Effects of Troponin Cardiomyopathy Mutations on the Calcium Binding Properties of the Troponin complex and Reconstituted Thin Filaments

by

Alison Yueh Li

M. Sc., Simon Fraser University, 2009

B. Sc., University of British Columbia, 2005

Thesis Submitted in Partial Fulfillment of the

Requirements for the Degree of

Doctor of Philosophy

in the

Department of Biomedical Physiology and Kinesiology

Faculty of Science

SIMON FRASER UNIVERSITY

Spring 2019

Approval

Name:	**Alison Yueh Li**
Degree:	**Doctor of Philosophy**
Title:	**Effects of Troponin Cardiomyopathy Mutations on the Calcium Binding Properties of the Troponin Complex and Reconstituted Thin Filaments**
Examining Committee:	**Chair: Will Cupples** Professor
	Glen F. Tibbits Senior Supervisor Professor
	Thomas Claydon Supervisor Associate Professor
	Lisa Craig Supervisor Associate Professor Molecular Biology and Biochemistry
	Damon Poburko Internal Examiner Associate Professor
	R. John Solaro External Examiner Distinguished University Professor Department of Physiology and Biophysics University of Illinois at Chicago
Date Defended/Approved:	April 18, 2019

Abstract

Hypertrophic cardiomyopathy (HCM) is the most common inherited cardiovascular disease that could result in sudden cardiac death. Mutations in the genes encoding sarcomeric proteins, including the thin filaments, are the most common cause of HCM. Thin filaments are an integral part of the cardiac muscle contractile unit, composed of actin, tropomyosin, and troponin (Tn) complexes which contain troponin C (TnC), troponin I (TnI) and troponin T (TnT). HCM molecular mechanisms remain unclear, partially due to the lack of a high-resolution thin filament structure and the complex molecular interactions between each component. My first goal was to investigate the effects of three TnT mutations, I79N, F110I and R287C, in human reconstituted thin filaments (RTF), using steady-state and stopped-flow fluorometry to determine Ca^{2+} sensitivity (K_d) and Ca^{2+} dissociation rates (k_{off}), respectively. Our data showed that I79N and R278C mutations significantly decreased K_d by lowering k_{off}, and all three mutations attenuated the functional effects of phosphomimetic TnI, suggesting an important role in impaired relaxation with HCM. My second goal was to investigate the effects of the I79N TnT mutation and the fetal cardiac R37C TnI mutation in their corresponding adult/fetal RTF. The I79N TnT mutation did not change the Ca^{2+} binding properties in fetal RTF but significantly decreased the K_d in adult RTF. In contrast, the R37C TnI mutation significantly increased the K_d in fetal RTF, yet its corresponding mutation, R68C TnI in adult RTF, exhibited reverse Ca^{2+} binding properties. My third goal was to use cryo-electron microscopy (EM) to solve the RTF structure. Optimal buffer conditions were found using negative-stain EM to ensure Tn binding on RTF with a periodicity of 38.5 nm; however, unexpected challenges arose during cryo data collection. Persistent filament aggregations obscured most of the cryo-images. Suggestions on how to address this problem are provided in the last chapter. In summary, using cardiac thin filaments as a physiologically relevant biochemical model allows us to investigate how HCM mutations alter Ca^{2+} binding properties. The resulting studies provide a better understanding of HCM molecular mechanism and can potentially help develop specific therapies that address the underlying causes of the disease.

Keywords: hypertrophic cardiomyopathy; troponin complexes; reconstituted thin filaments; steady-state fluorometry; stopped-flow fluorometry; cryo-electron microscopy

Acknowledgements

First and foremost, I would like to thank my senior supervisor, Dr. Glen F. Tibbits, whom I have had the pleasure to know since my master's study. I cannot express enough gratitude for his patience, understanding, motivation, immense knowledge, and great sense of humour especially when the times got difficult. Five years ago, I started my PhD after my maternity leave, and it was definitely not easy. However, because of Dr. Tibbits' genuine support, encouragement and trust in me, I know I made the right decision. Throughout my PhD years, he has provided opportunities for me to meet with other like-minded scientists through many national and international conferences and supported various opportunities to visit other research labs to learn new techniques. I'm forever grateful to Dr. Tibbits for the most fulfilling and rewarding educational experiences of my life and cannot imagine having a better supervisor and mentor for my PhD study.

I would also like to thank the rest of my thesis committee members, Dr. Thomas Claydon and Dr. Lisa Craig, for being there for me and believing in my academic potential. Their insightful comments, constant encouragement, and genuine curiosity for my project has propelled me and motivated me to widen my research from various perspectives. Also a special thanks to Dr. Craig for being a strong role model as women in science and teaching me negative staining technique and my early electron microscopy work at SFU.

My sincere thanks also goes to my collaborators. First, to Dr. Jonathan P. Davis from the Ohio State University, who provided me an opportunity to learn steady-state and stopped-flow techniques that are crucial for the data collection in my thesis. His meticulous way of performing an experiment and immense knowledge for biophysical experiments is infectious and inspiring. Also, for his former and current lab members, Dr. Sean Little and Dr. Svetlana Tikunova, for patiently showing me how to operate various instruments in the lab and teaching me all kinds of tricks for doing the most careful fluorometry work. Without their generous support, it would not be possible to learn the techniques and conduct this research. The other special thanks goes to Dr. Thomas Walz from Rockefeller University in New York City. I had some of the most joyful research days during the two separate trips I took to the Walz lab to learn the electron

microscopy related work. Seeing those world-renowned scientists conducting experiments in one of the most cutting-edge electron microscopes is awe-inspiring. I'm forever grateful for his warm hospitality for me to be in his lab, generous support for my experiments and incredible knowledge for cryo-EM. Same goes to one of my dear friends, Dr. Kelly Kim, who has been an important ally for me since our early grad school days. She made me feel so welcomed in her NYC home and the Walz lab, and patiently taught me everything about negative-stained and cryo-EM techniques. I will forever cherish those memories in NYC.

The members of the Tibbits group have contributed immensely to my time at the Molecular and Cellular Physiology Group (MCPG). The group has been a source of friendship as well as collaboration for my PhD study. I am especially grateful for my dear friend and lab sister, Dr. Sanam Shafaattalab, who has shown incredible perseverance and dedication in her stem cells projects. I have had the privilege to witness her impeccable work ethic, genuine passion for science and incredible strength to overcome challenges and hardships. I'm thankful for being able to work alongside with someone who provides such strong friendship, support, and encouragement throughout my grad school career. I would like to thank our lab manager Haruyo Kashihara, post-docs Dr. Eric Lin and Dr. Helen Sheng for their invaluable assistance to my project; I would also like to thank Deidre Jong-Wong for proofreading of my entire PhD thesis. I would like to thank the molecular team members Bo Liang and Kaveh Rayani, whom I have worked closely with for many years for the troponin project. I would also like to thank the other group members that I have had the pleasure to spend time with, including: graduate students Marvin Gunawan, Sabi Sangha, Lisa Lin, Drake Comber, and Kevin Ye for their friendship and laughter; my incredibly helpful and talented undergraduate student Tiffany Barszczewski; other past group members Dr. Laura Dewar, Dr. Charles Stevens, Dr. Christine Genge, Lillian Lee, Cindy Li, Tina Lu, Amanda Ribeiro and many others who have come through the Tibbits lab. I'm sincerely thankful for the people who have become a part of my life and made my time in the Tibbits lab and MCPG enjoyable.

Lastly, I would like to thank my family for their unconditional love and unwavering support in my academic pursuit. Starting my PhD after my maternity leave was definitely a challenge, and I could not have done it without the love and support of my parents, Jimmy and Penny. They have helped me through countless days and nights to take care of my young daughter. Their help was crucial especially at the early times of my PhD

study when my husband was completing his medical residency at the University of British Columbia. We could not have survived the long hours of studying, researching and training without the generous and unconditional help from my parents, my brother and sister in-laws, Lisa and Jack, my lifelong friend Jasmine, as well as many supportive and loving family friends, including the Peng family, the Fan family, and the Fu family, to name a few. I would like to thank my brother Jeff and his family, who have always believed in me. I would also like to thank my husband, Dr. Johnny Lee, for providing his insightful clinical perspectives for my project, working tirelessly to support our family, and loving me and believing that we can complete this journey together. Johnny has always been able to shift my perspective when I am stuck with a problem and ensuring me that everything will be okay. Last but not least, I would like to thank my beloved now six-year old daughter, Katelyn. Because of her, I want to be the best version of me that I can possibly be. Finding the balance for research and family has never been easy, but I want to be a role model to Katelyn just like the many amazing women scientists and mothers that I have had the privilege to meet throughout my grad school career. As I am writing this acknowledgment, I am 32-week pregnant with my second baby daughter. I cannot wait to tell her this amazing journey that I have completed with so many loved ones in my life. I am forever grateful for the most wonderful family, friends, mentors and colleagues that I can ever ask for. Thank you.

Table of Contents

List of Tables

List of Figures

List of Acronyms

ATP	adenosine triphosphate
AV node	atrioventricular node
Ca^{2+}	Calcium
Cav1.2	L-type Ca^{2+} channel
CM	Cardiomyocytes
DTT	dithiothreitol
EDTA	ethylene diamine tetraacetic acid
EGTA	ethylene glycol tetraacetic acid
F-actin	Filamentous actin
HCM	Hypertrophic cardiomyopathy
IAANS	2-(4'-(iodoacetamido)anilino)naphthalene-6-sulfonic acid
hiPSC	human induced pluripotent stem cells
K_d	dissociation constant
k_{off}	dissociation rate
MOPS	3(N-morpholino)propanesulfonic acid
NCX	Sodium calcium exchanger
NHE	Sodium hydrogen exchanger
PDB	Protein Data Bank
PLB	phospholamban
RTF	Reconstituted thin filaments
RyR	Ryanodine receptor
SA node	sinoatrial node
SERCA	Sarcoplasmic reticulum Ca^{2+}-ATPase
SR	Sarcoplasmic reticulum

Tm	Tropomyosin
Tn	Troponin
TnC	Troponin C
TnI	Troponin I
TnT	Troponin T
TnC^{T53C}	human cardiac TnC with T53C mutations for IAANS labeling at Cys53 and with C35S and C84S mutations
T-tubule	Transverse tubule
Uniprot	Universal Protein Resources
Vm	Membrane voltage

Chapter 1.

Introduction

1.1. Structure of cardiac myocytes

Every vertebrate organism possesses a heart. Its major function is to pump freshly oxygenated blood to other organs and throughout the body. An average adult human heart pumps about 60-90 mL of blood per beat, adding up to approximately 7500 L per day (College, 2013). To accomplish this task, the musculature of the heart is impressively robust; its contraction delivers blood throughout the body on a beat-to-beat basis over the course of a lifetime.

Many cell types exist in adult human hearts. Cardiomyocytes account for 30-40% of the cells in the mammalian heart, and the rest of the heart consists of a variety of non-CM cells, including fibroblasts, endothelial cells, peri-vascular cells, and neurons that are important for proper heart function (Pinnell J., 2007; Zhou and Pu, 2016). Cardiomyocytes occupy most of the volume of the mammalian heart and are divided into myocardial contractile and pacemaker cells. Contractile cells make up the atria and ventricles of the heart and enable the shortening and lengthening of the muscle fibers necessary for muscle contraction and relaxation to occur. Pacemaker cells are found in the sinoatrial (SA), atrioventricular (AV) nodes, bundle of His, bundle branches and Purkinje fibres. These cells are able to generate electric impulses spontaneously, controlling the rate of contraction and therefore regulating heart beat (Pinnell J., 2007).

As shown in Figure 1.1, cardiac muscle fibers are made up of cardiomyocytes, each containing 1-3 nuclei surrounded by a plasma membrane called the sarcolemma, part of which forms an intercalated disc at the interface of one myocyte to another (College, 2013). The cardiomyocytes are densely packed with mitochondria (30-35% by volume) to provide an ample supply of ATP which is required for muscle contraction (Gustafsson and Gottlieb, 2008). Each cardiomyocyte can be further dissected into several organizational levels, beginning with bundles of myofibrils, rod shaped units that are further composed of myofilaments (College, 2013). Each myofilament consists of a repeating parallel array of the most basic contractile unit, the sarcomere, and in turn,

each sarcomere is composed of thick and thin filaments (College, 2013). Thick filaments are made primarily of myosin, myosin-binding protein C and titin, while thin filaments are composed of primarily of actin, tropomyosin, and troponin (Tn) complexes. The Tn complex serves as a critical regulator of cardiac muscle contraction and relaxation.

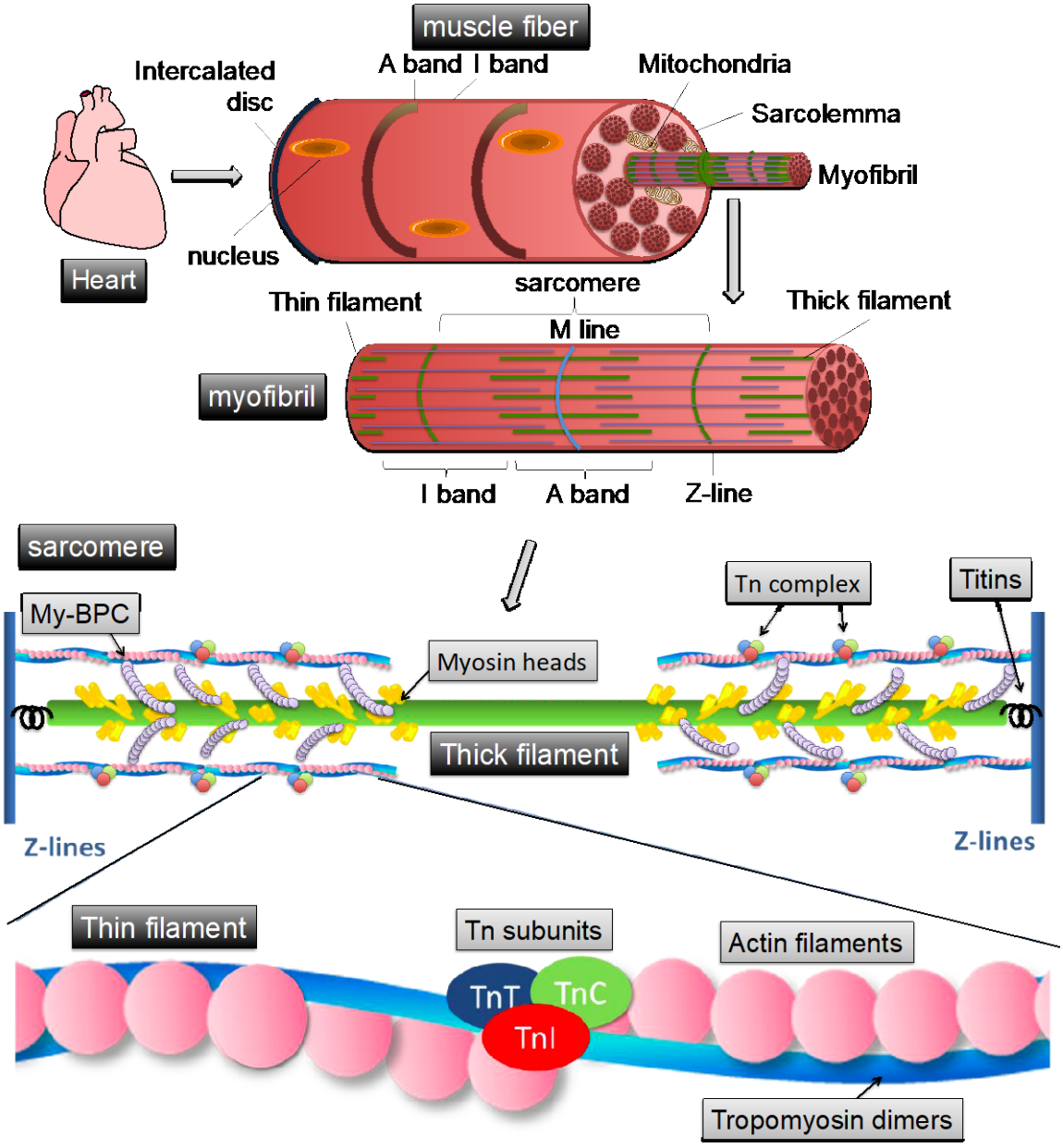

Figure 1-1 Schematic of the cardiac muscle fiber and its components.

The vertebrate heart is composed of billions of muscle fibers or cardiomyocytes, which are connected to each other through intercalated discs. Each cardiomyocyte contains hundreds to thousands of myofibrils that confer on it a striated pattern. Each myofibril consists of sarcomeres, in which the boundaries are defined by Z lines. In the middle of the A-band lies another line called the M-line. Each sarcomere is made up by parallel arrays of thick and thin filaments. The thick filament consists of myosin, myosin binding protein C (My-BPC) and titin while the thin filaments are composed of actin filaments, tropomyosin and troponin complexes. Parts of this image are adapted from (Web, 2017).

1.2. Excitation-contraction coupling of the heart

Cardiomyocytes are activated by signals from the cardiac electrical conduction system, transmitted from the pacemaker cells (Irisawa, 1978). The electrical signal normally is initiated by the sino-atrial (SA) node and generates an action potential that first travels to the atria via gap junctions to reach the atrio-ventricular (AV) node (Irisawa, 1978). Then, the electrical signal is conducted through the Bundle of His, along the bundle branches, and down to the Purkinje fibers to stimulate the right and left ventricles (Irisawa, 1978). The action potential causes rapid depolarization of the cardiomyocytes due to the opening of the Na^+ channels (NaV1.5) in the T-tubules (Irisawa, 1978). Figure 1.2 illustrates the action potential movement from the SA node to the Purkinje fibers and into the T-tubules of the ventricular cardiomyocytes.

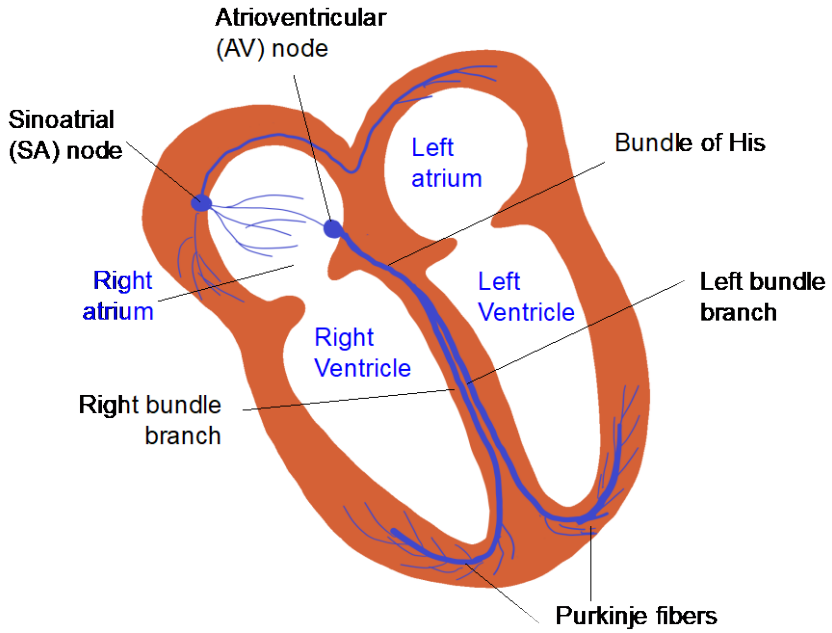

Figure 1-2 Cartoon representation of the conduction system of the heart.

The main components of the cardiac conduction system are the SA node, AV node, bundle of His, bundle branches and Purkinje fibers. The SA node starts the wave signal of depolarization causes the atria to contract. Next the signal travels to AV node, through the bundle of His, down the bundle branches and through the Purkinje fibers, causing the ventricles to contract.

Depolarization leads to the opening of the voltage-gated L-type Ca^{2+} channels (CaV1.2) (I_{ca}) (Irisawa, 1978) as shown in Figure 1.3. This opening causes an increase in the cytosolic Ca^{2+} concentration from the low nanomolar range (~100 nM) to a higher concentration of 500-1200 nM (Bers, 2002). Higher cytosolic Ca^{2+} concentration further

induces the release of Ca^{2+} from the sarcoplasmic reticulum (SR) through the ryanodine receptor (RyR2) by means of Ca^{2+}-induced Ca^{2+} release (CICR) (Bers, 2002; Gordon et al., 2000). This drives a further increase in cytosolic Ca^{2+} levels so Ca^{2+} can now bind to the major Ca^{2+} sensor protein, cardiac troponin C (cTnC). cTnC binds approximately 50% of Ca^{2+} released from the SR during a typical heart beat and thus is the largest cytosolic Ca^{2+} buffer in cardiomyocytes (Bers, 2002). Binding of Ca^{2+} to cTnC elicits a cascade of protein conformational changes that eventually lead to muscle contraction. This process by which an electrical stimulus triggers the release of Ca^{2+} by the SR, resulting in cardiac muscle contraction is termed “excitation-contraction coupling”, also known as the “EC-coupling” (Bers, 2002).

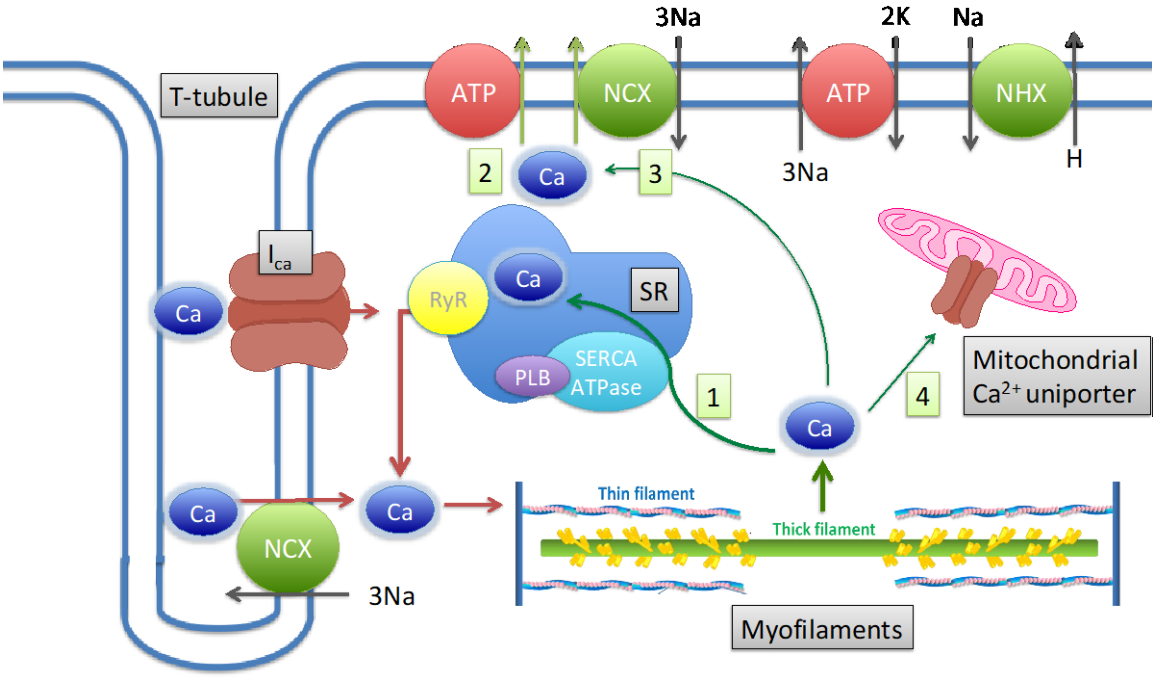

Figure 1-3 The excitation-contraction coupling process and relaxation process in ventricular cardiac myocytes.

During relaxation, Ca^{2+} is released from TnC and is mediated by four pathways: 1) the SR Ca^{2+} ATPase pump, SERCA2A, which regulated by phospholamban (PLB); 2) the sarcolemmal Na^{+}/Ca^{2+} exchanger 1 (NCX1); 3) the sarcolemmal Ca^{2+} ATPase pump and, 4) the mitochondrial Ca^{2+} uniporter. The SR Ca^{2+}-ATPase sequesters about ~60-70% of the Ca^{2+}, NXC extrudes ~30-40%, and the remaining 1% goes to the sarcolemmal Ca^{2+} ATPase pump and the mitochondrial Ca^{2+} uniporter. NHE: sodium hydrogen exchanger. This figure is adapted from Bers et. al. (Bers, 2002).

1.3. Molecular regulation of cardiac muscle contraction

As mentioned previously, cardiac muscle is highly responsive to the cytosolic levels of Ca^{2+}, and the largest cytosolic buffer that binds to Ca^{2+} is cTnC. cTnC belongs to an essential heterotrimeric complex cardiac troponin (cTn) that regulates muscle contraction and relaxation (Katrukha, 2013). The other two subunits of cTn include the inhibitory subunit, cardiac troponin I (cTnI), and the tropomyosin (Tm) binding subunit, cardiac troponin T (cTnT). The cTn complex binds to the thin filaments with a regular periodicity at every seventh actin subunit and one Tm dimer (Katrukha, 2013). Bound to the thin filament, together these proteins interact with the thick filament to promote force-generating cross-bridges that use the chemical energy generated from ATP hydrolysis (Katrukha, 2013). Figure 1.4 illustrates the crystal structure of the core domain of the human cTn complex.

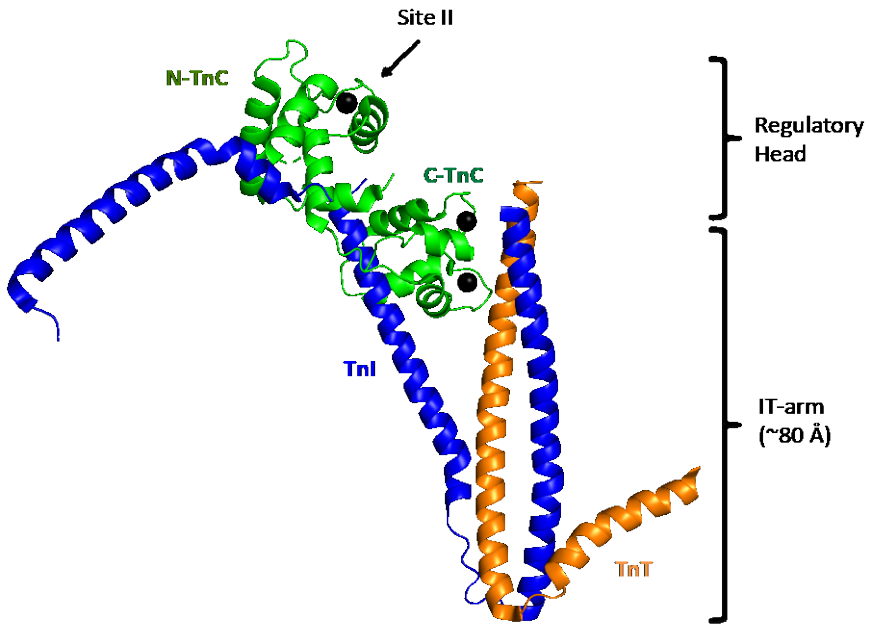

Figure 1-4 The structure of the core domain of the human cTn complex.

TnC (green), TnI (blue), and TnT (orange). The Ca^{2+} ions bound to TnC are represented as black spheres. The regulatory head region includes the N-terminal regulatory domain of TnC (N-cTnC) and part of TnI. Site II of the N-cTnC is indicated as the Ca^{2+} sensing site that elicit the muscle contraction. The coiled-coil region formed by the TnI and TnT chains, namely the IT arm, acts as a scaffold that holds the C-terminal structural domain of TnC (C-TnC). The IT-arm region spans ~80 Å. (PDB: 4Y99) (Takeda, 2016). This figure was generated using PyMol (Delano, 2015).

Following the excitation-contraction coupling process, relaxation of the myofilaments begins with the active removal of cytosolic Ca^{2+} via two pathways (see Figure 1.3). Through the first pathway, the majority of the Ca^{2+} ions are pumped back into the SR by the Ca^{2+} ATPase pump (SERCA2A). The rate at which Ca^{2+} is sequestered into the SR is regulated, in part, by the level of phospholamban (PLB) phosphorylation (Bers, 2002). When PLB is phosphorylated, it removes the inhibition of SERCA2a and facilitates the Ca^{2+} intake to SR. The second pathway by which Ca^{2+} is removed from the cytosol--in this case, extruded from the cell rather than sequestered in the SR--is via the sodium/calcium exchanger (NCX1) (Bers, 2002). NCX1 transports one Ca^{2+} ion out of the cell at the expense of allowing entry of three Na^{+} ions into the cell. As the cytosolic Ca^{2+} concentration decreases through these two major pathways, Ca^{2+} then dissociates from Site II of cTnC, ultimately leading to cardiac muscle relaxation (Hazard et al., 1998). This relaxation process is further enhanced by the phosphorylation of Ser23/24 of cTnI during β-adrenergic stimulation (Figure 1-5) (Solaro and Kobayashi, 2011). When this process is disturbed, it can greatly affect the ability of the cardiac muscle to relax, resulting in complex cardiomyopathies that will be discussed in a later section of this chapter.

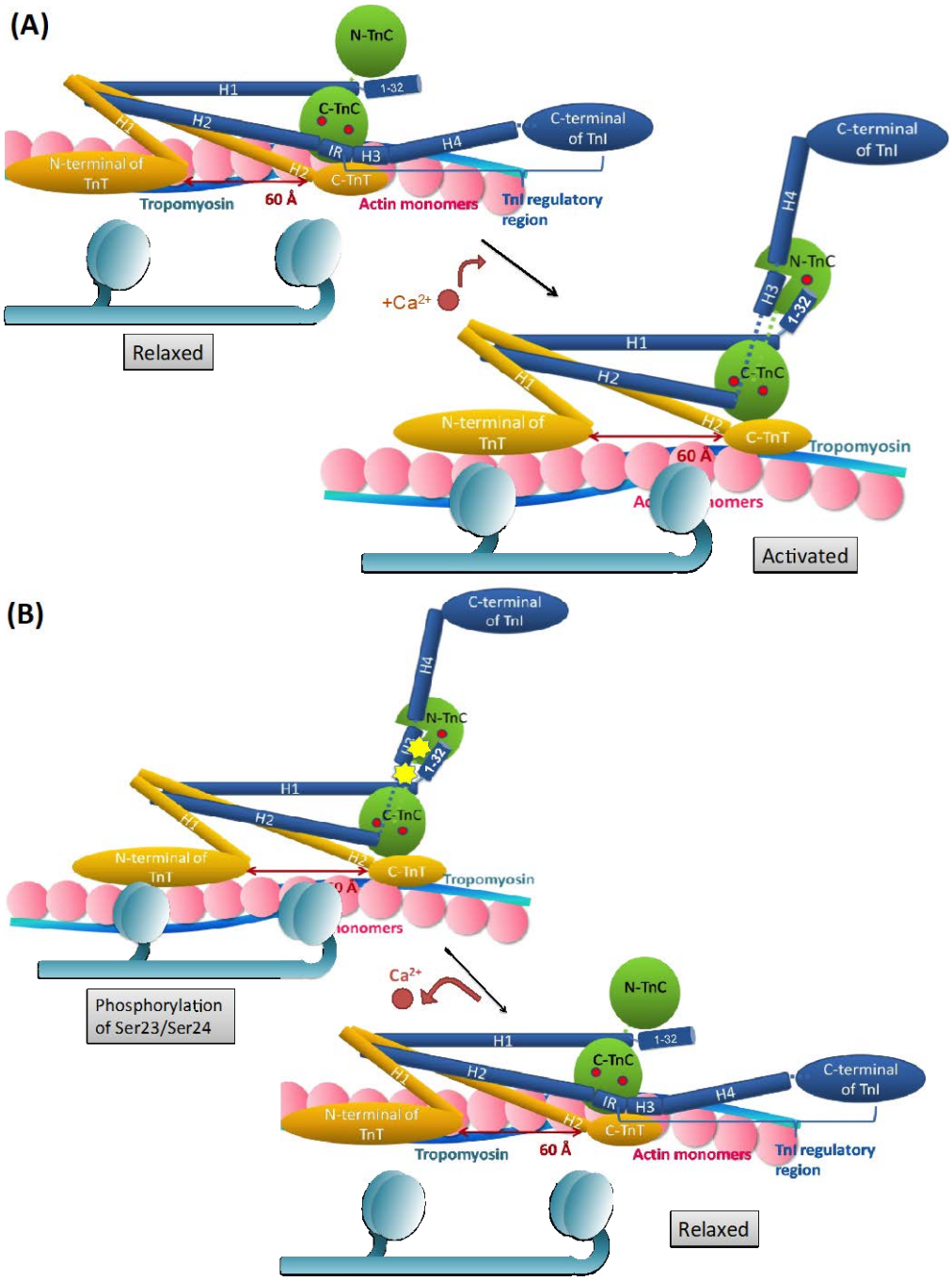

Figure 1-5 The schematic of the cardiac contraction and relaxation.

(A) shows the relaxed form of the Tn complex without Ca^{2+} binding. When Ca^{2+} binds to site II of TnC, it opens up the hydrophobic binding pocket of TnC, allowing helix 3 (H3) of TnI to bind. This removes the inhibitory effect of TnI from actin so that the myosin heads from the thick filaments can bind to actin filaments. As more myosin heads bind to the actin, the thin filaments enter the fully activated form. (B) During β-adrenergic stimulation, cardiac output is increased up to five-fold; this requires faster relaxation and hence faster Ca^{2+} removal from site II of TnC. This Ca^{2+} removal is facilitated by phosphorylation of Ser23/Ser24 of TnI allowing the myofilaments to return to the relaxed form more quickly.

The molecular regulation of the cardiac muscle contraction can be described by a "Three-state model". The Three-state model, as shown in Figure 1-6, includes the Blocked state (B-state), the Closed state (C-state), and the Open state (M-state) (Tardiff, 2011). In the Blocked state, which occurs in diastole or when cytosolic Ca^{2+} concentration is maintained at around 100 nM, nominally no Ca^{2+} is bound to Site II of cTnC and Tm blocks the actin from binding to myosin preventing cross-bridge activity from occurring. In the Closed state, Ca^{2+} binds to the regulatory domain of cTnC but only weak cross-bridge activity is observed. In the Open (M-state), the conformational change occurring when Ca^{2+} binds to TnC is propagated through TnT and Tm to the rest of the thin filament, causing Tm to move closer to the groove along the surface of the actin monomers (Tardiff, 2011). The binding site on actin that was previously blocked by cTnI is now exposed for the myosin heads to bind. As more myosin heads bind to actin, it causes the thin filaments to produce strong force generating cross-bridges, allowing the thick and thin filaments to slide past each other to produce muscle contraction (Tardiff, 2011). The whole process is reversed for muscle relaxation to occur (see Figure 1.6). Taken together, thin filament cooperativity is fundamental to proper cardiac function at the molecular level. However, their dynamic regulation processes largely remain unclear.

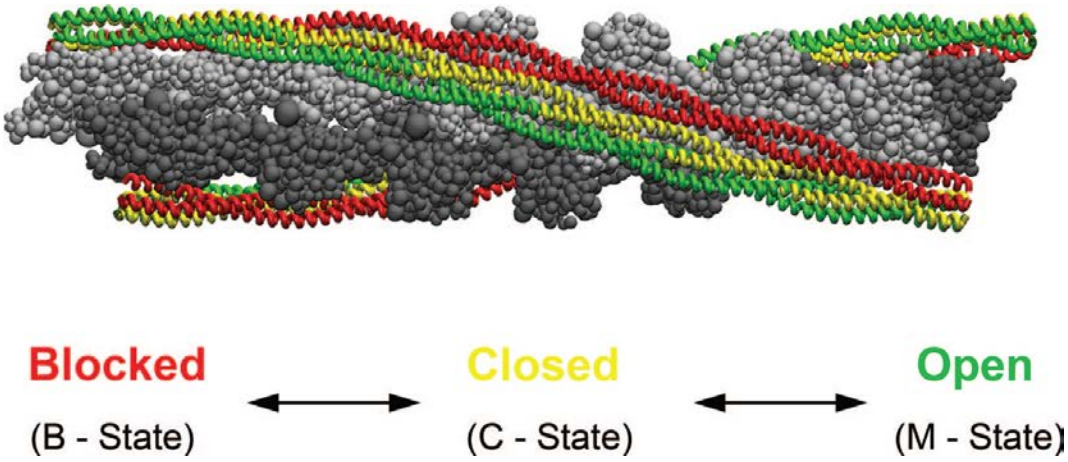

Figure 1-6 The three-state model of myofilament activation.

A section of simulated tropomyosin-actin structure is shown here in three different myofilament states: Blocked state (red), Closed state (yellow), and Open state (green). The colour of the long helices of Tm corresponds to the position of the myofilament. Without Ca^{2+} binding to TnC, the myofilament remains in the Blocked state (B-state). Ca^{2+} binding to TnC induces an azimuthal shift to the weakly bound state (C-state) and subsequent binding of myosin drives the C-state to the fully activated open conformation (M-state). Reprinted with permission (Tardiff, 2011).

1.4. Structure and function of cardiac thin filaments

Cardiac thin filaments form a dynamic, multi-subunit regulatory machine that requires the cooperativity of each component for the proper function of the cardiac muscle. It is a system that is highly dynamic and flexible in order to execute their respective functions; in particular, the transition between the three states of muscle activation. One important property that is intrinsic to thin filament activation is the cooperative mechanism between the neighbouring units (Moss et al., 2004; Tobacman, 1996). Each regulatory unit of the thin filament is generally considered to be one Tn complex and one Tm dimer associated with seven actin molecules. These regulatory units are in communication and do not function independently; Ca^{2+} binding to TnC promotes further binding of Ca^{2+} to the neighbouring TnC and so on (Moss et al., 2004). The cooperative activation propagates along the Tm-Tm overlap on the actin filaments as well as through the neighbouring Tn complexes. These regulatory units require precise protein-protein interactions and coordination to activate the thin filaments, and perturbation of any component can result in changes that propagate along the entire filament (Tardiff, 2011; Tobacman, 1996). The following sections will discuss the structure and function of each thin filament component, and their isoform and paralog switch during cardiac development.

1.4.1. Actin

Actin is one of the most highly conserved and abundant proteins in eukaryotic cells (Dominguez and Holmes, 2011). From *S. cerevisiae* (yeast) actin to human actin, which represents more than one billion years of evolution, 94% of the overall amino acid sequence is conserved (Kudryashov and Reisler, 2013). In humans, actin is expressed by six different genes, with two expressed in striated muscles: the α-skeletal actin *ACTA1* and α cardiac actin *ACTC* (Dominguez and Holmes, 2011). There are 377 amino acids in total for both paralogs but only 375 residues for the mature polypeptides due to the removal of the initiator Met and the subsequent Cys residue at the second position (Dominguez and Holmes, 2011). The actin used throughout this thesis was obtained from the rabbit skeletal muscle, which has >99% protein sequence identity compared to that of the human cardiac actin (Figure 1-7).

```
human       MCDDEETTALVCDNGSGLVKAGFAGDDAPRAVFPSIVGRPRHQGVMVGMGQKDSYVGDEA 60
rabbit      MCDEDETTALVCDNGSGLVKAGFAGDDAPRAVFPSIVGRPRHQGVMVGMGQKDSYVGDEA 60
            ***::**********************************************************

human       QSKRGILTLKYPIEHGIITNWDDMEKIWHHTFYNELRVAPEEHPTLLTEAPLNPKANREK 120
rabbit      QSKRGILTLKYPIEHGIITNWDDMEKIWHHTFYNELRVAPEEHPTLLTEAPLNPKANREK 120
            ************************************************************

human       MTQIMFETFNVPAMYVAIQAVLSLYASGRTTGIVLDSGDGVTHNVPIYEGYALPHAIMRL 180
rabbit      MTQIMFETFNVPAMYVAIQAVLSLYASGRTTGIVLDSGDGVTHNVPIYEGYALPHAIMRL 180
            ************************************************************

human       DLAGRDLTDYLMKILTERGYSFVTTAEREIVRDIKEKLCYVALDFENEMATAASSSSLEK 240
rabbit      DLAGRDLTDYLMKILTERGYSFVTTAEREIVRDIKEKLCYVALDFENEMATAASSSSLEK 240
            ************************************************************

human       SYELPDGQVITIGNERFRCPETLFQPSFIGMESAGIHETTYNSIMKCDIDIRKDLYANNV 300
rabbit      SYELPDGQVITIGNERFRCPETLFQPSFIGMESAGIHETTYNSIMKCDIDIRKDLYANNV 300
            ************************************************************

human       LSGGTTMYPGIADRMQKEITALAPSTMKIKIIAPPERKYSVWIGGSILASLSTFQQMWIS 360
rabbit      MSGGTTMYPGIADRMQKEITALAPSTMKIKIIAPPERKYSVWIGGSILASLSTFQQMWIT 360
            :************************************************************:

human       KQEYDEAGPSIVHRKCF    377
rabbit      KQEYDEAGPSIVHRKCF    377
            *****************
```

Figure 1-7 Sequence alignment between human cardiac actin and rabbit skeletal actin.

The sequence alignment file was performed using Clustal Omega (Sievers et al., 2011).

Actin has a molecular weight of approximately 42 kDa and an overall globular shape (Dominguez and Holmes, 2011; Kudryashov and Reisler, 2013). There are two major domains, a small (outer) domain and a large (inner) domain, which further divide into four subdomains: subdomains 1 through 4, as shown in Figure 1-8. The two main domains are separated by a cleft where divalent ions, Mg^{2+} or Ca^{2+}, and nucleotides, ATP or ADP + Pi, are bound. More than 80 X-ray crystallographic structures have been determined for actin in the monomeric form (known as globular or G-actin), in complex with actin binding proteins or small molecules (Dominguez, 2011). Regardless of the binding molecule or the nucleotide state, the conformation of the actin monomer remains similar and very stable. With the recent advancement of cryo-electron microscopy (cryo-EM), many actin structures in the polymer form (known as filamentous or F-actin) (Figure 1-9) with various binding proteins have also been determined (Pospich et al., 2017; von

der Ecken et al., 2016; von der Ecken et al., 2015). These structures of filamentous actins indicate that the subdomains of the large domain—subdomains 3 and 4--are located towards the center of the filament helix, whereas the subdomains of the small domain—subdomains 1 and 2--are exposed to the solvent. The DNase I-binding loop, termed the D-loop, mediates important interactions in the complex with DNase I and acts as a central region for longitudinal inter-subunit contacts in the actin filaments through various hydrophobic and electrostatic interactions (Durer et al., 2012; Kabsch et al., 1990). In addition, the negatively-charged Tm interacts with a positively charged grove on F-actin (von der Ecken et al., 2015), and the negatively charged N-terminus of actin interacts with a conserved basic motif of myosin (von der Ecken et al., 2016).

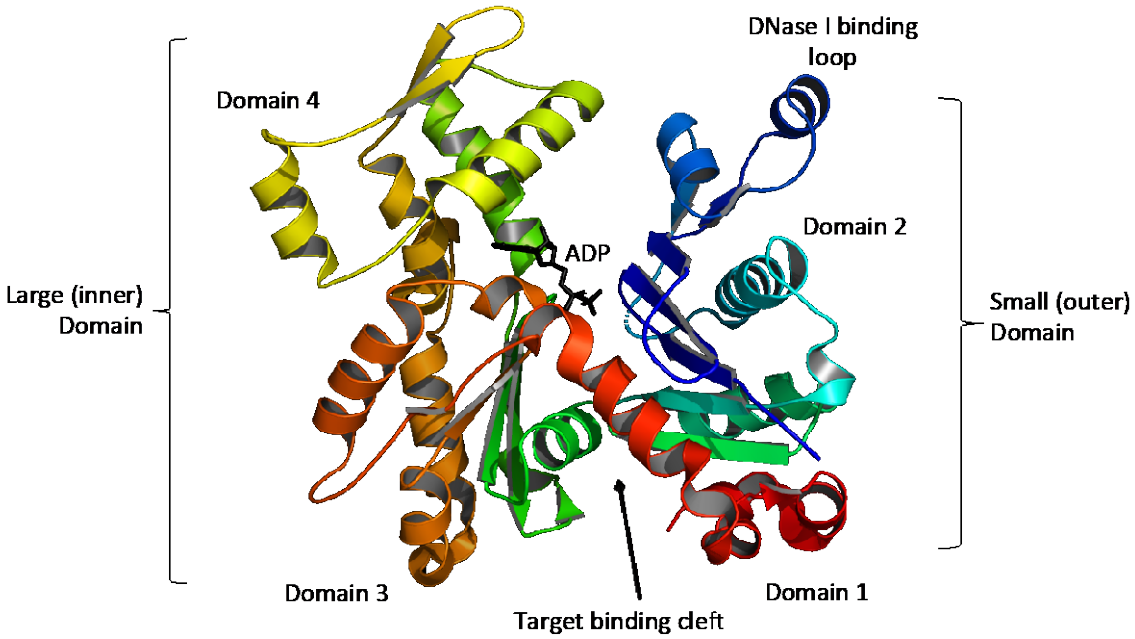

Figure 1-8 Crystal structure of the rabbit skeletal actin monomer in the ADP state.

There are four subdomains in the full-length actin monomer in the ADP (shown as the black stick) bound form. The small outer domain consists of subdomains 1 and 2, and the large inner domain consists of subdomains 3 and 4 (PDB: 1J6Z) (Otterbein et al., 2001). The DNase I binding loop would become disordered and usually is missing in the crystal structure of the ATP-bound form (Graceffa and Dominguez, 2003). The structure is coloured spectrally from the N-terminus (blue) to the C-terminus (red) and generated by PyMol (Delano, 2015).

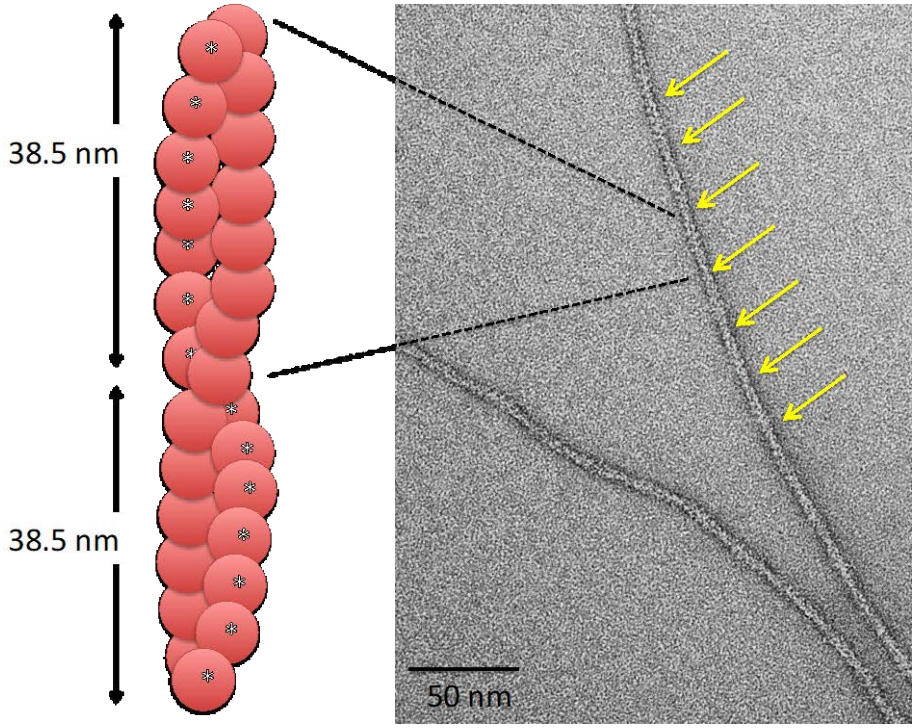

Figure 1-9 G-actins assemble into F-actin filaments.

Cartoon representation of seven G-actin monomers assembled into a F-actin filament with a periodicity of 38.5 nm. The twist can be seen in my negatively-stained EM image on the right with yellow arrows indicating the twists at every 38.5 nm. F-actin was stained with 0.75% uranyl formate and imaged with a CM10 Philips electron microscope.

As mentioned previously, not only is actin a highly-conserved protein but it is also the most abundant protein in eukaryotic cells. It plays a critical role in many cellular processes, including cell motility, muscle contraction, organelle movement, establishment of cell junctions and maintenance of cell shape. The versatile functions of actin arise from its ability to transition between monomeric actin (G-actin) and filamentous actin (F-actin) and interact with more than 150 actin binding proteins (dos Remedios et al., 2003; Lodish H, 2000). In general, actin polymerization occurs over three phases: a nucleation phase, an elongation phase and a steady-state phase. Starting with three actin monomers, a stable actin nucleus is formed. Once more monomers are added to the actin nucleus, the elongation phase accelerates as monomers are rapidly added to the filaments at the plus (barbed) end (Figure 1-10). Under steady-state conditions in the presence of ATP, actin from the minus (pointed) end bound with ADP dissociate from the filaments while actin monomers bound with ATP bind to the plus end. Actin-bound ATP is hydrolyzed upon incorporation of G-actin into the filaments, and subsequently the inorganic phosphate is released. Consequently,

the barbed ends of the filaments are enriched with ATP where monomers are rapidly associated, and the pointed end where enriched with ADP-monomers are rapidly dissociated (Lodish H, 2000). This ATP-hydrolysis driven process is termed as "treadmilling" in which the shortening of the pointed end is balanced by elongation of the barbed end of the filaments (Figure 1-10). This process is crucial in cell migration and invasion, even in resting cells (Lodish H, 2000).

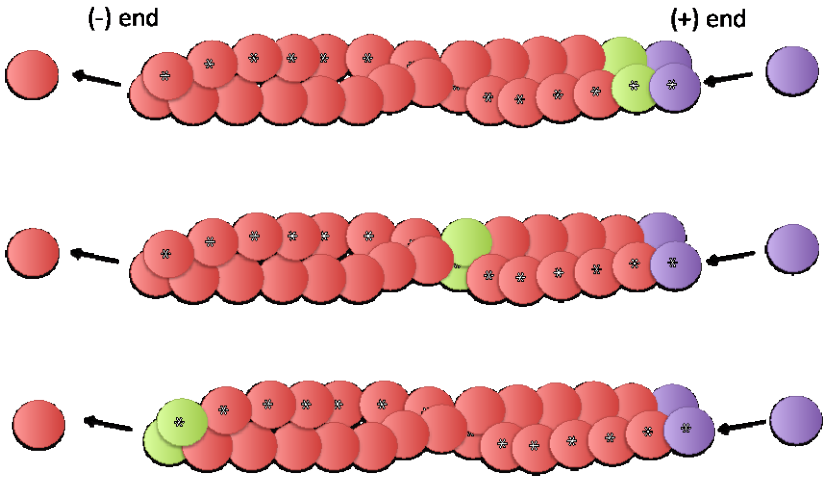

Figure 1-10 Treadmilling of actin filaments.

Subunits undergo a net assembly at the (+) end and disassembly at the (-) end with the polymer remaining a constant length when both ends of the polymer are exposed. The green monomers indicate the movement of the individual actin monomers from the (+) end to the (-) end. The purple monomers are the new actin monomers being added to the (+) during the treadmilling process.

However, in cardiac muscle, thin filaments maintain a constant ~1 μm length, despite the actin subunits continuously associating and dissociating from both the plus and minus ends of the filaments (Lodish H, 2000). Many factors contribute to the regulation of the constant thin filament length, and it has been an active research area over the last several decades. These factors include regulation by the capping protein tropomodulin (Tmod) at the pointed end, coordination by various other actin-binding proteins such as cofilin, profilin and the Arp2/3 complex, and binding with nebulin and/or titin as a molecular ruler (Lodish H, 2000). Regardless of the mechanisms, actin serves a crucial role in the allosteric regulation of the thin filaments through its interactions with Tm and Tn complexes. As will be discussed in later sections, a single amino acid mutation within the Tn complex or Tm located far from the Ca^{2+} binding site of TnC can

have varying impacts on the overall Ca^{2+} binding properties of the sarcomere through direct or allosteric interactions with actin, resulting in complex cardiomyopathies.

1.4.2. Tropomyosin

There are four human Tm genes, *TPM1*, *TPM2*, *TPM3*, and *TPM4*, which encode for the striated tropomyosin proteins α1-Tm, β-Tm, α3-Tm, and α4-Tm, respectively (Schevzov et al., 2011). Each gene can produce multiple isoforms through alternative splicing. In small mammals such as mice and rabbits, there is a progressive increase of the expression ratio of α-Tm to β-Tm during development, until α-Tm becomes the predominant tropomyosin expressed in the adult heart. In larger mammals such as cow or sheep, the expression ratio of β-Tm to α-Tm is approximately 1:4 (Leger et al., 1976). However, the developmental changes in human cardiac Tm are not well understood, and no protein data are available yet. Purified human ventricular Tm has been reported to be exclusively α1-Tm (Purcell et al., 1999).

Tropomyosin (Tm) is an α coiled-coil protein consisting of 284 amino acid residues, as shown in Figure 1-11 (Smillie, 1979). Tm-dimer molecules bind to actin filaments in a head-to-tail fashion via overlaps at their amino and carboxyl terminal ends and defines the periodicity of the Tn complex at every 38.5 nm on the actin filaments (Brown et al., 2001). Each Tm has a heptad repeat that extends throughout the full length Tm; these seven residues are labeled *a* to *g.* Residues *a* and *g* are hydrophobic, contributing to the hydrophobic core of the parallel strands, whereas residues *e* and *g* form salt bridges providing further stability and specificity of the coiled-coil structure (Monteiro et al., 1994; Smillie et al., 1980). These residues at the N-terminus of Tm are highly conserved from *Drosophila* to human (Basi and Storti, 1986), since they are crucial for the promotion of binding actin to Tm. The structure of Tm is well understood since there have been more than 90 structures of Tm or Tm complexes with various interacting proteins solved to date using X-ray crystallography or cryo-EM.

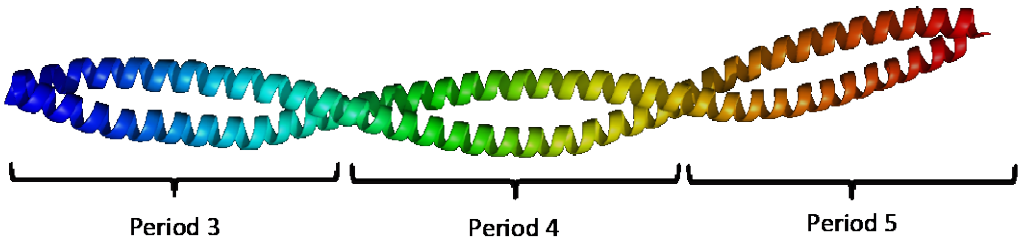

Figure 1-11 Cryo-EM structure of a section of mouse Tm.

This portion of Tm was included in the high-resolution cryo-EM structure of the actin-Tm complex (PDB: 4A7L) (von der Ecken et al., 2015). The full-length Tm, with 284 residues, spans seven actin monomers. It is divided into seven pseudo-repeat regions, which consist of ~40 residues, corresponding to seven actin interaction sites. The structure is coloured spectrally from the N-terminus (blue) to the C-terminus (red). The figure was generated using PyMol (Delano, 2015).

The adjoining Tm homo-dimers are a critical component of the cooperative three-state muscle activation model through their interactions with actin and Tn complexes (Tardiff, 2011). At low Ca^{2+} concentrations, Tm sterically blocks the myosin-binding site of actin during the relaxation state. As Site II of TnC becomes saturated with Ca^{2+}, Tm moves away from the blocked position to allow myosin to bind to actin. The initial myosin binding further changes the actin conformation, resulting in an azimuthal shift of the Tm position, and promoting stronger binding of myosin to the actin groove (Tardiff, 2011). Subsequently, fully active cross-bridges form. The precise mechanism through which Tm modulates the conformational changes of sarcomeric proteins has been an active research area over the past two decades (Li et al., 2011; Seymour and O'Brien, 1980; Xu et al., 1999), but it is still not well understood. It is clear that Tm plays a pivotal role in regulating actin-myosin interactions and controlling the flexibility and dynamics of the thin filaments to facilitate the coordination between myosin and actins.

Tm binds to F-actin with very low affinity (Kd~10^{-3} M), and its incorporation into the actin filament requires precise formation of the head-to-tail Tm dimers assembly along the actin filaments (Tobacman, 2008). Native human Tm is not easily obtained and as a result, many previous experiments used native bovine Tm (Davis et al., 2007). In this thesis project, I used recombinant human Tm because it can be generated in high quantity in *Escherichia coli* (*E. coli*) and any desired mutations can be introduced by site-directed mutagenesis in the recombinant form than it is to isolate and purify from slaughterhouse bovine hearts. However, the disadvantage is that the post-translational modification of recombinant Tm is missing in the *E. coli* system (Rosano and Ceccarelli, 2014). In particular, the initiation Met in the naturally expressed Tm is acetylated,

whereas the initiation Met in recombinant Tm expressed in *E. coli* is not acetylated (Coulton et al., 2006). Consequently, the unacetylated Met in recombinant Tm is removed by Met aminopeptidase during the *E. coli* co-translational process, leaving the charged Asp exposed (Monteiro et al., 1994). This negatively charged Asp is predicted to oppose the hydrophobic core of the Tm dimer, reducing the stability of the coiled-coil structure in this region, and thereby impairing head-to-tail polymerization (Monteiro et al., 1994). For this reason, all recombinant Tm used for the generation of reconstituted thin filament used throughout the thesis project required the fusion of the peptide Met-Ala-Ser (MAS-) or Met-Gly-Ser (MGS-) at the N-terminus, leaving the hydrophobic Ala or Gly residue after the removal of the initiation Met (Coulton et al., 2006; Monteiro et al., 1994).

1.4.3. Cardiac troponin C (cTnC)

cTnC is a small, 161 amino acid, protein molecule which adopts the shape of a "dumbbell" consisting of two globular domains (Figure 1-12) connected by a long flexible linker (Katrukha, 2013). In the C terminal structural domain, there are two ion binding sites which are made of two helix-loop-helix (EF-hand) motifs, termed Site III and Site IV (Katrukha, 2013). Under physiological conditions, these two ion binding sites are almost always occupied by Mg^{2+} and Ca^{2+}, with a binding affinity K_d of 10^{-4} M and 10^{-7} M, respectively, maintaining the structural integrity with the rest of the cTn complex (Katrukha, 2013). In the N terminal regulatory domain, Site I is dysfunctional in cardiac but not skeletal muscle, meaning it does not binding to ions under normal physiological conditions. Site II is the main Ca^{2+} sensing site that binds to Ca^{2+} with a binding affinity K_d of 10^{-5} M responsive to Ca^{2+} concentration increases from the nanomolar range to micromolar range (Katrukha, 2013). Upon Ca^{2+} binding to Site II of TnC, the hydrophobic binding pocket opens to allow the binding of the switch peptide of TnI (residue 147-163), removing the inhibition of TnI on actin. Myosin heads can now bind to the newly exposed actin molecules, allowing muscle contraction to occur (Katrukha, 2013) (Figure 1-5).

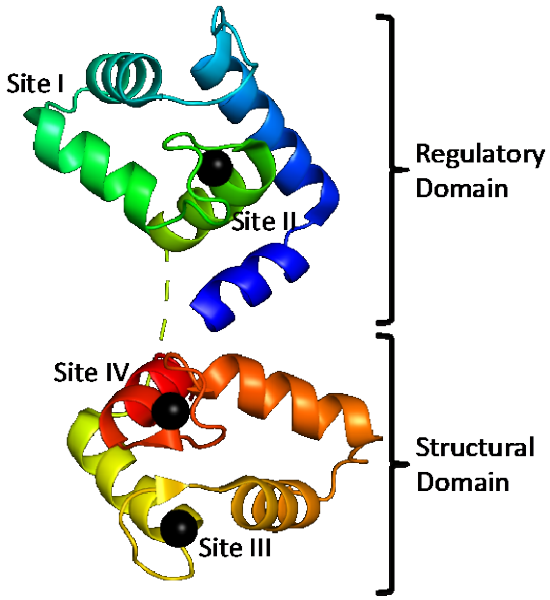

Figure 1-12 Crystal structure of the full-length human TnC.

cTnC is a protein molecule that resembles the shape of a dumbbell. It consists two domains: a regulatory domain and a structural domain that are connected by a flexible linker region. cTnC is coloured spectrally from the N-terminus (blue) to the C-terminus (red). The Ca^{2+} ions are represented as black spheres. Site I does not bind any ion in the cardiac isoform of TnC in the crystal structure, whereas Sites II to IV exhibit Ca^{2+} binding. (PDB: 4Y99) (Takeda, 2016). The figure was generated using PyMol (Delano, 2015).

cTnC is a highly conserved protein molecule across many different species (Li and Hwang, 2015) and binds to more than 50% of the Ca^{2+} released from the SR, serving as the major Ca^{2+} cytosolic buffer in cardiomyocytes (Li and Hwang, 2015). Interestingly, many of the cardiomyopathy-related mutations known occur are in regions located remotely from the TnC- Ca^{2+} binding site. However, these mutations have “long-range effects” that propagate along the thin filaments, causing perturbation of the Ca^{2+} binding kinetics on TnC and resulting in complex cardiomyopathies (Tardiff, 2011). In order to study these cardiomyopathies at the molecular level, measuring the changes in the Ca^{2+} binding kinetics of TnC using steady-state and stopped flow fluorescence techniques in various biochemical systems of increasing complexity has been developed over the past two decades (Davis et al., 2007; Li et al., 2013a; Liu et al., 2012b; Tikunova and Davis, 2004; Tikunova et al., 2010). These data provide important biochemical information on the changes in Ca^{2+} binding kinetics and their relation to Ca^{2+} mishandling in cardiomyocytes derived from the human-derived pluripotent stem cells (hiPSC) (Shafaattalab et al., 2019).

1.4.4. Cardiac troponin I (cTnI)

cTnI is the inhibitory subunit of the cTn complex, switching its inhibitory peptide between actin and the hydrophobic pocket of the regulatory domain of TnC during cardiac muscle contraction and relaxation (Katrukha, 2013). It is composed exclusively of α-helices made up of 211 amino acid residues, with the initiator Met being cleaved after post-translational modification, leaving the mature protein with 210 amino acids. The entire molecule is divided into five domains, including the N-terminal domain (residues 2-32), the IT arm (residue 32-136), the inhibitory domain (residue ~137-146), the regulatory/switch domain (residues ~147-163), and the mobile domain (163-210) as shown in Figure 1-13 (Manning et al., 2011; Tardiff, 2011).

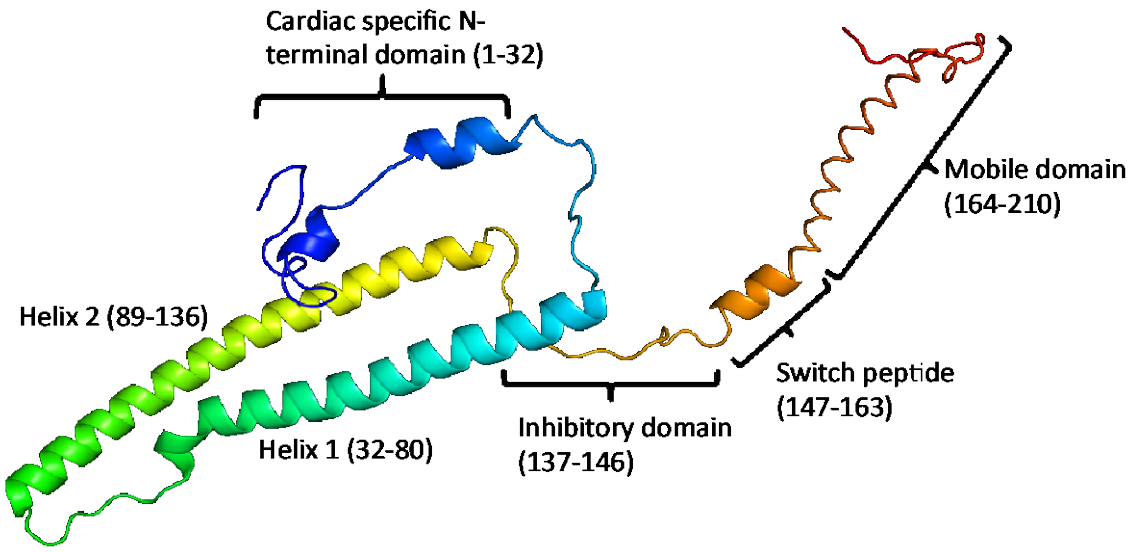

Figure 1-13 Structure and functional domains of human cTnI.

The predicted structure of the full-length cTnI was built from the crystal structure of cTnI (PDB: 1J1E) with the missing regions constructed by the secondary structure prediction program PSIPRED (Bryson, 2005; Jones, 1999; Bryson, 2005) and from homology with chicken fast skeletal Tn (Manning et al., 2011). The original TnI structure included in the core domain of the cTn complexes contains only Helices 1 and 2 and the switch peptide region. The structure is coloured spectrally from the N-terminus (blue) to the C-terminus (red). The figure was generated using PyMol (Delano, 2015).

There are three main TnI paralogs found in humans, which are encoded by *TNNI* for slow skeletal muscle TnI (ssTnI), *TNNI2* for fast skeletal muscle TnI (fsTnI), and *TNNI3* for cardiac TnI (cTnI), respectively (Sheng and Jin, 2016). The paralogs are expressed in a developmentally regulated manner specific to different muscle types. During the embryonic stage of heart development, *TNNI1* (ssTnI) is the predominant

paralog of TnI expressed in the human fetal/neonatal heart until it is completely replaced by cTnI nine months (or possibly longer) after birth, but congenital malformations may delay the paralog switching up to two years after birth (Hunkeler et al., 1991; Sasse et al., 1993). The TnI paralog switch has been shown to have significant impact on fine-tuning myofilament Ca^{2+} binding properties and pH tolerance as an adaption to changes in the cellular environment and contractile characteristics (Westfall et al., 1997). More specifically, this process contributes to the major differences between neonate and adult contractile function, in which the cardiac contractile apparatus transitions from being highly sensitive to Ca^{2+} with slower kinetics of activation and relaxation in neonatal myocytes, to being less sensitive to Ca^{2+} with higher rates of contractile properties in the adult myocardium (Gomes et al., 2004; Marston and Redwood, 2003; Nakanishi and Jarmakani, 1984; Racca et al., 2016; Schiaffino et al., 1993). Structurally, the major difference between ssTnI and cTnI lies in the N-terminal region-- the first 31 amino acid residues are truncated in ssTnI compared to cTnI (Kranias and Solaro, 1982; Robertson et al., 1982; Solaro et al., 1976) as seen in Figure 1-14. This cardiac-specific N-terminal domain contains two serines at residues 23 and 24, which are essential for protein kinase A (PKA) phosphorylation during β-adrenergic stimulation (Kranias and Solaro, 1982; Robertson et al., 1982; Solaro et al., 1976).

```
cTnI   MADGSSDAAREPRPAPAPIRRRSSNYRAYATEPHAKKKSKISASRKLQLKTLLLQIAKQE   60
ssTnI ------------------------------MPEVERKPKITASRKLLLKSLMLAKAKEC   29
                                     *.::* **:***** **:*:*  **:

cTnI   LEREAEERRGEKGRALSTRCQPLELAGLGFAELQDLCRQLHARVDKVDEERYDIEAKVTK   120
ssTnI WEQEHEEREAEKVRYLAERIPTLQTRGLSLSALQDLCRELHAKVEVVDEERYDIEAKCLH   89
       *:* ***..** * *: *   *:  **.:: ******:***:*: **********  :

cTnI   NITEIADLTQKIFDLRGKFKRPTLRRVRISADAMMQALLGARAKESLDLRAHLKQVKKED   180
ssTnI NTREIKDLKLKVMDLRGKFKRPPLRRVRVSADAMLRALLGSKHKVSMDLRANLKSVKKED   149
      *  ** **. *::********* *****:*****::****:: * *:****:**.*****

cTnI   TEKEN-REVGDWRKNIDALSGMEGRKKKFES-------   210
ssTnI TEKERPVEVGDWRKNVEAMSGMEGRKKMFDAAKSPTSQ   187
      ****.  ********::*:******** *::
```

Figure 1-14 Sequence alignment between human cTnI and ssTnI.

The sequence identity between human cTnI (Uniprot ID: P19429) and human ssTnI (Uniprot ID: P19237) is ~63% (UniProt Consortium, 2018). The sequence alignment file was generated on Clustal Omega (Sievers et al., 2011). Ser23 and ser24 are critical PKA targets during β-adrenergic stimulation and are highlighted in red.

Under acute exercise or stress conditions, the healthy heart is able to increase its cardiac output nearly five-fold within seconds (Solaro et al., 2008). This “flight or fight” response is mediated, at least in part, by the release of norepinephrine and epinephrine, which act as substrates that initiate cyclic AMP (cAMP) production via adenylyl cyclases (AC). Subsequently, cAMP activates protein kinase A (PKA), which then phosphorylates Ser 23 and Ser 24 in cTnI to facilitate the Ca^{2+} dissociation from the N-terminal domain of TnC (Solaro et al., 2008). cTnI activity is not only regulated by PKA phosphorylation but also by protein phosphatases types 1 (PP1) and 2A (PP2A) that are responsible for dephosphorylation, although the mechanism of these phosphatases remains much less clear than kinases (Jideama et al., 2006). The coordinated nature between the kinases and phosphatases dictate the degree of cTnI phosphorylation, which in turn regulates the myofilament Ca^{2+} sensitivity of force generation, cross-bridge cycling rate, and the rate of relaxation (Rao et al., 2014; Solaro et al., 2008). Any disturbance of the balance between kinases and phosphatases activities can impact or attenuate the functional effects of PKA-phosphorylated TnI, compromising the relaxation properties of the cardiac muscle as seen in many end-stage failing hearts (Kooij et al., 2010).

1.4.5. Cardiac troponin T (cTnT)

cTnT is the tropomyosin-binding protein that anchors the entire Tn complex to the rest of the thin filaments at a periodicity of 38.5 nm. It is considered the “touchdown” protein that dynamically interacts with components in the thin filaments to conduct the Ca^{2+} regulation of cardiomyocyte excitation-contraction cycles (Katrukha, 2013). In particular, its interaction with Tm directly modulates the average position of Tm in the three-state model of muscle activation. Like the other two Tn subunits, it is entirely composed of α-helices, making it extremely dynamic and flexible (Katrukha, 2013).

There are four human cardiac TnT isoforms which are splice variants of the *TNNT2* gene: TnT1, TnT2, TnT3, and TnT4 (Gomes et al., 2002) (Figure 1-15). The four isoforms have a molecular weight of 30-33 kDa and range from 223 to 305 residues due to the variable length of the N-terminal region. In the fetal heart, TnT1, TnT2, and TnT4 are expressed, with TnT1 being the predominant form (Gomes et al., 2002). As the heart goes through perinatal development, the expression level of TnT1 decreases and TnT3 becomes the predominant isoform in the adult cardiac muscle. TnT4 is re-expressed in some failing adult hearts. TnT1, the isoform that expresses predominantly in fetal hearts,

has both exons 4 and 5, whereas TnT3 has exon 5 removed. Only the N-terminal region is highly variable due to alternative splicing, while the amino acid sequences of the middle and C-terminal domains are highly conserved (Gomes et al., 2002).

```
TnT1      MSDIEEVVEEYEEEEQEEAAVEEEEDWREDEDEQEEAAEEDAEAEAETEETRAEEDEEEE     60
TnT2      MSDIEEVVEEYEEEEQ-----EEEEDWREDEDEQEEAAEEDAEAEAETEETRAEEDEEEE     55
TnT3      MSDIEEVVEEYEEEEQEEAAVEE----------QEEAAEEDAEAEAETEETRAEEDEEEE     50
TnT4      MSDIEEVVEEYEEEEQEE--------------QEEAAEEDAEAEAETEETRAEEDEEEE     45
          ****************                 ***************************

TnT1      EAKEAEDGPMEESKPKPRSFMPNLVPPKIPDGERVDFDDIHRKRMEKDLNELQALIEAHF     120
TnT2      EAKEAEDGPMEESKPKPRSFMPNLVPPKIPDGERVDFDDIHRKRMEKDLNELQALIEAHF     115
TnT3      EAKEAEDGPMEESKPKPRSFMPNLVPPKIPDGERVDFDDIHRKRMEKDLNELQALIEAHF     110
TnT4      EAKEAEDGPMEESKPKPRSFMPNLVPPKIPDGERVDFDDIHRKRMEKDLNELQALIEAHF     105
          ************************************************************

TnT1      ENRKKEEEELVSLKDRIERRRAERAEQQRIRNEREKERQNRLAEERARREEEENRRKAED     180
TnT2      ENRKKEEEELVSLKDRIERRRAERAEQQRIRNEREKERQNRLAEERARREEEENRRKAED     175
TnT3      ENRKKEEEELVSLKDRIERRRAERAEQQRIRNEREKERQNRLAEERARREEEENRRKAED     170
TnT4      ENRKKEEEELVSLKDRIERRRAERAEQQRIRNEREKERQNRLAEERARREEEENRRKAED     165
          ************************************************************

TnT1      EARKKKALSNMMHFGGYIQKQAQTERKSGKRQTEREKKKKILAERRKVLAIDHLNEDQLR     240
TnT2      EARKKKALSNMMHFGGYIQKQAQTERKSGKRQTEREKKKKILAERRKVLAIDHLNEDQLR     235
TnT3      EARKKKALSNMMHFGGYIQKQAQTERKSGKRQTEREKKKKILAERRKVLAIDHLNEDQLR     230
TnT4      EARKKKALSNMMHFGGYIQKQAQTERKSGKRQTEREKKKKILAERRKVLAIDHLNEDQLR     225
          ************************************************************

TnT1      EKAKELWQSIYNLEAEKFDLQEKFKQQKYEINVLRNRINDNQKVSKTRGKAKVTGRWK       298
TnT2      EKAKELWQSIYNLEAEKFDLQEKFKQQKYEINVLRNRINDNQKVSKTRGKAKVTGRWK       293
TnT3      EKAKELWQSIYNLEAEKFDLQEKFKQQKYEINVLRNRINDNQKVSKTRGKAKVTGRWK       288
TnT4      EKAKELWQSIYNLEAEKFDLQEKFKQQKYEINVLRNRINDNQKVSKTRGKAKVTGRWK       283
          ************************************************************
```

Figure 1-15 Sequence alignment for TnT isoforms from the human gene *TNNT2*.

The human *TNNT2* gene produces four cTnT isoforms via alternative splicing of exons 4 and 5. TnT1 (also known as isoform 1: Uniprot number P45379-1) has 298 residues with a molecular weight of 35,924 Da. TnT1 is the predominant isoform that has all exons expressed in fetal cardiac muscle. TnT2 (known as isoform 8; Uniprot number: 45379-8) has 293 residues (residue 18-22 missing from TNT1) with a molecular weight of 35,424 Da. TnT3 (known as isoform 6; Uniprot number P45379-6) has 288 residues (residue 23-32 residues missing from TnT1) with a molecular weight of 34,590 Da. TnT3 is the predominant isoform expressed in the adult cardiac muscle. TnT4 (known as isoform 7; Uniprot number: P45379-7) has 283 residues (residue 18-23 missing from TnT1) with a molecular weight of 34,091 Da (UniProt Consortium, 2018).

Early limited chymotrypsin digestion experiments generated two fragments of TnT: T1 and T2 (Ohtsuki, 1979). T1 (residues 1-97) contains the hypervariable region

and a highly conserved central region which serves to anchor the N-tail of cTnT to the rest of the thin filament through interactions with Tm. The T2 (residues 98-288) region interacts with the rest of the cTn complex as well as with actin and Tm (Ohtsuki, 1979).

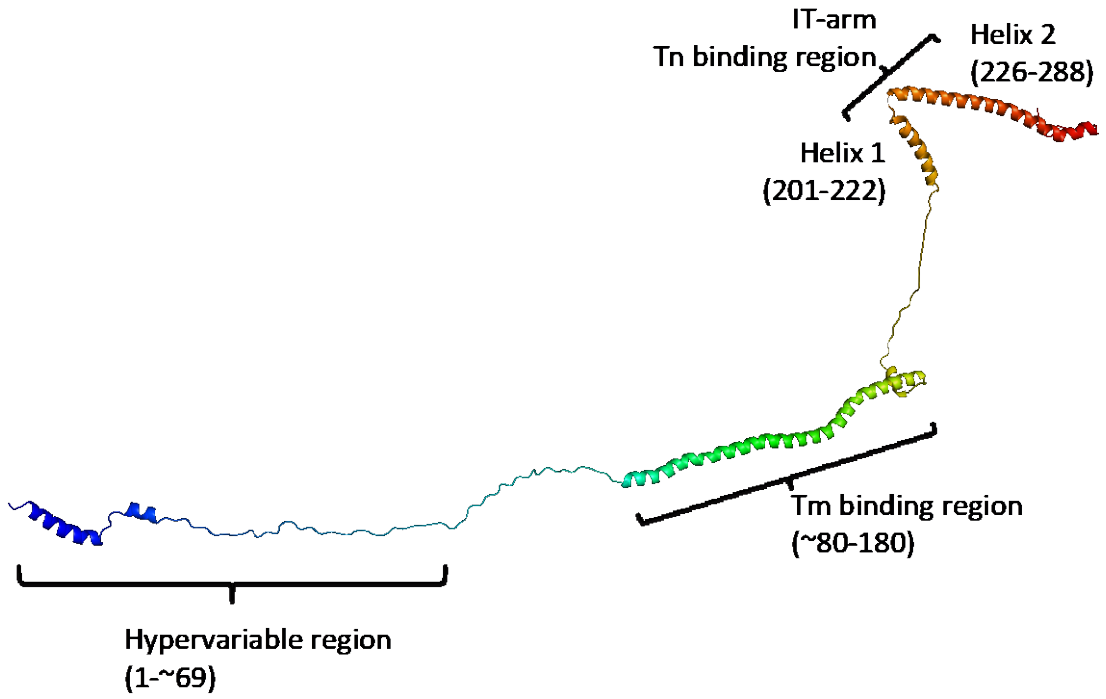

Figure 1-16 Modeled structure of human cTnT.

Depicted is the predicted full-length structure of cTnT. Like the full-length structure of cTnI in Figure 1-13, this structure was constructed from a crystal structure which contains only helices 1 and 2 with the missing regions built from PSIPRED and a homology model of the chicken fast skeletal Tn complex (Manning et al., 2011). cTnT is highly flexible and dynamic. A large portion of TnT is unwound, without binding to Tm and/or actin. This figure was generated using PyMol (Delano, 2015).

Only the C-terminal portion of TnT, which spans residues 199-272, has been solved in the high-resolution crystallographic structure of the core domain of the Tn complex (PDB: 4Y99) shown in Figure 1-16 (Takeda, 2016). However, more than 90% of the known diseases causing mutations in cTnT occur in the unresolved regions (Tardiff, 2011). These regions present a challenge for structural determination by X-ray crystallography due to their high flexibility and extended nature (Takeda et al., 2003). However, the N-terminal tail region is of high importance since it is directly responsible for positioning Tm along the actin groove and stabilizes the head-to-tail arrangement of Tm. Although some cTnT mutations occur at a great physical distance from the

regulatory cTn complex, any changes in the local protein-protein interactions may often be propagated and transduced to the rest of the thin filaments, causing complex cardiomyopathies (Tardiff, 2011).

1.5. Familial hypertrophic cardiomyopathy

Hypertrophic cardiomyopathy (HCM) is one of the most prevalent cardiomyopathies, affecting one in every 500 individuals (Ashrafian and Watkins, 2007). A major subset of HCM is familial hypertrophic cardiomyopathy (FHC). It is the most commonly occurring autosomal dominant cardiomyopathy and is the leading cause of sudden cardiac death (SCD) in young athletes and individuals under the age of 35 (Maron et al., 1996). In general, people with HCM have an asymmetrically thickened left ventricular and interventricular septal walls, which decreases the cavity size of the ventricle and can cause obstruction to blood flow (Ashrafian and Watkins, 2007). It is a disease with progressive symptoms, ranging from the clinically less symptomatic, to development of some advanced thickening of the heart muscle, to the most serious consequence, SCD (Prinz et al., 2011). Most often, young athletes with HCM suddenly collapse and die in the field during or shortly after performing some vigorous physical activity. It is a devastating disease since it affects a younger population and most FHC patients who die from SCD do not manifest any obvious symptoms (Maron et al., 1996).

Since the discovery of the first FHC-causing mutation in the gene that encodes for the β-myosin heavy chain (*MYH7*) (Geisterfer-Lowrance et al., 1990; Jarcho et al., 1989), more than 1,000 individual mutations in genes encoding 20 mostly sarcomeric proteins have been found to be linked with FHC, including α-tropomyosin (*TPM1*), myosin binding protein C (*MYBPC3*/MYBPC), ventricular myosin light chains 1 and 2 (MLC-1 and -2), cardiac troponin T (cTnT), cardiac troponin I (cTnI), cardiac troponin C (cTnC), actin and titin (Fung et al., 1999; Willott et al., 2010). Despite the discovery of many FHC-associated sarcomeric protein mutations, the molecular pathway leading to various complex cardiomyopathies within the descriptor of FHC remains unclear. One hypothesis is that FHC leads to decreased cardiac contractile function, resulting in compensatory hypertrophy (Lankford et al., 1995; Sata and Ikebe, 1996). This was challenged by several clinical and laboratory observations in which some proteins exhibit have gain of function (Lowey, 2002), and many FHC-associated mutant proteins have increased Ca^{2+} sensitivity of force generation (Dweck et al., 2008). Therefore, the

decreased contractile function cannot be an exclusive mechanism that causes hypertrophy in FHC. In addition, many patients develop the hypertrophy after puberty, and this contradicts the notion that the hypertrophy is a “compensatory” response since the inherited sarcomeric protein mutations are present at birth (Ashrafian et al., 2003). Other hypotheses are associated with inefficient ATP utilization of the myocytes leading to localized and compromised energetics, resulting in the delayed onset and asymmetrical hypertrophy in FHC (Ashrafian et al., 2003).

Another well-documented hypothesis contributing to FHC mechanism is that sarcomeric protein mutations cause an increase in myofilament Ca^{2+} sensitivity, meaning that the same amount of Ca^{2+} would elicit greater force of contraction (Dweck et al., 2008). This could turn on the gene expression program associated with hypertrophy via the Ca^{2+}-regulated nuclear factor of activated T-cells (NFAT)/calcineurin pathway (Hogan et al., 2003). Upon stimulation, Ca^{2+} will bind to calmodulin, and the Ca^{2+}-bound calmodulin will in turn activate a serine phosphatase, namely calcineurin. The activated calcineurin then dephosphorylates NFAT, allowing the dephosphorylated NFAT to be translocated into the nucleus and activate the transcription pathway associated with hypertrophy (Hogan et al., 2003).

However, some FHC-associated sarcomeric mutations do not necessarily cause any obvious structural remodelling but are, however, associated with a high incidence of sudden cardiac death, such as some well-documented mutations in *TNNT2* gene. *TNNT2* variants are responsible for approximately 7% of all FHC, making them the third most common cause of FHC (Knollmann et al., 2001; Knollmann et al., 2003). Unlike the general anatomical abnormalities typically found in FHC patients, hearts from patients harbouring cTnT variants show significantly less ventricular hypertrophy compared to other FHC-associated mutations such as those in the β-MHC gene (Watkins et al., 1995). This low degree of penetrance of the classical clinical phenotype associated with the cTnT variants makes them difficult to detect by echocardiography (Knollmann et al., 2001). This suggests that additional mechanisms, such as sarcomeric Ca^{2+} mishandling that disturbs the delicately balanced Ca^{2+} homeostasis in the myocytes, might present significant contributions to the arrhythmia susceptibility in the FHC-causing cTnT mutations (Baudenbacher et al., 2008; Schober et al., 2012; Wang et al., 2018). In addition, identical mutation occurring within the same family can result in HCM, dilated cardiomyopathy (DCM), restrictive cardiomyopathy (RCM), or even transition from one

phenotype to another during the disease progression (Menon et al., 2008). Therefore, assigning a clinical phenotype can be very difficult and complex. Regardless of the complexity and challenge of linking a particular mutation to a specific clinical diagnosis, change in myofilament Ca^{2+} sensitivity as a result of a sarcomeric mutation is often used as an indicator of cardiac muscle function (Chung et al., 2016; Ren et al., 2018).

Currently the treatment for HCM relies on symptom relief and complication management since no compounds exist that are known to treat or prevent sarcomeric cardiomyopathies (Tardiff et al., 2015). β-adrenergic agonist blockers, Ca^{2+} channel blockers and various other drugs have been used to improve the symptoms but do not prevent the disease progression (Tardiff et al., 2015). The focus of HCM treatment needs to gradually shift from simply alleviating the patients' symptoms to a more complex and mechanistic approach, with the goal to design targeted therapeutics to intervene in the natural course of the disease progression before end-stage irreversible remodelling occurs (Tardiff et al., 2015). It is crucial to understand the cellular and molecular mechanisms that contribute to HCM, in particular, how changes in myofilament Ca^{2+} sensitivity relate to the disease. Many factors collaboratively contribute to the changes of myofilament sensitivity Ca^{2+}, and it is difficult to fully explain the complex integration of all the components regulating thin filaments. The following sections will discuss the major mechanisms that contribute to sarcomeric regulation and how sarcomeric mutation can modulate these mechanisms at the molecular level.

1.5.1. β-adrenergic activation

Under stress or exercise conditions, the adrenal gland releases epinephrine and norepinephrine to activate the cascade events of the β-adrenergic pathway in cardiomyocytes. Activated PKA (protein kinase A), as the main driving force of this signalling pathway, phosphorylates several key regulatory proteins in the cardiomyocytes. (Solaro and Kobayashi, 2011; Solaro et al., 1976; Solaro et al., 2008; Solaro and van der Velden, 2010). Ser23/Ser24 phosphorylation of cTnI is one of the most well understood post-translational modifications in cardiac thin filaments. Not only are Ser 23/Ser24 phosphorylated by PKA, but they also can be activated by a series of other kinases, including PKG, PKC beta, PKC gamma, and PKD1 (Solaro et al., 2008). These two serines are located in the cardiac specific N-terminal region of cTnI, a highly solvent accessible and intrinsically disordered region (Hwang et al., 2014). Because of

its highly dynamic and flexible nature, the structure of this region has not yet been solved by any structural biology techniques (Takeda et al., 2003). Recently, multinuclear multi-dimensional solution NMR spectroscopy has been used to map out the important protein-protein interactions between the cTnI peptide from residues 1-73 with full-length cTnC (Hwang et al., 2014). cTnI residues 19-37 are now understood to be electrically "tethered" to the negatively charged surface of cNTnC, thereby directly fixing the orientation of cTnC relative to the rest of the Tn complex (Siddiqui et al., 2016). Under non-phosphorylated conditions, cTnC is well positioned to bind to the switch peptide of TnI148-158 (TnI_{sw}) (Siddiqui et al., 2016). When the hydrophobic binding pocket of TnC opens upon Ca^{2+} binding, this pocket is available for TnI_{sw} to bind (Siddiqui et al., 2016), increasing the effective concentration of the TnI_{sw} presented to cTnC, and driving cTnC toward its Ca^{2+} activated state to increase the overall myofilament Ca^{2+} sensitivity. Upon phosphorylation of Ser23/Ser24 of cTnI, this domain positioning of cNTnC is disrupted, facilitating the release of Ca^{2+} from cNTnC and subsequently the switch peptide from the hydrophobic pocket, thereby decreasing the myofilament sensitivity to Ca^{2+} (Siddiqui et al., 2016).

Many of the HCM-associated Tn mutations disrupt this process, including Li et al.'s L29Q cTnC mutation, the first HCM-associated mutation discovered in human cTnC (Li et al., 2013a). Many other Tn mutations are also located remotely from the TnI-TnC interaction site but still have long-range effects that propagate along the thin filaments and result in modulating the functional effects of the TnI phosphorylation (Cheng et al., 2015b; Li et al., 2013a; Lu et al., 2013; Memo et al., 2013; Messer et al., 2016). Regardless of the level of complexity in the biochemical systems, HCM-associated sarcomeric mutations often abolish the Ca^{2+} desensitization induced by TnI phosphorylation, causing the myofilaments to have higher Ca^{2+} sensitivity and impaired relaxation. As demonstrated in many *in vitro* kinetic measurements, the large increase of Ca^{2+} dissociation (k_{off}) is no longer seen in constructs containing the mutations, resulting in Ca^{2+} binding to TnC for a longer period of time (Albury et al., 2012; Dong et al., 2008; Li et al., 2013a).

1.5.2. Myofilament length-dependent activation

More than one century ago, Otto Frank and Ernst Starling determined the relationship between the extent of ventricular filling and the pump function of the heart,

later described as the Frank-Starling law of the heart (Allen and Kurihara, 1982; Kentish et al., 1986; Parmley and Chuck, 1973). More specifically, at the whole heart level, the stroke volume of the heart increases in response to an increase in the ventricular volume at the end of diastolic phase. With an increase in the end diastolic volume (EDV), the blood stretches the cardiac muscle, leading to an increase in force production. Length-dependent activation (LDA) is an important physiological process that underlies the main cellular mechanism of the Frank-Starling relationship. It describes that the responsiveness of cardiac myofilaments to activating calcium Ca^{2+} increases when the sarcomeric length (SL) is increased.

Several theories and factors have been proposed over the past few decades to describe the underlying mechanism of LDA (de Tombe et al., 2010). The earlier "inter-filament spacing theory" proposes that the impact of the sarcomere length on myofilament Ca^{2+} sensitivity is due to changes in the spacing between the thick and thin filaments. Upon stretching the sarcomeric length (SL), there is a decrease of the lattice spacing between the thick and thin filament, allowing more overlap between them and hence producing more force-generating cross-bridges. This was further supported by the utilization of a strong-binding non-tension-generating derivative of myosin S1 (NEM-S1) to increase the formation of strongly bound cross-bridge at short SL, producing a Ca^{2+} sensitivity that was similar to that of long SL (Fitzsimons and Moss, 1998). They suggested the formation of strong-cross bridges due to the decrease of myofilament spacing is the key that contributes to molecular mechanism of LDA (Fitzsimons and Moss, 1998). However, this theory was later challenged by several experiments, most noticeably by the use of high molecular weight molecules (e.g. dextran), which cannot enter the myofilament lattice but was able to exert osmotic compression. Although dextran compression resulted in a filament spacing that was matched to that attained at longer SL, myofilament Ca^{2+} sensitivity was not changed by the osmotic compression. This suggests that inter-filament spacing may not be the primary mechanism of LDA and remains controversial, and likely other mechanisms are involved (Konhilas et al., 2002b).

Later studies done by de Tombe's group show that myosin head orientation is a major cellular mechanism of LDA that contributes to the Frank-Starling relationship (Farman et al., 2011). They utilized the small-angle X-ray diffraction on intact, electrically-stimulated myocardium to correlate the generating force as a function of SL. From the reflection and the intensity of the X-ray diffraction pattern, the proximity of

myosin heads to thin filaments as well as the orientation of the myosin head with respect to the axis of the filament were assessed (Farman et al., 2011). They were able to observe that upon the stretch of SL, there was an increase of orientation ordering of myosin heads perpendicular to the filaments. This potentially minimizes the volume that myosin heads need to search to obtain an optimal stereo-specific binding site on actin, thereby increasing the probability of productive myosin-actin interactions (Farman et al., 2011).

Another factor that contributes to the molecular basis of LDA is the cooperative interactions between components of myofilaments. Since myofilaments are highly cooperative and function as a large macromolecular machine, any changes in one regulatory unit can affect the neighbouring unit (Dobesh et al., 2002; Kobayashi et al., 2008; Razumova et al., 2000). Starting from Ca^{2+} binding to TnC and inducing the conformational change of the Tn complex, then leading to the filaments forming weakly-bound cross-bridges and transitioning to strongly-bound cross-bridges, this process can recruit the neighbouring unit and propagate along the thin filaments until full myofilament activation occurs. Modulation of any step in the process can have an impact on LDA, abolishing the highly balanced mechanism among the regulatory units of the myofilaments (Razumova et al., 2000). Many of the missense HCM-associated mutations abolish the myofilament LDA, resulting in higher Ca^{2+} sensitivity regardless of sarcomeric length (Li et al., 2013a). A study done by Sequeira et. al even showed that the direction and the magnitude of the Ca^{2+} sensitivity change is dependent on the affected gene, but all the HCM cardiomyocytes isolated from human heart uniformly blunted the response to LDA due to altered Ca^{2+} handling and potentially serve a substrate for arrhythmia (Sequeira et al., 2013). In addition, some Tn mutations may seem benign in *in vitro* studies where LDA could not be factored in due to experimental limitation, but they distinctively exerted their effects on modulating Ca^{2+} sensitivity when the mutation was incorporated into constructs where sarcomeric length was manipulated (Farman et al., 2007; Li et al., 2013a).

Several protein molecules also serve as important regulator for myofilament LDA (Konhilas et al., 2003). Troponin I, the inhibitory subunit of Tn complexes, plays a pivotal role in regulating the signal transduction process within the sarcomere. It is well documented that PKA-dependent phosphorylation of cTnI enhances LDA in cardiomyocytes (Konhilas et al., 2003; Li et al., 2013a). More specifically, when cTnI is

phosphorylated, the magnitude of the myofilament Ca^{2+} sensitivity change is larger upon the stretch of the myofilament compared to that of the wild type (WT) (Konhilas et al., 2003). This phenomenon is clearly observed in cardiac muscle but completely blunted in slow skeletal muscle (Konhilas et al., 2003). In addition to the PKA-phosphorylated Ser23/Ser24 in the cardiac specific domain of TnI, a threonine at position 144 within the cardiac TnI is a PKC target and of particular importance in relation to LDA (de Tombe et al., 2010). At the equivalent position, this residue is replaced with a Proline residue in the slow skeletal TnI (de Tombe et al., 2010). It has been shown that replacement of cTnI with ssTnI in transgenic mice completely abolishes LDA, and that the mutation from Pro to Thr was able to restore myofilament LDA (de Tombe et al., 2010). Evidently, cardiac TnI phosphorylation plays a major role in modulating myofilament LDA, and many HCM-associated mutations abolish this functional effect of TnI (Li et al., 2013a).

Other myofilament proteins, such as titin and cardiac myosin binding protein C (cMyBP-C), also contribute to the elasticity of muscle fiber and affect the molecular mechanism of LDA (Ait-Mou et al., 2016; Li et al., 2019; Methawasin et al., 2014). Titin, the molecular giant in which a single molecule spans more than 1 μm in length, (i.e. half the sarcomere from M line to Z line), acts as a molecular spring in the I-band region (Figure 1-1) (Herzog, 2018). Its main function is to develop passive tension during relaxation as the sarcomeres are stretched (Granzier and Labeit, 2006). While there are multiple titin isoforms, isoforms that include the motif N2B, are unique to the myocardium (Granzier and Labeit, 2006). N2BA, which includes both the N2B and N2A motifs, is a more compliant form than N2B, and it is often expressed at a higher level with various cardiac diseases including dilated cardiomyopathy (Nagueh et al., 2004). A recent study using in situ fluorescence resonance energy transfer (FRET) demonstrates that the compliance of titin can modulate sarcomeric length-dependent activation through regulating the interactions between the thin and thick filaments at different cross-bridges states under the ATP- or ADP- bound conditions (Li et al., 2019). Specifically, in WT mice myocardium, the increase of sarcomeric length also increased the tension developed via Ca^{2+}-bound Tn complexes and strongly bound cross-bridges; this effect was evidently lost in mice that expressed higher level of the more compliant N2BA titin isoform at different SL (Li et al., 2019). Any modulation of titin has shown to significantly reduce myofilament LDA and the passive elasticity of the cardiac muscle, resulting in

numerous cardiomyopathies (LeWinter and Granzier, 2010; Li et al., 2019; Nagueh et al., 2004).

cMyBP-C also plays a significant role in modulating sarcomeric function including LDA through its direct interactions with both thin and thick filaments. Though its mechanism of action is less well understood, it has been shown recently that the N-terminal domain of cMyBP-C may bind to F-actin whereas the C-terminal domain binds to myosin thick filaments by cryo-EM, suggesting its important structural role of associating thin and thick filaments together (Harris et al., 2016). In addition, Kampourakis et al. used fluorescence probe on TnC to monitor the thin filament structural changes and showed that the N-terminal region also binds to thick filaments and stabilize thin and thick filaments during different activation states of the thin filaments (Kampourakis et al., 2014). Although the structure and function of cMyBP-C remains controversial, it is evident that cMyBP-C plays an important role of regulating the cooperative activation of the myofilaments. During β-adrenergic stimulation, cMyBP-C is also one of the PKA phosphorylation targets in ventricular myocytes, and phosphorylation of cMyBP-C has been shown to increase the proximity of actin and myosin heads and affect the rates of cross-bridge cycling during Ca^{2+} activation in normal myocardium (Colson et al., 2008; Coulton and Stelzer, 2012; Mamidi et al., 2016). In a myocardium with decreased cMyBP-C phosphorylation, it was shown that the kinetics of cross bridge activation and relaxation was severely blunted at various SL, suggesting the sarcomeric length dependence is also highly dependent on the functional effects of cMyBP-C phosphorylation (Mamidi et al., 2016).

In summary, myofilament LDA is a fundamental cardiac property that regulates the ability of the heart to increase the strength and rate of contraction (Konhilas et al., 2002a) as a function of sarcomere length. At the whole-heart level, it increases ventricular pressure in response to increased ventricular filling. At the cardiomyocyte level, it is an enhancement in force generation upon increase of the sarcomeric length. At the myofilament level, it increases the myofilament responsiveness to Ca^{2+}, the rate of cross-bridge cycling, and the recruitment of neighbouring units of thin filaments (Farman et al., 2010). Any changes in this complex interplay due to sarcomeric mutation can result in changes in Ca^{2+} buffering in the cardiomyocytes, blunted the LDA response and provide a substrate for arrhythmia (Sequeira et al., 2013).

1.5.3. Implications in Arrhythmia

Cardiac arrhythmias refer to conditions in which the electrical activity of the heart is disturbed in various ways that cause the heart to beat too fast, too slow, or in an irregular manner. Many arrhythmias are relatively benign, and patients may not have clinically overt symptoms, but some may have symptoms such as dizziness, shortness of breath, palpitation, and in the most serious cases, sudden cardiac death. Slow heart rhythms are readily treated with pacemakers, but pharmacological treatment is still problematic for rapid heart rhythms (Fu, 2015).

The excitation-contraction coupling in the heart requires the conversion of electrical activation into mechanical force that results in muscle contraction. This process, known as the EC-coupling, requires the coordinated movement of Ca^{2+} ions governed by numerous channels, exchangers, and sarcomeric proteins to maintain a balanced Ca^{2+} homeostasis within the cardiomyocytes. Any disruption in the electrical activity of the heart and cytosolic Ca^{2+} cycling is implicated in the underlying mechanisms of arrhythmogenesis (Bers, 2008).

Normal ventricular activation is dependent on action potential duration (APD), which in turn is reliant on balanced inward and outward currents maintaining by various ion channels. The coordinate opening and closing of these ion channels is crucial in mediating cardiac action potential and maintain a stable heart rhythm. These channels include voltage-gated Ca^{2+} channels (Cav1.2), several types of potassium and sodium channels that embedded in the ventricular plasma membrane, as well as ryanodine receptor (RyR) and sarcoplasmic reticulum Ca^{2+} ATPase (SERCA) that control the Ca^{2+} release and uptake of the SR. Gene mutations in these ion channels may lead to arrhythmia, and these abnormal ion channels activities define a class of cardiac diseases, “ion channelopathies”, which remain the major cause for arrhythmia (Ashcroft, 2006; Behere and Weindling, 2015).

It is well-documented that channelopathies, along with other cardiac structural maladaptation associated with classic HCM phenotypes, including fibrosis, myofibrillar disarray, and hypertrophy, may serve as a “substrate” for predisposing arrhythmia (Landstrom et al., 2017; O'Mahony et al., 2013). These substrates can cause impaired conduction of the electrical activity either within a small region of heart or between atria

and ventricles, a phenomenon known as re-entry (Tse, 2016). In the case of channelopathies, it is categorized as a functional obstacle in which in the absence of a block (anatomical obstacle), differential conduction velocity occurs due to the abnormal function of a particular ion channel (Behere and Weindling, 2015). The resulting arrhythmia include the most common cardiac channelopathy, Long QT syndrome with the occurrence of 1 in 2500 people, short QT syndrome, and catecholaminergic polymorphic ventricular tachycardia (CVPT) among others (Behere and Weindling, 2015). Cardiac channelopathies account for approximately one-third of sudden unexpected death (Behere and Weindling, 2015). On the other hand, HCM-associated mutations are found in 1 in 500 people and are the most common cause of sudden cardiac death (O'Mahony et al., 2013). HCM cardiac maladaptation due to hypertrophy, myofibrillar disarray and fibrosis present themselves as an “anatomical obstacle” that can physically provide a “block” in a small region of a conduction pathway (Huke et al., 2013; O'Mahony et al., 2013). In this case, the normal heart excitation does not self-terminate and re-excited previously excited tissue in an unregulated manner (Landstrom et al., 2017). The occurrence of re-entry involving an anatomical obstacle is highly dependent on the conduction velocity and refractory period of an action potential (Landstrom et al., 2017). Whatever the substrate might be, it should be noted that people with channelopathies or structural abnormalities might carry on their normal life for many years before a “trigger” occurs. A trigger can include, but not limited to, exercise, pharmacological agents, stress-inducing life events, or combinations of these that could induce a higher heart rate (Ziegelstein, 2007). A trigger in addition to the presence of pre-existing substrate could form a “perfect storm” that leads to arrhythmia, and in the most serious cases, result in sudden cardiac death.

In the past decade, a growing set of compelling data has indicated that changes in myofilament Ca^{2+} sensitivity in sarcomeric protein mutations can also be attributed to HCM-associated arrhythmia (Allen and Kurihara, 1982; Baudenbacher et al., 2008; Huke and Knollmann, 2010; Huke et al., 2013; Schober et al., 2012; Schober and Knollmann, 2007). Patients with some sarcomeric protein mutations may not necessarily develop structural remodelling in their heart but cause disturbance to the delicately balanced Ca^{2+} dynamics. Among these, HCM-associated TnT mutations have been shown to have minimal hypertrophy present in the patient’s heart and thus often remained undetected, but sometimes the first sign of symptom could be arrhythmia or even sudden cardiac

death (Knollmann and Potter, 2001). Several TnT mutations are associated with high incident of sudden cardiac death, with 75% of death occurring to patients under the age of 45 (Watkins et al., 1995). Studies performed by Knollmann's group have shown the close link between altered myofilament Ca^{2+} sensitivity due to HCM-associated TnT mutations and the occurrence of arrhythmia (Baudenbacher et al., 2008; Knollmann et al., 2001; Schober et al., 2012).

Baudenbacher et al.'s experiments showed that arrhythmias can be initiated by fast pacing rates in transgenic mice with Ca^{2+} sensitizing TnT mutations, such as I79N and F110I TnT mutations (Baudenbacher, 2008). This corroborates the observation that HCM patients often experience fast heart rates prior to an arrhythmia event. In addition, optical mapping experiments, which measure the speed with which an electrical impulse is transmitted through cardiac tissues, known as the conduction velocity (CV), indicate that there is an increased spatial dispersion of CV during rapid pacing in cardiac tissue harbouring the Ca^{2+} sensitizing mutation. This phenomenon was recapitulated when wild type control tissues were treated with the Ca^{2+} sensitizer EMD 57033, suggesting that the abnormal electrical activity was directly associated with the myofilament Ca^{2+} sensitization rather than any structural abnormalities in the mutant cardiac myocytes (Baudenbacher et al., 2008). They found that repetitive activation pattern form long last rotors, generating a substrate for re-entry loop associated with arrhythmia (Baudenbacher et al., 2008).

Several hypotheses have been proposed to explain the arrhythmic events associated with altered myofilament Ca^{2+} sensitivity. There is a clear relationship between Ca^{2+} handling and the ventricular cardiac membrane potential. Specifically, Ca^{2+} ion movement through the L-type Ca^{2+} channels is the major contributor to maintain the plateau phase of an action potential. When a Ca^{2+} sensitizing mutation is present, this can cause several possibilities that affect the Ca^{2+} handling. First, the peak Ca^{2+} concentration may be reduced due to a decreased off-rate constant of Ca^{2+} from TnC. This could affect the L-type Ca^{2+} channel inactivation that normally occurs as a protective mechanism, enabling more Ca^{2+} to enter through L-type Ca^{2+} channel. As more Ca^{2+} enters through the myocardium, this will increase the overall cytosolic Ca^{2+} level, and consequently, increasing the SR Ca^{2+} load. This in turn could cause a spontaneous Ca^{2+} release from the SR and affect the Ca^{2+} transport through NCX. Second, Ca^{2+} transients are reduced but prolonged due to a reduced Ca^{2+} off-rate

constant from TnC, and this in turn could affect the NCX activity. Since the Ca^{2+} ions are coming off more slowly from TnC, this will potentially decrease NCX activity, shortens the AP duration and causes AP “triangulation”. As a result, this could trigger an un-stimulated (ectopic) beat followed by a normal, electrically-stimulated beat, resulting in either early after-depolarization (EAD) or delayed after-depolarization (DAD). Whether EAD or DAD happens depends on the timing of when the ectopic beat occurs relative to the normal beat. Third, the prolonged Ca^{2+} transients are more likely to develop Ca^{2+} transient alternans under fast heart rates conditions. Alternans are characterized when the consecutive membrane voltage (Vm) and Ca^{2+} transients are periodically out of phase, also serving as a substrate for arrhythmia to occur. Although the exact mechanisms are complex and remain unclear, these speculations suggest a strong link of Ca^{2+} mishandling and arrhythmogensis (Huke and Knollmann, 2010; Huke et al., 2013).

1.6. Research hypothesis and objectives

A major challenge to characterize various cardiomyopathies is to link the biophysical characterizations of a particular sarcomeric mutation to the diverse phenotypes presented in patients. It is well-documented that linking a genotype to its phenotype can be difficult, and often the first manifestation of the cardiomyopathy can be quite severe with some Tn mutations. Investigating the structure and function of the thin filaments can significantly advance our understanding of the complex clinical problems of inherited cardiomyopathy. Based on the literature, most functional studies of various cardiomyopathies utilized murine including transgenic mice, which have provided valuable data in the characterization of the cardiomyopathies but one should be cautious when interpreting the data due to the fundamental differences between human and rodent cardiomyocytes. Hence it is important to study the behaviours of the mutations in more human-related models at the biochemical and whole-cell level. In addition, to date there is no structural information available for the entire human cardiac thin filaments. Although there are separate structure available for the core domain of the Tn complex and the filament structure of actin and Tm, obtaining the entire structure of the cardiac thin filaments is crucial since it functions as a highly allosteric multi-molecular complex. We hypothesize that any non-conserved amino acid substitution occurring in the crucial region of Tn complexes will have an impact on the structure and the Ca^{2+} binding

properties of the thin filaments. This could lead to the arrhythmias observed in HCM or other cardiomyopathy diseases at the whole heart level, potentially resulting in sudden cardiac death in the most serious cases. Having a more complete understanding of the structure and function of the thin filaments will allow us to risk-stratify a particular sarcomeric mutation and better link the genotype-phenotype in HCM.

To test this hypothesis, several experimental techniques were carried out. First, functional studies on the Ca^{2+} binding properties of the Tn complexes and reconstituted thin filaments were performed using the steady-state and the stopped-flow fluorometry to determine the Ca^{2+} sensitivity and Ca^{2+} off rate constant, respectively. Second, the structural studies on the reconstituted thin filaments were performed using the negative-stain electron microscopy and cryo-electron microscopy. Specifically, we chose several cardiomyopathy-related Tn mutations with the following aims to investigate the changes in the Ca^{2+} binding properties of three adult cTnT mutations (I79N, F110I, and R278C) and a novel mutation of fetal/neonatal ssTnI (R37C), at the molecular level in systems of increasing complexity. The primary goals of this thesis were to:

1. Establish the expression and purification protocol for Tn complex and reconstituted thin filaments system utilizing rabbit skeletal actin, human recombinant tropomyosin, human recombinant Tn subunits for data collection on the steady-state and the stopped-flow experiments (Chapter 2).

2. Investigate the effects of the three adult cTnT mutations (I79N, F110I, and R278C) on the Ca^{2+} binding properties of the Tn complex and reconstituted thin filaments (RTF). In addition, investigate their modulation on the functional effects of the phosphomimetic cTnI (Chapter 3).

3. Investigate the changes in Ca^{2+} binding properties of the fetal R37C ssTnI and the adult I79N cTnT mutations and their corresponding adult R68C cTnI and fetal I89N cTnT mutations, respectively, to understand the fetal/adult environmental impacts on the mutant phenotypes (Chapter 4).

4. Investigate the overall structure of the entire reconstituted cardiac thin filaments (Chapter 5).

I first established expression and purification protocols for each of the thin filament components, including various recombinant human Tn subunits, recombinant human Tm and rabbit skeletal actin, and generated a series of Tn complexes and RTF (Table 2-1, Chapter 2). I then characterized the Ca^{2+} binding properties of various Tn and RTF constructs using steady-state and stopped-flow fluorescence techniques. I also carried out preliminary structural studies on the reconstituted thin filaments using negative stain EM and cryo-EM.

Chapter 2.

Materials and Methods

This chapter describes the general experimental approach and common procedures used throughout the entire thesis for the functional Ca^{2+} binding studies. More detailed materials and methods specific for each experiment are provided in each subsequent chapter.

2.1. Overview of Experimental Approaches

As mentioned previously, the main goal of my thesis was to investigate the changes in the Ca^{2+} binding properties for various troponin (Tn) complexes and reconstituted human cardiac thin filaments (RTF) constructs with different HCM-associated TnT mutations, a novel neonatal TnI mutation as well as their response to acidotic conditions for adult and fetal constructs (Figure 2-1). The initial stage of the thesis project was to focus on establishing optimized methods for protein expression and purification for each protein component that is listed in Table 2-1. After I established purification protocols specific to each protein component, I generated various Tn complexes and RTF constructs that were specific to the experimental conditions described in each chapter. Each Tn complex and RTF were subjected to two experiments for the investigation of Ca^{2+} binding properties. First, steady-state fluorescence experiments allowed the determination of Ca^{2+} sensitivity (represented by K_d) and the cooperativity of each construct (represented by Hill coefficient, η). Second, the stopped-flow experiments allowed the observation of the fast kinetics reactions that determined the Ca^{2+} dissociation rate (denoted as k_{off}). I then carried out the data analysis and investigated the significance of the altered Ca^{2+} binding properties due to a specific mutation or change in the environment. These data have given us invaluable insight on how these mutations change the Ca^{2+} binding properties at the biochemical level of Tn complexes and RTF and help us ascertain the functional differences of adult and neonatal constructs in response to different conditions in the presence of a particular cardiomyopathy-related mutation. More importantly, some of the data in this thesis were used to support and offer explanation of the potential mechanism(s) for the

mutant cardiomyocytes derived from the human induced pluripotent stem cells (hiPSC) in the Tibbits Lab (Shafaattalab et al., 2019). This allows us to investigate the effects of a particular mutation from the most basic Tn complex level, to the reconstituted thin filament and eventually at the whole cell level using hiPSC-derived cardiomyocytes (hiPSC-CMs).

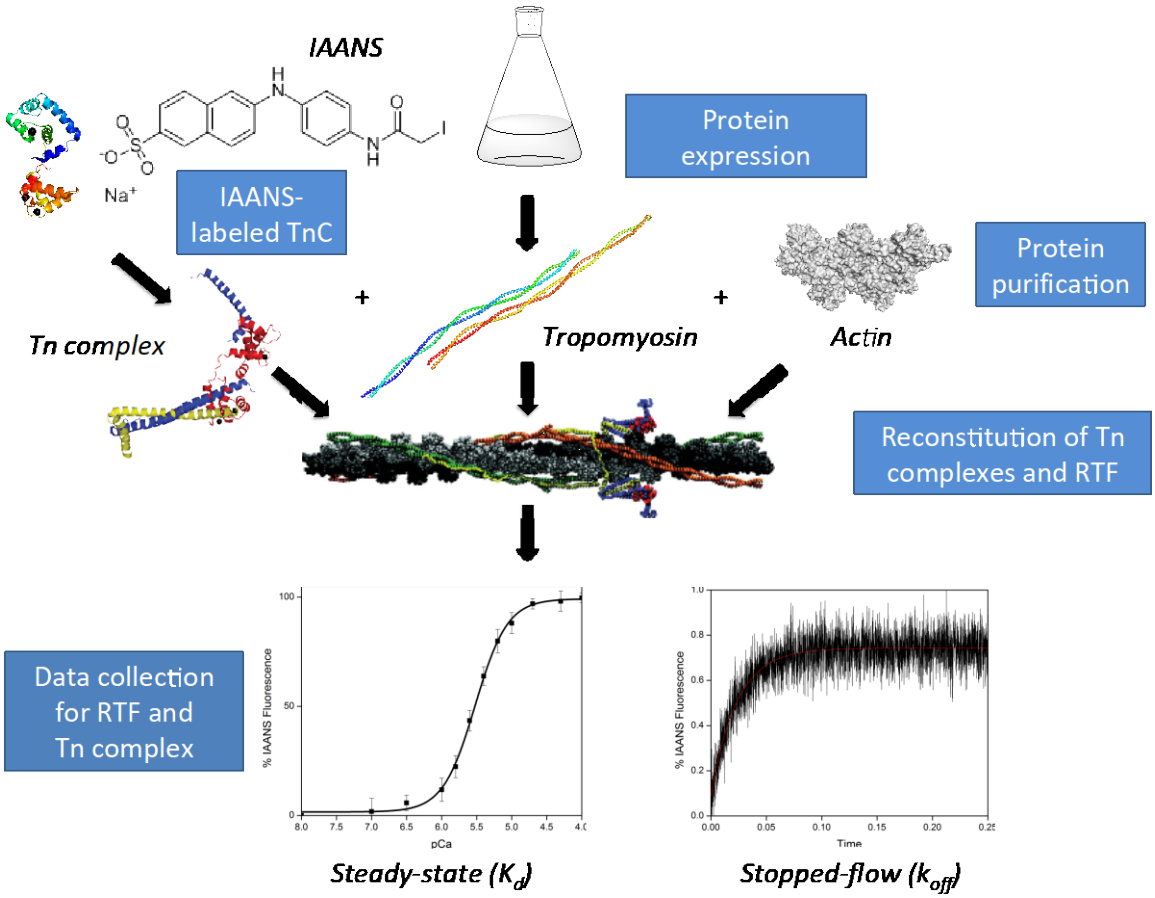

Figure 2-1 Overview of the experimental approaches.

This schematic represents the overall workflow for the characterization of the Ca^{2+} binding properties of Tn complexes and RTF. First it involves the protein expression for each of the protein construct. Then each protein was purified according to the purification protocol specific for each protein component. TnC is labeled with the fluorophore IAAANS before binding with TnI and TnT to make Tn complexes. Tropomyosin and actin are also purified separately before reconstitution with Tn complexes to generate RTF. Once purified Tn complexes and RTF are generated, they are subjected to the steady-state and stopped-flow experiments to determine the K_d and k_{off} values, respectively.

2.2. List of the constructs

Various constructs were outsourced from Genscript or obtained from the glycerol stock that have been established over the past decade in the Tibbits Lab. Site-directed mutagenesis (Quickchange site directed mutagenesis kit, Sigma) was performed to make mutations of interest using the corresponding wild type DNA templates. Some point mutations were generated by Genscript mutagenesis service. The sequence of each construct was confirmed by DNA sequencing before attempting protein expression and purification. All the constructs used in this thesis are listed in Table 2-1.

Table 2-1 List of constructs used in this thesis

Construct	Gene Name	Description	Length	Molecular Weight (kDa)	Extinction Coefficient ($M^{-1}cm^{-1}$)	Uniprot ID
WT $cTnC^{T53C}$	*TNNC1*	Full length TnC with three mutations (T53C, C35S, C84S) for fluorescence labeling specifically at T53C for functional studies.	161	18	4470	P63316
Human Adult Troponin I and Troponin T Subunits						
WT cTnI	*TNNI3*	Full length WT cTnI.	211	24	9970	P19429
SD cTnI	*TNNI3*	Full length TnI with Ser23 and Ser24 mutated to Asp23 and Asp24 to mimic the phosphorylation of cTnI.				
R68C cTnI	*TNNI3*	Full length TnI with R68C mutation, which was the corresponding mutation of R37C found in the ssTnI.				
WT cTnT	*TNNT2*	Full length WT cTnT (isoform 6).	288	35	16960	P45379
I79N cTnT	*TNNT2*	Full length cTnT with I79N mutation.				
F110I cTnT	*TNNT2*	Full length cTnT with F110I mutation.				
R278C cTnT	*TNNT2*	Full length cTnT with R278C mutation.				
Human Fetal/Neonatal Troponin I and Troponin T Subunits						
WT ssTnI	*TNNI1*	Full length slow skeletal troponin I.	187	22	13980	P19237
R37C ssTnI	*TNNI1*	ssTnI with R37C mutation				
WT cTnT	*TNNT2*	WT cTnT (isoform 1)	298	36	22460	P45379
I89N cTnT	*TNNT2*	cTnT with I89N mutation, which was the corresponding mutation of I79N found in adult cTnT.				
Other constructs						
MAS-αTm	*TPM1*	Full length Tm with the additional tri-peptide (Met-Ala-Ser) to the N-terminus to mimic acetylation process in native Tm and ensure the binding to actin filaments.	287	33	8940	P09493

2.3. Protein Overexpression

Each expression plasmid (pET21a(+) or pET28a(+)) coding for the protein of interest was transformed into *E. coli* BL21(DE3) expressing cells. The transformed cells were grown overnight in 100 mL LB and used to inoculate each liter of LB with 1:100 back dilution (10 mL of overnight culture in 1 liter of LB) supplemented with appropriate antibiotics (Ampicillin or Kanamycin, with a final concentration of 100 µg/mL and 50 µg/mL, respectively). Cell cultures were grown at 37ºC until the OD^{600} reached 0.6-0.8, which normally occurred within about 3-4 hours. To facilitate the growth of the cell, the LBs were pre-warmed to 37 ºC. The protein overexpression was then induced with 1 mM IPTG for an additional 3-4 hours. The cells were then harvested by centrifugation at 6,000 x g for 6 mins, and the collected cell pellets were stored at -80ºC.

2.4. Protein Purification

The general protein purification protocol for each thin filament component is discussed in detail in the following sections. The representative FPLC chromatogram and the corresponding SDS-PAGE gels are included in the supporting materials in the Appendix A. Individual Tn subunits were expressed and purified in a denatured form and then re-natured together to form Tn complexes and RTFs.

2.4.1. Purification of TnC

The TnC construct used for the functional studies contained three mutations (T53C, C35S, and C84S, termed as TnC^{T53C}) for the fluorescence labeling with 2-(4'-(iodoacetamido)anilino)naphthalene-6-sulfonic acid (IAANS). TnC^{T53C} has proven to be very effective and widely used in reporting the fluorescence change upon Ca^{2+} binding and dissociation from TnC (Davis 2006). For the structural studies, only the WT TnC was utilized since fluorescence labeling was not required. Both TnC and TnC^{T53C} were purified using identical protocols as described below.

The cell pellets collected from six liters of overexpressed cell solution were first thawed in buffer A (50 mM Tris-HCl, 100 mM NaCl, 2 mM $MgCl_2$, 1 mM DTT). After the cell pellets were completely resuspended in buffer A, the cells were sonicated at 30% amplitude for 30 seconds on and 30 seconds off 1 mM PMSF and 5 µL of benzonase

(Sigma-Aldrich) was added per 40 mL of the cell solution. The cell solution was then incubated on ice for 30 mins to digest of the bacterial DNA. until the solution was no longer viscous. The cell solution was then centrifuged at 28,900 g for 30 mins at 4ºC (Fiberlite F13-14 × 50 cy fixed angle rotor). The supernatant was obtained and filtered using a 0.45 µm filter to ensure the solution was clear before being loaded onto an anionic exchanger, HiTrep DEAE fast-flow (FF) column (GE Healthcare). After applying the lysate onto the column, the solution was run at 5 mL/min with a gradual gradient mixing with Buffer A and Buffer B (Buffer A + 0.55 M NaCl) starting from 0% Buffer B up to 100% Buffer B by the end of the run. Identity of the fractions under the peaks were confirmed by 12% SDS-PAGE.

All the fractions containing partially pure TnC were concentrated to 3 mL using an Amicon ultra-centrifuge filter device (Millipore) with a 10 kDa molecular weight cut off (MWCO). The concentrated protein sample was further purified by size-exclusion chromatography (Sephacryl S-100 HiPrep 26/60 column) in buffer A on an AKTA Prime system (GE Healthcare) at room temperature and a flow rate of 1 mL/min. Before loading on the column, the concentrated protein solution was spun at 28,900 g for 30 mins using a tabletop centrifuge or filtered through 0.45 µm filter to remove any possible precipitant. The purity of the protein was once again confirmed by a 12% SDS-PAGE. All fractions containing purified TnCs were combined and kept in -80 ºC.

2.4.2. Fluorescence Labeling of TnC

Purified TnC^{T53C} was thawed and dialyzed against IAANS labeling buffer (6 M urea, 50 mM Tris-HCl, 90 mM KCl, 1 mM EGTA, 1 mM DTT, pH 7.5) overnight. The next day, TnC^{T53C} was dialyzed against the same buffer without DTT to remove excess reducing agent. This step was only performed for 1 exchange for 4 hours since the Cys residue in TnC is very active (Putkey et al., 1993), so one exchange step was sufficient. The concentration of TnC^{T53C} was then measured using the Bradford assay. Meanwhile, the concentrated IAANS stock solution (Sigma-Aldrich) was prepared by dissolving 10 mg of the IAANS powder in 1 mL of DMSF. IAANS labeling to TnC was initiated by the addition of a three-to five-fold molar excess of IAANS to TnC^{T53C}. The labeling reaction was allowed to proceed in the dark, by wrapping the Falcon tube with aluminum foil, for 5-8 hours with gentle rocking at 4ºC. The reaction was then stopped by the addition of 2

mM DTT. Unreacted IAANS was then removed by exhaustive dialysis against 4 liters of a solution containing 10 mM MOPS, 90 mM KCl, pH 7.0 with minimal three exchanges.

2.4.3. Purification of TnI

The protocol for the purification of TnI was modified from the technique described by Kruger et. al. (Kruger et al., 2003). All adult cTnI and fetal ssTnI were purified using the same protocol and yielded similar purity. Cell pellets were first thawed in TnI lysis buffer (6 M urea, 25 mM TEA-HCl, 2 mM $MgCl_2$, 1 mM DTT, 1 mM PMSF, pH 7.5). After completely resuspending the cell pellet in the lysis buffer, 5 µL of benzonase (Sigma-Aldrich) was added to the cell solution to ensure the digestion of DNA. Next, the cell solution was sonicated at 30% amplitude for 30 seconds on and 30 seconds off for 5 minutes, or until there was no visible viscosity. The cell solution was then centrifuged at 28,900 g for 30 mins and the supernatant was obtained. Twenty-five grams of ammonium sulphate was added per 100 mL of supernatant and the solution was stirred on ice for 30 mins. The solution was further centrifuged at 28,900 g for 30 mins, and the solution was dialyzed against Column buffer A (6 M urea, 25 mM TEA-HCl, 2 mM EDTA, and 1 mM DTT at pH 7.5). Three exchanges of buffer A were required to ensure the removal of ammonium sulphate before loading onto the anionic exchange column, CM Sepharose Fast Flow (FF) column (GE Healthcare). If the solution was somewhat cloudy, then the solution could be cleared by either centrifugation at 28,900 g for 30 mins or by filtering through 0.45 µm filter. TnI was eluted with a linearly increasing NaCl gradient (0-500 mM) in buffer A on a CM Sepharose FF column with a flow rate of 5 mL/min. The identity of fractions under each peak on a chromatogram was confirmed by 12% SDS-PAGE gel. All fractions containing TnI were pooled together and further dialyzed against buffer B (6 M urea, 20 mM Tris-HCl, 1 mM EDTA, and 0.5 mM DTT at pH 8.0) with three exchanges. The protein samples were then loaded onto an anionic exchange column DEAE-Sepharose Fast Flow column (GE Healthcare) and the *flow through* was collected while other remaining contaminant proteins bound to the column. After confirming the purity of TnI on a 12% SDS-PAGE gel, all the fractions containing purified TnI were then pooled together and dialyzed extensively with 1 mM HCl prior to lyophilisation and long-term storage at -80ºC.

2.4.4. Purification of TnT

All TnT proteins were purified using the protocol described by Kruger et. al. with minor modifications (Kruger et al., 2003). TnT cell pellets were first thawed in TnT lysis buffer (6 M urea, 50 mM sodium citrate, 2 mM $MgCl_2$, 0.1 mM DTT at pH 6.0). After the cell pellet was fully resuspended in the lysis buffer, 5 µL of benzonase (Sigma-Aldrich) was added to ensure the digestion of bacterial nucleic acid. The cell solution was then sonicated at 80% amplitude for 30 seconds on and 30 seconds off for 5 mins or until no visible viscosity was observed. The protein was dialyzed against Column Buffer A (6 M urea, 50 mM sodium citrate, 1 mM EDTA, and 0.1 mM DTT at pH 6.0) with two exchanges. The cell solution was then loaded on the cationic exchange column, CM-Sepharose Fast Flow column and TnT was eluted by applying a linearly increasing gradient from 0 to 100% of 500 mM NaCl in Buffer A. The identity of the fractions under each peak were confirmed by a 12% SDS-PAGE gel, and fractions containing TnT were combined and dialyzed against Buffer B (6 M urea, 50 mM Tris-HCl, 1 mM EDTA, and 0.1 mM DTT at pH 8.0) with three exchanges. TnT was eluted by applying a linearly increasing gradient from 0 to 100% of 500 mM NaCl in Buffer B on a DEAD FF column. Presence of pure TnT in the elution fractions were confirmed by 12% SDS-PAGE. The elution fractions containing TnT were then pooled, dialyzed against 4-5 mM ammonium hydrogen carbonate or 0.1% formic acid to avoid precipitation, lyophilized and stored at -80°C.

2.4.5. Purification of Tropomyosin

Tm is a coiled-coil protein in which its position on actin is important in modulating the three-states of muscle contraction/relaxation. Unlike native Tm in which the first initiation Met is acetylated, the recombinant Tm produced in *E. coli.* does not undergo an acetylation process. The un-acetylated initiation Met has a net positive charge and the two protonated amino groups from un-acetylated Tm are predicted to electrostatically oppose each other in the hydrophobic core of the coiled coil. Therefore, previous literature has suggested to fuse a short tri-peptide (Met-Ala-Ser or Met-Gly-Ser) at the N-terminus to Tm (Monteiro et al., 1994). After the initial Met is removed, Ala or Gly would be exposed as the first residue in the heptad repeat followed by Ser, mimicking the acetylation process in the native Tm and restoring recombinant Tm binding to actin

(Coulton et al., 2006; Monteiro et al., 1994). Hence, all Tm used in this thesis had the tri-peptide MAS- fusion to the N-terminus of Tm.

Cell pellets were first thawed and resuspended in Tm lysis buffer (20 mM Tris-HCl, 100 mM NaCl, and 5 mM $MgCl_2$ at pH 7.5) with the addition of 5 µL of benzonase (Sigma) per 40 mL of cell solution. The cell solution was then sonicated at 60% amplitude for 10 seconds on and 10 seconds off for 3 mins or until no visible cell clumping or viscosity was observed. The cell lysate was then centrifuged at 28,900 g for 30 mins and the supernatant was collected. The supernatant was heated at 80°C for 10 mins, and the solution turned white almost immediately. Then the protein solution was centrifuged at 28,900 g for 30 mins and the supernatant was collected in which the soluble Tm was collected. 1N of HCl was added slowly, drop-by-drop, to the protein solution which was immersed in an ice bath and with gentle stirring, until the pH reached to 4.5-4.6. Once the pH had reached pH 4.5 – 4.6, the solution was stirred gently on ice for another 20 mins. The protein solution was then spun down at 28,900 g for 30 mins, and the cell pellet was collected. The cell pellet was further re-suspended in 10-20 mL of Buffer A (10 mM PO_4^-, 100 mM NaCl at pH 7.0). After the resuspension, the solution was kept stirring on ice for additional 30 mins or until the protein solution was not cloudy anymore. The solution was then dialyzed against buffer A overnight to ensure the proper refolding of Tm.

The next day Tm was purified by anion exchange column, HiTrap Q FF, on a FPLC system (GE Healthcare). Tm was eluted by applying a linearly increasing gradient from 0 to 100% of 900 mM NaCl in Buffer A. All fractions under the peak were confirmed by 12% SDS-PAGE and further concentrated to 3 mL using an Amicon ultra-centrifugal filter device filter with MWCO of 15 kDa (Millipore). The next day, the concentrated protein sample was purified further by size-exclusion chromatography (Sephacryl S-100 HiPrep 26/60 column) in Buffer B (10 mM MOPS, 150 mM KCl, 3 mM $MgCl_2$, and 1 mM DTT at pH 7.0). Fractions containing Tm were combined together, lyophilized and stored at -20°C.

2.4.6. Purification of rabbit skeletal actin

The protocol for actin purification was modified based on the Davis' lab protocol on actin purification (Spudich et al., 1972). Dry rabbit muscle powders were purchased

from Sigma-Aldrich. The day before purification, four liters of G-buffer (2 mM Tris, 1 mM NaN_3, 0.25 mM $CaCl_2$ and 0.25 mM DTT at pH 8.0) was prepared and kept at 4°C. Since actin is susceptible to proteolysis from bacterial contamination, it is important to add sodium azide (1 mM or 0.1%) if the solution is prepared from stock buffer.

On the first day of purification, fresh 0.1 mM ATP was added to the 4 liters of G-buffer. Five grams of acetone powder were weighed in 400 mL beaker and the acetone powder were further cut and grinded into a finer powder form before dissolving in cold 100 mL G-buffer (20 mL of G buffer/gram of powder). The acetone powder was stirred within the G-Buffer in the cold room or on ice or 1 hour with occasional mixing of the contents with a plastic rod. After one hour of mixing, the solution was filtered through eight layers of cheesecloth into a clean beaker. The solution was then centrifuged using a Ti70 rotor at 40,000 g for 30 mins at 4°C. The supernatant was collected and some of the pellet would become loose and cloudy. Therefore, the solution was then filtered through a 0.45 µm syringe tip filters. Next, 50 mM KCl, 1 mM ATP, and 2 mM $MgCl_2$ was added to the solution and incubated in the refrigerator at 4°C where F-actin was formed. At this stage, a visible increase in the solution viscosity was observed, indicating the formation of F-actin. After 2 hours of incubation at 4°C, solid KCl was slowly added with stirring to a final concentration of 0.6 M on ice for 30 mins. This high salt wash step ensured the removal of native Tm in the solution. The polymerized actin was then centrifuged at 150,000 g for 1 hour at 4°C. To obtain optimal purity, the remaining contaminant was removed by homogenizing the F-actin pellet with 25 mL G buffer with the addition of solid 0.6 M KCl, 1 mM ATP, 2 mM $MgCl_2$. The F-actin was then centrifuged at 150,000 g for 1 hour at 4°C. The resulting F-actin pellet was resuspended with 10 mL G-buffer, homogenized thoroughly with the buffer, and put in the dialysis against G-buffer.

On the second day of the purification, the buffer was exchanged two more times with the 1 litre G-buffer with rapid constant stirring at 4°C. After two exchanges against fresh G-buffer, the actin preparation was spun at 150,000 g for 1 hour at 4°C in an ultracentrifuge. Actins used for structural studies were further purified by size-exclusion chromatography (Sephacryl S-100 HiPrep 26/60 column) in G-buffer on a FPLC system (GE Healthcare) with a flow rate of 1-1.3 mL/min. The actin preparation was concentrated to 3 mL with an Amicon ultra-centrifugal filter device filter with MWCO of 15 kDa (Millipore) before loading onto the column. Fractions containing the pure G-actins

were confirmed on an SDS-PAGE gel, combined and further concentrated to approximately 20-25 mL using an Amicon ultra-centrifugal filter device filter with MWCO of 15 kDa (Millipore). Purification by size-exclusion chromatography was not necessary for the actins used for the functional studies.

On the last day of the actin purification, 50 mM KCl, 1 mM ATP, and 2 mM $MgCl_2$ were then slowly added to the actin solution in this order by gentle twirling of the Falcon tube. After addition of each chemical, the tube was inverted gently to complete mixing. Immediately, the viscosity of the solution increased as the G-actin polymerized to F-actin. It is important to store the actins in the filamentous form since G-actin solutions begin to lose polymerization activity after 2-3 days even in the presence of 1 mM ATP. After the contents were mixed, the solution was mixed in the refrigerator for 1.5-2 hours with no stirring for polymerization. Next, the solution was centrifuged at 150,000 g at 4°C for 1 hour, and the resulting pellets were clear and big. The cell pellets were then suspended in 7 mL of actin storage buffer (10 mM MOPS, 90 mM KCl, 1 mM $MgCl_2$ and 0.5 mM DTT at pH 7.0) and it was important to ensure that the cell pellets were dislodged completely from the walls of the centrifuge tubes. The solution was then homogenized by using the douncer to dounce around 40 times with a tight pestle. The suspended F-actins were placed into a dialysis bag and the dialyzed against 2-4 liters of fresh actin storage buffer with 3 exchanges in the cold room. After three exchanges, the concentration of F-actin was measured using a Nanodrop (ND-1000 UV-Vis) and an equal molar amount of phalloidin (Sigma-Aldrich) with 1:1 ratio of actin: phalloidin was added immediately to stabilize the F-actin. Phalloidin-bound F-actin was stored in 4°C up to four weeks.

2.4.7. Generation of troponin complex and reconstituted thin filament

Lyophilized purified TnI and TnT (approximately 6 mg/ml) were dissolved in 2 liters of Tn subunit dissolving buffer (10 mM MOPS, 4.6 M urea, 0.5 mM DTT and 0.01% NaN_3) for at least four hours. After dialysis, the concentration of the TnI and TnT were determined using Bradford Assay. The subunits were mixed at a molar ratio of 1:1.5:1.5 (TnC/TnI/TnT) and incubated at room temperature for 20 mins with aluminum foil wrapped around the Falcon tube. The complexes were subsequently dialyzed against buffers with decreasing concentration of urea and KCl, with 10 mM MOPS, 3 mM $MgCl_2$, 0.5 mM DTT and 1) 4 M urea, 1 M KCl; 2) 2 M urea, 750 mM KCl, 3) 500 mM KCl, and

4) 150 mM KCl. The last buffer exchange was repeated three times. After the sequential dialysis, any non-complexed TnI and TnT were precipitated after centrifugation at 28,900 g for 30 mins at 4°C. An example of purified reconstituted Tn complexes is shown on Figure A8 in the Appendix.

For functional studies, thin filaments were generated by combining phalloidin-actin, MAS-Tm, and cTn complexes in a molar ratio of 4:2:0.6, respectively. This is different from the physiological stoichiometric ratio (7:1:1) since the higher molar ratio of the recombinant MAS-Tm had to be used to ensure the complete binding of cTn onto the actin filaments so no free cTn were in the solution before the functional studies. This was confirmed by the stopped-flow experiments listed in section 2.5.1. First, actin and MAS-Tm were combined in thin filament buffer (10 mM MOPS, 150 mM KCl, 3 mM $MgCl_2$, 1 mM DTT at pH 7.0) and incubated on ice for 20 mins. cTn complexes were subsequently added to the actin-Tm solution and incubated on ice for additional 15 mins. For structural studies, thin filaments were generated using the same method except that the cTn complexes used were reconstituted with TnC without the IAANS labeling.

2.5. Methods of determining Ca^{2+} binding properties on the Tn complexes and reconstituted thin filaments

The purified Tn complexes and RTF were subjected to functional characterization using fluorescence technique to determine their Ca^{2+} binding properties. The Ca^{2+} sensitivity of the construct, represented by K_d, was extrapolated from the data obtained from the steady-state experiment. The Ca^{2+} dissociation constant, denoted as k_{off}, was determined from the stopped-flow fluorescence apparatus. Here are the descriptions of the basic principles behind the steady-state and the stopped flow fluorescence experiments.

The experimental approach to assess thin filament or Tn complex Ca^{2+} sensitivity was to construct the IAANS-pCa fluorescence curve and determine the left- or right-ward shift of the mutants relative to the WT curve. A left-ward shift indicates an increase of Ca^{2+} sensitivity while the right ward shift indicates a decrease of Ca^{2+} sensitivity. In other words, the same amount of free Ca^{2+} will generate more of the 50% of IAANS fluorescence for the thin filaments with higher Ca^{2+} sensitivity. The Ca^{2+} sensitivity of the thin filament, represented by the equilibrium dissociation constant K_d, is a ratio between

the Ca^{2+} association rate constant (K_{on}) and the Ca^{2+} dissociation rate constant (k_{off}) (Figure 2-2).

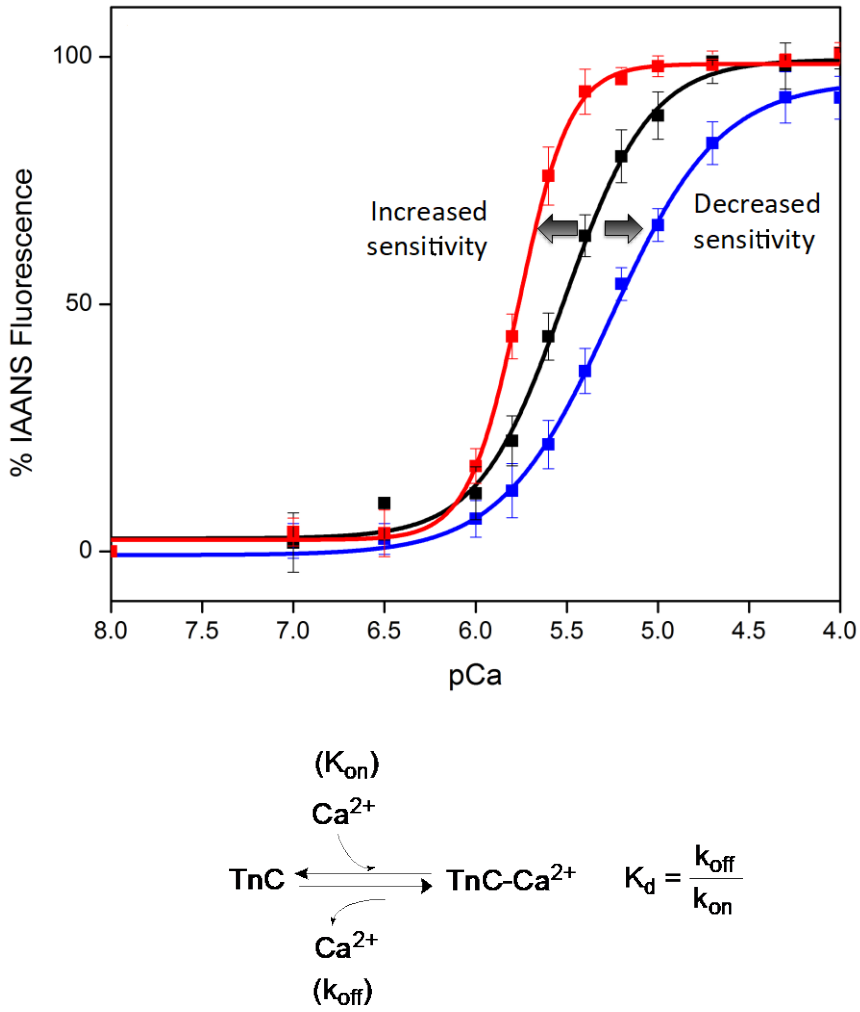

Figure 2-2 % IAANS fluorescence-pCa curve demonstrating leftward and rightward shift of the curve.

The top panel shows %IAANS-fluorescence-pCa curve for WT RTF (black), SD RTF (blue) which contains the pseudo-phosphorylation TnI that renders the RTF to have decreased Ca^{2+} sensitivity (shown by the rightward shift), and I79N RTF (red) which harbours the Ca^{2+} sensitizing I79N cTnT mutation that increase the Ca^{2+} sensitivity as demonstrated by the leftward shift. The bottom panel is the equation that demonstrates the relationship between equilibrium dissociation constant (K_d), k_{on}, and k_{off}. This figure was adapted from Chung et al. 2016 (Chung et al., 2016).

Before attempting the steady-state data collection, stopped-flow kinetics experiments were carried out to ensure the quality of the Tn complexes and RTF. Because each level of biochemical system complexity has a distinct fluorescence curve characteristic to the system (Davis et al., 2007), one is able to use this assure that there is no free cTnC in Tn complex and the stoichiometry of the complex is correct. The

fluorescence curve of the Tn complex goes upward while that of the RTF goes downward as shown Figure 2-4. Therefore, if the Tn complex has free TnC or the RTF has free Tn complexes, then the fluorescence curve will gradually appear in the opposite direction as expected.

2.5.1. Stopped-flow data collection and analysis

Stopped-flow is one of the most frequently used kinetic techniques. It involves rapidly mixing two solutions in the mixing chamber, and the mixed solutions are passed into a measurement flow cell. As the solution flows through, a steady-state equilibrium is getting established and the resultant solution is only a few milliseconds old as it enters the observation cell. The mixed solution then passes into a stopping syringe where the flow of mixed solutions can be instantaneously stopped. The kinetics of the Ca^{2+} removal (k_{off}) by EGTA causes the conformational change of TnC that is reflected by the fluorescence change of the fluorophore that is covalently attached to TnC (Li et al., 2013a) (Davis et al., 2007). This fluorescence change can be followed, monitored, and recorded in a computer device. In our case, the IAANS-TnC incorporated in Tn complexes or RTF were saturated with Ca^{2+} in one syringe and the other syringe contains the same buffer compositions with EGTA. As the two solutions rapidly mixed together, EGTA chelates Ca^{2+} from TnC and this Ca^{2+} dissociation causes a conformational change of TnC that was reported by IAANS (Figure 2-3).

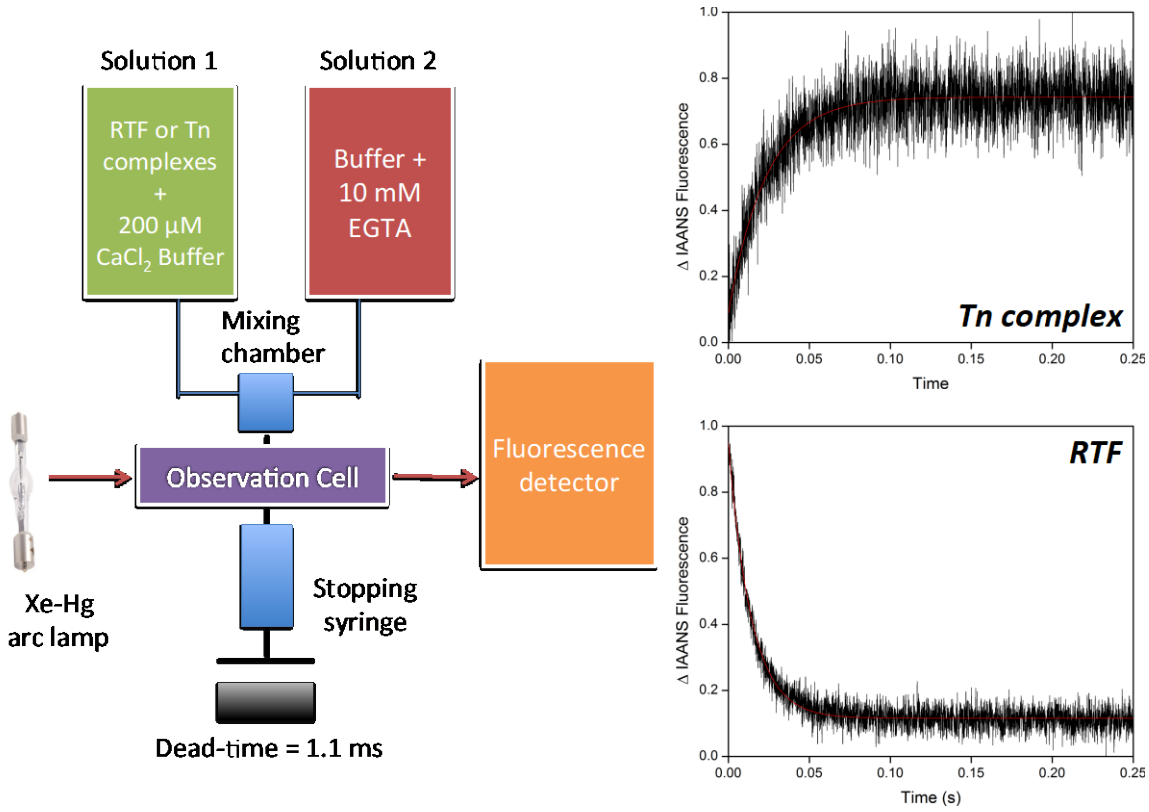

Figure 2-3 Schematic for the stopped flow apparatus.

In a stopped-flow apparatus, one syringe is filled with purified Tn complexes or RTF saturated with $CaCl_2$, and the second syringe is filled with the same buffer but with EGTA instead of $CaCl_2$. The two solutions are pushed simultaneously by the driver ram into the mixing chamber, and then the solution flows into the observation cell where the signal is recorded. The dead-time, which is the time from the end of the mixing of the two solutions and the time of the observation, is 1.1 ms in the Chirascan stopped-flow apparatus.

All stopped-flow kinetic measurements were carried out using a Chirascan Stopped-flow apparatus, which is almost identical to the SX20 series with a dead-time of 1.1 ms at 15ºC (Applied Photophysics, Leatherhead, UK). The IAANS was excited at 330 nm with a bandwidth of 10 nm and monitored through a 510/42 nm single-band bandpass filter (Semrock, Rochester, NY). One syringe was filled with either cTn complexes or RTF in the thin filament buffer (10 mM MOPS, 150 mM KCl, 3 mM $MgCl_2$, 1 mM DTT at pH 7.0) saturated with 200 µM of $CaCl_2$, and the other syringe was filled with 10 mM EGTA with the same buffer composition as the first syringe without the addition of purified protein samples and calcium. To obtain data traces, the solution from the two syringes were mixed rapidly in the mixing chamber, and the EGTA-induced Ca^{2+} dissociation from TnC was monitored by the IAANS fluorescence change. Before attempting the data collection on the RTF, the Ca^{2+} dissociation kinetics was always

performed to ensure the quality of the cTn complexes (i.e. no free cTnC in solution). This can be done routinely using the stopped-flow since TnC at different level of complexity that has an opposite trend of the IAANS fluorescence curve.

The rate decay of fluorescence after introduction of EGTA was fit with a single exponential equation as the following:

$$F_{(t)} = F_{(0)} e^{(-k_{off} \cdot t)}$$

where $F_{(t)}$ equals the fluorescence at time = t, $F_{(0)}$ is the fluorescence amplitude at time equals zero, k_{off} is the rate coefficient (s^{-1}) for a single exponential equation and t is the time.

Each k_{off} value represents an average of at least five traces that were fitted with a single exponential equation, and each trace was repeated more than 15 times. The data in the final analysis represent at least three to five separate stopped-flow data collection for each Tn or RTF complex. The background traces were obtained by injecting 5 mM EGTA in the syringe containing the protein sample and mixed it rapidly with the buffer with 10 mM EGTA. Background EGTA traces were then subtracted from the IAANS fluorescence curve to correct for scattering artifacts. Noted that the IAANS fluorescence curve obtained for Tn complexes and RTF are distinctive and opposite from each other (Figure 2-4).

2.5.2. Steady-state fluorescence data collection

A steady-state experiment (Figure 2-4), performed by the serial addition of Ca^{2+} into the solution, results in a hydrophobic binding pocket of TnC opening up as Ca^{2+} binds to site II of TnC and induces a conformational change that is reported by the change of IAANS fluorescence (Δ IAANS).

All steady-state fluorescence measurements were carried out using a Cary Eclipse Fluorescence Spectrophotometer (Agilent) at 15ºC. IAANS fluorescence was induced by excitation at 330 nm and monitored at 450 nm with the excitation and emission bandwidth filters set at ± 20 nm. The PMT voltage was kept at the default setting of 600 V. The titration buffer of 390 mM MOPS, 150 mM KCl, 3 mM $MgCl_2$, 4 mM

EGTA and 1 mM DTT at pH 7.0 were prepared fresh and stored at 4ºC. Hellma absorption cuvettes (Sigma-Aldrich) with a chamber volume of 3,500 µL were used. In brief, 1,050 µL of each of the purified Tn complexes or reconstituted thin filaments were combined with 1,050 µL of titration buffer, so that the final buffer composition in the cuvette chamber is 200 mM MOPS, 150 mM KCl, 3 mM $MgCl_2$, 2 mM EGTA and 1 mM DTT at pH 7.0. A minimal total volume of 2,100 µL was used during the steady-state data collection since the Z-dimension, defined as the distance from the bottom of the cuvette cell compartment to the center of the light beam, was 20 mm. After mixing the protein solution and the titration buffer, the solution was incubated at 15ºC in the spectrophotometer for 5 minutes before data collection. Microliter amounts of $CaCl_2$ were added to the protein solution with constant stirring. The $[Ca^{2+}]_{free}$ was calculated using a MaxChelator program (http://maxchelator.stanford.edu/downloads.htm). All fluorescence values obtained at 450 nm were normalized, fitted with a Dose Response sigmoidal equation (mathematically equivalent to the Hill equation) in Origin 8.6 (OriginLab, Northampton, MA) as the following:

$$F = F_{min} + \frac{F_{max} - F_{min}}{1 + 10^{\,n\,(pCa_{1/2} - pCa)}}$$

where F_{min} and F_{max} represent the minimal and maximal IAANS fluorescence, η is the Hill coefficient. $pCa_{1/2}$ is the negative log of the $[Ca2+]_{free}$ that produces half-maximal IAANS fluorescence. Note that the fluorescence-pCa curve generated for the Tn complexes and RTFs have the completely opposite trend, in which the IAANS fluorescence starts from 100% at pCa 8.0 to 0% at pCa 4.0 for the Tn complex while it is the reversed for the RTF (Figure 2-4). The Ca^{2+} sensitivity values were reported as a dissociation constant $K_{d,}$ and each K_d represents a mean of three to five separate titration ± standard error of the mean (SEM).

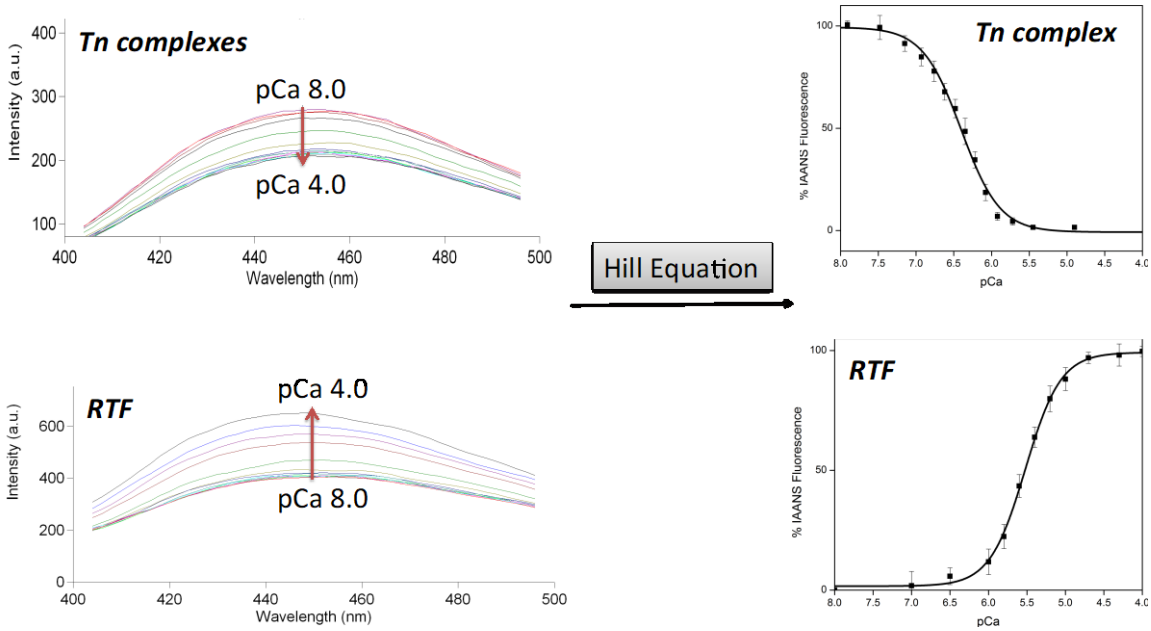

Figure 2-4 Data collection and analysis of the steady-state experiments.

The left side of the graph shows the IAANS emission spectra from 400 nm to 500 nm with the peak of the emission at 450 nm. Each line represents the IAANS fluorescence curve with each addition of Ca^{2+} during the course of titration. As indicated, the intensity of the IAANS fluorescence of Tn complexes gradually decreases from pCa 8.0 (apo-state) to pCa 4.0 (Ca^{2+} - saturated state). RTF has a completely reversed trend in which the intensity of the IAANS fluorescence gradually increases upon each addition of Ca. After normalizing the data and fitting with the Hill equation, the % IAANS fluorescence-pCa curve is constructed shown on the right side of the figure. Subsequently, pCa_{50}, which is converted to K_d and Hill coefficient are obtained after fitting with Hill equation.

2.5.3. Data analysis

Data throughout this thesis were analyzed using Origin 8.6 software (OriginLab, Northampton, MA). Statistical analysis was performed using one-way (one factor) analysis of variance (ANOVA) followed by Tukey's post-hoc test to determine if there were significant differences between the means. A p-value less than 0.05 was considered statistically significant.

Chapter 3.

Impact of pseudo-phosphorylation of TnI on the functional effect of hypertrophic cardiomyopathy-associated-troponin T mutations

3.1. Introduction

Hypertrophic cardiomyopathy (HCM) is one of the most commonly inherited cardiomyopathies, affecting 1 in 500 individuals (Maron et al., 1995; Maron et al., 2012). It is the major cause of the sudden cardiac death (SCD) in young athletes and individuals under the age of 35 (Watkins et al., 1995). In general, people with HCM have thickened left ventricular and interventricular septal walls that decrease the cavity size for the ventricle and can cause obstruction to blood flow (Maron and Maron, 2013). It is a disease with progressive symptoms, ranging from clinically less symptomatic, to the advanced thickening of the cardiac muscle that could potentially result in SCD (Maron et al., 2012). More than 1000 individual mutations in genes encoding 20 mostly sarcomeric proteins have been found to be associated with HCM (Maron et al., 2012).

Mutations found in the cardiac TnT gene (*TNNT2*) are responsible for approximately 7% of all HCM and are the third most common cause of HCM after β-myosin heavy chain and myosin binding protein-C mutations (Knollmann and Potter, 2001). Unlike the general anatomical abnormalities found in HCM patients, hearts from patients harbouring cardiac troponin T (cTnT) mutations show significantly less ventricular hypertrophy compared to other HCM-associated mutations (Knollmann and Potter, 2001). This low degree of clinical penetrance of the cTnT mutations makes them difficult to detect by echocardiography. However, patients with cTnT mutations are at high risk of SCD. This suggests that the degree of hypertrophy does not necessarily correlate with the risk of SCD, and that other mechanisms may contribute to the devastating outcomes for the patients with cTnT mutations (Knollmann and Potter, 2001).

cTnT belongs to a trimeric troponin (cTn) complex that serves as the essential regulator for cardiac muscle contraction and relaxation (Katrukha, 2013). The main

function of cTnT is to anchor the cTn complexes on actin filaments at a periodicity of 38.5 nm (Katrukha, 2013). The other two subunits include cardiac troponin C (cTnC), the calcium (Ca^{2+}) binding subunit, and cardiac troponin I (cTnI), the inhibitory subunit. cTn binds to actin filaments with a regular periodicity of 7 actin monomers and one tropomyosin (Tm) molecule (Katrukha, 2013). Together, these proteins form the thin filaments that interact with the thick filaments to promote force-generating cross-bridges that use the chemical energy generated from ATP hydrolysis (Katrukha, 2013).

A cascade of protein conformational changes is triggered when Ca^{2+} binds to cTnC, ultimately leading to muscle contraction. As Ca^{2+} dissociates from cTnC, the entire process is reversed, and the muscle relaxes mechanically. During β-adrenergic stimulation, the Ca^{2+} dissociation process is further enhanced by protein kinase A (PKA) phosphorylation of Ser23/Ser24 of cTnI, facilitating Ca^{2+} removal from cTnC (Solaro and Kobayashi, 2011). Many *in vitro* studies have shown that HCM-associated cTn mutations increase basal myofilament Ca^{2+} sensitivity, but more importantly, they compromise the enhanced Ca^{2+} dissociation process facilitated by cTnI phosphorylation (Messer et al., 2016). It is intriguing that many of these mutations are located remotely from the Ca^{2+} binding site of cTnC and phosphorylation sites of cTnI. However, they can still have "long-range" or allosteric effects that propagate along the thin filaments, altering the Ca^{2+} binding properties of the thin filaments and resulting in complex cardiomyopathies (Tardiff, 2011).

In this study, we investigated the altered Ca^{2+} binding properties induced by three cTnT mutations: I79N, F110I, and R278C in a human reconstituted cardiac thin filament system. Studies on transgenic mice harbouring these mutations show that they induce varying degrees of pathogenicity and arrhythmogenicity in which I79N exhibits the highest susceptibility to cardiac arrhythmia, F110I exhibits an intermediate susceptibility, and R278C behaves closer to that of the wild-type (WT) (Baudenbacher et al., 2008; Schober et al., 2012). Previous *in vitro* studies on these mutations utilizing mice, rat, or rabbit myofibrils or myofilaments yielded inconsistent results. For example, the I79N mutation has been reported to either increase the force per cross bridge in a mouse model (Miller et al., 2001) or decrease in cTn complexes exchanged into bovine skinned muscle fibers (Bai et al., 2013). The mutation has no effect on the ATPase activity or changes in Ca^{2+} sensitivity in the equivalent residue position in rat cTn complexes (Lin et al., 1996), yet it increases the Ca^{2+} sensitivity in human cTn complexes reconstituted in

porcine skinned fibers (Szczesna et al., 2000). The Ca^{2+} sensitivity of force generation was higher in cTn complexes exchanged into rabbit muscle fibers (Morimoto et al., 1998) but a Ca^{2+} desensitization was observed when the mutation was introduced into rat ventricular myocytes via adenoviral gene transfer (Rust et al., 1999). Although small mammals are valuable animals models due to their short gestation time and easy manipulation to generate transgenic strains, the translational aspects to human cardiac diseases are limited due to fundamental differences of the contractile properties of the heart (Wessels and Sedmera, 2003). In addition, several studies suggest that myofilament Ca^{2+} sensitization is the cause of the increased susceptibility to cardiac arrhythmia, however the molecular mechanism is still unknown (Baudenbacher et al., 2008; Schober et al., 2012).

We used human recombinant cTn complexes and human recombinant Tm reconstituted into thin filaments to determine the changes in Ca^{2+} sensitivity and Ca^{2+} dissociation rate using steady-state and stopped-flow fluorescence techniques, respectively. Additionally, we included phosphomimetic cTnI in which Ser23/Ser24 were mutated to Asp and examined how these mutations modified the functional effects of cTnI. Our results show that I79N and R278C cTnT mutations significantly increase myofilament Ca^{2+} sensitivity and that all three mutations, including F110I, attenuate the functional effects of phosphomimetic cTnI at the thin filament level. The R278C cTnT mutation, which was previously suggested as a benign mutation, most notably shows the highest Ca^{2+} sensitizing ability and blunting response to phosphomimetic cTnI.

3.2. Materials and Methods

3.2.1. Bioinformatics

Full-length cTnT protein sequences from each species were obtained from UniProt and the NCBI protein database (UniProt Consortium, 2018). Sequence alignment was conducted through Clustal Omega (Sievers et al., 2011). The secondary prediction program was performed by PSIPRED (Buchan et al., 2013).

3.2.2. Protein over-expression and purification of recombinant cTnC, cTnI and cTnT, Tm and actin extraction from rabbit skeletal muscle powder

All protocols associated with thin filament protein expression and purification, generation of Tn complexes and reconstituted thin filaments, data collection using the steady-state and the stopped flow fluorescence spectrometry are described in Chapter 2. All cTn subunits and Tn complexes generated specific to this chapter with various combinations of cTnI and cTnT are listed in Table 3-1 and Table 3-2, respectively.

Table 3-1 List of Protein Constructs in Thin Filament Preparation

Construct	Gene Name	Description	Length	Molecular Weight (kDa)*	Extinction Coefficient ($M^{-1}cm^{-1}$)*	Uniprot ID
# WT $cTnC^{T53C}$	*TNNC1*	Full length TnC with three mutations (T53C, C35S, C84S) for fluorescence labeling specifically at T53C for functional studies.	161	18	4470	P63316
Troponin I and Troponin T Subunits						
WT cTnI	*TNNI3*	Full length WT cTnI.	211	24	9970	P19429
SD cTnI	*TNNI3*	Full length TnI with Ser23 and Ser24 mutated to Asp23 and Asp24 to mimic the phosphorylation of cTnI.				
WT cTnT	*TNNT2*	Full length WT cTnT (isoform 3).	288	35	16960	P45379
I79N cTnT	*TNNT2*	Full length cTnT with I79N mutation.				
F110I cTnT	*TNNT2*	Full length cTnT with F110I mutation.				
R278C cTnT	*TNNT2*	Full length cTnT with R278C mutation.				
Other constructs						
Alpha MAS-Tm	*TPM1*	Full length Tm with the additional tri-peptide (Met-Ala-Ser) to the N-terminus to mimic acetylation process in native Tm and ensure its binding to actin filaments.	287	33	8940	P09493

*Both the molecular weight and extinction coefficients were calculated by ProtParam (Gasteiger et al 2005).

All cTn and RTF utilized in this study were labeled with IAANS at T53C position with the two additional mutations C35S and C84S (Davis et al., 2007). For simplicity, cTn and RTF mentioned in the text do not have T53C superscript and IAANS subscript included.

Table 3-2 List of cTn complexes in the current study.

Recombinant cTn complexes for data collection*	Composition
WT cTn^{T53C}	WT $cTnC^{T53C}$, WT cTnI, WT cTnT
I79N cTn^{T53C}	WT $cTnC^{T53C}$, WT cTnI, I79N cTnT
F110I cTn^{T53C}	WT $cTnC^{T53C}$, WT cTnI, F110I cTnT
R278C cTn^{T53C}	WT $cTnC^{T53C}$, WT cTnI, R278C cTnT
SD cTn^{T53C}	WT $cTnC^{T53C}$, SD cTnI, WT cTnT
I79N SD cTn^{T53C}	WT $cTnC^{T53C}$, SD cTnI, I79N cTnT
F110I SD cTn^{T53C}	WT $cTnC^{T53C}$, SD cTnI, F110I cTnT
R278C SD cTn^{T53C}	WT $cTnC^{T53C}$, SD cTnI, R278C cTnT

*All the RTF constructs contained the above various cTn complexes with 2 to 4 μM Tm and 4 μM actin filaments.

3.3. Results

3.3.1 Sequence alignment of cTnT

Human cTnT and cTnT from many other species are subjected to alternative splicing during the myocardial transition from fetal to adult heart or in response to pathological perturbations such as heart failure (Anderson et al., 1991; Sasse et al., 1993). To understand the conservation of the chosen three cTnT mutations, sequence alignment was performed from human to zebrafish, which represents more than 450 millions of year apart (Genge et al., 2016). Only the canonical sequences from each species were used in the sequence alignment as shown in Figure 3-1. The secondary structure was predicted by PSIPRED (Buchan et al., 2013). The algorithm predicts that TnT is made of entirely α-helices that are connected by loop regions, making it a highly flexible protein molecule that likely enables its mobile movement along the thin filaments in response to the different states of thin filament activations (Tardiff, 2011).

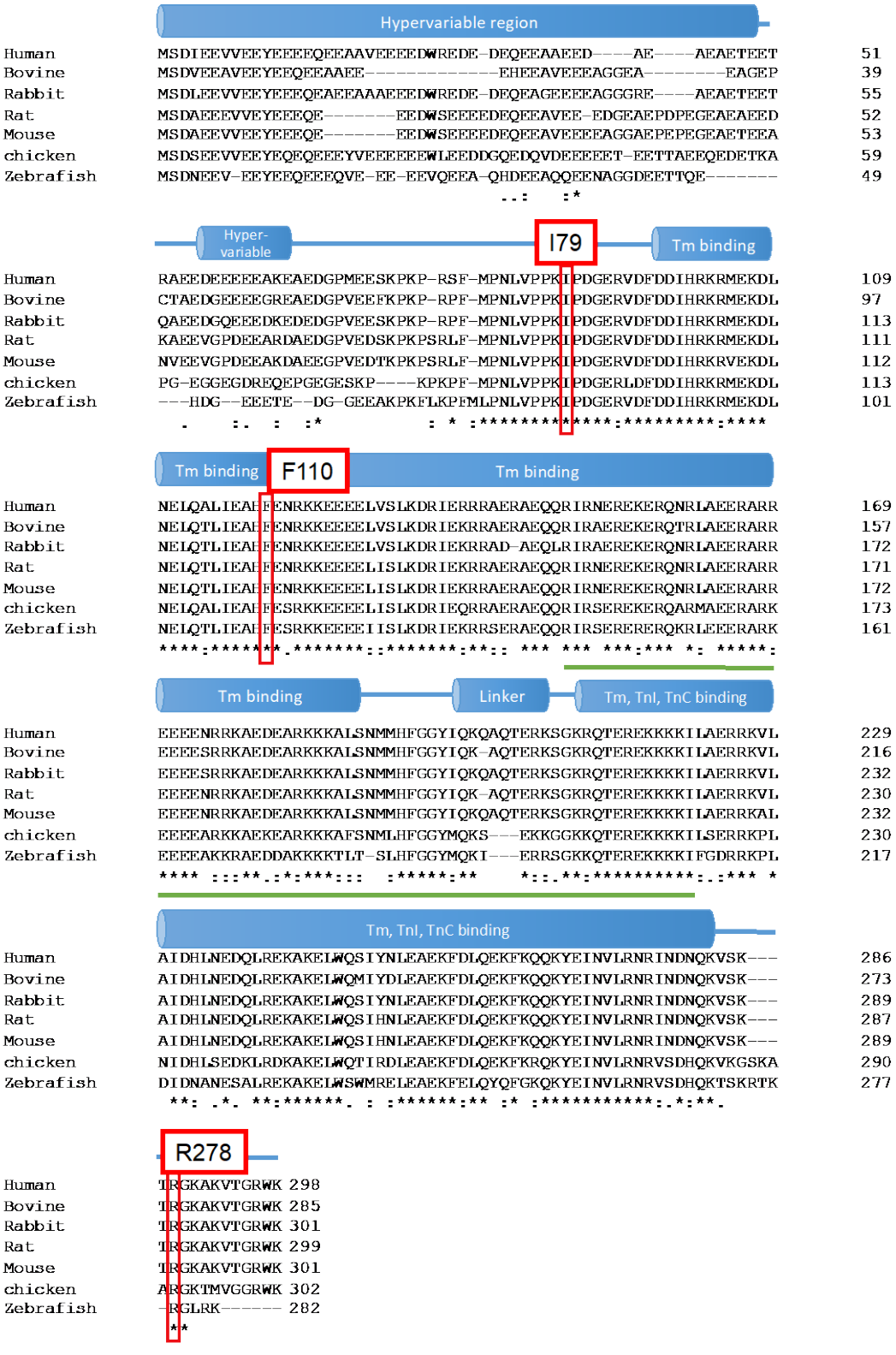

Figure 3-1 Sequence alignment of the full-length cTnT protein among different species.

A multiple sequence alignment of the full-length canonical cTnT protein (isoform 1) from human (Uniprot ID: P45379), bovine (Uniprot ID: P13789), rabbit (Uniprot ID: P09741), rat (Uniprot ID: P50753), mouse (Uniprot ID: P50752), chicken (Uniprot ID: P02642), and zebrafish (Uniprot ID: Q90Y46) was performed using Clustal Omega (Sievers et al., 2011). I79, F110, and R278 are boxed in red and they are highly conserved across different species. Secondary structures of the human cTnT, mainly alpha helices (shown by blue cylinder) and loop (blue lines) region, were predicted by PSIPRED webserver and modified accordingly (Buchan et al., 2013). The green line represents the residues (residue 199-272) in the core domain of cTn complexes solved by X-ray crystallography (PDB: 4Y99) (Takeda, 2016).

3.3.1. Effects of the cTnT mutations on the Ca^{2+} sensitivity of cTn complexes

The stopped-flow protocols were carried out to ensure there were no free cTnC in the cTn complex solution and no free cTn complexes in the RTF solution before data collection. To observe the quality of cTn complexes or RTF, a longer period (10 seconds) of monitoring was used (data not shown).

To determine the Ca^{2+} sensitivity of the cTn complexes, steady-state fluorescence experiments were carried out. At the cTn complex level, a measurable Ca^{2+}-dependent IAANS fluorescence decrease was observed for all eight cTn complexes (Figure 3-2). Consistent with the literature, there were no significant differences in the Ca^{2+} sensitivity as indicated by the K_d, the concentration required to elicit 50% of IAANS fluorescence (Table 3-3) at the cTn complex level. The Hill coefficients (η_H) were all within the range of 1.4-1.7 (Table 3-3) and no significant differences were observed among different cTn complexes.

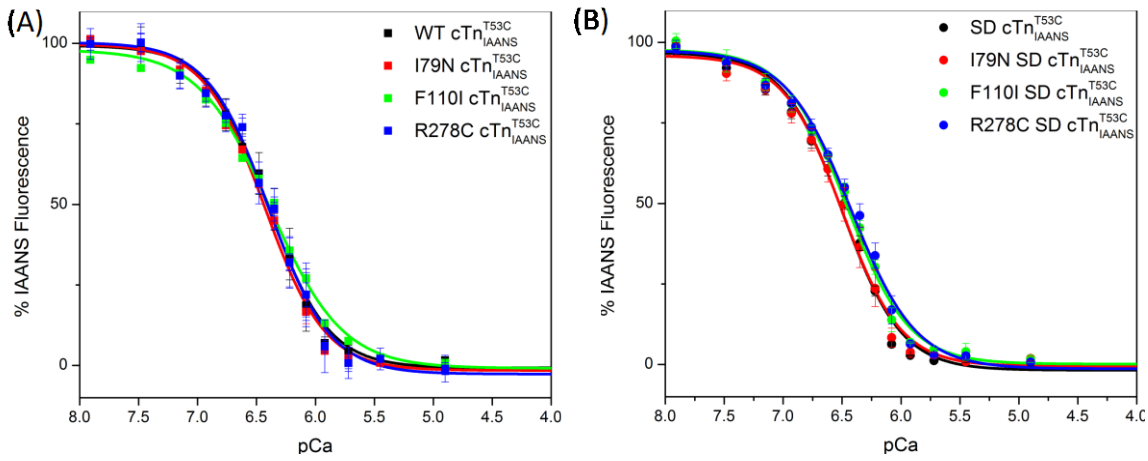

Figure 3-2 Effects of the three cTnT mutations on the Ca2+ binding affinity of cTn complexes with (A) WT cTnI and (B) SD cTnI.

Panel (A) shows the change in fluorescence, represented by % IAANS fluorescence in various cTn complexes as a function of free Ca^{2+}. The data were normalized by setting the fluorescence at pCa 8.0 equal to 100% and the fluorescence at pCa 4.0 equal to 0. Control WT cTn is shown in solid black square, I79N cTn in solid red square, F110I in solid green square and R278C in solid blue square. Panel (B) shows the change in fluorescence for cTn constructs with SD cTnI. SD cTn is shown in open black square, I79N SD cTn in open red square, F110I SD cTn in open green square and R278C in open blue square.

3.3.2. Effects of the cTnT mutations on the Ca^{2+} sensitivity of reconstituted thin filaments (RTFs)

Steady-state fluorescence measurements were carried out on RTFs with various combinations of cTnT and cTnI. A Ca^{2+}-dependent IAANS fluorescence increase was observed for all eight RTF constructs. Differences in the Ca^{2+} sensitivity observed at the cTn-complex level became apparent at the RTF level (Figure 3-3). Both R278C and I79N cTnT mutations showed a significant increase in Ca^{2+} sensitivity of ~1.7- and ~2-fold ($p<0.05$), respectively (Figure 3-3A, Table 4).

3.3.3. Effects of the cTnT mutations with SD cTnI on the Ca^{2+} sensitivity of RTFs

As predicted, the Ca^{2+} sensitivity for SD RTFs containing phosphomimetic cTnI (S23D/S24D) were ~2.2-fold lower compared to that of the WT ($p<0.05$). This result confirms that *in vitro* RTF is able to recapitulate the functional effects of SD cTnI observed under physiological conditions. All three mutations, I79N SD RTF, F110I SD

RTF, and R278C SD RTF exhibited a significant decrease in K_d compared to WT SD RTF by ~1.8-fold, ~2.4-fold and ~4-fold ($p<0.05$), respectively (Figure 3-3B, Table 3-4).

As anticipated, the Hill coefficients (η_H) for the RTFs were higher overall than that of the Tn complexes, and all were found to be within a range of 2.1-3.8. No significant differences of the Hill coefficient were observed among various RTF constructs (Table 3-4).

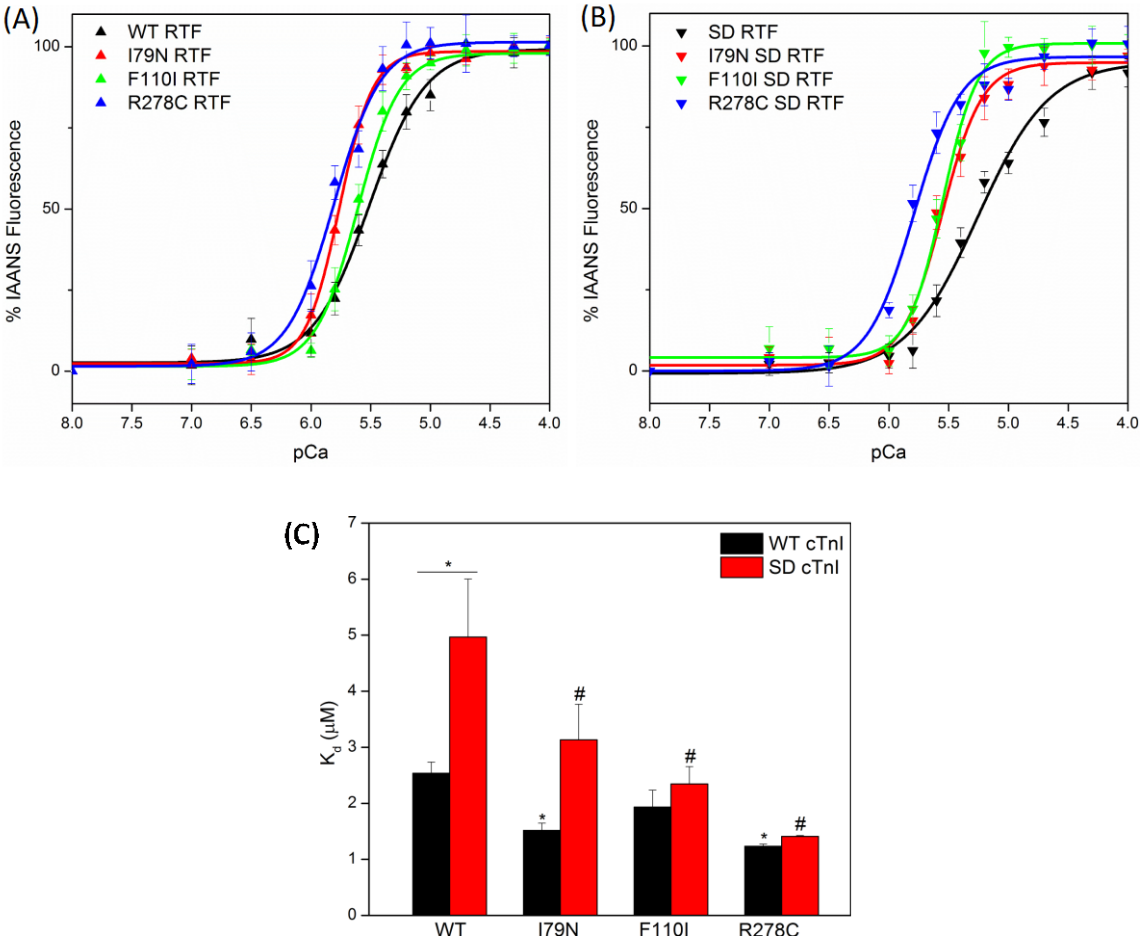

Figure 3-3 Effects of the three cTnT mutations on the Ca^{2+} sensitivity of reconstituted thin filaments with (A) WT cTnI and (B) SD cTnI.

Panel (A) shows the change in fluorescence, represented by % IAANS fluorescence in various RTF preparations as function of free Ca^{2+}. The data were normalized by setting the fluorescence at 8.0 equal to 0 and the fluorescence at pCa 4.0 equal to 100%. Control WT RTF is shown in solid black triangle, I79N RTF in red, F110I RTF in green and R278C RTF in blue. Panel (B) shows the change in fluorescence for RTF constructs with SD cTnI. SD RTF is shown in inverted black triangle, I79N SD RTF in red, F110I SD RTF in green and R278C SD RTF in blue. Panel (C) shows the summary of the K_d in which black bars represent the RTF reconstituted with WT cTnI and red bars represent the RTF reconstituted with SD cTnI. The asterisk (*) indicates $p<0.05$ versus the WT RTF, and the pound sign (#) indicates $p<0.05$ versus the SD RTF.

3.3.4. Effects of the cTnT mutations on the Ca^{2+} dissociation rates from cTn complexes

Stopped-flow fluorescence spectroscopy was used to determine the Ca^{2+} dissociation rates from the cTn complexes. Upon addition of EGTA, Ca^{2+} was rapidly removed from TnC, inducing a conformational change from cTnC in which the fluorescence modification was recorded.

An increase in IAANS fluorescence as Ca^{2+} was removed by EGTA was observed for all cTn complexes. All cTn complexes were subjected to a 10-second time period to detect the presence of any free cTnC, as the presence of free cTnC would show a downward fluorescence curve over a longer period of time. All cTn complexes remained stable as shown in a plateau fluorescence curve over a 10-second period after the initial fluorescence increase. All cTn complexes exhibited k_{off} values in the range of 45 to 47 s^1, and no significant differences were observed among all eight cTn complexes (Figure 3-4, Table 3-3).

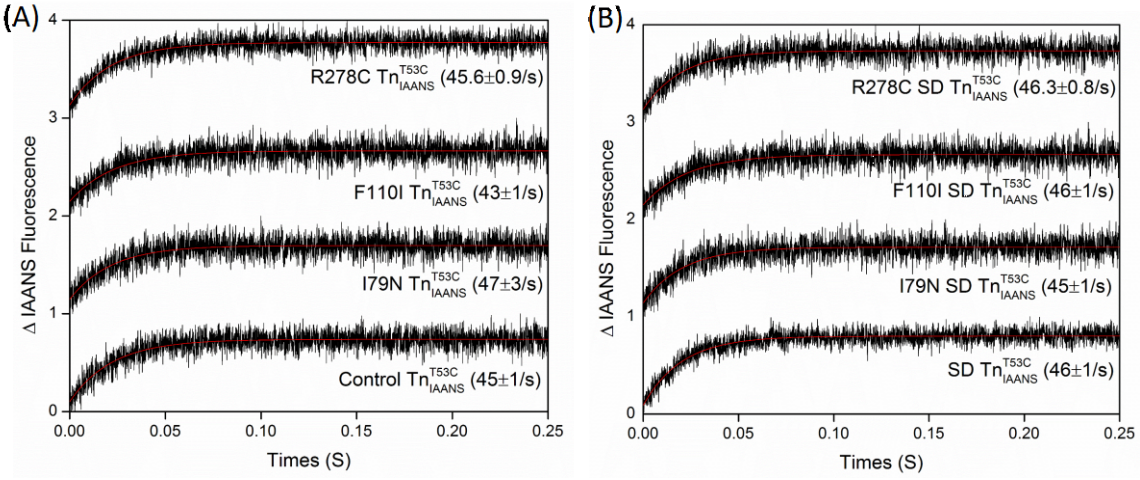

Figure 3-4 Effects of the three cTnT mutations on the rate of the Ca2+ dissociation from the cTn complexes with (A) WT cTnI and (B) SD cTnI.

Panel (A) shows the time course of the increases in IAANS fluorescence as 200 μM Ca^{2+} was removed by 10 mM EGTA from control WT cTn, I79N cTn, F110I cTn, and R278C cTn. Panel (B) shows the time course of the increases in IAANS fluorescence as 200 μM Ca^{2+} was removed by 10 mM EGTA from SD cTn, I79N SD cTn, F110I SD cTn, and R278C SD cTn.

3.3.5. Effects of the cTnT mutations with SD cTnI on the Ca^{2+} dissociation rates from RTFs

As the cTn complexes were reconstituted with Tm and actin in the RTF system, a Ca^{2+}-dependent IAANS fluorescence decrease was observed for all RTF constructs. To detect the presence of any free cTn complexes, the fluorescence was recorded over a 10-second period. At this stage, it was observed that higher concentrations of human recombinant Tm (2 µM to 4 µM) were required to ensure all cTn complexes were bound to thin filaments, compared to previous studies where native bovine Tm were used for RTF (Davis et al., 2007; Li et al., 2013a). After adjusting the Tm concentration, all RTF constructs showed a stable recording of fluorescence decrease over a 10-second period (data not shown).

RTFs containing both I79N and R278C cTnT mutations showed a significant decrease in k_{off} compared to the WT counterpart, increasing the Ca^{2+} sensitivity by ~1.2-fold and ~1.5-fold ($p<0.05$), respectively (Figure 3-5, Table 3-4). As shown in Figure 3-5, phosphomimetic cTnI significantly decreased the Ca^{2+} sensitivity of the RTF by ~2.4-fold ($p<0.05$) compared to the WT, consistent with our steady-state data as well as previous findings (Li et al., 2013a). Interestingly, all three cTnT mutations, I79N SD, F110I SD, and R278C SD RTF demonstrated a significant decrease in the k_{off} from the WT SD RTF construct by ~1.9-fold, ~1.5-fold, and ~2-fold ($p<0.05$), respectively (Figure 3-5, Table 3-4). F110I RTF, which did not show any significant difference in k_{off} values when reconstituted with WT cTnI, showed a significant decrease in k_{off} ($\Delta k_{off} = 76\ s^{-1}$) with phosphomimetic cTnI.

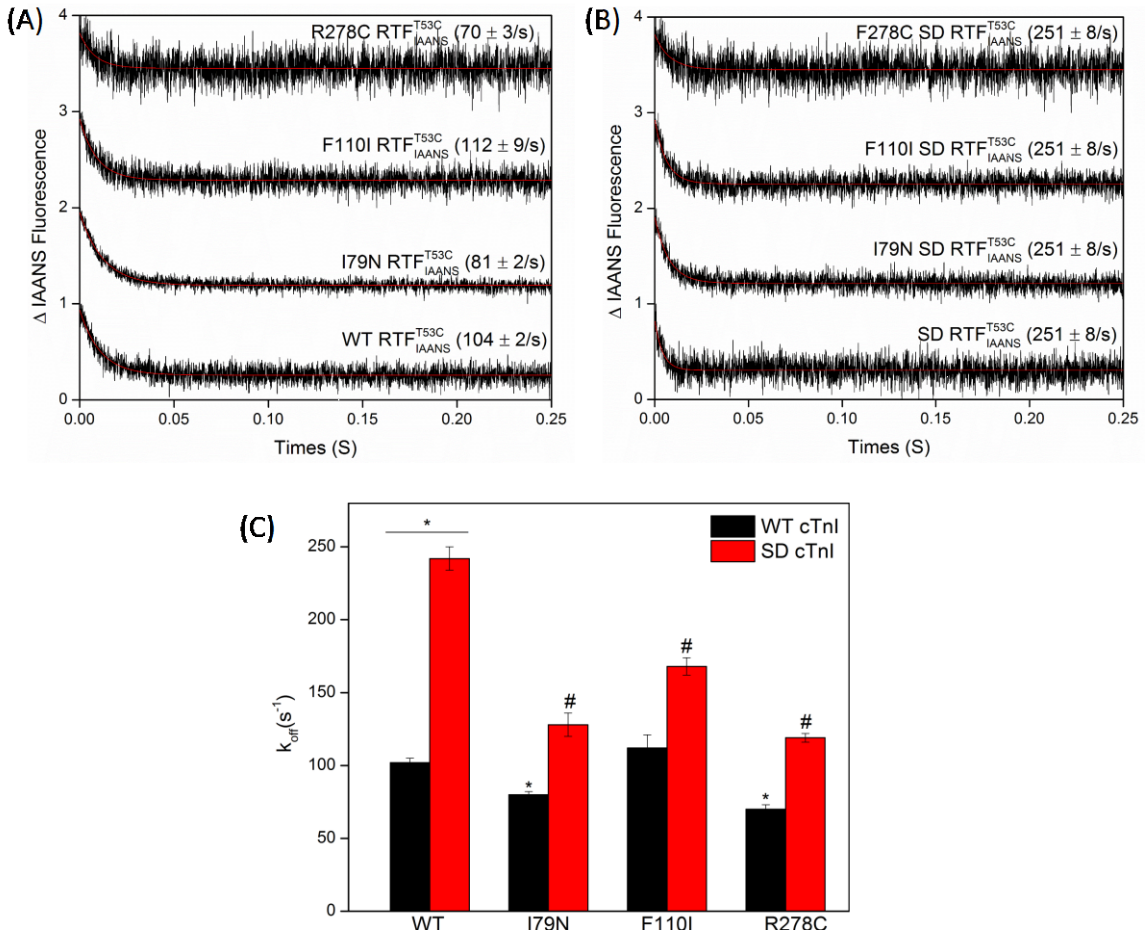

Figure 3-5 Effects of the three cTnT mutations on the rate of the Ca^{2+} dissociation from the RTF reconstituted with (A) WT cTnI and (B) SD cTnI.

Panel (A) shows the time course of the decreases in IAANS fluorescence as 200 μM Ca^{2+} was removed by 10 mM EGTA from control WT RTF, I79N RTF, F110I RTF, and R278C RTF. Panel (B) shows the time course of the decreases in IAANS fluorescence as 200 μM Ca^{2+} was removed by 10 mM EGTA from SD RTF, I79N SD RTF, F110I SD RTF, and R278C SD RTF. Panel (C) is the bar graph that shows the Ca^{2+} dissociation rates, represented by the k_{off} obtained from the fitting of the single exponential equation. Black bars represent the RTF reconstituted with WT cTnI and red bars are the ones with SD cTnI. The asterisks (*) indicates $p<0.05$ versus the WT RTF, and the pound sign (#) indicates $p<0.05$ versus the SD RTF.

Table 3-3 The Ca^{2+} binding properties of the cTn complexes using the $cTnC^{T53C}$ IAANS reporter.

cTn constructs	Kd (uM)	Hill coefficient (η)	K_{off} ($/s^{-1}$)
WT cTn^{T53C}	0.41 ± 0.06	1.76 ± 0.03	45 ± 1
I79N cTn^{T53C}	0.38 ± 0.02	1.71 ± 0.09	47 ± 3
F110I cTn^{T53C}	0.42 ± 0.02	1.44 ± 0.09	43 ± 1
R278C cTn^{T53C}	0.42 ± 0.05	1.73 ± 0.25	43 ± 1
SD cTn^{T53C}	0.31 ± 0.01	1.73 ± 0.06	47 ± 1
I79N SD cTn^{T53C}	0.31 ± 0.04	1.71 ± 0.07	45 ± 1
F110I SD cTn^{T53C}	0.35 ± 0.02	1.61 ± 0.06	46 ± 1
R278C SD cTn^{T53C}	0.37 ± 0.03	1.59 ± 0.02	46 ± 1

Table 3-4 The Ca^{2+} binding properties of the reconstituted thin filament preparation using the cTnCT53C IAANS reporter.

	K_d (μM)	Relative change in Ca^{2+} sensitivity (in folds)*	Hill coefficient (n)	k_{off} (s^{-1})	Relative change in Ca^{2+} k_{off} (in folds)*
WT RTF	2.5 ± 0.2[b]	--	2.3 ± 0.5	103 ± 2[b]	--
I79N RTF	1.5 ± 0.1[a,b]	↓1.7	3.3 ± 0.5	85 ± 2[a,b]	↓0.8
F110I RTF	1.9 ± 0.3	↓1.3	3.0 ± 0.8	112 ± 9[b]	↑1.1
R278C RTF	1.23 ± 0.04[a,b]	↓2.0	3.8 ± 0.5	70 ± 3[a,b]	↓1.5
SD RTF	5.6 ± 1.2[a]	--	1.9 ± 0.8	244 ± 8[a]	--
I79N SD RTF	3.1 ± 0.6[a,b]	↓1.8	3.1 ± 0.9	128 ± 8[a,b]	↓1.9
F110I SD RTF	2.3 ± 0.3	↓2.4	2.1 ± 0.6	168 ± 6[a,b]	↓1.5
R278C SD RTF	1.41 ± 0.02[a,b]	↓4.0	3.8 ± 0.6	119 ± 4[a,b]	↓2.1

[a] Significantly different from their respective WT values ($p<0.05$, unpaired t-test versus WT control RTF).

[b] Significantly different from their respective SD values ($p<0.05$, unpaired t-test versus SD RTF).

*All the relative changes of K_d and k_{off} for I79N, F110I, R278C RTF are in comparison to the control WT RTF, and I79N SD RTF, F110I SD RTF and R278C SD RTF are in comparison to the SD RTF.

3.4. Discussion

3.4.1. Structural prediction and sequence alignment of cTnT proteins

The N-terminal end (~first 70 amino acids) of cTnT is a hypervariable region, and to date there are no cardiomyopathy-related mutations found in this region (Tardiff, 2011). Perhaps this region is more tolerant to amino acid changes since it is highly variable and subjected to alternative splicing. PSIPRED predicted that the cTnT is composed entirely of alpha helices and a loop region (Figure 3-1). Due to its highly flexible nature, most regions of the cTnT remain structurally unsolved except for residues 199-272 that are included in the high-resolution crystal structure (PDB: 4Y99) (Takeda, 2016). However, 90% of the HCM-causing cTnT variants occur in the

unresolved region, including the three cTnT mutations assessed in the current study (Tardiff, 2011).

Sequence alignment shows that the three residues, I79, F110, and R278 are highly conserved across a broad phylogenetic spectrum from human to zebrafish, spanning an evolutionary scale of more than 400 millions of years (Figure 3-1). One can predict that any non-conserved substitution of these amino acids could have a structural impact on the rest of the thin filaments. For example, the amino acid substitution of the non-polar Ile to polar Asn at position 79 for the I79N mutation could affect the protein-protein interactions between the loop region of TnT and Tm. If this region becomes less flexible, then it could have an allosteric effect on the position of TnI in which it is less likely to bind to Tm-actin but switches its binding to the regulatory domain of TnC when TnC is bound with Ca^{2+}. This could strengthen the binding of Ca^{2+} to TnC and indirectly increase myofilament Ca^{2+} sensitivity. For the case of R278C TnT mutation, residue 278 is located at the end of the C-terminal region of TnT that is close to the docking region of Tn complexes on actin filaments based on the secondary structural prediction. The non-conserved amino acid substitution from a large, polar charged Arg to a small, less polar Cys at this position could also have an impact on how TnT interacts with the rest of the Tn complex. It could indirectly change the dynamic interactions between TnI and TnC and shift the binding equilibrium of TnI between TnC and actin. For the case of F110I mutation, the amino acid substitution from the non-polar Phe and to Ile is a more conserved substitution; nevertheless, the loss of a phenyl ring could also affect the local protein-protein interactions between TnT and Tm, indirectly affecting the TnI binding to TnC and attenuating the myofilament Ca^{2+} sensitivity. Although these three TnT mutations are located in the regions that are remote from the Ca^{2+} binding to TnC, any allosteric interactions that could affect the interactions between TnC and TnI could have an impact on myofilament Ca^{2+} sensitivity (Siddiqui et al., 2016).

3.4.2. Functional studies of the three cTnT mutations by steady-state and stopped-flow fluorescence spectroscopy

Clinically, the general consensus for patients carrying cTnT mutations is that they present with a mild left-ventricular hypertrophy or remodeling of the heart compared to other sarcomeric HCM-associated mutations, such as in myosin binding protein-C or myosin heavy chain (Knollmann and Potter, 2001). Nevertheless, the first manifestation

of the HCM could be SCD that can occur at various ages. We were particularly interested in the three cTnT mutations because transgenic mouse studies showed that they induce varying degrees of severity in arrhythmogenicity with I79N being the most severe mutation, F110I being the intermediate and R278C the least malignant (Baudenbacher et al., 2008; Schober et al., 2012). Numerous clinical, functional and animal studies have been performed to characterize the effects of these mutations. Although different animal models and/or species have been extensively used, some functional species-specific differences cannot be disregarded. Sometimes the results can be conflicting, even for the same mutation (Bai et al., 2013; Lin et al., 1996; Morimoto et al., 1998; Rust et al., 1999; Schober et al., 2012; Szczesna et al., 2000). Therefore, we used entirely human cTn subunits as well as human recombinant Tm to generate cTn complexes and RTFs.

At the cTn complex level, neither the Ca^{2+} binding affinity nor the Ca^{2+} dissociation rates were different among the various cTn complexes (Figure 3-2, Figure 3-4, Table 3-3). Likewise, no significant differences in Ca^{2+} binding affinity or kinetics of isolated adult cTn complexes containing phosphomimetic cTnI among the adult cTn complexes were observed. These results agree with previous studies in which the effects of the cardiomyopathy-associated mutations often do not manifest their effects at simplest biochemical levels (Li et al., 2013a; Liu et al., 2012b; Tikunova and Davis, 2004; Tikunova et al., 2010), although there are few exceptions, such as the case for the L48Q cTnC (Tikunova and Davis, 2004) or R37C ssTnI (Shafaattalab et al., 2019) mutation in which its ability to change Ca^{2+} sensitization is consistently demonstrated regardless of the complexity of the biochemical system.

The next level of complexity for the biochemical system in our experimental design is the reconstituted thin filaments (RTFs) which also include Tm and actin filaments. During steady-state conditions, both I79N and R278C cTnT significantly increase the Ca^{2+} sensitivity of the adult RTF, while F110I cTnT did not (Figure 3-3).

The most unanticipated results arise from the changes in the Ca^{2+} sensitivity and kinetics associated with the R278C cTnT mutation in the RTF. Previous literature suggests that it is a more benign, late-onset disease in which SCD is uncommon in young people, albeit there are a few, but is more common in older patients (Fujita et al., 2013; Garcia-Castro et al., 2003; Lin et al., 2000; Olivotto et al., 2008; Pasquale et al.,

2012; Ripoll-Vera et al., 2016; Sirenko et al., 2006; Theopistou et al., 2004; Torricelli et al., 2003; Watkins et al., 1995) (Table 3-5, supporting materials). Although the transgenic mice expressing the R278C cTnT mutation show a more benign phenotype (Baudenbacher et al., 2008; Schober et al., 2012), in our hands using human recombinant proteins, both steady-state and kinetics data show that it causes a similar magnitude of Ca^{2+} sensitization compared to that of the I79N cTnT mutation (Figure 3-3, Figure 3-5, Table 3-4). It is possible that the transgenic mice, which were 3-4 months old, might need more time to develop the pathophysiological phenotypes associated with this late-onset mutation (Hernandez et al., 2005). In addition, these were transgenic mice over expressing the mutant proteins that could have some effects on the manifestation of the phenotypes, and thus making it difficult to directly correlate the observations seen in mice to those in humans. Although mice models may provide valuable insight to the mechanisms of human diseases, one cannot disregard the fundamental differences between the mice and human myocytes, such as the heart rate (600 bpm in mice versus 60-80 bpm in human) (Wessels and Sedmera, 2003), expression of various cardiac protein isoforms (predominant β-MHC in human versus α-MHC in mice) (Krenz and Robbins, 2004), or differences in Ca^{2+} fluxes in cardiomyocytes (~92% Ca^{2+} reuptake to mice SR versus ~60-70% in larger mammals) (Bers, 2002). It is possible that some phenotypes of a particular mutation could be masked by those differences. Therefore, one should be cautious when interpreting and correlating the results obtained from mice to human studies, which has been observed in human inflammatory response studies in mice models (Seok et al., 2013). On the other hand, it is also important to note the limitation of our experimental study, which is the phenotype manifested in our set up mimics the homozygous mutation, since there is no mixture of the WT and mutant Tn complex or RTFs to mimic the heterozygous mutation seen in the patients or the animal subjects. Therefore, it is possible that the more severe phenotype that we observed for the R278C mutation is because the virtue of our experimental setup. One powerful tool is to study the human diseases in the iPSC-derived cardiomyocytes, to better correlate the results observed at the biochemical level using human recombinant proteins to human myocytes, enabling us to elucidate new mechanisms for understanding human diseases (Shafaattalab et al., 2019).

Patients with the F110I cTnT mutation have a more favorable prognosis, and in general, SCD in not common among these patients. Previous clinical reports indicate

that patients with a heterozygous F110I cTnT mutation exhibit mild hypertrophy, and some carriers were completely asymptomatic (Table 3-5) (Anan et al., 1998; Fujita et al., 2013; Lin et al., 2000). Several functional studies show that this mutation has more moderate effects on Ca^{2+} sensitivity in force generation, ATPase measurement, and susceptibility to arrhythmogenesis (Hernandez et al., 2005; Palm et al., 2001). Our data show that F110I cTnT is a more benign mutation in comparison to I79N and R278C, where it did not change the Ca^{2+} sensitivity or Ca^{2+} dissociation rates when reconstituted with WT cTnI. Nevertheless, it diminished the functional effects of phosphomimetic cTnI in the adult RTF as demonstrated in the steady-state and Ca^{2+} kinetics studies.

The prognosis for patients harboring the I79N cTnT mutation is poor as it tends to be malignant and is associated with a high rate of SCD at a young age (Menon et al., 2008; Pasquale et al., 2012; Thierfelder et al., 1994; Watkins et al., 1995). Studies on transgenic mice demonstrate that I79N cTnT significantly increases the myofilament Ca^{2+} sensitivity, which is likely culpable in an increase in susceptibility of ventricular arrhythmia (Baudenbacher et al., 2008), an increase in end-diastolic Ca^{2+} concentration at fast pacing rates, and enhanced sarcoplasmic reticulum (SR) Ca^{2+} content and release (Schober et al., 2012). The study by Schober et al. suggests that the I79N cTnT mutation prolonged Ca^{2+} binding to TnC, and it may even stay bound at the end of diastole (Schober et al., 2012). Our stopped-flow kinetic data on the I79N cTnT RTF directly supports that premise in which the Ca^{2+} dissociation rate is significantly slower with much lower k_{off} in the presence of the mutation. This prolongation may increase cytosolic Ca^{2+} during each subsequent beat, thus increasing the Ca^{2+} being removed by the sodium-calcium exchanger (NCX) of the cardiomyocytes and potentially resulting in triggered electrical activity or delayed after-depolarization (DADs). In addition, a heterozygous I79N cTnT mutation was found in a family with nine affected members and caused substantially different phenotypes indicative of restrictive cardiomyopathy (RCM), dilated cardiomyopathy (DCM), HCM and mixed cardiomyopathy within the same family (Table 3-5) (Menon et al., 2008). This example suggests that the malignant cTnT mutation results in complex cardiomyopathies with a great diversity of morphological, functional and clinical features, potentially caused by different cellular mechanisms that arise from F110I or R278C cTnT mutations.

Chronic changes in myofilament Ca^{2+} sensitivity of cardiac muscle could eventually lead to cardiomyopathy, although the link between altered Ca^{2+} properties

and a specific type of cardiomyopathy remains less clear. It is generally believed that HCM-related mutations sensitize the myofilament to Ca^{2+} and slow the mechanical relaxation, whereas DCM-associated mutations have the opposite effect where decreased myofilament Ca^{2+} sensitivity and increased Ca^{2+} dissociation are observed. Recent work done by Davis et. al. (Davis et al., 2016) has shed more light on the direct relationship between altered Ca^{2+} sensitivity and changes in myocyte growth specific to HCM or DCM. A particular mutation may change the signaling activity of the two important regulators that modify the myocyte growth in width and mass (Davis et al., 2016). The first regulator is the Ca^{2+} responsive serine-threonine phosphatase, calcineurin and its downstream transcriptional effector nuclear factor of activated T-cells (NFAT) (Houser and Molkentin, 2008), and the second one is the extracellular-signal regulated kinase, ERK1/2 (Bueno et al., 2000; Kehat and Molkentin, 2010). The signaling of these two regulators changes depending on a specific mutation, in which the ERK/12 singling dictates the changes in myocyte width whereas the activation calcineurin-NFAT signaling is associated with cardiac hypertrophy. In particular, an HCM-associated mutation, L48Q cTnC, induces concentric hypertrophy with an increase of myocyte width and cardiac mass, whereas a DCM-linked mutation, I61Q TnC, causes eccentric hypertrophy with minimal change in myocyte width but an increase in cardiac mass. In addition to thin filament mutations, mutations in the thick filament proteins, such as myosin heavy chain, also have shown to increase tension that contributes to the increased mechanical performance as one of the underlying mechanisms of HCM. Therefore, a concerted effort has been made in the past decade to develop small molecules that depress tension in HCM, with the aim to rebalance the contractility in HCM and potentially prevent or delay the disease progression before irreversible cardiac remodelling occurs (Tardiff et al., 2015).

Although it is sometimes difficult to link a particular mutation, such as I79N cTnT, to a clinically well-defined cardiomyopathy phenotype (Menon et al., 2008), it is clear that a heart needs to operate within a delicately balanced homeostatic zone of Ca^{2+} response, and any perturbation of this balance for sustained periods of time can result in maladaptive responses and have deleterious effects of the heart (Davis et al., 2016). Even in our simplified biochemical system, it is clear that mutations occurring on the same protein yet at different location result in vastly different alterations in the Ca^{2+} binding properties, demonstrating the complex nature of the cardiomyopathies.

3.4.3. Impact of the phosphomimetic cTnI on the functional changes induced by HCM-related mutations

One of the most important mechanisms that regulates the intricate Ca^{2+} fluxes and Ca^{2+} responses of the myofilaments is the PKA-phosphorylation of residue 23/24 of cTnI during β-adrenergic stimulation. These two residues were among the earliest phosphorylation sites identified on cTnI, and their modulatory effects on myofilament Ca^{2+} sensitivity are well documented. (Kobayashi and Solaro, 2005; Metzger and Westfall, 2004; Solaro and Kobayashi, 2011; Solaro and van der Velden, 2010). PKA phosphorylation serves as an important protective mechanism for the heart to meet higher physiological demands during a flight or fight response (Solaro and Kobayashi, 2011). For this reason, we generated phosphomimetic cTnI in which Ser23/Ser24 were mutated to Asp23/Asp24 to mimic the PKA-phosphorylated state of the cTnI.

In the RTF with phosphomimetic cTnI, all three cTnT mutations significantly diminished the Ca^{2+} desensitization effects associated with phosphomimetic cTnI (Figure 3B, 5B). Our thin-filament kinetic data consistently agree with our steady-state studies in which both I79N and R278C cTnT significantly decrease the Ca^{2+} dissociation rate when reconstituted with both WT cTnI and phosphomimetic cTnI. In addition, the seemly more benign F110 RTF, which did not demonstrate any significant changes in Ca^{2+} sensitivity and Ca^{2+} dissociation rates when reconstituted with WT cTnI, also shows a significant decrease in Ca^{2+} dissociation rate when phosphomimetic cTnI is included in the RTF. Our steady-state and the kinetic data clearly show that all three HCM-associated cTnT mutations abolish the functional effects of phosphomimetic cTnI, a phenomenon consistent with our previous study on one of the HCM-associated cTnC mutations (Li et al., 2013a) and other cTnT mutations (Messer et al., 2016). This delayed Ca^{2+} dissociation from cTnC could result in an increase of diastolic Ca^{2+} concentration, thereby increasing the propensity for arrhythmias because the amount of Ca^{2+} released must be extruded from the cell via electrogenic NCX. This outcome corroborates well with the fact that reduced phosphorylation of cTnI, among other PKA-phosphorylation targets such as phospholamban and myosin-binding protein C, occurs in the failing heart due to diastolic dysfunction (Li et al., 2013a; Lovelock et al., 2012; Messer et al., 2016). Recently it has been shown that the attenuation of the increased myofilament sensitivity, in particular, via the incorporation of the phosphomimetic cTnI, can delay and even prevent the progression of the HCM phenotype. Specifically, the increased myofilament

Ca^{2+} sensitivity of a mouse with HCM-associated E180G tropomyosin mutation was significantly reduced when these mice were crossed with other mice expressing the phosphomimetic cTnI. This indicates an important role for desensitizing myofilaments to Ca^{2+} as a one of the therapeutic targets for HCM patients (Alves et al., 2014).

3.5. Conclusions

Our study shows that among the three cTnT mutations, I79N and R278C have the highest Ca^{2+} sensitizing effects at the thin-filament level. I79N cTnT has consistently been shown in previous clinical reports to be a malignant mutation in which the patient prognosis is poor and SCD is common among the youth. It is clear that the I79N mutation demonstrates the marked increase of the Ca^{2+} sensitivity both in our hands and in Knollmann's studies in transgenic mice with high susceptibility to arrhythmia associated with this mutation (Baudenbacher et al., 2008; Schober et al., 2012). The most surprising result found in our study using RTFs is that R278C cTnT also appears to be a severe mutation that significantly increases Ca^{2+} sensitivity. It has been clinically suggested that the prognosis of R278C cTnT is more favorable compared to I79N in terms of SCD onset (Elliott et al., 1999), and in transgenic mice studies R278C cTnT behaves similarly to the WT (Baudenbacher et al., 2008; Schober et al., 2012). In our system, which represents the homozygous mutation, the phenotype manifested could be more severe than the heterozygous mutation seen in the patients or the transgenic mice. In addition, a protracted longitudinal study could potentially help to observe the long-term effects of the R278C cTnT in those animal subjects. Furthermore, it is possible that younger patients died due to this mutation remained undocumented before the widespread use of next-generation DNA sequencing techniques to perform routine mutational screening for family members of a proband. It is therefore difficult to draw definitive genotype-phenotype conclusions because the number of patients carrying these mutations is very limited. In the presence of phosphomimetic cTnI, all three mutations significantly diminished the functional effects of the phosphomimetic cTnI, rendering the RTFs to have higher Ca^{2+} sensitivity. This suggests that the protective adaption of β-adrenergic desensitization of the myofilament is compromised. Our kinetic data directly support that HCM-associated cTn mutations increase myofilament Ca^{2+} sensitivity, thereby slowing the rate of Ca^{2+} dissociation from cTnC. Therefore, the

delayed Ca^{2+} and force transients could result in diastolic dysfunction in a more physiological scenario.

In conclusion, the cardiac thin filament is a multi-subunit, allosterically regulated complex that is fully dependent on the precise coordinated movements of all protein components. Any disruption of this highly tuned molecular complex can result in pathological consequences. Our *in vitro* study shows that increasing myofilament Ca^{2+} sensitivity and uncoupling of the functional effects of phosphomimetic cTnI are caused by these cTnT mutations at the thin-filament level. These are factors that increase the pro-arrhythmogenic susceptibility at the cellular level which has been recently shown by iPSC-CMs harboring the I79N cTnT mutation (Wang et al., 2018). Linking genotype to phenotype for a particular HCM mutation remains a challenge since the phenotypic outcomes are often complex and diverse. The presence of modifier genes, additional mutations, epigenetic differences and environmental factors could all contribute to the complexity of the disease (Tardiff, 2011; van der Velden et al., 2015). Current treatments can only provide relief from symptoms but do not target specific HCM pathways. Therefore, understanding the molecular mechanism of these HCM-associated mutations, as demonstrated in our current study that examined changes at the biochemical level of the thin filaments, is crucial to provide information regarding altered Ca^{2+} binding properties and help develop specific therapies that address the underlying cause of the disease.

Table 3-5 Summary of the clinical reports for patients harbouring I79N, F110I and R278C cTnT mutation.

R278C cTnT mutation							
Study	*Family/Patient	Age at the time of the study /sex	Age of diagnosis (year)	LVMT (mm)	Presentation	Symptoms	Mortality
Ripoll-Vera et al. 2015 (180 families)	12 proband	47/M	18	23	Routine ECG	no	no
	12 father	71/M	57	35	Routine ECG	LVOT Obstruction	no
	12 cousin	40/M	37	16	Family screening	no	no
	13 proband	41/F	37	18	Dyspnea	no	no
	13 brother	44/M	42	22	Family screening	no	no
	13 mother	75/F	N/A	10	Mutation carrier	no	no
	14 proband	68/M	55	30	Chest pain	VT	no
	14 daughter	29/F	N/A	9	Mutation carrier	no	no
Pasquale et al. 2012 (552 unrelated HCM patients)	1 patient	44/F	26	23	Resuscitate after ventricular fibrillation	VF	no
	2 patient	65	N/A	N/A	Heart failure	VT	yes
Olivotto et al. 2008 (203 unrelated HCM patients)	2 probands	N/A	N/A	N/A	Mutation Carriers	N/A	no
Theopistou et al. 2004 (143 patients)	A-proband (IV-1)	40/M	33	22	Asymmetric septal hypertrophy	LVOT obstruction	no
	A-mother (III-6)	68/F	50	after 40	Arterial hypertension	AF	yes
	A-aunt (III-14)	64/F	64	after 40	Abnormal echo and ECG	mild concentric hypertrophy, arterial hypertension, paroxysmal AF	no

	A-aunt's first son (IV-14)	41/M	N/A	N/A	Mutation carrier; no hypertrophy; normal echo and ECG	no	no
	A-aunt's second son (IV-16)	38/M	N/A	N/A	Mutation carrier; no hypertrophy; normal echo and ECG	no	no
	A-aunt's granddaughter (V-11)	14/F	N/A	N/A	Mutation carrier; no hypertrophy	no	no
	A-3 family members (III-8, III-10, II-4)	64/M, 62/M, 70/M	N/A	N/A	N/A	sudden death	yes
	B-proband (II-2)	15/M	13	23	Parents and sister had normal echo and ECG but refused further genetic testing; no family history of SCD	die during doing daily normal activities	yes
Driest et al. 2003 (389 unrelated HCM patients)	1 patient	57/M	54	20	Asymptomatic	none	no
	2 patient	66/M	31	15	Angina	Dyspnea	no
	3 patient	74/M	69	23	Dyspnea	Dyspnea	no
Torricelli et al. 2003 (150 unrelated HCM patients)	1 proband	66/M	62	24	LOVT Obstruction	LVH, T-wave inversion V4-V6	no
Castro et al. 2003 (30 unrelated HCM patients)	1 proband	60/F	60	22	Hypertrophy	severe concentric hypertrophy	no
	1 sister	55/F	N/A	normal	Mutation carrier; no hypertrophy	no	no
	1 daughter	35/F	N/A	normal	Mutation carrier; no hypertrophy	no	no

Watkin et al. 1995 (27 families)	1 patient	17/F	17	normal	resuscitated after cardiac arrest	cardiac arrest	Yes
	Family WW - 3 members	N/A	N/A	16 +/-6	family screening	no	1 death
F110I cTnT mutation							
Study	Family/Patient	Age at the time of the study /sex	Age of diagnosis (year)	LVMT (mm)	Presentation	Symptoms	Die
Fujita et al. 2013 (173 unrelated HCM patients)	A-proband (III-2)	12/F	12	<20	sinus rhythm, CRBBB, Vf survivor	LVH, ASH, LV relaxation abnormalities; with additional R139C cTnT mutation from the mother.	no
	A-brother (III-1)	deceased	14	<20	SR, CRBBB	LVH, ASH, LV relaxation abnormalities; with additional R130C TnT mutation from the mother.	yes
	A-father (II-6)	55/M	N/A	<20	mild HCM	CAVB, LV relaxation abnormalities	no
	A-uncle (II-1)	deceased	N/A	N/A	mild HCM	CAVB	yes
Anan et al 1998 (46 HCM patients)	KC proband (II-1)	38/F	N/A	27	unexplained cardiac hypertrophy by ECG and echo	LOVT obstruction	no
	KD proband (II-1)	69/F	N/A	22	unexplained cardiac hypertrophy by ECG and echo	Type III LVH; ST-T	no
	KD sister	deceased	33	N/A	N/A	died suddenly	yes

	KD daughter (III-1)	47/F	N/A	20	unexplained cardiac hypertrophy by ECG and echo	Type III LVH; ST-T	
	KE proband (I-1)	87/F	N/A	16	Chest pain	Type IV LVH; ST-T	no
	KE son (II-1)	48/M	N/A	15	family screening	Type IV LVH; ST-T	no
	KE daughter (II-2)	42/F	N/A	11	family screening	None	no
	KF proband (II-1)	64/M	N/A	23	Hypertrophy	Type II LVH; ST-T	no
	KG proband (III-1)	24/F	N/A	20	family screening	Type IV LVH; ST-T	no
	KG maternal grandfather (I-1)	70/F	N/A	20	family screening	ST-T	no
	KG mother (II-2)	47/F	N/A	13	family screening	Type III LVH; ST-T	no
	KG uncle (II-3)	45/M	N/A	12	family screening	ST-T	no
	KG aunt (II-4)	39/F	N/A	13	family screening	Type III LVH; ST-T	no
	KH proband (II-1)	56/F	56	19	unexplained cardiac hypertrophy by ECG and echo	ST-T	no
	KH brother (II-2)	53/M	N/A	15	family screening	ST-T	no
	KH sister	deceased	N/A	N/A	N/A	N/A	yes
	KH daughter (III-1)	31/F	N/A	21	family screening	ST-T	no
	KH daughter (III-2)	28/F	N/A	10	family screening	ST-T	no
Lin et al. 2000 (14 individuals of the same family)	I-1	72/M	N/A	17	family screening (hetero)	type II LVH; SVPC; ST-T;	no
	I-3	69/F	N/A	11	family screening	N/A	no
	I-4	65/F	N/A	29	family screening (hetero)	ST-T and Q abnormality	no
	I-5	58/F	N/A	18	family screening (hetero)	type II LVH; ST-T and Q abnormality	no

	II-1	54/M	N/A	19	family screening (homo)	type III LVH; RVH, RSC, AF, abnormalities of ST-T and Q wave	no
	II-2	49/M	N/A	21	family screening (homo)	RVH, RSC, abnormalities of ST-T waves	no
	II-3	deceased	18/F	N/A	N/A	died while running	yes
	II-4	45/F	N/A	8	family screening	N/A	no
	II-5	43/F	N/A	10	family screening (hetero)	N/A	no
	II-6	41/M	N/A	17	family screening (hetero)	abnormalities of ST-T waves	no
	II-7	37/F	N/A	9	family screening (hetero)	N/A	no
	II-8	34/F	N/A	7	family screening	N/A	no
	III-1	16/M	N/A	10	family screening	N/A	no
	III-2	12/M	N/A	7	family screening (hetero)	N/A	no
	III-3	6/F	N/A	6	family screening (hetero)	N/A	no
Watkins et al, 1995 (27 families)	2 patients	N/A	N/A	17	Echo and ECG screening	hypertrophy	no
I79N cTnT mutation							
Study	Family/Patient	Age at the time of the study /sex	Age of diagnosis (year)	LVMT (mm)	Presentation	Symptoms	Die
Thierfelder et al, 1994 (5 families); Watkins et al. 1995 (27 families)	Family AW	N/A	N/A	~ 13	Echo and ECG screening	N/A	5 deaths

Menon et al. 2008 (17 individuals of the same family)	II-11 proband	63/M	53	14	RCM: dyspnea on exertion, palpitations and exercise intolerance	AF, SB, RAD, AVB, LBBB, LAE, ST-T	No
	I-1 Mother	Deceased at 71	N/A	N/A	N/A	Heart disease	Yes
	I-2 Father	Deceased at 94	N/A	N/A	N/A	Stroke	yes
	II-2 sister	deceased at 64	50	N/A	DCM: right heart enlargement	Heart failure	Yes
	II-4 sister	deceased at 73	68	normal	DCM: AF and signs of heart failure	AF/AFL, SB, BFB, LAE, ST-T; heart failure	Yes
	II-6 sister	70/F	66	N/A	HCM: asymmetrical septal hypertrophy	NSVT, BAE, ST-T, LVH	no
	II-7 brother	deceased at 69	46	N/A	Mixed cardiomyopathy: found during routine ECG	AF/AFL	Yes (due to cancer)
	II-9 brother	69/M	58	normal	RCM: dyspnea on exertion and AF	AF, RAD, LAE, ST-T, LVH	no
	III-3 niece	49/F	49	N/A	HCM: initial pulmonary hypertension	LAVE, IRBBB, ST-T	no
	III-4 niece	45/F	40	N/A	HCM: asymmetrical septal hypertrophy	SVT, LAE, LVH, ST-T	no
	III-6 niece	51/F	48	N/A	Echo screening showed mild left atrial enlargement.	SB	no
Pasquale 2012 (552 unrelated HCM patients)	1 proband	deceased	16	9	no echo abnormalities	N/A	yes
	1 cousin	deceased	N/A	N/A	N/A	Death due to complications during an ICD lead extraction.	yes

LVMT: left ventricular myocardial thickness; N/A: Not available; ECG electrocardiography; VT: ventricular tachycardia; LVOT: left ventricular outflow tract; AF: atrial fibrillation; Echo: echocardiography; LVH: left ventricular hypertrophy; ASH; Asymmetric septal hypertrophy; LV: left ventricle; CAVB: complete right bundle branch block; ST-T: non-specific ST-T wave changes; SVPC: supraventricular premature contraction; RVH: right ventricular hypertrophy; RSC: reversed septal curvatures; SB, sinus bradycardia; RAD, right axis deviation; AVB, atrioventricular block, LBBB, left bundle branch block; LAE, left atrial enlargement; BFB, bifascular block; AFL, atrial flutter; RAD, right axis deviation; SVT, supraventricular tachycardia; LAV, left atrial enlargement. IRBBB: incomplete right bundle branch block.

*Family/patient's assignment in letters and numbers are obtained from the original clinical reports.

Chapter 4.

Altered Ca^{2+} binding properties of cardiomyopathy-related troponin I and troponin T mutations in fetal and adult cardiac thin filaments

Note regarding contributions:

Part of the data presented in this chapter was published in the Proceedings of the National Academy of Sciences, USA. The authors and the full reference for the article are listed below:

Shafaattalab S., **Li A.Y.**, Lin E., Stevens C.M., Dewar L., Lynn F.C., Sanatani S., Laksman Z., Morin R.D., van Petegem F., Hove-Madsen L., Tieleman D.P., Davis J.P., and Tibbits G.F. (2019). In vitro analyses of suspected arrhythmogenic thin filament variants as a cause of sudden cardiac death in infants. *Proc Natl Acad Sci USA*. Vol 116, Issue 14, Pages 6969-6974.

4.1. Introduction

In the last two decades, advances in and availability of genetic testing have lead to the discovery of a large number of previously unknown mutations associated with various types of cardiomyopathies (Ho et al., 2015). Most of the mutations are found in the sarcomeres, which are the basic building units of cardiac muscles. Sarcomeric mutations are one of the most common causes of sudden cardiac death (SCD) in patients between 20 and 50 years old (Wijnker et al., 2018). Some patients have earlier onset, under the age of 18, and as such are categorized with the pediatric cardiomyopathies (Lee et al., 2017). Pediatric cardiomyopathies are considered rare diseases with an incidence of 1.1 to 1.5 per 100,000 in children under 18 years of age (Lee et al., 2017). Despite the low incidence of pediatric cardiomyopathies, often the first presenting event can be cardiac arrest or sudden death in a previously healthy child, which is devastating for their parents and families (Lee et al., 2017). Therefore, identifying patients at risk for cardiomyopathies is important in risk stratification, and periodic screening for the children of the affected individuals throughout childhood can be beneficial. Children who carry the variant gene can be followed closely for disease development over a range of several years and given trials for intervention to prevent progression of the phenotype.

Despite the similarities between adult and pediatric cardiac morphologies in various cardiomyopathies, they have distinct clinical outcomes, requiring different treatments (Colan, 2010). For example, in the case of dilated cardiomyopathy (DCM), which is characterized by dilation and enlargement of the left ventricle, is the most common cause for heart transplantation in children (Tatman et al., 2017). Medications that are routinely used in treating adult heart failure associated with DCM do not improve the outcomes in children (Patel et al., 2017). In the case of hypertrophic cardiomyopathy (HCM), which is the most commonly inherited cardiovascular disease and the leading cause of SCD in young adults, the left ventricular muscle thickens, resulting in a decrease in the size of the ventricular chamber (Houston and Stevens, 2014). The use of Implantable Cardioverter Defibrillator (ICD) is proven to be beneficial for some adult patients with an elevated risk of HCM-associated ventricular arrhythmia (Trivedi and Knight, 2016), but it is less effective in children than in adults (Alexander et al., 2004). The risk of device-related infections, ICD lead failures and complications, psychosocial impact is higher in children (Eicken et al., 2006; Opic et al., 2012). Although sudden

death is rare in pediatric HCM, deaths are clustered before the age of 1 and again between the ages of 8 and 17 (Lee et al., 2017). Regardless of the types of the cardiomyopathies, specific tests used for identifying at-risk adults, such as elevations in cardiac troponins, specific arrhythmia patterns, or blunted blood pressure response to exercise testing, have not been routinely assessed in children (Lee et al., 2017). Therefore, there is a clear need to establish clinical trials and design new approaches that can be used to identify the risk of the heart failure in children and to prevent the disease progression as they grow.

It is not surprising that adult and pediatric cardiomyopathies have very different outcomes. It is known during development of the heart, sarcomeric proteins undergo paralog/isoform switches to meet the specific demands of the structural and physiological changes of the cardiac muscle (Marston and Redwood, 2003). Each sarcomere is composed of parallel arrays of thick and thin filaments. Thick filaments consist primarily of the protein myosin, whereas thin filaments are composed of actin filaments, tropomyosin (Tm), and troponin (Tn) complexes. In particular, we will focus on the paralog and isoform switches of the thin filaments components, and how the isoform/paralog switches affect two cardiomyopathy-associated mutations occurring in the Tn complex.

Existing information suggest that α-actin remains the main isoform in both the fetal and adult hearts (Vandekerckhove et al., 1986). Developmental changes in human cardiac tropomyosin are not very well characterized, but α-Tm is the main isoform isolated from human cardiac samples (Purcell, 1999), although some literature suggests the transition of β-Tm to α-Tm increases during fetal myocardial development in mice (Muthuchamy et al., 1993). In contrast, troponin isoform/paralog switching has been well characterized in the developing heart (Metzger et al., 2003). Specifically, distinct TnT isoforms and TnI paralogs are expressed during the fetal to mature heart transition, and are responsible for the Ca^{2+} dependent regulation of contractile activities. These differentially regulated expressions affect the Ca^{2+} sensitivity of the myofilament as well as distinct response of adult and fetal myofilament response to hypoxia and acidosis, and β-adrenergic stimulation in adult and fetal systems (Fentzke et al., 1999; Marston and Redwood, 2003; Metzger et al., 2003; Wolska et al., 2001). The developmental transitions of human cardiac thin filament expression are summarized in Table 4-1 and more details pertaining to TnC, TnI and TnT switching are described.

Table 4-1 Developmental transitions of human thin filament protein expression (modified from Martson and Redwood, 2003) (Marston and Redwood, 2003).

Protein	Fetal Gene	Neonatal Gene	Adult Gene
Actin	Mainly α cardiac Some skeletal	Mainly α cardiac Some skeletal	α cardiac
Tropomyosin	mainly α-fast	Mainly α-fast	Mainly α-fast
TnC	cardiac	cardiac	cardiac
TnI	slow	slow/cardiac	cardiac
TnT	cTnT1/cTnT3	some cTnT1/mainly cTnT3	cTnT3

The cardiac slow skeletal isoform of the *TNNC1* gene, which encodes troponin C (TnC) protein, is expressed throughout development in both the fetal and adult heart. Unlike TnI and TnT, cardiac slow skeletal TnC is the only isoform that expresses exclusively in the heart (Li and Hwang, 2015). It differs from skeletal TnC in that it only contains three functional ion-binding sites: sites II, III, and IV, instead of four functional EF hand motifs that function as ion-binding sites in skeletal TnC (Li and Hwang, 2015). In site III and IV of TnC, they almost always bind to Mg^{2+} under physiological conditions, maintaining the structural integrity of TnC and interacting with the rest of the Tn complexes. Site II is the main Ca^{2+} sensing site, binding to Ca^{2+} when the increase of intracellular Ca^{2+} concentration rises from the nano-molar range to the micro-molar range. Binding of Ca^{2+} then opens the hydrophobic binding pocket of TnC and triggers a cascade of protein conformational changes that leads to muscle contraction. Hence, TnC is the most important Ca^{2+} sensor in the thin filaments, which regulate muscle contraction and relaxation.

TnI has two distinct paralogs, slow skeletal TnI (ssTnI), expressed from the *TNNI1* gene and cardiac TnI (cTnI), expressed from the *TNNT3* gene (Sheng and Jin, 2016). The term paralog is used since ssTnI and cTnI are expressed from two different genes. ssTnI is the predominant TnI paralog expressed in the heart throughout fetal/neonatal life, with its expression gradually decreasing until 8-9 months of age (Saggin et al., 1989; Sasse et al., 1993). cTnI then becomes the main paralog around 9 months postnatal and remains the predominant form throughout adult life, even in the failing heart (Saggin et al., 1989; Sasse et al., 1993). The major difference between the two paralogs lies in the first 31-residues in the N-terminal domain, which are only present

in the cardiac paralog. The sequence identity for the rest of cTnI and ssTnI is ~63%. As indicated in Figure 4-1, this specific cardiac N-terminal domain contains two phosphorylation sites, Ser23/Ser 24, that are absent in the ssTnI paralog. The functional significance of the two Ser23/Ser24 is well documented and explained in more detail in Chapter 3. Briefly, during β-adrenergic stimulation, Ser23/Ser24 act as two substrates for PKA phosphorylation. Phosphorylation of these two residues results in decreasing myofilament Ca^{2+} sensitivity and increasing cross-bridge cycling kinetics, accelerating cardiac muscle relaxation. In addition to PKA phosphorylation, PKC also phosphorylates three residues - Ser 43, Ser 45, and Thr 144 - resulting in an increase of Ca^{2+} sensitivity (Pi et al., 2002).

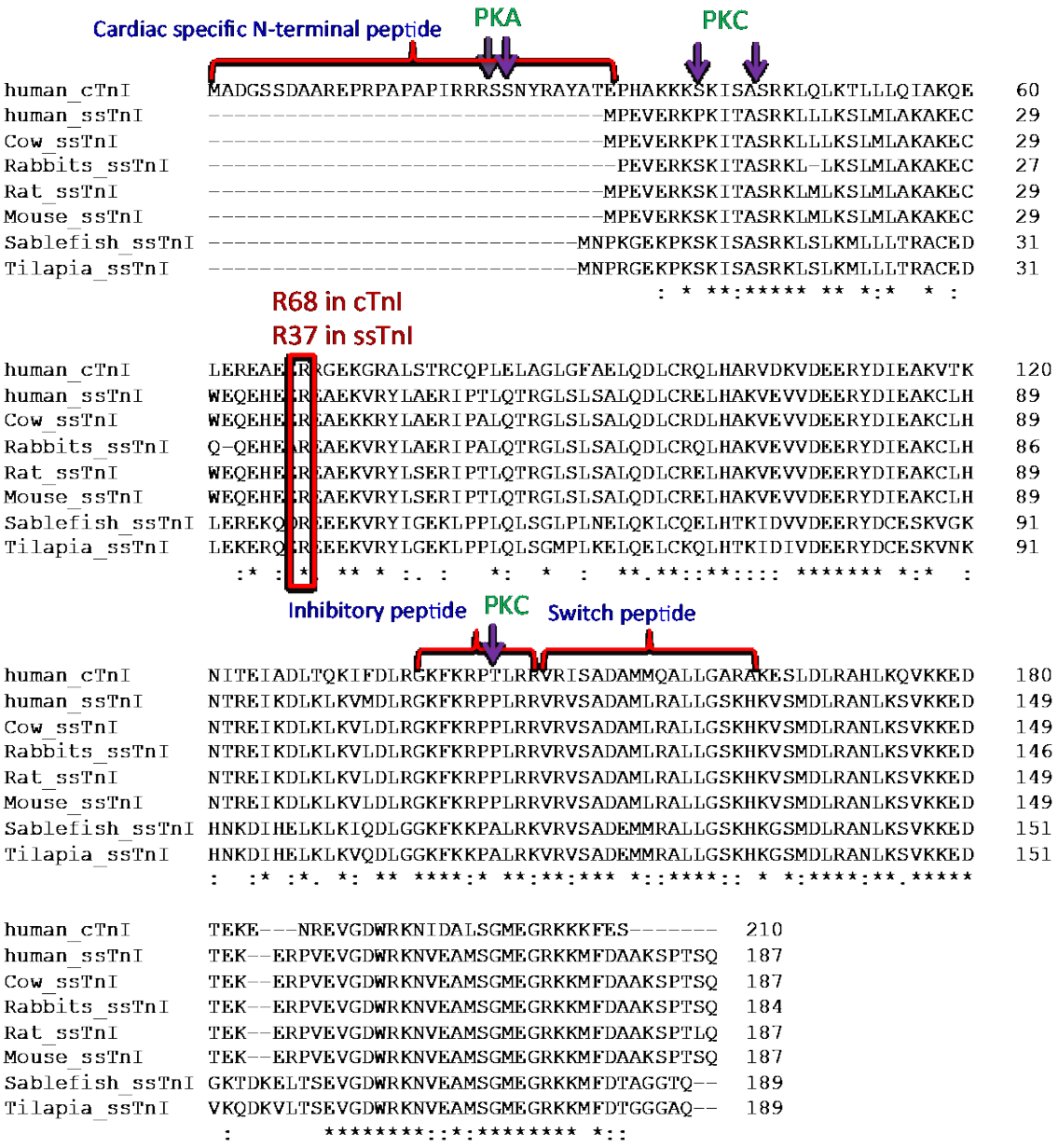

Figure 4-1 Sequence alignment among human cTnI, human ssTnI and ssTnI from various species.

The sequence from each species was obtained from Uniprot: human cTnI (P19429), human ssTnI (P48788), cow ssTnI (F8SWQ9), rabbit ssTnI (P02645), mouse ssTnI (Q9WUZ5), sablefish ssTnI (C3KHJ0), and tilapia ssTnI (I3KBM6). Important regions and phosphorylation sites specific to cTnI are indicated by purple arrows. PKA phosphorylates Ser23 and Ser24 of cTnI during β-adrenergic stimulation, resulting in a decrease in Ca^{2+} sensitivity, whereas PKC phosphorylates Ser43, Ser45, and Thr144, causing an increase in Ca^{2+} sensitivity. Important regions of cTnI include the cardiac specific N-terminal (residues 1-32), inhibitory peptide spans (residues 137-146), and switch peptide region (residues 148-163). The mutation of interest--Arg at 37 in ssTnI, corresponding to Arg 68 in cTnI--is a highly conserved residue across many different species. Sequence alignments were generated using ClustalOmega (Sievers et al., 2011).

The *TNNT2* gene encodes the four human cardiac TnT isoforms: TnT1, TnT2, TnT3 and TnT4, as a result of alternative splicing (Gomes et al., 2002) (Figure 4-2). In the fetal heart, TnT1, TnT2, and TnT4 are expressed, with TnT1 being the predominant form. As the heart goes through perinatal development, the expression level of TnT1 decreases as TnT3 increases until TnT3 becomes the predominant isoform expressed in the adult heart. TnT4 may be re-expressed in the failing adult heart. TnT1, the isoform that expresses predominantly in fetal hearts, has both exons 4 and 5 whereas TnT3 has exon 5 sliced out. The four isoforms have a molecular weight of 30-33 kDa and range from 223 to 305 residues due to the variable length of the N-terminal region. Only the N-terminal region is highly variable, due to alternative splicing while the amino acid sequences of the middle and C-terminal domains are highly conserved (Gomes et al., 2002). So far, no pathogenic point mutations have been identified in the hypervariable region, whereas multiple mutations associated with HCM have been located outside of the hypervariable region, indicating the highly plastic nature and hence higher tolerance for mutations within the N-terminal variable region (Tardiff, 2011).

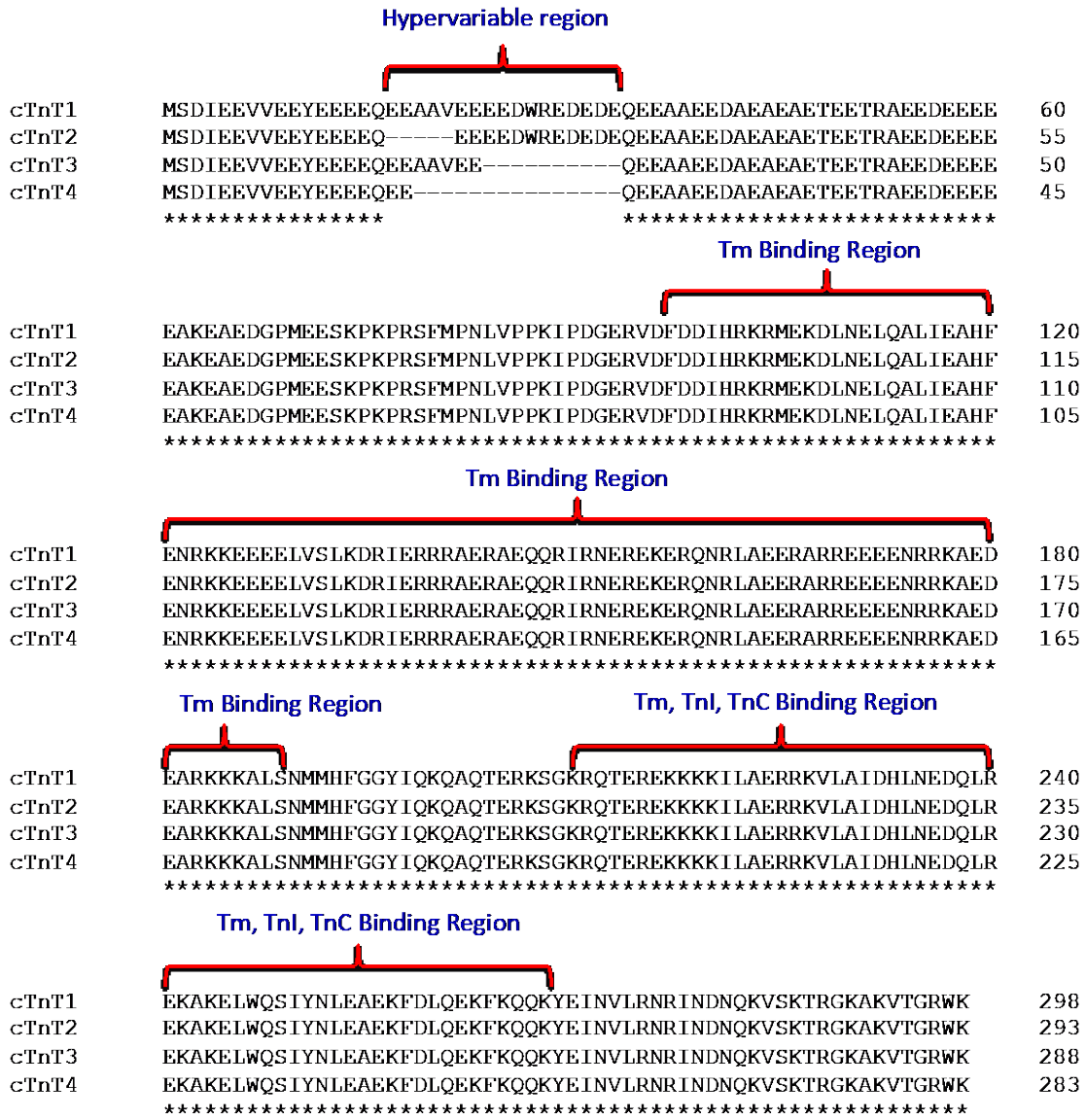

Figure 4-2 Sequence alignemnt of the human four cTnT isofroms encdoning from the *TNNT2* gene (Uniprot ID: P45379).

The sequences of the cTnT isoforms, from cTnT1 to cTnT4, were obtained from Uniprot with ID: P45379. cTnT1 is the predominant form in fetal cTnT. cTnT2 lacks exon 4, which translate to amino acid residues 17-21. cTnT3 lacks exon 5, which corresponds to amino acid residues 24-33. cTnT3 is the predominant cTnT isoform found in the adult heart. cTnT4 has residues 19-33 missing compared to the canonical cTnT1 sequence. The hypervariable region corresponds to the amino acids translated from exon 4 and exon 5. The sequence alignment was generated using Clustal Omega (Sievers et al., 2011).

Since both TnI and TnT go through the paralog/isoform switch during development, we are particularly interested in investigating two cardiomyopathy mutations associated with poor diagnosis. First is the Arg to Cys mutation at residue 37

(R37C) found in ssTnI, which is the paralog of TnI found in the neonatal heart. R37C ssTnI is a novel heterozygous variant discovered in 10 infants out of 191 post mortem tissues obtained from infants/children who died suddenly and unexpectedly (Dewar et al., 2017). To our knowledge, this is the very first ssTnI mutation that has been found to be associated with any of the cardiomyopathies linked to the human *TNNI1* gene (Dewar et al., 2017; Sheng and Jin, 2016).

All infants died under the age of 20 months with this mutation, and we have previously shown that this mutation is associated with arrhythmogenicity in cardiomyocytes generated from the induced human-pluripotent cells (Shafaattalab et al., 2019). The fact that this identical mutation occurs to 10 infants makes it unlikely a *de novo* mutation, suggesting that at least one of their parents is a mutational carrier. However, it is unknown as to why and how parents of these infants survived past the fetal/neonatal stage carrying this mutation. We generated a corresponding mutation, R68C cTnI, in the adult thin filaments and examined the changes in the Ca^{2+} sensitivity and binding kinetics of this particular mutation in hopes of answering this mystery.

The second mutation is the I79N cTnT mutation found in young patients. It is associated with a high rate of SCD (Wang et al., 2018; Watkins et al., 1995). This particular mutation is mostly associated with HCM, although it has been found associated with dilated cardiomyopathy (DCM), restrictive cardiomyopathy (RCM), and even mixed cardiomyopathy (Menon et al., 2008). The prognosis of patients associated with the I79N cTnT mutation is poor, with mild or no hypertrophy detected in the echocardiography (Knollmann and Potter, 2001). It will be intriguing to discover how these patients carry this mutation past the fetal and neonatal stages. To find the answer, we generated an equivalent mutation in fetal cTnT, I89N, and investigated the altered Ca^{2+} binding properties of adult and fetal Tn complexes and RTF harbouring this mutation.

The various combinations of fetal and adult Tn complexes and RTF containing these mutations are listed in Table 4-2. In this study, we investigated their impact on the Ca^{2+} sensitivity and binding kinetics of their corresponding mutation in the adult and fetal counterparts. The main goal was to gain insight into how the paralog/isoform switches impact Ca^{2+} handling at the biochemical level in the Tn complexes and RTF. In addition, since cardiac failure is often associated with changes in protein phosphorylation--in

particular, the phosphorylation of Ser23/Ser24 of the adult cTnI paralog, we also included the phosphomimetic cTnI (Ser23/Ser 24 mutated to Asp23/Asp24) in the adult thin filaments. These two phosphorylation sites are specific to adult cTnI since the fetal ssTnI lacks the 31 residues where the two phosphorylation sites reside in its N-terminal domain.

Table 4-2 List of protein constructs in the fetal and adult Tn complexes and thin filament preparation.

Protein	Gene Name	Description	Length	Molecular Weight (kDa)*	Extinction Coefficient ($M^{-1}cm^{-1}$)*	Uniprot ID
WT $cTnC^{T53C}$	*TNNC 1*	Full length TnC with three mutations (T53C, C35S, C84S) for fluorescence, labeling specifically at T53C for functional studies.	161	18	4470	P63316
Adult Troponin I and Troponin T Subunits						
WT cTnI	*TNNI3*	Full length WT cardiac TnI.	211	24	9970	P19429
SD cTnI	*TNNI3*	Full length TnI with Ser23 and Ser24 mutated to Asp23 and Asp24 to mimic the phosphorylation of cTnI.				
WT cTnT3	*TNNT 2*	Full length WT cTnT isoform 3, the predominant adult cTnT isoform.	288	35	16960	P45379
I79N cTnT	*TNNT 2*	Full length cTnT with I79N mutation (isoform cTnT3).				
Fetal Troponin I and Troponin T Subunits						
WT ssTnI	*TNNI1*	Full length slow skeletal TnI, which differs from adult cTnI because it lacks the N-terminal specific cardiac domain of residues 1-31.	187	22	14105	P19237
R37C ssTnI	*TNNI1*	Full length ssTnI with R37C mutation.				
WT cTnT1	*TNNT 2*	Full length WT cTnT isoform 1, the predominant fetal cTnT isoform.	298	36	22460	P45379
I89N cTnT	*TNNT 2*	Full length WT cTnT with I89N mutation.				
Other constructs						
Alpha MAS-Tm	*TPM1*	Full length Tm with the additional tri-peptide (Met-Ala-Ser) added to the N-terminus to mimic acetylation process in native Tm and ensure its binding to actin filaments.	287	33	8940	P09493

Our data showed that the fetal cTnT isoform (cTnT1) did not show the increased Ca^{2+} sensitivity produced by the equivalent adult I79N cTnT mutations. In addition, the fetal R37C ssTnI and its adult corresponding R68C cTnI mutation both cause effects on Ca^{2+} binding kinetics. In particular, R37C ssTnI significantly decreases myofilament Ca^{2+} sensitivity and increases Ca^{2+} dissociation from TnC, whereas R68C cTnI shows the reverse trend of Ca handling. Our data suggest that the cTnT-HCM mutations are "rescued" when they occur in the fetal Tn environment due to the presence of ssTnI and the fetal cTnT1 isoform. However, a severe mutation, such as R37C occurring in the ssTnI, can produce detrimental effects that are also unlikely to be benign in the adult Tn environment.

4.2. Materials and Methods

All protocols describing the thin filament protein expression and purification, generation of Tn complexes and reconstituted thin filaments, data collection using the steady-state and the stopped flow fluorescence spectrometry are described in Chapter 2. All cTn complexes generated specific to this chapter with various combinations of cTnI and cTnT are listed in Table 4-3.

Table 4-3 List of Tn complexes used in the current chapter.

Recombinant cTn complexes for data collection*	Composition
Adult Tn complexes	
WT Tn	WT $cTnC^{T53C}$, WT cTnI, WT cTnT3
R68C Tn	WT $cTnC^{T53C}$, R68C cTnI, WT cTnT3
I79N Tn	WT $cTnC^{T53C}$, WT cTnI, I79N cTnT3
I79N SD	WT $cTnC^{T53C}$, SD cTnI, I79N cTnT3
Fetal Tn complexes	
Fetal WT	WT $cTnC^{T53C}$, WT ssTnI, WT cTnT1
R37C Tn	WT $cTnC^{T53C}$, R37C ssTnI, WT cTnT1
I89N Tn	WT $cTnC^{T53C}$, WT ssTnI, I89N cTnT1

*Both the molecular weights and extinction coefficients were calculated by ProtParam (Wilkins et al., 1999).

All cTn and RTF utilized in this study were labeled with IAANS at the T53C position with the two additional mutations C35S and C84S (Davis et al., 2007). For simplicity, Tn complexes and RTF constructs mentioned in the text do not have T53C superscript and IAANS subscript included.

*All the RTF constructs contained the above various cTn complexes with 2 to 4 μM Tm and 4 μM actin filaments.

4.3. Results

4.3.1. Differences in the Ca^{2+} binding properties of the WT fetal and adult Tn complexes and reconstituted thin filaments (RTF)

At the Tn complex level, measurable Ca^{2+} dependent IAANS fluorescence decreases were observed for all Tn complexes. The K_d for these complexes were within the range of 0.35-0.42 μM, and there were no significant differences in the Ca^{2+} sensitivity in any of the Tn complexes (Table 4-4). Moreover, from the Ca^{2+} binding kinetics experiments, a Ca^{2+}-dependent increase in IAANS fluorescence was observed for all Tn complexes. All Tn complexes have a k_{off} in the range of 45 s^{-1} to 47 s^{-1} and no significant differences were observed among them (Table 4-4).

Figure 4-3 A shows the Ca^{2+}-dependent decreases in IAANS fluorescence in both fetal and adult Tn complexes obtained from the steady-state experiments. The Ca^{2+} sensitivity of fetal Tn was 1.75-fold lower than that of adult Tn (comparison of K_d values shown in Table 4.4). To determine the differences in Ca^{2+} kinetics in fetal and adult Tn complexes, EGTA-induced time courses of Ca^{2+} dissociation from Tn reported by an increase in IAANS fluorescence was performed in the stopped-flow apparatus (Figure 4-3 B). Consistent with fetal Tn exhibiting a higher Ca^{2+} sensitivity than adult Tn, the rate of Ca^{2+} dissociation from fetal Tn was ~4 fold lower than that of adult Tn (Table 4-4). Hill coefficients associated with adult Tn were generally higher than that of fetal Tn (Table 4-4). They were within a range of 1.12-1.7, indicating some positive cooperativity among Tn complexes.

Introducing the next level of complexity, by adding actin and MAS-Tm to form the reconstituted thin filaments (RTF), Figure 4-3 C and D shows the Ca^{2+} sensitivity and Ca^{2+} dissociations for comparison of the fetal and adult RTF. Fetal RTF had a 3-fold increase of Ca^{2+} sensitivity compared to adult RTF in the steady-state experiment (Figure 4-3 C). Table 4-5 shows that the Hill coefficients associated with RTF were within a range of 2.1-3.8, which was expected since more components were included in the system and they induced a positive cooperativity Ca^{2+} binding process. Figure 4-3 D shows the EGTA-induced Ca^{2+}-dependent fluorescence decrease as the Ca^{2+} was rapidly removed from the adult and fetal RTF. Consistent with the lower Ca^{2+} sensitivity presented when Tn was incorporated in the RTF, both adult RTF and fetal RTF showed

a higher k_{off} than the isolated Tn by ~2.3 fold and ~7 fold, respectively. Furthermore, fetal RTF also has a 1.4-fold lower k_{off} compared to that of the adult RTF (Table 4-5).

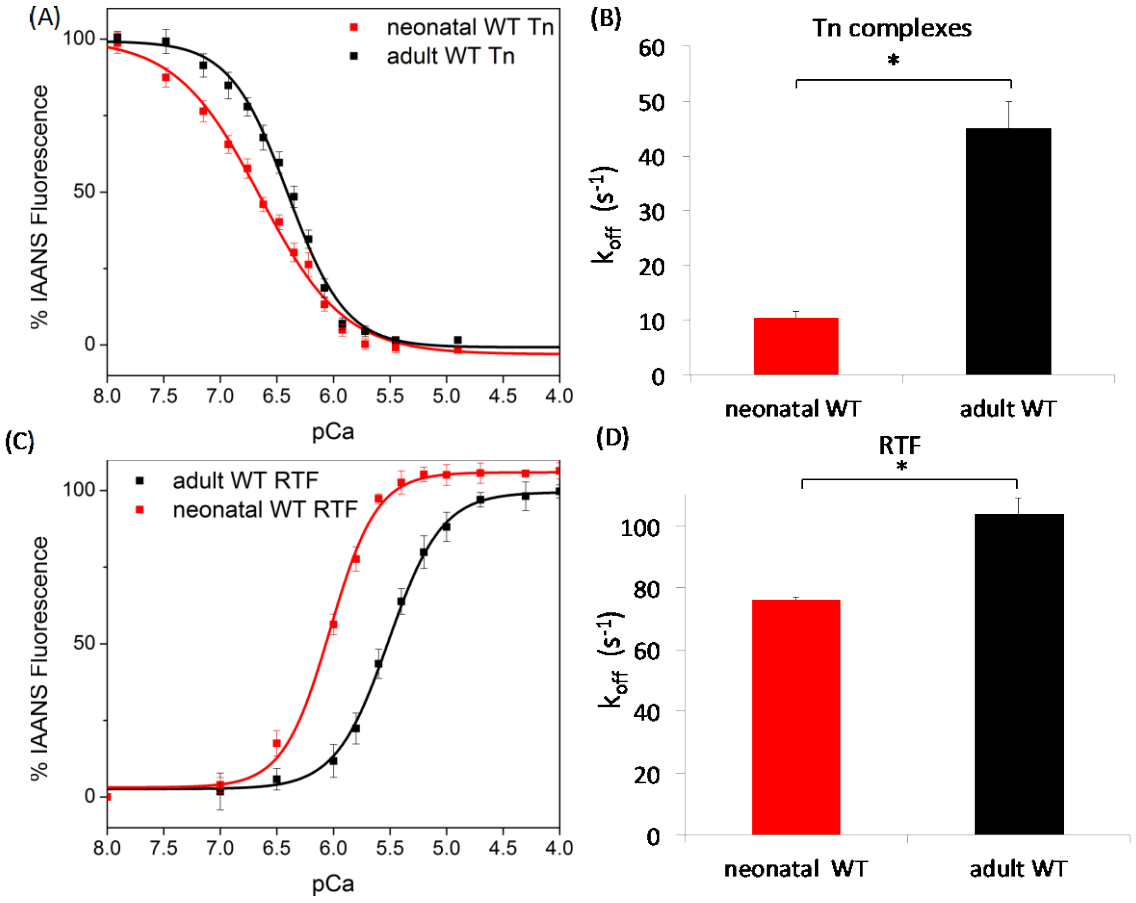

Figure 4-3 Ca^{2+} binding properties and Ca^{2+} dissociation rates from the WT fetal and WT adult Tn complexes and RTF.

Panel (A) shows the change in fluorescence, represented by % IAANS fluorescence in WT adult Tn (black) and WT fetal Tn (red) as a function of free Ca^{2+}. The data were normalized by setting the fluorescence at pCa 8.0 as 100% and the fluorescence at pCa 4.0 equal to 0. Panel (B) shows the Ca^{2+} dissociation rate, k_{off} (s^{-1}) of neonatal (red) and adult (black) WT Tn complexes determined by stopped-flow fluorescence. Panel (C) shows the change in fluorescence for the WT adult RTF (black) and WT fetal RTF (red) as a function of free Ca^{2+}. The data were normalized by setting the fluorescence at pCa 8.0 as 0% and pCa 4.0 as 100%. Panel (D) shows the Ca^{2+} dissociation rate, k_{off} (s^{-1}) of neonatal (red) and adult (black) WT RTF determined by stopped-flow fluorescence.

Table 4-4 Summary of the Ca^{2+} binding properties of the Tn complexes.

cTn constructs*	K_d (μM)	Hill coefficient (η)	k_{off} (s^{-1})
Adult Tn complexes			
WT cTn^{T53C}	0.35 [C] ± 0.02	1.73 ± 0.02	45[C] ± 1
SD cTn^{T53C}	0.31 [C] ± 0.02	1.73 ± 0.06	47[C] ± 1
I79N cTn^{T53C}	0.38 [C] ± 0.02	1.71 ± 0.09	47[C] ± 3
I79N SD cTn^{T53C}	0.31 [C] ± 0.04	1.71 ± 0.07	45[C] ± 1
R68C cTn^{T53C}	0.49 [C] ± 0.08	1.64 ± 0.07	50[C] ± 3
Fetal Tn complexes			
WT cTn^{T53C}	0.20 [a, b] ± 0.02	1.17 [a,b] ± 0.05	10.4 [a,b] ± 0.6
I89N cTn^{T53C}	0.31 [c] ± 0.04	1.12 [a,b,c] ± 0.04	13.3 [a,b,c] ± 0.4
R37C cTn^{T53C}	0.36 [c] ± 0.02	1.34 [a,b,c] ± 0.04	14.3 [a,b,c] ± 0.2

*For simplicity, the superscript "T53C" is omitted throughout the text of this chapter.

Significantly different from adult WT Tn values ($p<0.05$, unpaired t-test).

Significantly different from adult SD Tn values ($p<0.05$, unpaired t-test).

Significantly different from fetal WT Tn values ($p<0.05$, unpaired t-test).

Table 4-5 The Ca^{2+} binding properties of the reconstituted thin filament preparation.

	K_d (μM)	Relative change in Ca^{2+} sensitivity (in folds)	Hill coefficient (n)	k_{off} (s^{-1})	Relative change in Ca^{2+} k_{off} (in folds)*
Adult RTF					
WT RTF^{T53C}	2.8 ± 0.2[b,c]	--	2.2 ± 0.5	104 ± 5[b, c]	--
SD RTF^{T53C}	5.6 ± 1.2[a,c]	↑2.0*	2.1 ± 0.9	244 ± 8[a, c]	↑2.3
I79N RTF^{T53C}	1.5 ± 0.1[a,b,c]	↓1.9*	3.3 ± 0.5	81 ± 2[a, b, c]	↓1.3
I79N SD RTF^{T53C}	3.1 ± 0.7[a,b,c]	↓1.8[#]	3.0 ± 0.8	128 ± 8[a, b, c]	↓1.9
R68C RTF^{T53C}	1.8 ± 0.1[a,b,c]	↓1.6*	3.8 ± 0.5	83 ± 2[a, b, c]	↓1.3
Fetal RTF					
WT RTF^{T53C}	0.9 ± 0.2[a,b]	--	3.1 ± 0.9	76 ± 1[a, b]	--
I89N RTF^{T53C}	1.0 ± 0.1[a,b]	--	2.1 ± 0.6	78 ± 4[a, b]	--
R37C RTF^{T53C}	1.3 ± 0.1[a,b,c]	↑1.4[¶]	3.8 ± 0.6	104 ± 6[b, c]	↑1.4

Significantly different from adult WT Tn values ($p<0.05$, unpaired t-test).

Significantly different from adult SD Tn values ($p<0.05$, unpaired t-test).

Significantly different from fetal WT Tn values ($p<0.05$, unpaired t-test).

*relative change in comparison to adult WT RTF; # relative change in comparison to adult RTF; ¶ relative change in comparison to fetal WT RTF.

4.3.2. Effects of the I79N cTnT mutation on the Ca^{2+} binding properties of the adult Tn complexes and RTF

At the Tn complex level, there were no significant differences between the I79N Tn complex and the WT complex in both the steady-state (Figure 4-4 A) and the stopped-flow (Figure 4-4 B) experiments. At the RTF level, the differences in Ca^{2+} sensitivity and Ca^{2+} dissociation among different RTF constructs became evident. I79N showed a leftward shift of the IAANS-fluorescence pCa curve compared to the WT (Figure 4-4 C) and demonstrated a significant increase of Ca^{2+} sensitivity by ~1.7 ($p<0.05$) (Table 4-5). In addition, agreeing with the steady-state data, RTF containing the

I79N cTnT mutation show a significant decrease in k_{off} compared to WT counterpart, decreasing the Ca^{2+} dissociation rate by ~1.2 fold (Figure 4-4 D, Table 4-5).

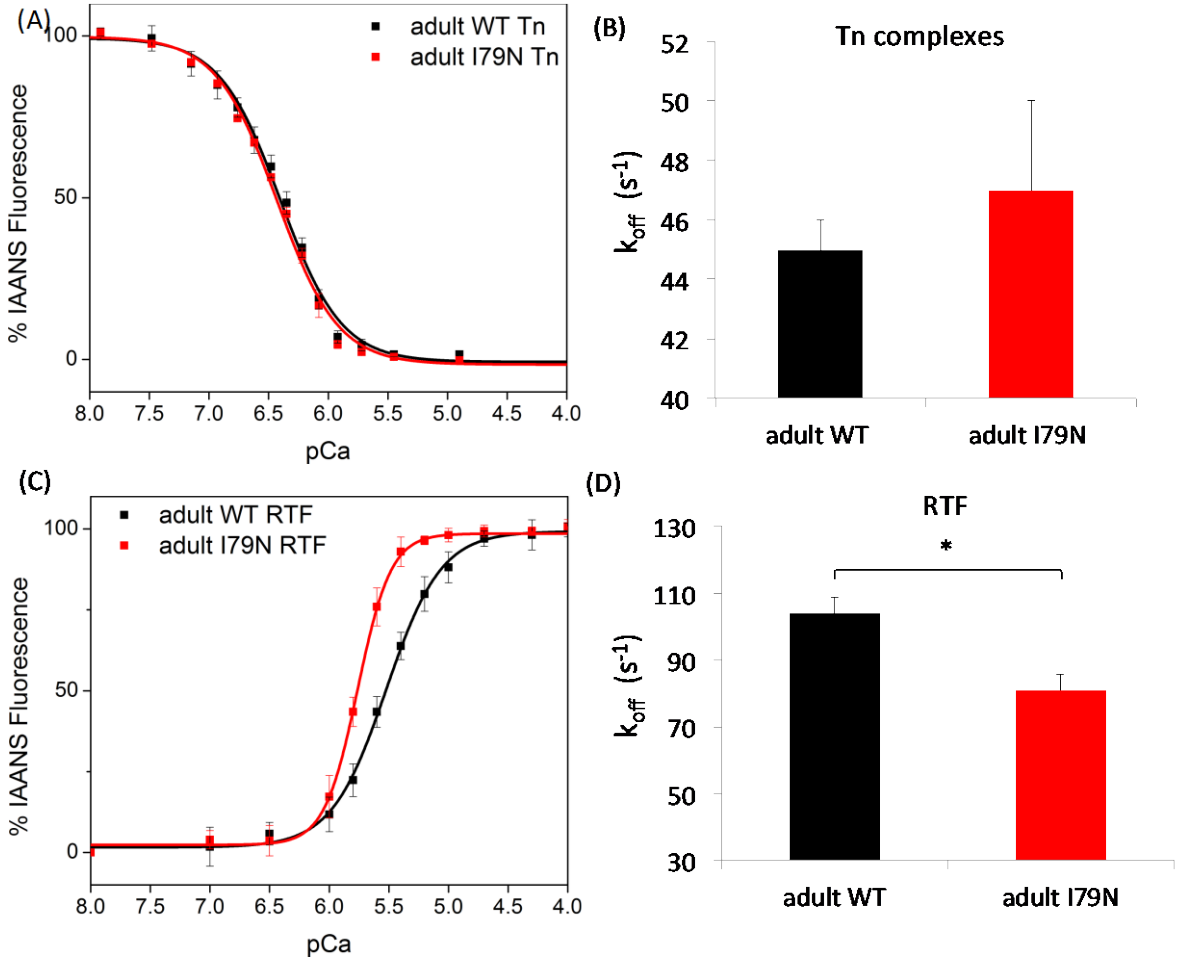

Figure 4-4 Effects of the I79N cTnT mutation on the Ca^{2+} binding properties and Ca^{2+} dissocation rate in adult cTn complexes and RTF.

Panel (A) shows the Ca^{2+} dependent decrease in IAANS fluorescence of adult WT and I79N cTn. Panel (B) shows the Ca^{2+} dissociation rate, k_{off} (s^{-1}) of adult WT (black) and I79N (red) Tn complexes determined by stopped-flow fluorescence. Panel (C) shows the Ca^{2+}-dependent increase in IAANS fluorescence of adult WT RTF and I79N RTF. Panel (D) shows the Ca^{2+} dissociation rate, k_{off} (s^{-1}) of adult WT (black) and I79N (red) RTF determined by stopped-flow fluorescence.

4.3.3. Effects of the I79N cTnT mutation on the Ca^{2+} binding properties with phosphomimetic cTnI of the adult Tn complexes and RTF

Many of the cardiomyopathy-associated Tn mutations down-regulate and desensitize the β-adrenergic stimulation. At the level of the myofilaments, these

mutations reduce the degree of Ca^{2+} desensitization on the PKA phosphorylated Ser23/Ser24 of cTnI. This process is specific to adult myocardium since the fetal ssTnI lacks the first 31 residues at the N-terminal domain where the two phosphorylation sites Ser23/Ser24 are located. For this reason, Ser 23/Ser 24 phosphomimetic cTnI mutated to Asp23/Asp24 (namely SD cTnI) were included in the adult Tn and RTF for the following data collection.

At the Tn complex level, the Ca^{2+} sensitivity (Figure 4-5 A) or the Ca^{2+} dissociation (Figure 4-5 B) was different for the complexes containing SD cTnI with and without the cTnT mutation. As predicted, at the RTF level, the Ca^{2+} sensitivity for SD RTF containing SD cTnI was 2.2-fold lower compared to that of the WT ($p<0.05$) (Table 4-5). This confirms that *in vitro* RTF is able to recapitulate the functional effects of SD cTnI in physiological conditions. The I79N cTnT mutation significantly increased the Ca^{2+} sensitivity by ~1.8 fold ($p<0.05$) compared to the SD RTF (Figure 4-5 C, Table 4-5). RTF containing the I79N cTnT mutation shows a significant decrease of k_{off} compared to their WT counterpart, decreasing the Ca^{2+} dissociation by ~1.2 fold ($p<0.05$), respectively (Figure 4-5 D, Table 4-5). SD cTnI significantly increased the Ca^{2+} dissociation of the RTF by ~2.4 fold ($p<0.05$) compared to the WT, consistent with our steady-state data.

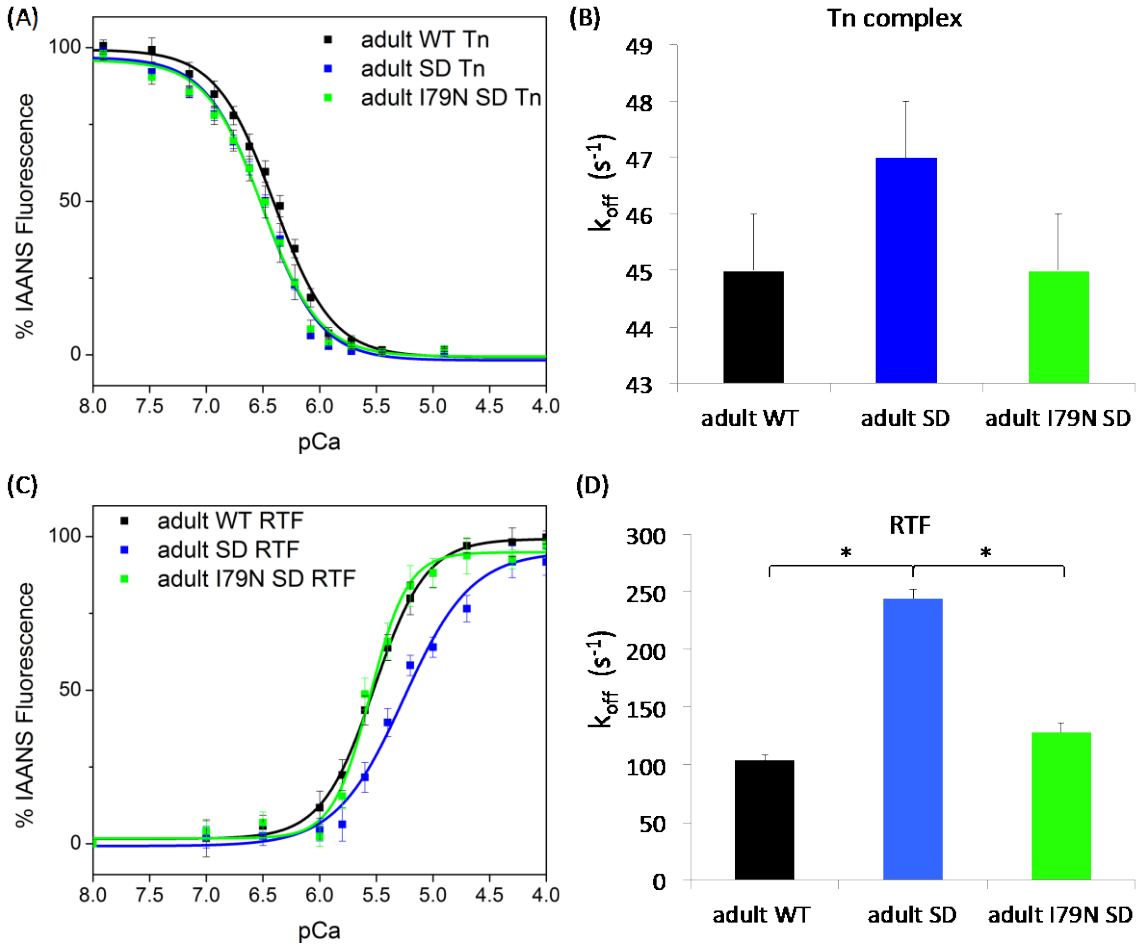

Figure 4-5 Effects of the I79N cTnT mutation on the Ca^{2+} binding properties and Ca^{2+} dissocation rate with the SD cTnI in adult cTn complexes and RTF.

Panel (A) shows the Ca^{2+} dependent decrease in IAANS fluorescence of the adult WT cTn, SD cTn, and I79N SD cTn. Panel (B) shows the Ca^{2+} dissociation rate, k_{off} (s^{-1}) of adult WT (black), SD (blue) and I79N SD (green) Tn complexes determined by stopped-flow fluorescence. Panel (C) shows the Ca^{2+} -dependent increase in IAANS fluorescence of adult WT RTF, SD RTF, and I79N SD RTF. Panel (D) shows the Ca^{2+} dissociation rate, k_{off} (s^{-1}) of adult WT (black), SD (blue) and I79N SD (green) RTF determined by stopped-flow fluorescence.

4.3.4. Effects of the fetal I89N cTnT mutation on the Ca^{2+} binding properties of the fetal Tn complexes and fetal RTF

To determine the effects of the I79N mutation in the fetal environment, the corresponding mutations were generated in the fetal isoform of cTnT1, which contains exon 4, translating to 10 extra amino acid residues compared to that of the adult isoform of cTnT3. Unlike the adult Tn complexes in which no significant differences were observed, the fetal I89N Tn complexes showed a significant increase in K_d by ~1.6 fold

(Figure 4-6 A, Table 4-4). Correspondingly, fetal I89N Tn complexes also significantly increase the k_{off} by 1.4-fold (Figure 4-6 B, Table 4-4).

Interestingly, when the fetal I89N Tn complexes were reconstituted with actin and Tm, no differences in the Ca^{2+} sensitivity (Figure 4-6 C) or Ca^{2+} dissociation rates (Figure 4-6 D) were observed. The significant Ca^{2+} binding and disassociation changes observed in the isolated fetal Tn complex were diminished in the fetal RTF.

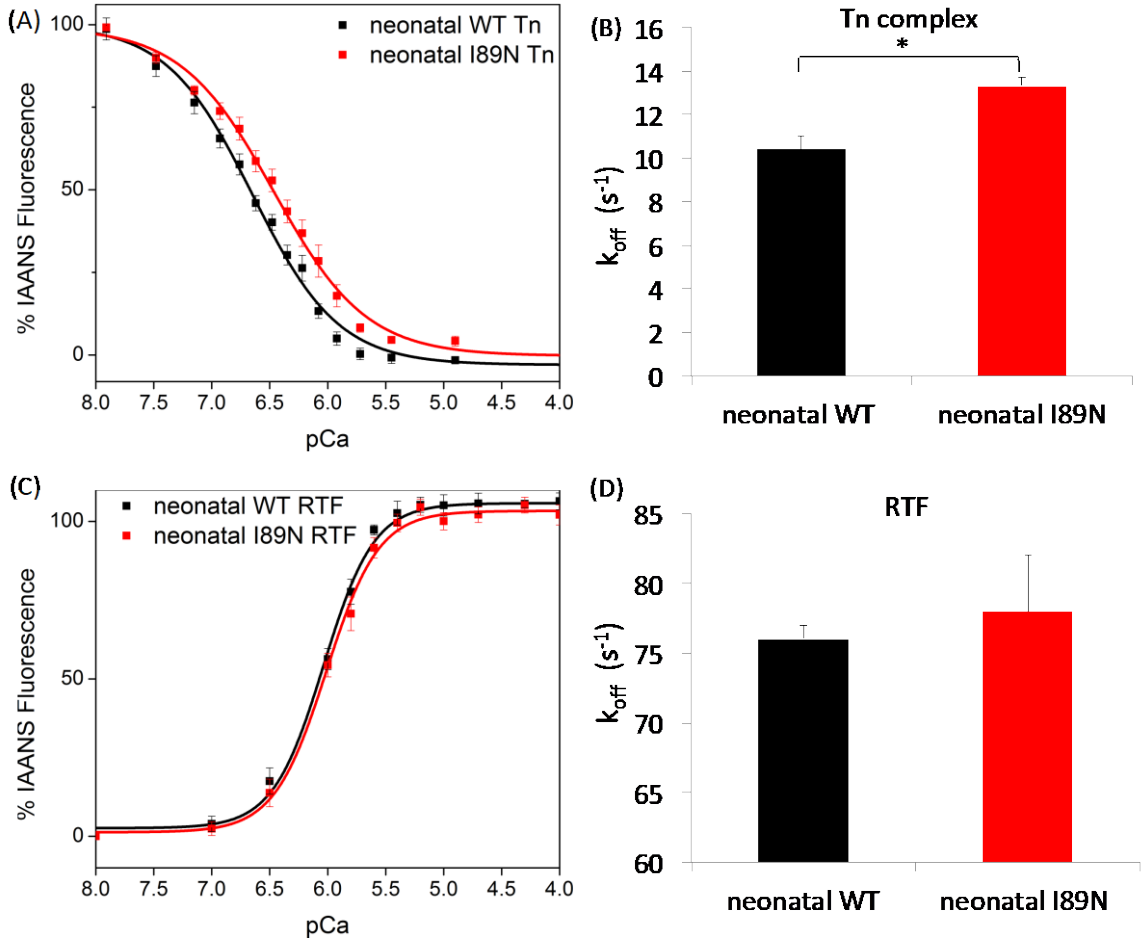

Figure 4-6 Effects of the I89N cTnT mutation on the Ca^{2+} binding properties and Ca^{2+} dissociation rate in fetal Tn complexes and RTF.

Panel (A) shows the Ca^{2+} dependent decrease in IAANS fluorescence of fetal WT and fetal I89N Tn complex. Panel (B) shows the Ca^{2+} dissociation rate, k_{off} (s^{-1}) of neonatal WT (black) and I89N (red) Tn complexes determined by stopped-flow fluorescence. Panel (C) shows the Ca^{2+} dependent increase in IAANS fluorescence of fetal WT RTF and I89N RTF. Panel (D) shows the Ca^{2+} dissociation rate, k_{off} (s^{-1}) of neonatal WT (black) and I89N (red) RTF determined by stopped-flow fluorescence.

4.3.5. Effects of the R37C ssTnI mutation on the Ca^{2+} binding properties in the fetal Tn complexes and RTF

At the Tn complex level, R37C ssTnI decreased the Ca^{2+} sensitivity in the steady-state conditions, as demonstrated in the rightward shift of the fluorescence pCa curve with a ΔpCa of 0.16 ($p<0.05$) (Figure 4-7 A) It also significantly increases the Ca^{2+} dissociation rate with Δk_{off} of 28 s^{-1} compared to that of the fetal WT Tn (Figure 4-7 B).

Similar Ca^{2+} desensitization effects, associated with R37C ssTnI, are also observed in the fetal RTF system. Figure 4-7 C demonstrates that when R37C ssTnI was reconstituted in the fetal RTF, it induced a rightward fluorescence-pCa curve, increasing the K_d by ~1.3 fold (Table 4-5). Consistent with the lower Ca^{2+} sensitivities of the R37C RTF, it increased the Ca2+ dissociation rate with a k_{off} that was nearly identical as the adult WT RTF (Figure 4-7 D, Table 4-5).

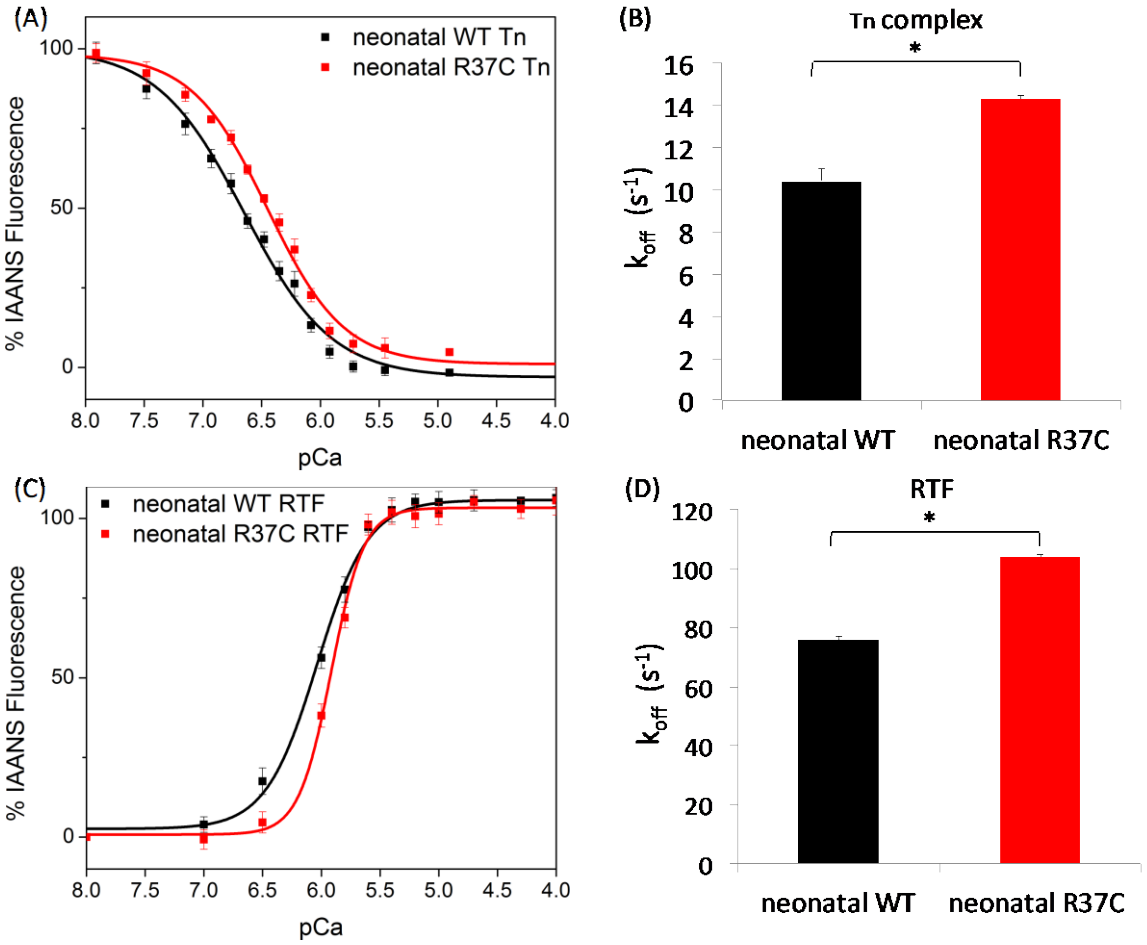

Figure 4-7 Effects of the R37C ssTnI mutation on the Ca^{2+} binding properties and Ca^{2+} dissociation rate in fetal Tn complexes and RTF.

Panel (A) shows the Ca^{2+} dependent decrease in IAANS fluorescence of fetal WT and fetal R37C Tn complex. Panel (B) shows the Ca^{2+} dissociation rate, k_{off} (s^{-1}) of neonatal WT (black) and R37C (red) Tn complexes determined by stopped-flow fluorescence. Panel (C) shows the Ca^{2+} dependent increase in IAANS fluorescence of fetal WT RTF and R37C RTF. Panel (D) shows the Ca^{2+} dissociation rate, k_{off} (s^{-1}) of neonatal WT (black) and R37C (red) RTF determined by stopped-flow fluorescence.

4.3.6. Effects of the R68C ssTnI mutation on the Ca^{2+} binding properties in the adult Tn complexes and RTF

To examine the corresponding mutation of R37C in the cTnI paralog, the R68C mutation was introduced in cTnI and reconstituted into the adult Tn complex and adult RTF. As predicted, at the Tn complex level, no significant differences were observed for either Ca^{2+} sensitivity (Figure 4-8 A) or Ca^{2+} dissociation rates (Figure 4-8 B) compared

to those of the WT. However, at the adult RTF level, this corresponding R68C cTnI mutation causes the adult thin filaments to have a higher Ca^{2+} sensitivity as demonstrated in the leftward shift curve from that of the WT (Table 4-5). It decreased the K_d by ~1.6 fold (Figure 4-8 C) and increases the k_{off} by ~1.2 fold (Figure 4-8 D), which is the opposite of how R37C ssTnI behaved in the fetal RTF.

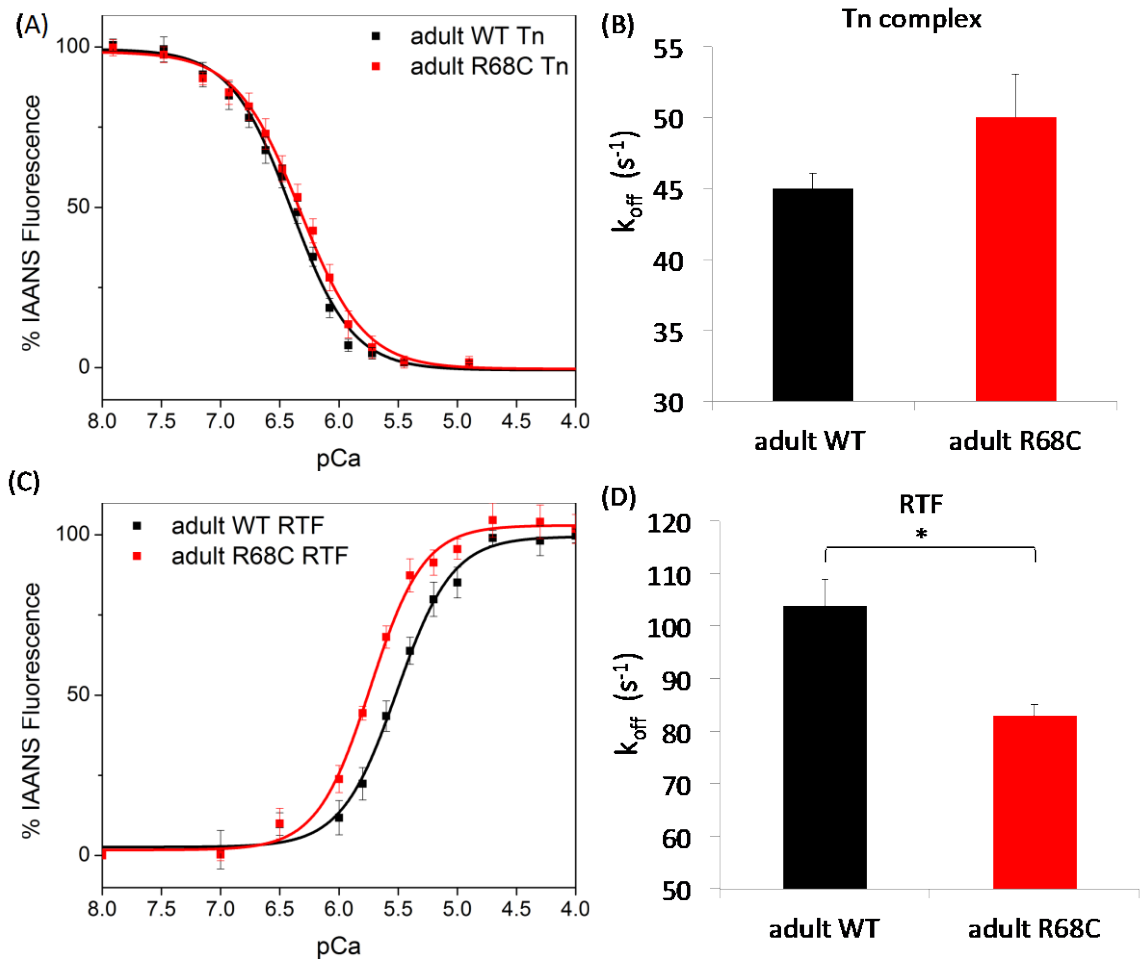

Figure 4-8 Effects of the R68C cTnI mutation on the Ca^{2+} binding properties and Ca^{2+} dissociation rate in adult cTn complexes and RTF.

Panel (A) shows the Ca^{2+} dependent decrease in IAANS fluorescence of adult WT and R68C cTn. Panel (B) shows the Ca^{2+} dissociation rate, k_{off} (s^{-1}) of adult WT (black) and R68C (red) Tn complexes determined by stopped-flow fluorescence. Panel (C) shows the Ca^{2+} dependent increase in IAANS fluorescence of adult WT RTF and R68C RTF. Panel (D) shows the Ca^{2+} dissociation rate, k_{off} (s^{-1}) of adult WT (black) and R68C (red) RTF determined by stopped-flow fluorescence.

4.4. Discussion

Several findings demonstrate the changes in cardiac contractility as the human fetal heart develops into the postnatal and adult heart (Elmstedt et al., 2012; Elmstedt et al., 2013; Racca et al., 2016). At the whole heart level during development, heart rate decreases as the diastolic filling, atrial contraction and ventricle ejection increases (Elmstedt et al., 2012; Elmstedt et al., 2013). Electron micrographs show that as the fetal cardiac muscle develops, the density of Tn and myofibrils increase, with the myofibrils becoming wider, more elongated and organized (Racca et al., 2016). These changes in the ultrastructure might contribute to the increase in force. As the number of cross bridges increases, the force generating capacity increases, a necessity as the cardiac muscle matures (Racca et al., 2016). At the molecular level of thin filaments and Tn complexes, the cardiac isoform of the *TNNC1* gene is expressed in both fetal and adult heart tissue. Both TnI paralogs and TnT isoforms are expressed in a developmentally regulated manner. Previous literature suggests that TnI paralog and TnT isoform switches are important adaptive mechanisms in Ca^{2+} handling as the cardiac contractile apparatus transitions from being highly sensitive to Ca^{2+} in the fetal environment to being less sensitive in the adult heart (Gomes et al., 2004; Westfall et al., 2002).

In this chapter, we explored the differences in the Ca^{2+} binding properties of the fetal and adult Tn complexes, as well as in the reconstituted thin filaments level. In addition, we investigated the changes in the Ca^{2+} binding properties of the I79N cTnT mutation found in the adult heart and one recently discovered novel ssTnI mutation, R37C ssTnI, found in infants who died suddenly without previous overt symptoms (Dewar et al., 2017). We generated the corresponding mutation in their adult/fetal counterparts with the main goal of examining the different effects caused by the mutation on Ca^{2+} handling in the parallel adult and fetal environments.

In the absence of cardiomyopathy-related mutations, the WT fetal Tn complex has an ~1.8-fold lower K_d and an ~4 fold lower k_{off} than the WT adult Tn complex; at the RTF level, WT fetal RTF demonstrated an ~3-fold lower K_d and an ~1.4-fold lower k_{off} compared to its WT adult counterpart. This confirms several previous findings that regardless of the complexity of the biochemical system utilized, the fetal system always has a higher Ca^{2+} sensitivity and lower Ca^{2+} dissociation rate, due to the presence of the ssTnI paralog and the fetal cTnT1 isoform (Gomes et al., 2002; Gomes et al., 2004). The

clear difference of Ca^{2+} binding properties between the adult and fetal systems can be recapitulated in isolated Tn and RTF constructs in *in vitro* experimental conditions.

The protective role of ssTnI is evident as the Ca^{2+} sensitizing effects of the I79N cTnT mutation are mitigated in the fetal RTF. In particular, the apparent Ca^{2+} sensitizing effects associated with the I79N cTnT mutation observed in the adult RTF (Figure 4-4 and 4-5) were diminished in the fetal RTF (Figure 4-6). This phenomenon of mutations being rescued in the fetal or slow skeletal muscle environments have been observed in several other studies on human cardiomyocytes, including two RCM-associated TnT mutations (Pinto et al., 2011) and several HCM-linked TnC mutations (Veltri et al., 2017). In adult rat and mouse cardiomyocytes, ssTnI also enhances the contractile sensitivity to Ca^{2+} activation under physiological and acidic pH conditions (Fentzke, 1999). However, after the ssTnI paralog switches to cTnI, the protective mechanism is lost in which the Ca^{2+} sensitization due to the mutation becomes evident. This results in the marked Ca^{2+} sensitization of the I79N cTnT when the ssTnI is replaced with cTnI in the adult RTF.

When a mutation occurs in ssTnI, such as the case of R37C ssTnI mutation, it is evident that it has more severe effects than those mutations specific to the adult cardiac muscle type. To our knowledge, this is the very first human disease that has been reported with a mutation in ssTnI (Dewar et al., 2017). The majority of the slow skeletal muscle related diseases that have been reported to date are associated with fast-twitch muscle expressed from the *TNNT2* gene, causing distal arthrogryposes (Robinson et al., 2007). Arg37 is a highly conserved residue between human skeletal and cardiac TnI (Arg 68) and across many different species (Figure 4-1). The non-conserved substitution from Arginine to Cysteine suggests that this substitution is likely to be structurally substantive by changing nearby protein-protein interactions. This is demonstrated by our previous molecular dynamics (MD) simulations experiments (Shafaattalab et al., 2019). Since there is no structural information available for the fetal ssTnI in the fetal Tn complexes, MD simulation was carried out by substituting the corresponding mutation, R68C, in the adult Tn complex (Shafaattalab et al., 2019). It is evident that mutation at this location has a significant impact on the protein-protein interactions between TnI, TnT and ultimately TnC, in which the extensive hydrogen bonding network is clearly lost in the presence of this mutation (Shafaattalab et al., 2019).

In the current study, R37C ssTnI consistently increases both K_d and k_{off} compared to the WT counterpart, regardless of the complexity of the system. Unlike the majority of the Tn mutations in which the effects are usually not evident at the level of the Tn complex, severe Tn mutations such as R37C ssTnI and L48Q cTnC consistently show their effects in biochemical systems through the range of increasing complexity (Feest et al., 2014; Tikunova et al., 2010; Wang et al., 2012). The results obtained from the current biochemical studies corroborated well with the physiological data obtained from the hiPSC-CMs in which the heterozygous *R37C+/- TNNI* mutation was introduced using the genome-editing method of CRISPR/Cas9 (Shafaattalab et al., 2019). More specifically, using optical mapping techniques to compare the voltage and Ca^{2+} transients of the *R37C*$^{+/-}$ *TNNI* variant CMs to the isogenic control, the variant showed no indication of restitution over a range of stimulation frequencies and displayed alternans at 75 bpm or higher, in which both phenomena were absent in the WT cells. This suggests that the presence of this variant renders the CMs pro-arrhythmic, strongly suggesting that the underlying pathogenicity is closely associated with altered Ca^{2+} handling (Shafaattalab et al., 2019). Furthermore, other possibility for the severity of the ssTnI mutation is that slow skeletal muscle is present in a large percentage of the human body (Scott et al., 2001). It is possible that this mutation could potentially have profound effects on other crucial skeletal muscle-related functions, such as the diaphragm or any regions composed of predominately slow-twitch muscle fibers (Meznaric and Cvetko, 2016).

Having 10 children with the identical mutation die makes the R37C ssTnI mutation unlikely as a *de novo* mutation. It is likely that one of the parents is a mutational carrier, although this warrants further investigation of the genotypes of their parents. If in fact one of the parents is a mutational carrier, it is unclear why and how they can survive past the fetal stage and successfully transition from ssTnI to the cTnI paralog during the first few months after birth. Although earlier literature suggests that the amount of ssTnI is not detectable after 8-9 months of age, some reports suggest that congenital malformation of the heart can delay the ssTnI to cTnI paralog switch up to 2 years of age (Sasse et al., 1993). Nevertheless, the reasons the parents with this mutation survive remain unclear. For the purpose of investigating the potential consequences of this mutation in the adult environment, we introduced the corresponding mutation, R68C, into adult cTnI. Surprisingly, adult R68C RTF shows an opposite trend in Ca^{2+} binding

properties compared to that of the fetal R37C RTF. The R68C cTnI mutation causes the adult RTF to have a higher Ca^{2+} sensitivity and a lower Ca^{2+} dissociation rate, instead of the overall Ca^{2+} desensitization observed in the fetal R37C Tn complex and RTF. It is intriguing that the corresponding adult R68C cTnI mutation has the reverse effect on Ca^{2+} handling from fetal R37C ssTnI. Nevertheless, these results suggest that this mutation is not benign and more investigation, particularly the family medical history and genetic information of at-risk family members, is essential in understanding the disease mechanism for this novel ssTnI mutation.

4.5. Conclusion

Our functional data strongly support the notion that different TnI paralogs are involved in fine-tuning myofilament Ca^{2+} sensitivity and cooperativity as an adaptation to the cellular environment and contractile performance. The presence of ssTnI and the fetal cTnT1 isoform provide some cardio-protective effects throughout fetal and neonatal life and gradually decrease during the first few months of postnatal development. This is demonstrated well in the mutation of I79N cTnT in which its Ca^{2+} sensitizing effect is significantly mitigated when it is in the fetal environment. In contrast, when a severe mutation occurs in ssTnI, as in the case of the R37C ssTnI mutation, significant changes in Ca^{2+} binding properties persist, regardless of the complexity of the system. Our functional studies provide insightful information on how cardiomyopathy-associated Tn mutations behave differently in the adult and neonatal contractile elements and highlight the need for more understanding on the molecular level, in order to help us comprehend the different disease outcomes in adult and pediatric cardiomyopathies.

Chapter 5.

Three-dimensional structural determination of the thin filaments using negative-stain EM and Cryo-EM

5.1. Introduction

Cardiac thin filament is a multi-subunit, allosterically regulated macromolecular structure, fully dependent on the precise coordinated movements of actin filaments, and tropomyosin (Tm) and troponin (Tn) complexes. Thin filaments, particularly Tm and Tn complexes, are highly dynamic and flexible in order to execute their respective functions, transitioning between the three states (blocked → closed → open) of muscle activation (Manning et al., 2011). To date, parts of the cardiac thin filaments have been solved by X-ray crystallography and more recently, by cryo-electron microscopy (cryo-EM) (Table 5-1). The core domain of the human Tn complex was solved by X-ray crystallography to a 3.3 Å resolution more than a decade ago (Takeda et al., 2003) and recently refined to a 2.2 Å resolution (Takeda, 2016). However, the most flexible parts of the troponin complex, the TnT N-tail domain and the terminal regions of TnI remain unresolved (Tardiff, 2011). Unfortunately, more than 90% of the cardiomyopathy-related mutations occur in these unresolved regions, highlighting the importance and the challenge of obtaining the complete Tn complex structure at high resolution (Tardiff, 2011). In addition, although high-resolution structures of the actin-Tm complexes or actin-related structure were solved by cryo-EM in recent years, none of the structures included the Tn complexes. Obtaining a high-resolution structure of the cardiac thin filaments will significantly enhance our understanding of the molecular mechanisms for these cardiomyopathy-associated mutations and provide important structural insights which will aid in the development of novel drugs.

Single-particle Cryo-EM has become a very useful technique to solve high-resolution structures of many macromolecular complexes, due to recent hardware and software development (Bai et al., 2015; Nogales, 2016). Structures of large protein complexes are often not attainable by X-ray crystallography due to their difficulty of crystallization, or by NMR spectroscopy due to its upper molecular weight limit of 50

kDa. However, they may be ideal candidates for single-particle cryo-EM structural determination (Bai et al., 2015; Nogales, 2016). For structure determination by cryo-EM, the protein samples are plunge-frozen in liquid ethane so that the protein molecules are embedded in a thin layer of vitreous ice (Cheng et al., 2015a). This ensures that hydration of the complex biological structure is maintained without having the water molecules forming cages that can distort the molecules as in crystalline ice (Cheng et al., 2015a). Following the vitrification of the samples, a series of images are collected under cryo conditions to produce thousands of 2D images (Cheng et al., 2015a). The images are collected as a series of “movies” and each frame is illuminated with a small dose of electrons. As a result, tens or hundreds of images are collected under 1 second or less as video files, and they can be used to reduce image blurring caused by beam-induced motion and/or stage instabilities. The video frames are motion-corrected and summed to produce 2D images (Campbell et al., 2012; Li et al., 2013b). Protein particles are then selected either manually or automatically from each image, and those particles are digitally aligned and classified according to their orientations. The resulting 2D averages are then used for 3D reconstruction to produce an initial 3D map. Heterogeneity in the protein sample, such as that resulting from different conformation states or partial complex formation, can then be sorted out by 3D classification and further refined to obtain the final density map (Figure 5-1) (Cheng et al., 2015a). The first EM reconstruction was accomplished in the late 1960’s (De Rosier and Klug, 1968), and the single-particle reconstruction technique has been established since 1995 (Lata et al., 1995). However, it is only recently that cryo-EM has become a mainstream structural biology technique, due to its vastly improved technology. In particular, the combination of direct-electron detectors (DED) (McMullan et al., 2009) and improved image and data processing (Li et al., 2013b) has enabled a quantum leap for cryo-EM structural determination.

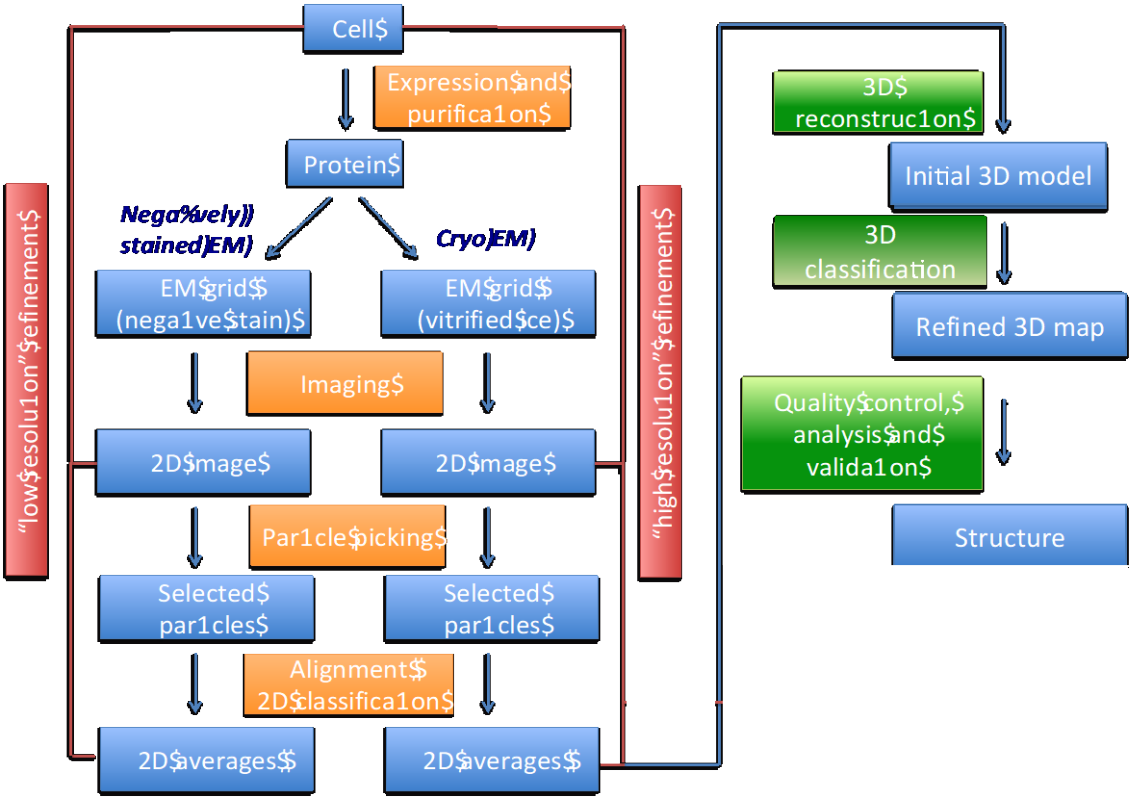

Figure 5-1 The workflow involved in structure determination by single particle cryo-EM.

The workflow typically starts with evaluating the homogeneity of the sample by negative stain EM. When negatively-stained EM images are satisfactory, that is, the particles show minimal aggregation and heterogeneity, then the sample is ready for cryo-EM analysis. The 2D classification, 2D averages and 3D maps generated from the vitrified sample may require multiple rounds of sample improvement or structural refinement to reach a high-resolution structure of the protein sample. The figure was adapted from Cheng *et. al* (Cheng et al., 2015a).

It is important to look at the progress of the thin filament structural determination. The process originated in the early 1980's with the development of negative-stain EM. This approach remained the major technique used to solve the structure until the recent advancements in cryo-EM. With negative-stain EM, structures were determined at an average of 25 Å resolution or 20 Å at best, so no atomic details were resolved Nevertheless, these low-resolution structures provided an important foundation for the visualization of the overall architecture of the thin filaments and paved the way for higher-resolution filament-related structures.

One of the earlier thin filament models that clearly demonstrates the periodic distribution of the troponin, every 38.5 nm on the actin filament, is the native filament

isolated from *Limulus polyphemus* (the horseshoe crab) (Lehman et al., 1994). The position of Tm is clearly resolved in the Ca^{2+}-bound and Ca^{2+}-free states, revealing that Tm binds to actin domains 3 and 4, leaving domains 1 and 2 exposed for myosin binding. Other thin filament-related structures that have been studied are listed in Table 5-1. A few of the thin filament structures that are of particular interest are: the structures of the reconstituted thin filaments in the Ca^{2+}-activated and relaxed states (Pirani et al., 2006; Pirani et al., 2005); the native thin filament isolated from porcine cardiac muscle (Yang et al., 2014); the more recent high-resolution structure of the reconstituted rigor actin-Tm-myosin complex (Behrmann et al., 2012; von der Ecken et al., 2016); and the reconstituted actin-tropomyosin complex (von der Ecken et al., 2015).

5.1.1. Structure of the reconstituted thin filament in the Ca^{2+}-bound and apo-states

Although the position of Tm relative to the actin filaments is well defined, it has been a challenge to fit the Tn structure into the EM density map for several reasons. First, the symmetry of Tn on the thin filament is different from the helical symmetry of actin and Tm. If helical reconstruction is applied with respect to the symmetry of actin, the density of Tn is averaged out and lost. Second, since Tn is composed entirely of α-helices in all three subunits, the high degree of flexibility induces conformational dynamics to the cTn complex, compromising the isolation of near identical filament segments for single-particle reconstruction. Third, it is difficult to ensure the continuous or uniform distribution of Tn on the filaments, especially for the reconstituted thin filaments (Pirani et al., 2006; Pirani et al., 2005; Yang et al., 2014).

The structure of the reconstituted thin filaments by Pirani et. al was generated by mixing rabbit skeletal actin, bovine Tn and Tm in a ratio higher than the physiological ratio (1: 3.2:3.2) to ensure the full decoration of Tn on the filament (Pirani et al., 2005). The negative-stain EM images of the reconstituted thin filament in the Ca^{2+} bound and the apo states were processed to ~25 Å. Their structures demonstrate that Tm binding to actins is flexible and transient, allowing the thin filaments to switch between the three states of muscle regulation. Parts of the filaments remain in the relaxed conformation under the Ca^{2+} bound condition, whereas other parts adopt the activated position during the apo state. Their results suggest that the interactions between actin and Tm are in

dynamic equilibrium, allowing a rapid transition between different states (Pirani et al., 2005).

Later Pirani et al. generated a structural model of the thin filament (Pirani et al., 2006), built from the crystal structure of the core domain of Tn (Takeda et al., 2003), Tm (Whitby and Phillips, 2000), and cryo structures of actin (Holmes and Schroder, 2003) based on published distance measurements (Figure 5-2). This initial model of the thin filament, which had Tn bound to the first and second actin monomers from the barbed end, was used as a reference to align and classify the thin filaments. Alternative models were built by placing Tn at different periodic locations with respect to actin. The accuracy of the models was determined by fitting the collected EM images to them. After iterations of 40-60 rounds, the initial model yielded the most stable outcome as the other ones diminished or became very noisy with indistinct Tn densities (Pirani et al., 2006).

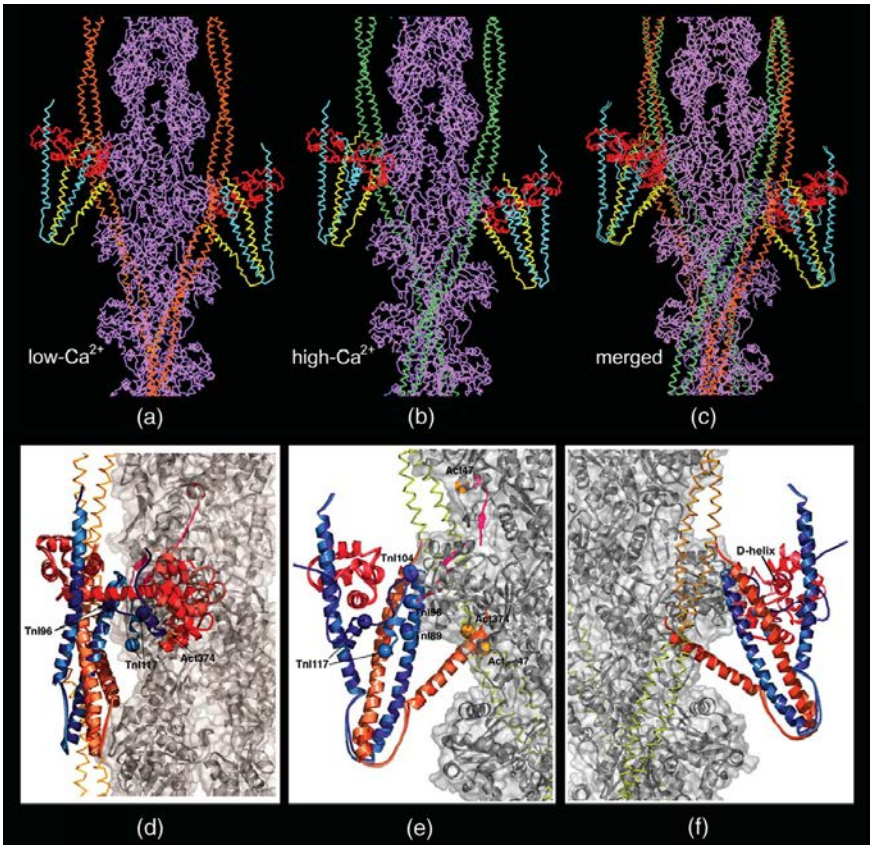

Figure 5-2 Atomic model of actin-Tm-Tn in the (a) low Ca^{2+} state, (b) high Ca^{2+} state, and (c) merged structure of the low and high Ca^{2+} state.

The core domain of Tn was obtained from Takeda's crystal structure (Takeda et al., 2003) (TnC is colored in red, TnI in cyan, and TnT in yellow). Each Tn binds to subdomain 1 of the actin monomers which are colored lavender. (d) to (f) show three enlarged superimposed views of the Tn core domain at low Ca^{2+} state (faded colors) and high Ca^{2+} state (saturated color). (d) shows that the TnC binds perpendicularly to the actin filaments; (e) shows the binding region on the actin filaments with the TnI binding regions highlighted in pink; (f) uses a 180-degree rotation of (d) to show the relative position of the D-helix of TnC to Tm and actin. Figure reused with permission (Pirani et al., 2006).

5.1.2. Structure of the native thin filament using negative-stain EM

Native thin filaments isolated directly from fresh muscle generally have higher Tn decoration than the thin filaments generated from reconstitution of recombinant proteins, including the thin filaments isolated from porcine cardiac muscle (Yang et al., 2014), *Drosophila* flight muscle (Cammarato et al., 2004) and goldfish skeletal muscle (Paul et al., 2009).

The most recent thin filament EM structure, including the density for Tn complex, was obtained from the native thin filaments isolated from porcine cardiac muscles

(Figure 5-3) (Yang et al., 2014). Their single-particle reconstruction of the negatively stained native thin filaments clearly demonstrates the density of Tn and show features that were not included in the previous models. Although nine different starting models were used, all produced the same final structure, confirming the validity of the reconstruction. At 25 Å resolution, two novel features stand out from the structure. First, the orientation of TnT and the Tn core domain were shown on the thin filaments. Density is observed for the TnT1 tail domain, spread over three actin subunits in the direction of the filament's barded ends (Figure 5-4). Second, the reconstruction clearly shows the density attributed to the mobile C-terminal domain of TnI bound to Tm during blocked states. This position of the C-terminal domain of TnI coincides with the reconstruction of the thin filament that includes not the full length, but only the C-terminal 80-residue fragment of TnI (Galinska-Rakoczy et al., 2008)

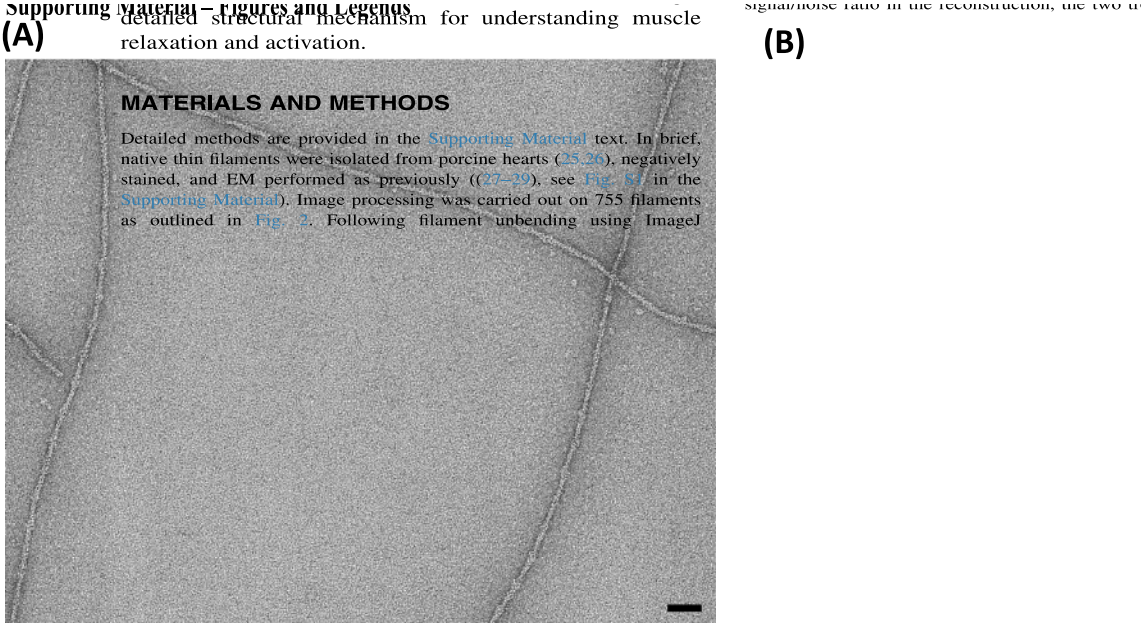

Figure 5-3 (A) The representative negative-stained image of the porcine native thin filaments with two parallel strands showing periodic Tn binding and one horizontal strand with no visible Tn binding. (B) Negative-stained EM images of the thin filament.

In Panel B-(a), periodic Tn densities are clearly visible at intervals of every ~385 3 Å. In (b), Tn is not clearly seen, but it is possible that these thin filaments were without Tn complexes binding, or Tn complexes were bound on the top and the bottom of the filaments, so they cannot be seen visibility from the top view. In (c), there are no signs of Tn in the image or Fourier transforms. Only 10% of the images have no visible Tn binding. Each scale bar represents 500 Å (Yang et al., 2014). This figure is reused with copyright permission.

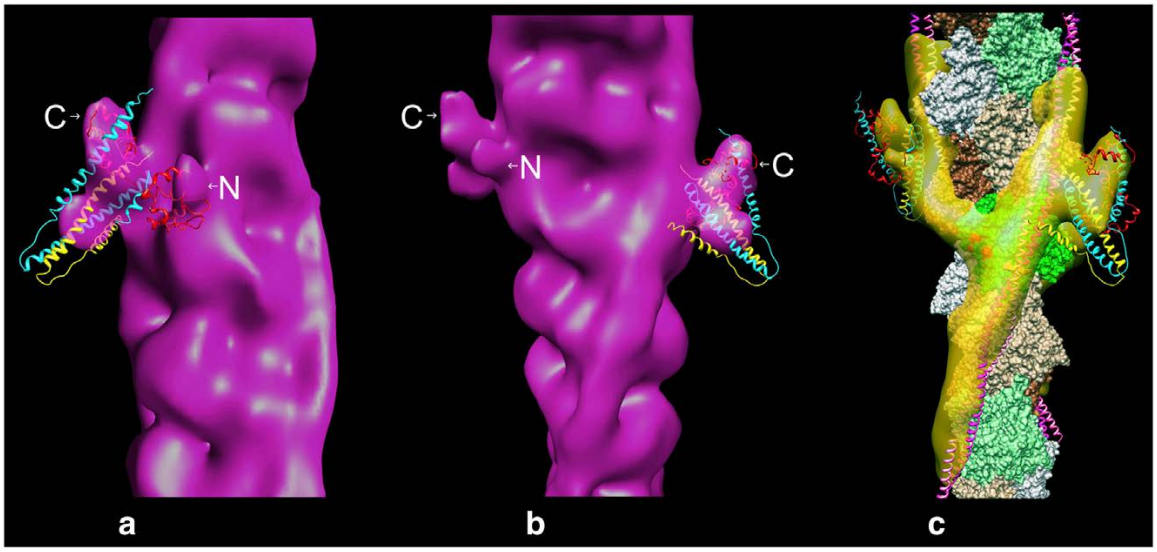

Figure 5-4 Fitting of the crystal structure of the core domain of the Tn complex (PDB ID: 1J1E) into the EM density map.

(a) and (b) show the two views of the Tn complexes fitting into the EM density map. TnC is coloured in red, TnI is colored in cyan and TnT is coloured in yellow. (c) The atomic model of actin-Tm (Li et al., 2011) was fitted into the reconstruction and superimposed with the Tn complex crystal structure. This figure is reused with copyright permission.

5.1.3. Structure of the reconstituted thin filament by cryo-EM

With the “resolution revolution” development of cryo-EM, more structures are being solved at an atomic resolution than was previously achievable through X-ray crystallography or NMR spectroscopy. Even though more non-filament structures have been solved at 3 Å or higher resolution, the highest resolution obtained for filament-related structures still remains around 3.3 Å (Pospich et al., 2017). The major challenge in solving the thin filament structure is the intrinsic flexibility of the filaments, which are of variable lengths that bend, twist, or even aggregate, thereby imposing challenges when going through the classification process for these heterogeneous filamentous structures.

Despite the challenges to the determination of the filamentous structure, Raunser’s group has successfully solved many cryo-EM structures at reasonably high resolution (von der Ecken et al., 2016; von der Ecken et al., 2015). The most relevant structures related to thin filaments include the actin-Tm-myosin complex at ~7.7 Å resolution (Behrmann et al., 2012), F-actin at 3.7 Å and in complex with Tm at 6.5 Å (von der Ecken et al., 2015), and the latest actin-Tm-myosin complex at 3.9 Å resolution (von der Ecken et al., 2016). The structure of the rigor actin-Tm-myosin complex was tackled

first because it is the most stable form of the filaments in the nucleotide free state, but many different combinations of F-actin and myosin motor domains were screened to obtain the straight and unbundled rigor complex. The resulting structure shows the actin-myosin interface creates a neutral groove with positively charged patches that can optimally accommodate negatively charged areas on Tm. Binding of myosin results in a large 23 Å shift of Tm along actin and conformational change of myosin itself, but no major conformational change was observed in actin (von der Ecken et al., 2015). This structure provides an important basis for understanding how Tm modulates myosin binding to actin. Subsequently, higher resolution structure for actin-Tm, at 6.5 Å, confirmed the central region as the area for hydrophobic and electrostatic interactions that stabilize the F-actin, and determined that the D-loop of actin acts as the key mediator, becoming ordered upon polymerization of the actin molecules (von der Ecken et al., 2015). This structure also confirms the negatively charged Tm interacts with the positively charged groove on F-actin, in more detail than previous structures. More recently, the human rigor actomyosin complex was solved at an average resolution of 3.9 Å, revealing the hydrophobic interactions that stabilize the actomyosin interface as well as many more atomic details that were not discovered in the previous version (von der Ecken et al., 2016). These structures provide structural details that potentially help the understanding of the molecular mechanism of filaments-related diseases (Figure 5-5).

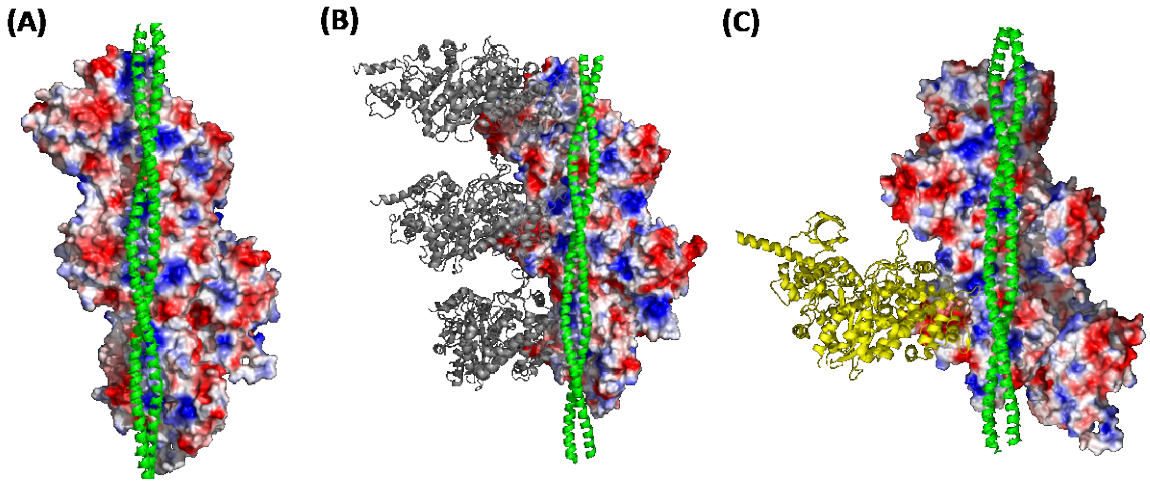

Figure 5-5 High-resolution cryo-EM structure of the thin filaments solved by Raunser's group.

(A) Rabbit skeletal actin with alpha-MAS-Tm from mouse at a resolution of 6.5 Å (PDB: 3J8A) (von der Ecken et al., 2015). (B) A 7 Å resolution structure of thin filament consisting of rabbit actin, human alpha-MAS-Tm, and the motor domain of *Dictyostelium discoideum* myosin. It is a fast, single molecular motor involved in the uptake of solid particles, bacteria and yeast cells and it binds well to the actin-Tm complex (PDB: 4A7L) (Behrmann et al., 2012). (C) G-actin (ACTG1 from human) recombinantly expressed using the *baculovirus/Sf9-cell* system with human MAS-Tm and the motor domain of non-muscular myosin-2C isolated from human directly fused to a lever arm of alpha-actinin. The structure was solved at an average resolution of 3.9 Å (PDB: 5JLH) (von der Ecken et al., 2016). The figure was generated using PyMol (Delano, 2015).

However, as mentioned previously, none of the high-resolution structures include Tn complexes. In order to achieve near-atomic resolution of a structure, the averaging process requires many particles with different orientations, preferably stable without aggregation and too much flexibility. I spent the first two years of my PhD studies pursuing the structural determination of the reconstituted cardiac thin filaments in collaboration with Drs. Thomas Walz and Kelly (Hyojin) Kim from Rockefeller University, New York, USA. We successfully screened and identified the optimal conditions for generating reconstituted thin filaments with a high percentage of Tn decorations using negative-stained EM. During our initial attempt with cryo-EM, different challenges appeared but we were able to collect several data sets under conditions that allowed initial 2D classification. The inherent challenges are several folds and remain as major obstacles preventing high-resolution structural determination of the thin filaments by cryo-EM. These difficulties precluded my completion of this project as part of my dissertation and are discussed in more detail in the Discussion section.

Table 5-1 Thin filament and Tn-related structures solved by negative-stained EM, Cryo-EM and X-ray crystallography.

Author	Structure	Source/Descriptor	Technique	Summary
Thin filament related structures				
Flicker et al., 1982, *JMB*	Troponin and its interaction with tropomyosin	EM of cTn complexes and co-complexes of cTn/Tm. Tn was isolated from the back/leg muscles of rabbits, the breast and leg muscles of the chicken and the back and legs of the mouse	Negative- stain EM	Tm Cys 190 interacts with all three cTn subunits (from cross linking experiments). The entire cTn complex is ~ 265 ± 40 Å long; the tail portion is 160 ± 35 Å long and 20 Å wide; isolated cTnT is ~185 ± 25 Å long. The re-assembled cTn/Tm can bind directly across from the same Tm, unlike the native cTn/Tm complex where only 1 cTn is bound to Tm.
Lehman et al., 1994, *Nature*	Ca^{2+}-induced tropomyosin movement in *Limulus* thin filaments revealed by EM at 20 A	Thin filaments isolated from *Limulus*	Negative- stain EM	The structure of TF in the apo and Ca^{2+} form shows the periodicity of Tn binding and the movement of Tm which provides support for steric effects in muscle activation.
Lehman et al., 2000, *JMB*	Tropomyosin and actin isoforms modulate the localization of Tm strands on actin filaments	Rabbit skeletal actin + bovine cardiac Tm and Tn	Negative- stain EM	For smooth muscles and non-muscle motile systems where cTn is absent, the binding of Ca to calmodulin couples a myosin light chain kinase phosphorylation cascade to activation of actomyosin ATPase. Even TF containing only cTnI caused Tm to localize on the outer domain of actin.
Pirani et al., 2005, *JMB*	Single particle analysis of relaxed and activated muscle thin filaments	Rabbit skeletal actin + bovine cTm and cardiac Tn	Negative- stain EM	The position of Tm on the actin filaments is dynamic, shown by having parts of the filaments maintained under relaxed conditions in the C (closed) state and some maintained in the B-state in the presence of Ca^{2+}.
Pirani et al., 2006, *JMB*	An atomic model of the thin filament in the relaxed and Ca^{2+} activated states	Rabbit skeletal actin + bovine cTm and cardiac Tn	Negative- stain EM	A low-resolution thin filament structure was obtained, saturated with Ca^{2+} and filled in the EM volume with the Tm, actin and core domain of Tn structure.

Mun et al., 2011, *JMB*	Electron microscopy and 3D reconstruction of F-actin decorated with cardiac myosin-binding protein C	F-actin purified from chicken pectoralis muscle and mouse cardiac cMyBP-C	Negative- stain EM	The orientation of the Tn complex docked on the actin-Tm filaments was established, as well as the position of the TnI mobile domain, placing Tm in the blocking position on actin in the apo condition.
Mun et al., 2014, *PNAS*	Myosin-binding protein C displaces Tm to activate cardiac thin filaments and governs their speed by an independent mechanism	F-actin isolated from chicken pectoralis muscle and native thin filaments from porcine cardiac muscle.	Negative- stain EM	Myosin binding protein C modulates thin filament activity by physically displacing Tm at the low Ca^{2+} position as shown in the EM images and in *in vitro* motility assays.
Ecken et al., 2016, *Nature*	Cryo-EM structure of a human cytoplasmic actomyosin complex at near-atomic resolution	Human G-actin was recombinantly expressed using baculovirus and purified with Tm 3.1 from *E. coli*. The motor domain of myosin was expressed from baculovirus.	cryo EM	The structure of the F-actin-myosin was solved to 3.8 A resolution.
Ecken et al., 2015, *Nature*	Structure of the F-actin-tropomyosin complex	Rabbit skeletal actin with recombinant mouse Tm	Cryo EM	The structure of the F-actin was solved at 7 A resolution and in complex with Tm at 6.5 A resolution.
Behrmann et al., 2012, *Cell*	Structure of the rigor actin-tropomyosin-myosin complex	Rabbit skeletal actin with recombinant Tm and myosin	Cryo EM	The structure of the F-actin-Tm-myosin complex was solved at 8 A resolution.
Sousa et al., 2013, *JMB*	Cryo-EM structures of the actin:Tm filament reveal the mechanism for the transition from C- to M-state	Rabbits skeletal actin with gizzard Tm	Cryo EM	The structure of the F-actin-Tm complex was solved at 8 A resolution

Yan et al., 2014, *Biophys. J*	Three-dimensional organization of troponin on cardiac muscle thin filaments in the relaxed state	Native thin filament isolated from the porcine heart	Negative- stain EM	This structure shows the Tn core domain is mounted on top of the TnT1 tail where it forms a scaffold for cNTnC and TnI; at low Ca^{2+},TnI bridges azimuthally adjacent actin subunits across the filaments, interacting with Tm or TnT1.
Troponin related structures				
White et al., 1987, *Nature*	Structure of co-crystals of tropomyosin & troponin	X-ray structure of glutaraldehyde-treated Tm with whole cTn or fragments of TnT at 17A	X-ray crystallography	The N-tail (residues 1-70) of TnT binds to the head-to-tail joint of the Tm filaments; residues 71-158 of TnT bind towards the middle of Tm, interacting in an antiparallel fashion (N of T spans the C of Tm). The head region of Tn binds 200 Å away, near residues 150-180 Å of theTm molecule. cTn is difficult to crystallize but pure Tm crystals with 0.1% glutaraldehyde stabilize the lattice and allow binding of Tn.
Ohtsuki et al., 1988 J. *Biochem*	Electron microscopic study of troponin	Troponin isolated from rabbit skeletal muscle	Rotary shadowed electron micrograph of Tn	TnT is subjected to chymotrypic digestion in which TnT1 (residues 1-158) binds to tropomyosin; TnT2 (C-terminal 101 residues~17 nm) binds to TnC, TnI and Tm. The intrinsic viscosity of Tn appears to be higher than that of fresh Tn after long term storage at -20 °C. Fresh Tn has a clear globular region; frozen Tn has a longer/thinner tail region; long-term freezing causes Tn to have longest/thinnest tail.
Vinogradova et al., 2005, *PNAS*	Ca^{2+}-regulated structural changes in troponin	Recombinant chicken skeletal troponin subunits	X-ray crystallography	The core domain of skeletal Tn was solved at 3 A in the Ca^{2+} activated state and at 8 Å in the apo state.
Takeda et al., 2003, *Nature*	Structure of the core domain of human cardiac troponin in the Ca^{2+}-saturated form	Recombinant human troponin subunits	X-ray crystallography	The core domain of the human Tn complexes were solved at 3.3 Å, then later refined to 2 Å resolution in 2016.

5.2. Materials and Methods

5.2.1. Thin filament preparation

Thin filaments were generated using the same methods described in section 2.3.7 except that the Tn complexes used here did not require the IAANS fluorescence labeling. RTF was prepared fresh at a concentration of 0.168 mg/mL (4 µM) and diluted 10 times with the reconstitution buffer prior to negative-stain grid preparation.

5.2.2. Preparation of uranyl formate stain

37.5 mg of uranyl formate was dissolved in 5 mL of boiling double-distilled water. After 5 minutes of stirring, 5 µL of 5 M NaOH was added to the solution and stirred for additional 5 minutes. The resulting 0.75% (wt/vol) uranyl formate solution was passed through a 0.20 µm syringe filter.

5.2.3. Negative-stain EM

An aliquot (3.5 µl) of thin filament protein sample of 400 nM was adsorbed to a glow-discharged 200-mesh copper grid covered with a thin carbon-coated plastic film. After adsorbing the sample for 45 s, the grid was blotted with a filter paper and washed twice with deionized water, and once with a 0.75% (wt/vol) uranyl formate solution, blotting the grid with filter paper between each drop. It was then stained for 15-20 s with the uranyl formate solution. After blotting the grid again with filter paper, the remaining solution was removed by vacuum aspiration (see (Ohi et al., 2004) for further details). Images were collected using an XR16L-ActiveVu charge-coupled device camera (AMT) on a Philips CM10 electron microscope (FEI) operated at an acceleration voltage of 100 kV. The calibrated magnification was 41,513× (nominal magnification of 52,000 ×), yielding a pixel size of 2.65 Å at the specimen level. The defocus was set to –1.5 µm.

5.2.4. Cryo-EM sample preparation and data collection

Freshly reconstituted RTF samples were concentrated to 0.16 mg/mL. Cryo-EM grids were frozen using a Vitrobot Mark IV (FEI) as follows: 3.5 µL of the concentrated sample were applied to a glow-discharged Quantifoil R1.2/1.3 holey carbon 400 mesh copper grid, blotted for 2-3 s at >90% humidity at room temperature, and plunge frozen in liquid ethane cooled by liquid nitrogen.

Cryo-EM data were recorded on a Talos Arctica (FEI) operated at 200 kV, equipped with a Gatan K2 Summit camera. Serial EM software was used for automated data collection. Video files were collected at a nominal magnification of 28,000 × in super-resolution mode resulting in a calibrated pixel size of 0.75 Å/pixel, with a defocus range of approximately –1.5 to –2.5 µm. Fifty frames were recorded over 15 s of exposure at a dose rate of 1.8 electrons per $Å^2$ per frame.

5.2.5. Image processing

For the WT thin filaments in apo conditions, two datasets were collected for the thin filaments after 2- and 5-fold dilution from the original concentration of 4 µM. A total of 1395 images were collected, and the image stacks were motion-corrected and binned over 2 x 2 pixels with MotionCor2 (Zheng et al., 2017), yielding a pixel size of 1.5 Å. The defocus values were estimated by CTFFIND4 (Rohou and Grigorieff, 2015). Each image was then manually inspected and rejected if considered to be of inadequate quality. Only 562 out of 1395 images were kept for further processing, due to a large amount of aggregates covering many of the entire images in some micrographs. 5600 particles were manually picked using the e2boxer.py command of the EMAN2 software package (Tang et al., 2007), and then extracted into 256 x 256-pixel boxes in RELION (Scheres, 2012). These particles were then subjected to reference-free 2D classification in RELION.

5.3. Results

5.3.1. Generation of thin filaments suitable for negative-stained EM

The biggest challenge to generating thin filaments suitable for negative-stained EM was obtaining thin filaments that were well separated, unbundled, and with a high amount of Tn binding to the actin-Tm filaments. Extensive troubleshooting processes were carried out, and various conditions were examined. These included but are not limited to: finding the optimal binding ratio of actin:Tm:Tn; varying the buffer compositions; changing the pH of the buffer; and determining the filaments concentration that allows optimal visualization under the microscope.

It was discovered that the buffer containing 25 mM imidazole, 25 mM KCl, 4 mM $MgCl_2$, 1 mM EGTA, and 1 mM DTT at pH 7.4 allowed the most Tn binding to the actin-Tm filaments. In addition, the optimal concentration and binding molar ratio for actin:Tm:Tn was determined to be 4:2:2. The samples were diluted 10-foldbefore being placed on the grid for the negative-stain EM. Therefore, the final concentration for visualization under the CM10 microscope was ~400 nM for actin:Tm:Tn. See Figure 5-6 for the representative images of WT RTF and RTF containing the I79N cTnT mutation.

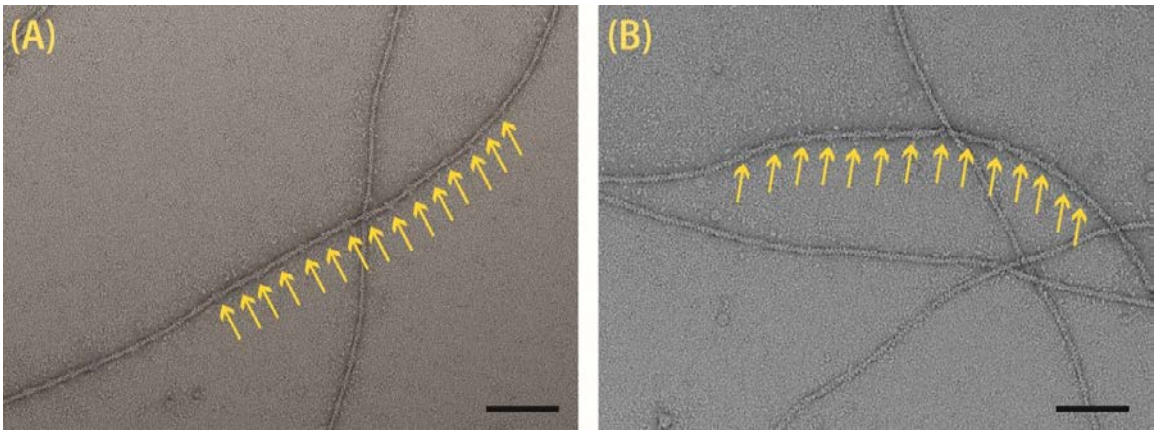

Figure 5-6 Representative negative-stained EM images of (A) WT RTF and (B) RTF containing the I79N cTnT mutation.

The regular distribution of the globular domain (yellow arrows) represents each Tn complex binding with a specific periodicity (~38.5 nm) on actin-Tm filaments. Scale bar = 100 nm.

RTF appeared cleanest and less likely to aggregate under the apo-condition without the addition of $CaCl_2$. When varying concentrations of $CaCl_2$ (0.1-0.4 mM) were

added to the purified RTF, RTF tended to aggregate or bundle with itself or neighbouring strands, generating non-specific protein-protein interactions. Therefore, no $CaCl_2$ was added to the RTF buffer, despite the fact that the original intent was to obtain structures of the RTF both with and without the presence of Ca^{2+}.

5.3.2. Generation of thin filaments suitable for cryo-EM

After extensive screening to identify the optimal negative-stain EM conditions for RTF, the next step was to transition to screening and data collection under cryo conditions for structure determination. Multiple freezing conditions were tested, leading to the determination of the optimal one. However, the initial cryo screening showed the sample concentration (0.4 μM) that worked well for negative-stain EM, which required a ten-fold dilution of the original protein concentration of 4 μM at the assembly of the reconstituted thin filaments, was too low for cryo-EM. Therefore, the samples were treated with serial dilutions from five- to two-fold and without dilution. Although serial dilution was applied to the protein samples, how the samples appeared under the microscope was not a direct reflection of the dilution factor. Ultimately, the 5 × dilution and 2 × dilution for the WT RTF gave the most promising results. Full day data collection was then collected for WT RTF under these conditions and the resulting images were processed.

5.3.3. Image processing

A few of the Tn complexes binding to actin-Tm filaments were very clear as shown in Figure 5-7 but most were not. Manual particle picking was performed by e2boxer.py command of the EMAN2 software package and those picked boxes were subjected to further image processing.

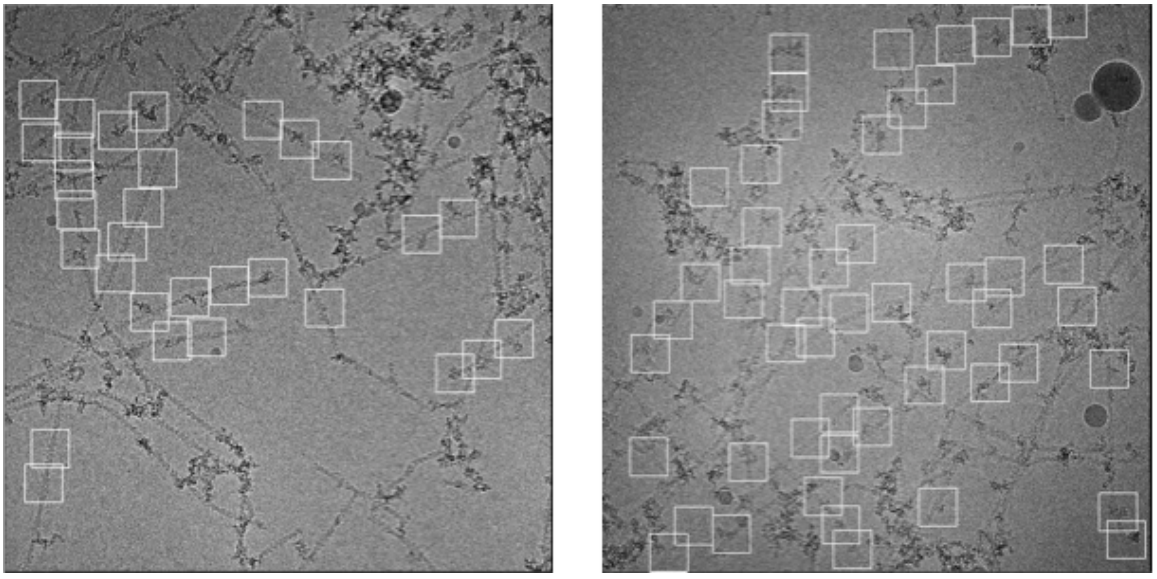

Figure 5-7 Manual particle picking process using the e2boxer.py commnad of the EMAN2 software package.

Each box was placed in a way such that each Tn complex was approximately located in the center of the box, representing one unit of a functional thin filament (7 actin:1 Tm: 1Tn). Each box size is 384 × 384 Å.

After image processing using RELION, the most clear density was shown for the actin-Tm that do not have any Tn complexes binding (as boxed in blue in figure 5-8), some Tn complex density alone without visible binding to the rest of the thin filaments (boxed in yellow in figure 5-8) and some Tn complex with actin and Tm (boxed in red in figure 5-8).

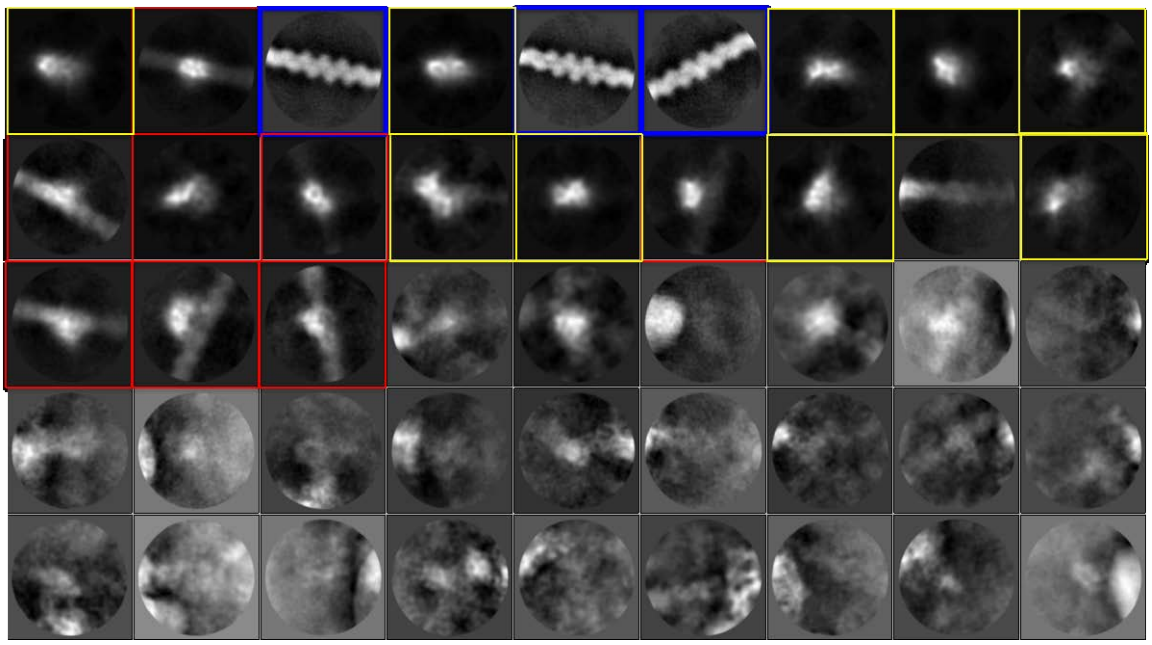

Figure 5-8 2D class averages obtained with RELION software.

Some Tn binding to actin-Tm filaments is clearly observed (red boxes), and clear averaged images of the filaments without the decoration of Tn complexes are also seen (blue boxes). Some images contain only Tn complexes (yellow boxes) without any visible filaments attached.

Serious challenges presented in the cryo-EM research and possible future directions to address these issues will be discussed in more detail in the next section.

5.4. Discussion

An exhaustive optimization process was undertaken in order to find the protein and buffer conditions that could ensure binding of at least 50% of the Tn complex to the thin filaments. Varying protein concentrations, binding ratios of each component, as well as concentrations of the salt, buffering agents, and pH were tested to identify the optimal combination for the formation of the thin filaments. Ultimately, the buffer that allowed the most Tn binding to the actin-Tm filaments contained 25 mM imidazole, 25 mM KCl, 4 mM $MgCl_2$, 1 mM EGTA, and 1 mM DTT at pH 7.4. However, although the decoration of the filaments with troponin complexes was high under the negatively stained conditions, protein aggregations were observed under the cryo conditions. Details of the serious challenges encountered in the cryo-EM step to determine the structure of the reconstituted cardiac thin filaments are discussed below.

The first challenge arose when the conditions that worked well to ensure higher Tn binding to the actin-Tm filaments and lower actin aggregation due to the presence of heavy metal salts did not work well for freezing cryo-EM grids. When using the same protein concentration as in the sample preparation step for the negative-stain EM, few or no RTF strands were present in the recorded images. However, increasing the sample concentration resulted in large aggregations that obscured clear observation of the thin filaments. A fine balance needs to be achieved to generate an adequate amount of thin filaments for each image without filament aggregation. More cryo-screening is required to find the right dilution of the thin filaments sample.

The second challenge is that, if in fact lower protein concentration has to be used to avoid the aggregation, then many more data collection sessions will be required to collect a reasonable number of images for data processing and reconstruction. Despite the fact that EM data collection has now become high throughput and automated, it is not without its caveats. The cost associated with equipment maintenance and data collection is still very high, typically in a range of ~ $2,000 per day, for the high-end cryo microscope such as Titan Krios, making experimental time scarce and expensive. Therefore, it is crucial to screen the most optimal conditions for the samples under the cryo conditions using less expensive but nevertheless sophisticated screening cryo microscope, such as Talos Artica.

Third, regardless of the choice of the microscope, reproducibility of sample preparation and data collection requires rigorous training and is still limited to experienced users. On-site assistance for the microscope is absolutely crucial. A cryo electron microscope, such as the Titan Krios microscope, is very expensive and difficult to manage and maintain (Alewijnse et al., 2017). In addition, high performance computer capabilities are required to store large amounts of data, typically in a range of a few terabytes for each data collection session (Alewijnse et al., 2017).

A fourth challenge is the flexible domains of the troponin complex which can hinder structural determination. In the reconstruction process, randomly-oriented particles are aligned, classified, superposed, and back-projected to obtain a three-dimensional structure of the protein. However, regions of high flexibility might be cancelled out after the averaging process, leaving only the stable regions visible. Since the regions of interests of the Tn complex on actin-Tm filaments are highly flexible, those regions may not be visible after the reconstruction process.

5.5. Future directions

Having actin-Tm filaments well decorated with troponin complexes and without aggregation is the primary goal for successful cryo-EM structural determination of cardiac thin filaments at high resolution. Each step should be carefully considered since many factors can influence the quality of the sample and ultimately affects the outcome for the analysis of the structure. This section discusses potential strategies that can be used, with a focus on sample preparation from the least formidable to more extensive optimization.

5.5.1. Vitrification process

In cryo-EM, vitrification of samples is achieved by blotting the samples on the grid to form in a thin layer of solution, then rapidly freezing the samples by plunging them into liquid ethane. Samples are then be embedded in a thin layer of ice, and the ice should be as thin as possible to fully include the specimen without distorting it. However, in our case, this resulted in aggregation that rendered more than 50% of the images unusable. One way to tackle this problem is to use a lower concentration (~0.4 μM) of protein as used in negative stain preparation, and carry out multiple blotting (Sievers et al., 2011) to

increase the particle density, avoiding the aggregation induced by higher concentration of filaments. This can potentially generate a cryo specimen that contains layers of sparse but well-separated filaments that might have a cumulatively significant number of filaments. However, ice thickness should be taken into consideration since increasing the ice thickness sacrifices the contrast. This can likely be overcome by increasing the blotting time. Multiple freezing and screening tests will be required to confirm the feasibility of this approach.

5.5.2. Use of continuous carbon film

As mentioned previously, a higher concentration of the filaments is required for cryo-EM. A key consideration in grid preparation is the type of the grid and support film used for the protein of interest. In cryo-EM, perforated carbon films are typically used to allow the specimen to be imaged in vitreous ice, suspended in the holes of the carbon film. Previous research has shown that the charge properties of the carbon film can have significant impact on how the particle partitions into the holes. Some samples tend to have higher affinity to the carbon film, and thus continuous carbon support films can be used to help the sample distribute homogenously, particularly for membrane proteins (Sgro and Costa, 2018). In addition, typically much less concentrated sample is required for the use of continuous carbon film, in which the concentration used is only slightly higher than one used for negative stain EM. In our case, although thin filaments are mainly hydrophilic and soluble, there might be areas that are largely hydrophobic and tend to cause the aggregation. Therefore, the use of continuous carbon layer film might be beneficial for homogeneous sample distribution on the grid.

5.5.3. Use of native thin filaments

If the problem of aggregation still persists in cryogenic visualization using the above-mentioned methodology, the use of native thin filaments might be an alternate approach. Currently reconstituted thin filaments are used, consisting of rabbit skeletal actin, recombinant human Tm and recombinant human troponin complex. Rabbit skeletal actin was used because it is relatively easy to isolate large amounts of actin from dried muscle powder, following a well-established and widely accepted protocol with a few modifications (Spudich et al., 1972). Since actin is a highly conserved protein, the sequence identity between rabbit skeletal actin and human cardiac actin is ~99% with

only four conserved substitutions. In addition, the use of recombinant Tm and Tn allows generation of many different combinations of thin filaments that contain the mutation of interest. However, it has been shown that reconstituted Tn complexes do not bind to reconstituted actin-Tm as well as they do to the thin filaments isolated from native muscle source. The reconstituted Tn complexes also tend to bundle with other filaments strands. Therefore, to use native thin filaments isolated from pigs, cows or chickens may be a more realistic alternative. Although ultimately, we are interested in human cardiac thin filaments, most thin filaments proteins among these species share a relatively high sequence identity with the human counterparts. If a high-resolution structure can be obtained for native thin filaments, they could serve as an important structural basis for human cardiac thin filaments.

5.5.4. Generation of mini filaments

Long filamentous structures have proven to be very challenging for structural determination since they can bend, twist and easily aggregate. Raunser's group has identified conditions for the binding of myosin or other proteins that can help unbundle and straighten the actin filaments (von der Ecken et al., 2016; von der Ecken et al., 2015). However, with the Tn complex having many flexible domains, it makes it very difficult to ensure the straightening of the filaments and a high decoration of Tn. To avoid the filament aggregation problems in the presence of the Tn complex, an approach that involves generating "mini-filaments" should be considered.

In 2005, Gong et al. published a protocol for the generation of mini filaments that contain approximate single regulatory units of ~40 nm in length and demonstrated their applicability to biochemical and structural analysis (Gong et al., 2005). The only disadvantage of this approach is that extensive modifications of some components are required. These include using gelsolin fused to the truncated N-terminus of TnT. Gelsolin is also used to cap the "barbed" end of the two actin strands, since each regulatory unit of thin filaments contain a double actin helix and a Tn-Tm complex in each strand. Furthermore, the other "pointed" end of the filaments is capped with tropomodulin which also interacts with the N-terminus of Tm. After the generation of stable mini-filaments, size-exclusion is used to further separate mini-filaments of the same size from other components that are not incorporated into the units. ATPase activity is carried out to validate the preservation of the function for these mini-filaments. With the recent

development of single particle cryo-EM, it could be promising to carry out cryo-EM on these mini-filaments and thus avoiding the aggregation caused by longer, unmodified filaments.

5.6. Summary

The cardiac thin filament is a large macromolecular complex whose function requires precise coordinated movements of all its protein components. As seen in many cases, the effects of one mutation in the Tn complex can propagate along the thin filaments, resulting in a complex cardiomyopathy. Therefore, obtaining a high-resolution structure of the entire cardiac thin filament can provide crucial details that could improve our understanding of the molecular mechanisms associated with various cardiomyopathies. Currently, cardiac sample preparation is the main bottleneck, due to the flexibility of the Tn complex and the heterogeneous nature of the thin filaments. Sample preparation requires as many Tn complexes binding to actin-Tm filaments as possible, without aggregation of the actin or uncomplexed protein components. Using the aforementioned approaches may be promising but are not without compromise. One limiting factor is the elevated cost of carrying out cryo-EM research, maintaining and using the cryo-EM microscope and the associated multiple freezing, screening, and data collection sessions. This technique is difficult, with a steep learning curve and necessary assistance from experienced cryo-EM researchers and technicians. Nevertheless, cryo-EM should be pursued for what it could do to aid in the successful solving of the structure of the cardiac thin filament. The resultant high-resolution structure will be able to provide invaluable insight into the molecular and disease mechanisms and facilitate rational drug design to combat cardiomyopathies.

Chapter 6.

General Discussion and Future Directions

The main objective of this thesis project was to determine the structure and function of the cardiomyopathy-associated reconstituted cardiac thin filaments. Cardiac thin filaments are the major components of sarcomeres, the basic building blocks of cardiac muscles. Each thin filament unit consists of seven actin monomers, one tropomyosin dimer, and one trimeric Tn complex made up of TnC, TnI, and TnT. Mutations found in each of these components have been shown to be associated with various cardiomyopathies, such as hypertrophic cardiomyopathy (HCM), dilated cardiomyopathy (DCM), or restricted cardiomyopathy (RCM). In particular, HCM is the most commonly inherited cardiac disorder that affects one in 500 individuals. The severity of its symptoms vary widely, ranging from asymptomatic to the most serious case, sudden cardiac death (SCD). HCM is the most common cause of sudden cardiac death in athletes and individuals under the age of 35. However, although current drug therapy aims for symptom management, there is no treatment to prevent disease progression. It is imperative to develop a more proactive approach that will enable clinicians to risk stratify at-risk patients and their family members who are also mutational carriers. Without a deeper understanding of the molecular basis of the disease mechanisms associated with cardiomyopathies, progress for cardiologists to initiate appropriate preventative therapy will be greatly hindered. Elucidating the structure and function of the thin filaments at the molecular level can provide insightful information on the disease mechanism in various cardiomyopathies.

The following sections describe each aim of this thesis project, and a summary of the research results and analyses.

6.1. Summary of findings

6.1.1. Generation of reconstituted thin filaments (RTFs)

The first aim of the thesis was to establish protein expression and purification protocols for each of the thin filament components in order to then carry out functional

and structural studies. Most of the RTFs generated from previous studies involved the use of a mixture of components from various species, such as native bovine tropomyosin and mouse or Tn complexes. Although bovine Tm and human Tm have a >99% sequence identity, isolation of bovine Tm is a complex process that involves obtaining fresh heart muscle from a slaughter house and executing extensive purification steps. In addition, expressing the protein from a human recombinant construct allows one to generate specific mutations or isoforms. In this thesis, the human recombinant Tm was utilized with a modified terminal extension of Met-Ala-Ser substituting functionally for the acetylation of the native N-terminus of Tm in eukaryotic cells (Brunet et al., 2014; Coulton et al., 2006; Monteiro et al., 1994). The recombinant Tm was found to be expressed very efficiently in bacterial *E. coli,* resulting in large quantities of purified recombinant Tm (>200 mg) being harvested from six liters of culture. The only limitation of the recombinant Tm was that a higher than the physiological stoichiometric ratio was required to ensure effective binding of Tn to Tm and actin to form complete RTF. After experimentation, it was determined that adding 2-3 μM of Tm to 4 μM of actin, followed by the addition of 0.6 μM of Tn complexes, was the most productive combination. Using this protein expression and purification protocol as described in Chapter 2, I successfully generated over 15 RTF constructs containing various HCM-related mutations, including a novel ssTnI R37C mutation in both fetal and adult counterparts. RTF generated using recombinant Tm gave rise to measurable changes in Ca^{2+} binding properties, comparable to those of the RTF reconstituted with native bovine Tm.

6.1.2. Effects of TnT mutations on TnI phosphorylation

The third aim of this thesis project was to perform functional studies on the Tn complexes and RTF containing three HCM-associated cTnT expressed from the cardiac *TNNT2* gene mutations. Specifically, to determine how the mutations affected the Ca^{2+} binding properties in the biochemical systems under steady-state and stopped-flow conditions. Patients with cTnT mutations do not necessarily develop hypertrophy but some specific mutations are associated with a high incidence of sudden cardiac death. Three cTnT mutations, I79N, F110I and R278C cTnT, were chosen because previous work on skinned papillary muscle isolated from the hearts of transgenic mice has shown that they have a varying degree of Ca^{2+} sensitization (I79N > F110I > R278C) that corresponds to their susceptibility to arrhythmia (Baudenbacher et al., 2008; Schober et

al., 2012). From their studies, it was shown that I79N has the most Ca^{2+} sensitizing ability, F110I being the intermediate and R278C behaving similarly to the WT.

Surprisingly, our functional studies show that the RTF containing R278C was as Ca^{2+} sensitizing as the I79N cTnT mutation, with F110I being the most similar to WT. The effects of TnI phosphorylation were also investigated. TnI phosphorylation is considered one of the most important downstream effects of the PKA signaling pathways that accelerates the Ca^{2+} turnover on TnC during β-adrenergic agonist stimulation. Under normal conditions, TnI phosphorylation of two serine residues at positions 23 and 24 facilitates Ca^{2+} dissociation from TnC, increasing the myofilament relaxation process. Our *in vitro* experiments directly recapitulated this phenomenon, in which the Ca^{2+} dissociation rate in the RTF containing the phosphomimetic cTnI is 2-fold the Ca^{2+} dissociation rate compared to that of the WT. Nevertheless, when cTnT mutations were incorporated in the RTF, the enhanced Ca^{2+} dissociation rate due to phosphomimetic cTnI was diminished. This suggests that all three cTnT mutations studied uniformly abolish the functional effects of TnI, compromising the relaxation process of the myofilaments. These findings suggest that TnT mutations exert their effects not only on the myofilament Ca^{2+} sensitization, but perhaps more importantly, on the interactions with cTnI especially during β-adrenergic agonist stimulation in which enhanced Ca^{2+} removal is required to meet the higher chronotropic state.

6.1.3. Difference between adult and neonatal Tn complex and RTF systems and the effects from the cardiomyopathy-associated mutations in adult and neonatal environment

The fourth aim of this project was to perform functional studies on the fetal and adult Tn complexes and RTF, and understand how cardiomyopathy mutations have different effects on the Ca^{2+} binding properties in the fetal and adult myofilaments. At the Tn complex level, it was evident that the WT fetal Tn complex had a much higher Ca^{2+} sensitivity compared to the adult Tn complex, consistent with previous literature (Elmstedt et al., 2012; Gomes et al., 2004; Pinto et al., 2011; Racca et al., 2016). This confirmed that our *in vitro* experiments were able to recapitulate the differences in Ca^{2+} binding properties observed in the *in vivo* and whole cell systems.

Two particular variants were selected for their severe phenotypes and association with sudden death: the I79N cTnT mutation expressed from isoform 3 in *TNNT2* gene (Uniprot ID: P45379-6) in adult patients and the R37C ssTnI mutation expressed from the *TNNI1* gene (Uniprot ID: P19237) in infants. The I79N cTnT mutation was selected due to its high rate of sudden cardiac death in adult patients. When this mutation was incorporated in the fetal TnT (isoform 1 in *TNNT2* gene), correspondingly, in the position of I89N, the Ca^{2+} sensitizing effect was diminished. This suggests that at the fetal/neonatal/infant stage, this comparable mutation potentially has not yet demonstrated its overt effects on myofilament Ca^{2+} sensitization. However, once the I79N mutation was in the adult environment with the switch of ssTnI to cTnI paralog in the Tn complexes, the marked Ca^{2+} sensitization was evident, explaining the cardiac dysfunction observed in patients and transgenic mice models (Baudenbacher et al., 2008; Knollmann et al., 2001; Schober et al., 2012).

The R37C ssTnI heterozygous mutation was the first mutation associated with ssTnI previously discovered by our group (Dewar et al., 2017). This mutation was found in ten out of 191 tissue samples isolated from infants under the age of two (Dewar et al., 2017). Unlike the I79N cTnT mutation, it decreases Ca^{2+} sensitivity at both the Tn complexes and RTF levels. The persistent Ca^{2+} desensitizing effect observed in both biochemical systems suggests that mutation associated with ssTnI is severe. In addition, when the corresponding mutation, R68C cTnI, was incorporated in the adult environment, it produces an opposite trend – it sensitizes the myofilament to Ca^{2+}. This indicates that this mutation is not benign in both fetal and adult environment, although it is still completely unknown as to why the adult mutation carriers survive past the fetal/neonatal/infant stages.

6.1.4. Cryo-EM on the reconstituted thin filaments (RTF)

The second aim of this thesis project was to solve the three-dimensional structure of the RTF. This part of the project was carried out in collaboration with Dr. Thomas Walz at Rockefeller University, USA. Together with Dr. Kelly Kim in Dr. Walz' lab, I used a negative-stain EM to screen for optimized RTF; those RTF with the highest number of Tn complexes bound to the filaments. An extensive optimization process was carried out at SFU to identify the ideal buffering agent, salt concentration, and pH range in both the apo- and Ca^{2+}-bound conditions. Ultimately, it was determined that the

binding ratio of 4 μM of actin, 4 μM of Tm and 2 μM of Tn was most effective at ensuring Tn binding in the apo- condition. The optimized buffer contained (in mM): 25 KCl, 25 imidazole, 4 $MgCl_2$, 1 EGTA, 1 DTT at pH 7.4. Under EM it was obvious that there was some unbound Tn, which did not interfere with the structural study but could with the functional studies. For functional studies, it was important that there would be no unbound, free Tn complexes in the solution because the fluorescence signal from those unbound Tn complexes would interfere with the signal from the RTF.

The conditions that worked well for the negative-stain EM resulted in large amounts of aggregation under the cryo conditions. Several data sets were collected, including the WT RTF and the RTF with the I79N TnT (*TNNT2* gene) mutation. The EM images collected for the WT RTF showed more filaments without aggregation than the I79N mutation, so only the WT RTF images were processed, motion corrected and subjected to 2D classification. Preliminary results revealed some filaments with bound Tn complexes, but there were many aggregated particles as well, likely between unbound Tn complexes and neighboring strands of filaments.

In order to decrease the amount of aggregation, samples of lower protein concentration may be required, and multiple blotting on the same grid with lower concentrated samples is the first reasonable step to attempt. Although the preliminary results were promising, this project could not be pursued further due to limited resources and access to the cryo-electron microscope at UBC.

6.2. Practical applications and limitations

6.2.1. Reconstituted thin filament system

One major advantage of RTF is that it is a very stable system, allowing incorporation of any desired mutation in the recombinant Tn subunit and recombinant Tm. In addition, it can accurately recapitulate changes in the Ca^{2+} binding properties observed in the cardiomyocytes, consistent with previous literature (Davis et al., 2007). Furthermore, data generated from the RTF are complementary to the techniques for the whole cell system utilized in our lab; for example, the same cardiomyopathy-associated mutation can also be engineered into the human induced pluripotent cells (hiPSC) using CRISPER/Cas9. This allows us to study a particular mutation at systems of increasing

complexity, enabling us to corroborate the molecular mechanism observed at the biochemical level to the pathogenicity occurring at the whole cell/tissue system (Shafaattalab et al., 2019).

As with any study, there were limitations to our techniques. One major limitation of the RTF system is that the length of the RTF cannot be controlled. After purification of the actin filaments, phalloidin was immediately added to stabilize the structure of actin. Phalloidin is a toxin isolated from the death cap mushroom which acts on the interface of actin, locking adjacent actin monomers together and stabilizing the actin filaments by preventing their depolymerization (Barden et al., 1987; Wehland et al., 1977). After the addition of phalloidin, the structure of the actin filaments became very stable without dissociation; however, the caveat is that the length cannot be neither determined nor controlled.

Another limitation is the use of the fluorophore that allows reporting of Ca^{2+} binding and dissociation in steady-state and stopped-flow experiments, respectively. Three mutations, C35S, C84S, and T53C, are required to generate a highly conserved protein TnC for the fluorophore IAANS to covalently attach to Thr53 of TnC. This engineered TnC was developed and tested (Davis et al., 2007) and the technique has been widely accepted in the last decade for its ability to accurately report the biochemical and biophysical changes to Ca^{2+} interactions with site II of TnC, similar to WT and endogenous TnC (Albury et al., 2012; Davis et al., 2007; Davis and Tikunova, 2008; Li et al., 2013a; Liu et al., 2012a; Liu et al., 2014; Tikunova et al., 2010). In addition, unlike endogenous Cys at positions 35 and 84, Thr 53 does not interact with residues that are in proximity to the hydrophobic core of TnC or the ion binding sites, while maintaining spectroscopically determined Ca^{2+} sensitivity (Davis et al., 2007; Davis and Tikunova, 2008). Furthermore, labeling at Cys35 and Cys84 has been shown to modify the Ca^{2+} binding properties of Tn complexes and Ca^{2+}-dependent ATPase activity at the thin filament level (Davis et al., 2007; Davis and Tikunova, 2008). Consequently, labeling at T53C TnC remains an ideal candidate for fluorophore labeling to examine the Ca^{2+} binding properties of Tn complexes and RTF.

6.3. Recommendations for future research

6.3.1. Direct extension of the current research

There is a huge range of possible cardiomyopathy-associated mutations that can be incorporated into each Tn subunit and the recombinant Tm. To date, there are more than 100 mutations found in genes encoding Tn subunits (Willott et al., 2010) and more than 15 mutations in Tm (Redwood and Robinson, 2013) that are associated with various cardiomyopathies. Each of the known mutations, and any newly discovered mutations, can be generated in the Tn complexes and RTF, and their corresponding Ca^{2+} binding properties characterized in steady-state and stopped-flow fluorescence experiments.

Furthermore, there is also the possibility of using Tn complexes and RTF for screening of potential drug candidates as Ca^{2+} sensitizers or desensitizers. A recent publication from Aprahamian et. al. demonstrates the potential of virtual screening, using molecular dynamics simulations from a list of possible chemical compounds and testing their ability to fine-tune Ca^{2+} sensitivity in the TnC and TnC-TnI complex using stopped-flow kinetics and steady-state fluorescence titrations (Aprahamian et al., 2017). A similar concept can be applied to the Tn complexes and RTF system to identify novel compounds that can be tested experimentally using the current established techniques described in this thesis.

Moreover, various experimental conditions can be tested to allow observation of factors that can influence Ca^{2+} sensitivity of Tn complexes and RTF. These include changing pH to investigate the effects of cytosolic acidosis on the fetal and/or adult Tn complexes and RTF. There is strong evidence of the pivotal role that TnI paralogs play in the pH-dependent Ca^{2+} response (Ball et al., 1994; Gomes et al., 2004). More studies can be carried out, to complement those already reported, to explore the different Ca^{2+} binding properties during acidosis conditions and in the presence of various mutations (Fentzke et al., 1999; Westfall et al., 1997; Wolska et al., 2001).

6.3.2. Broader issues to be covered

The next logical step to examine the effects of the cardiomyopathy-associated mutations is to incorporate the mutations into our established hiPSC-CM whole cell system and test their changes in voltage and Ca^{2+} dynamics compared to WT. We have

shown, in our most recent publications, that these techniques, on the RTF level and the whole cell level, are highly complementary and allow us to develop a platform that can be applied broadly when novel variants are identified and incorporated in the hiPSC-CMs using the CRISPER/Cas9 genome editing technique (Shafaattalab et al., 2019). This approach allows applications in disease modeling, discovery of new disease mechanisms, individualized risk stratification by cellular phenotyping, and drug safety testing that is specific to a patient or mutation (Eschenhagen et al., 2015).

6.4. Final conclusion

The work described within this thesis focused on the molecular mechanisms associated with changes in myofilament Ca^{2+} sensitivity and their contribution to the pathophysiology of the various cardiomyopathies. The functional characterizations of the three TnT mutations in Chapter 3 demonstrate that these HCM-associated mutations exert their effects through increasing Ca^{2+} sensitivity, thereby decreasing Ca^{2+} dissociation. This is especially true of the I79N mutation and the R278C mutation, which was previously thought to be a benign mutation. Moreover, all three TnT mutations, including the seemly benign mutation F110I, greatly attenuated the functional effects of the phosphomimetic cTnI, compromising the ability of the myofilament to relax during conditions that mimic β-adrenergic stimulation.

In Chapter 4, the differences between the protein isoforms/paralogs that comprise the adult and neonatal thin filaments are evident, whereby the neonatal constructs demonstrate a much higher Ca^{2+} sensitivity compared to that of the adults. The Ca^{2+}-sensitizing effect of the I79N TnT mutation becomes apparent in the adult construct, while the more severe ssTnI (*TNNI1* gene) mutation, R37C, demonstrates a persistent Ca^{2+} desensitization, regardless of the complexity of the system. These data provide important insight into how a particular cardiomyopathy-associated mutation affects the Ca^{2+} binding properties in the neonatal and adult environments at a molecular level, supporting the ongoing evidence that the pathophysiology of heart failure and arrhythmias in pediatric cardiomyopathy populations differ from adults. Although childhood cardiomyopathies are relatively rare compared to adult cardiac diseases, clinical trials and management that are specific to infants and children are urgently needed.

Identifying the pathophysiological mechanism(s) that underlie complex cardiomyopathies is by no means a straightforward task. Advances in cardiovascular genetics during the last three decades have identified a large number of mutations, some of which continue to be idiopathic. The ability for clinicians to risk-stratify patients who are mutational carriers remains to be challenging, since the link between genotype and phenotype can be weak, and background genetics, epigenetic, environmental and/or other still unidentified modifying factors can impact the severity of the disease. Using a comprehensive approach, combining *in vitro* and *in silico* biochemical studies as well as testing the mutations in a system closely resembling human cardiomyocytes, particularly hiPSC-derived cardiomyocytes, holds great promise. In the future, knowledge gained from molecular and cellular basic science research can be applied to the design of an integrative physiological clinical approach tailored to each specific mutation or patient, providing the basis for risk stratification and leading to the development of therapies to prevent cardiac dysfunction caused by sarcomeric mutations.

References

Ait-Mou, Y., K. Hsu, G.P. Farman, M. Kumar, M.L. Greaser, T.C. Irving, and P.P. de Tombe. 2016. Titin strain contributes to the Frank-Starling law of the heart by structural rearrangements of both thin- and thick-filament proteins. *Proceedings of the National Academy of Sciences of the United States of America*. 113:2306-2311.

Albury, A.N., N. Swindle, D.R. Swartz, and S.B. Tikunova. 2012. Effect of hypertrophic cardiomyopathy-linked troponin C mutations on the response of reconstituted thin filaments to calcium upon troponin I phosphorylation. *Biochemistry*. 51:3614-3621.

Alewijnse, B., A.W. Ashton, M.G. Chambers, S. Chen, A. Cheng, M. Ebrahim, E.T. Eng, W.J.H. Hagen, A.J. Koster, C.S. Lopez, N. Lukoyanova, J. Ortega, L. Renault, S. Reyntjens, W.J. Rice, G. Scapin, R. Schrijver, A. Siebert, S.M. Stagg, V. Grum-Tokars, E.R. Wright, S. Wu, Z. Yu, Z.H. Zhou, B. Carragher, and C.S. Potter. 2017. Best practices for managing large CryoEM facilities. *Journal of structural biology*. 199:225-236.

Alexander, M.E., F. Cecchin, E.P. Walsh, J.K. Triedman, L.M. Bevilacqua, and C.I. Berul. 2004. Implications of implantable cardioverter defibrillator therapy in congenital heart disease and pediatrics. *Journal of cardiovascular electrophysiology*. 15:72-76.

Allen, D.G., and S. Kurihara. 1982. The effects of muscle length on intracellular calcium transients in mammalian cardiac muscle. *The Journal of physiology*. 327:79-94.

Alves, M.L., F.A.L. Dias, R.D. Gaffin, J.N. Simon, E.M. Montminy, B.J. Biesiadecki, A.C. Hinken, C.M. Warren, M.S. Utter, R.T.R. Davis, S. Sakthivel, J. Robbins, D.F. Wieczorek, R.J. Solaro, and B.M. Wolska. 2014. Desensitization of myofilaments to Ca2+ as a therapeutic target for hypertrophic cardiomyopathy with mutations in thin filament proteins. *Circulation. Cardiovascular genetics*. 7:132-143.

Anan, R., H. Shono, A. Kisanuki, S. Arima, S. Nakao, and H. Tanaka. 1998. Patients with familial hypertrophic cardiomyopathy caused by a Phe110Ile missense mutation in the cardiac troponin T gene have variable cardiac morphologies and a favorable prognosis. *Circulation*. 98:391-397.

Anderson, P.A., N.N. Malouf, A.E. Oakeley, E.D. Pagani, and P.D. Allen. 1991. Troponin T isoform expression in humans. A comparison among normal and failing adult heart, fetal heart, and adult and fetal skeletal muscle. *Circulation research*. 69:1226-1233.

Aprahamian, M.L., S.B. Tikunova, M.V. Price, A.F. Cuesta, J.P. Davis, and S. Lindert. 2017. Successful Identification of Cardiac Troponin Calcium Sensitizers Using a Combination of Virtual Screening and ROC Analysis of Known Troponin C Binders. *Journal of chemical information and modeling*. 57:3056-3069.

Ashcroft, F.M. 2006. From molecule to malady. *Nature*. 440:440-447.

Ashrafian, H., C. Redwood, E. Blair, and H. Watkins. 2003. Hypertrophic cardiomyopathy:a paradigm for myocardial energy depletion. *Trends in genetics : TIG*. 19:263-268.

Ashrafian, H., and H. Watkins. 2007. Reviews of translational medicine and genomics in cardiovascular disease: new disease taxonomy and therapeutic implications cardiomyopathies: therapeutics based on molecular phenotype. *J Am Coll Cardiol*. 49:1251-1264.

Bai, F., H.M. Caster, J.R. Pinto, and M. Kawai. 2013. Analysis of the molecular pathogenesis of cardiomyopathy-causing cTnT mutants I79N, DeltaE96, and DeltaK210. *Biophysical journal*. 104:1979-1988.

Bai, X.C., G. McMullan, and S.H. Scheres. 2015. How cryo-EM is revolutionizing structural biology. *Trends Biochem Sci*. 40:49-57.

Ball, K.L., M.D. Johnson, and R.J. Solaro. 1994. Isoform specific interactions of troponin I and troponin C determine pH sensitivity of myofibrillar Ca2+ activation. *Biochemistry*. 33:8464-8471.

Barden, J.A., M. Miki, B.D. Hambly, and C.G. Dos Remedios. 1987. Localization of the phalloidin and nucleotide-binding sites on actin. *European journal of biochemistry*. 162:583-588.

Basi, G.S., and R.V. Storti. 1986. Structure and DNA sequence of the tropomyosin I gene from Drosophila melanogaster. *The Journal of biological chemistry*. 261:817-827.

Baudenbacher, F., T. Schober, J.R. Pinto, V.Y. Sidorov, F. Hilliard, R.J. Solaro, J.D. Potter, and B.C. Knollmann. 2008. Myofilament Ca2+ sensitization causes susceptibility to cardiac arrhythmia in mice. *The Journal of clinical investigation*. 118:3893-3903.

Behere, S.P., and S.N. Weindling. 2015. Inherited arrhythmias: The cardiac channelopathies. *Annals of pediatric cardiology*. 8:210-220.

Behrmann, E., M. Muller, P.A. Penczek, H.G. Mannherz, D.J. Manstein, and S. Raunser. 2012. Structure of the rigor actin-tropomyosin-myosin complex. *Cell*. 150:327-338.

Bers, D.M. 2002. Cardiac excitation-contraction coupling. *Nature*. 415:198-205.

Bers, D.M. 2008. Calcium cycling and signaling in cardiac myocytes. *Annual review of physiology*. 70:23-49.

Brown, J.H., K.H. Kim, G. Jun, N.J. Greenfield, R. Dominguez, N. Volkmann, S.E. Hitchcock-DeGregori, and C. Cohen. 2001. Deciphering the design of the tropomyosin molecule. *Proceedings of the National Academy of Sciences of the United States of America*. 98:8496-8501.

Brunet, N.M., P.B. Chase, G. Mihajlovic, and B. Schoffstall. 2014. Ca(2+)-regulatory function of the inhibitory peptide region of cardiac troponin I is aided by the C-terminus of cardiac troponin T: Effects of familial hypertrophic cardiomyopathy mutations cTnI R145G and cTnT R278C, alone and in combination, on filament sliding. *Archives of biochemistry and biophysics*. 552-553:11-20.

Buchan, D.W., F. Minneci, T.C. Nugent, K. Bryson, and D.T. Jones. 2013. Scalable web services for the PSIPRED Protein Analysis Workbench. *Nucleic acids research*. 41:W349-357.

Bueno, O.F., L.J. De Windt, K.M. Tymitz, S.A. Witt, T.R. Kimball, R. Klevitsky, T.E. Hewett, S.P. Jones, D.J. Lefer, C.F. Peng, R.N. Kitsis, and J.D. Molkentin. 2000.

The MEK1-ERK1/2 signaling pathway promotes compensated cardiac hypertrophy in transgenic mice. *The EMBO journal*. 19:6341-6350.

Cammarato, A., V. Hatch, J. Saide, R. Craig, J.C. Sparrow, L.S. Tobacman, and W. Lehman. 2004. Drosophila muscle regulation characterized by electron microscopy and three-dimensional reconstruction of thin filament mutants. *Biophys J*. 86:1618-1624.

Campbell, M.G., A. Cheng, A.F. Brilot, A. Moeller, D. Lyumkis, D. Veesler, J. Pan, S.C. Harrison, C.S. Potter, B. Carragher, and N. Grigorieff. 2012. Movies of ice-embedded particles enhance resolution in electron cryo-microscopy. *Structure*. 20:1823-1828.

Cheng, Y., N. Grigorieff, P.A. Penczek, and T. Walz. 2015a. A primer to single-particle cryo-electron microscopy. *Cell*. 161:438-449.

Cheng, Y., V. Rao, A.Y. Tu, S. Lindert, D. Wang, L. Oxenford, A.D. McCulloch, J.A. McCammon, and M. Regnier. 2015b. Troponin I Mutations R146G and R21C Alter Cardiac Troponin Function, Contractile Properties, and Modulation by Protein Kinase A (PKA)-mediated Phosphorylation. *The Journal of biological chemistry*. 290:27749-27766.

Chung, J.H., B.J. Biesiadecki, M.T. Ziolo, J.P. Davis, and P.M. Janssen. 2016. Myofilament Calcium Sensitivity: Role in Regulation of In vivo Cardiac Contraction and Relaxation. *Frontiers in physiology*. 7:562.

Colan, S.D. 2010. Hypertrophic cardiomyopathy in childhood. *Heart failure clinics*. 6:433-444, vii-iii.

College, O. 2013. Anatomy & Physiology. OpenStax CNX, Houston, TX.

Colson, B.A., T. Bekyarova, M.R. Locher, D.P. Fitzsimons, T.C. Irving, and R.L. Moss. 2008. Protein kinase A-mediated phosphorylation of cMyBP-C increases proximity of myosin heads to actin in resting myocardium. *Circulation research*. 103:244-251.

Coulton, A., S.S. Lehrer, and M.A. Geeves. 2006. Functional homodimers and heterodimers of recombinant smooth muscle tropomyosin. *Biochemistry*. 45:12853-12858.

Coulton, A.T., and J.E. Stelzer. 2012. Cardiac myosin binding protein C and its phosphorylation regulate multiple steps in the cross-bridge cycle of muscle contraction. *Biochemistry*. 51:3292-3301.

Davis, J., L.C. Davis, R.N. Correll, C.A. Makarewich, J.A. Schwanekamp, F. Moussavi-Harami, D. Wang, A.J. York, H. Wu, S.R. Houser, C.E. Seidman, J.G. Seidman, M. Regnier, J.M. Metzger, J.C. Wu, and J.D. Molkentin. 2016. A Tension-Based Model Distinguishes Hypertrophic versus Dilated Cardiomyopathy. *Cell*. 165:1147-1159.

Davis, J.P., C. Norman, T. Kobayashi, R.J. Solaro, D.R. Swartz, and S.B. Tikunova. 2007. Effects of thin and thick filament proteins on calcium binding and exchange with cardiac troponin C. *Biophys J*. 92:3195-3206.

Davis, J.P., and S.B. Tikunova. 2008. Ca(2+) exchange with troponin C and cardiac muscle dynamics. *Cardiovascular research*. 77:619-626.

De Rosier, D.J., and A. Klug. 1968. Reconstruction of three dimensional structures from electron micrographs. *Nature*. 217:130-134.

de Tombe, P.P., R.D. Mateja, K. Tachampa, Y. Ait Mou, G.P. Farman, and T.C. Irving. 2010. Myofilament length dependent activation. *Journal of molecular and cellular cardiology*. 48:851-858.

Delano, W.L. 2015. The PyMol molecular graphics system. The PyMOL Molecular Graphics System, Version 1.8. Schrödinger, LLC.

Dewar, L.J., M. Alcaide, D. Fornika, L. D'Amato, S. Shafaatalab, C.M. Stevens, T. Balachandra, S.M. Phillips, S. Sanatani, R.D. Morin, and G.F. Tibbits. 2017. Investigating the Genetic Causes of Sudden Unexpected Death in Children Through Targeted Next-Generation Sequencing Analysis. *Circulation. Cardiovascular genetics*. 10.

Dobesh, D.P., J.P. Konhilas, and P.P. de Tombe. 2002. Cooperative activation in cardiac muscle: impact of sarcomere length. *American journal of physiology. Heart and circulatory physiology*. 282:H1055-1062.

Dominguez, R., and K.C. Holmes. 2011. Actin structure and function. *Annual review of biophysics*. 40:169-186.

Dong, W.J., J. Xing, Y. Ouyang, J. An, and H.C. Cheung. 2008. Structural kinetics of cardiac troponin C mutants linked to familial hypertrophic and dilated cardiomyopathy in troponin complexes. *The Journal of biological chemistry*. 283:3424-3432.

dos Remedios, C.G., D. Chhabra, M. Kekic, I.V. Dedova, M. Tsubakihara, D.A. Berry, and N.J. Nosworthy. 2003. Actin binding proteins: regulation of cytoskeletal microfilaments. *Physiological reviews*. 83:433-473.

Durer, Z.A., D.S. Kudryashov, M.R. Sawaya, C. Altenbach, W. Hubbell, and E. Reisler. 2012. Structural states and dynamics of the D-loop in actin. *Biophysical journal*. 103:930-939.

Dweck, D., N. Hus, and J.D. Potter. 2008. Challenging current paradigms related to cardiomyopathies. Are changes in the Ca2+ sensitivity of myofilaments containing cardiac troponin C mutations (G159D and L29Q) good predictors of the phenotypic outcomes? *The Journal of biological chemistry*. 283:33119-33128.

Eicken, A., C. Kolb, S. Lange, S. Brodherr-Heberlein, B. Zrenner, C. Schreiber, and J. Hess. 2006. Implantable cardioverter defibrillator (ICD) in children. *International journal of cardiology*. 107:30-35.

Elliott, P.M., L. D'Cruz, and W.J. McKenna. 1999. Late-onset hypertrophic cardiomyopathy caused by a mutation in the cardiac troponin T gene. *N Engl J Med*. 341:1855-1856.

Elmstedt, N., K. Ferm-Widlund, B. Lind, L.A. Brodin, and M. Westgren. 2012. Fetal cardiac muscle contractility decreases with gestational age: a color-coded tissue velocity imaging study. *Cardiovascular ultrasound*. 10:19.

Elmstedt, N.N., J.J. Johnson, B.B. Lind, K.K. Ferm-Widlund, L.L. Herling, M.M. Westgren, and L.A. Brodin. 2013. Reference values for fetal tissue velocity imaging and a new approach to evaluate fetal myocardial function. *Cardiovascular ultrasound*. 11:29.

Eschenhagen, T., C. Mummery, and B.C. Knollmann. 2015. Modelling sarcomeric cardiomyopathies in the dish: from human heart samples to iPSC cardiomyocytes. *Cardiovascular research*. 105:424-438.

Farman, G.P., E.J. Allen, D. Gore, T.C. Irving, and P.P. de Tombe. 2007. Interfilament spacing is preserved during sarcomere length isometric contractions in rat cardiac trabeculae. *Biophysical journal*. 92:L73-75.

Farman, G.P., E.J. Allen, K.Q. Schoenfelt, P.H. Backx, and P.P. de Tombe. 2010. The role of thin filament cooperativity in cardiac length-dependent calcium activation. *Biophys J*. 99:2978-2986.

Farman, G.P., D. Gore, E. Allen, K. Schoenfelt, T.C. Irving, and P.P. de Tombe. 2011. Myosin head orientation: a structural determinant for the Frank-Starling relationship. *Am J Physiol Heart Circ Physiol*. 300:H2155-2160.

Feest, E.R., F. Steven Korte, A.Y. Tu, J. Dai, M.V. Razumova, C.E. Murry, and M. Regnier. 2014. Thin filament incorporation of an engineered cardiac troponin C variant (L48Q) enhances contractility in intact cardiomyocytes from healthy and infarcted hearts. *Journal of molecular and cellular cardiology*. 72:219-227.

Fentzke, R.C., S.H. Buck, J.R. Patel, H. Lin, B.M. Wolska, M.O. Stojanovic, A.F. Martin, R.J. Solaro, R.L. Moss, and J.M. Leiden. 1999. Impaired cardiomyocyte relaxation and diastolic function in transgenic mice expressing slow skeletal troponin I in the heart. *The Journal of physiology*. 517 (Pt 1):143-157.

Fitzsimons, D.P., and R.L. Moss. 1998. Strong binding of myosin modulates length-dependent Ca2+ activation of rat ventricular myocytes. *Circ Res*. 83:602-607.

Fu, D.G. 2015. Cardiac Arrhythmias: Diagnosis, Symptoms, and Treatments. *Cell biochemistry and biophysics*. 73:291-296.

Fujita, E., T. Nakanishi, T. Nishizawa, N. Hagiwara, and R. Matsuoka. 2013. Mutations in the cardiac troponin T gene show various prognoses in Japanese patients with hypertrophic cardiomyopathy. *Heart and vessels*. 28:785-794.

Fung, D.C., B. Yu, T. Littlejohn, and R.J. Trent. 1999. An online locus-specific mutation database for familial hypertrophic cardiomyopathy. *Hum Mutat*. 14:326-332.

Galinska-Rakoczy, A., P. Engel, C. Xu, H. Jung, R. Craig, L.S. Tobacman, and W. Lehman. 2008. Structural basis for the regulation of muscle contraction by troponin and tropomyosin. *J Mol Biol*. 379:929-935.

Garcia-Castro, M., J.R. Reguero, A. Batalla, B. Diaz-Molina, P. Gonzalez, V. Alvarez, A. Cortina, G.I. Cubero, and E. Coto. 2003. Hypertrophic cardiomyopathy: low frequency of mutations in the beta-myosin heavy chain (MYH7) and cardiac troponin T (TNNT2) genes among Spanish patients. *Clin Chem*. 49:1279-1285.

Geisterfer-Lowrance, A.A., S. Kass, G. Tanigawa, H.P. Vosberg, W. McKenna, C.E. Seidman, and J.G. Seidman. 1990. A molecular basis for familial hypertrophic cardiomyopathy: a beta cardiac myosin heavy chain gene missense mutation. *Cell*. 62:999-1006.

Genge, C.E., C.M. Stevens, W.S. Davidson, G. Singh, D. Peter Tieleman, and G.F. Tibbits. 2016. Functional Divergence in Teleost Cardiac Troponin Paralogs Guides Variation in the Interaction of TnI Switch Region with TnC. *Genome Biol Evol*. 8:994-1011.

Gomes, A.V., G. Guzman, J. Zhao, and J.D. Potter. 2002. Cardiac troponin T isoforms affect the Ca2+ sensitivity and inhibition of force development. Insights into the role of troponin T isoforms in the heart. *The Journal of biological chemistry*. 277:35341-35349.

Gomes, A.V., G. Venkatraman, J.P. Davis, S.B. Tikunova, P. Engel, R.J. Solaro, and J.D. Potter. 2004. Cardiac troponin T isoforms affect the Ca(2+) sensitivity of force development in the presence of slow skeletal troponin I: insights into the role of troponin T isoforms in the fetal heart. *The Journal of biological chemistry*. 279:49579-49587.

Gong, H., V. Hatch, L. Ali, W. Lehman, R. Craig, and L.S. Tobacman. 2005. Mini-thin filaments regulated by troponin-tropomyosin. *Proceedings of the National Academy of Sciences of the United States of America*. 102:656-661.

Gordon, A.M., E. Homsher, and M. Regnier. 2000. Regulation of contraction in striated muscle. *Physiol Rev*. 80:853-924.

Graceffa, P., and R. Dominguez. 2003. Crystal structure of monomeric actin in the ATP state. Structural basis of nucleotide-dependent actin dynamics. *The Journal of biological chemistry*. 278:34172-34180.

Granzier, H.L., and S. Labeit. 2006. The giant muscle protein titin is an adjustable molecular spring. *Exercise and sport sciences reviews*. 34:50-53.

Gustafsson, A.B., and R.A. Gottlieb. 2008. Heart mitochondria: gates of life and death. *Cardiovascular research*. 77:334-343.

Harris, S.P., B. Belknap, R.E. Van Sciver, H.D. White, and V.E. Galkin. 2016. C0 and C1 N-terminal Ig domains of myosin binding protein C exert different effects on thin filament activation. *Proceedings of the National Academy of Sciences of the United States of America*. 113:1558-1563.

Hazard, A.L., S.C. Kohout, N.L. Stricker, J.A. Putkey, and J.J. Falke. 1998. The kinetic cycle of cardiac troponin C: calcium binding and dissociation at site II trigger slow conformational rearrangements. *Protein science : a publication of the Protein Society*. 7:2451-2459.

Hernandez, O.M., D. Szczesna-Cordary, B.C. Knollmann, T. Miller, M. Bell, J. Zhao, S.G. Sirenko, Z. Diaz, G. Guzman, Y. Xu, Y. Wang, W.G. Kerrick, and J.D. Potter. 2005. F110I and R278C troponin T mutations that cause familial hypertrophic cardiomyopathy affect muscle contraction in transgenic mice and reconstituted human cardiac fibers. *The Journal of biological chemistry*. 280:37183-37194.

Herzog, W. 2018. The multiple roles of titin in muscle contraction and force production. *Biophysical reviews*. 10:1187-1199.

Ho, C.Y., P. Charron, P. Richard, F. Girolami, K.Y. Van Spaendonck-Zwarts, and Y. Pinto. 2015. Genetic advances in sarcomeric cardiomyopathies: state of the art. *Cardiovascular research*. 105:397-408.

Hogan, P.G., L. Chen, J. Nardone, and A. Rao. 2003. Transcriptional regulation by calcium, calcineurin, and NFAT. *Genes & development*. 17:2205-2232.

Holmes, K.C., and R.R. Schroder. 2003. Switch 1 opens on strong binding to actin. Molecular and cellular aspects of muscle contraction. *Advances in experimental medicine and biology*. 538:159-166; discussion 166-157.

Houser, S.R., and J.D. Molkentin. 2008. Does contractile Ca2+ control calcineurin-NFAT signaling and pathological hypertrophy in cardiac myocytes? *Science signaling*. 1:pe31.

Houston, B.A., and G.R. Stevens. 2014. Hypertrophic cardiomyopathy: a review. *Clinical Medicine Insights. Cardiology*. 8:53-65.

Huke, S., and B.C. Knollmann. 2010. Increased myofilament Ca2+-sensitivity and arrhythmia susceptibility. *Journal of molecular and cellular cardiology*. 48:824-833.

Huke, S., R. Venkataraman, M. Faggioni, S. Bennuri, H.S. Hwang, F. Baudenbacher, and B.C. Knollmann. 2013. Focal energy deprivation underlies arrhythmia susceptibility in mice with calcium-sensitized myofilaments. *Circulation research*. 112:1334-1344.

Hunkeler, N.M., J. Kullman, and A.M. Murphy. 1991. Troponin I isoform expression in human heart. *Circulation research*. 69:1409-1414.

Hwang, P.M., F. Cai, S.E. Pineda-Sanabria, D.C. Corson, and B.D. Sykes. 2014. The cardiac-specific N-terminal region of troponin I positions the regulatory domain of troponin C. *Proceedings of the National Academy of Sciences of the United States of America*. 111:14412-14417.

Irisawa, H. 1978. Comparative physiology of the cardiac pacemaker mechanism. *Physiological reviews*. 58:461-498.

Jarcho, J.A., W. McKenna, J.A. Pare, S.D. Solomon, R.F. Holcombe, S. Dickie, T. Levi, H. Donis-Keller, J.G. Seidman, and C.E. Seidman. 1989. Mapping a gene for familial hypertrophic cardiomyopathy to chromosome 14q1. *The New England journal of medicine*. 321:1372-1378.

Jideama, N.M., B.H. Crawford, A.K. Hussain, and R.L. Raynor. 2006. Dephosphorylation specificities of protein phosphatase for cardiac troponin I, troponin T, and sites within troponin T. *International journal of biological sciences*. 2:1-9.

Kabsch, W., H.G. Mannherz, D. Suck, E.F. Pai, and K.C. Holmes. 1990. Atomic structure of the actin:DNase I complex. *Nature*. 347:37-44.

Kampourakis, T., Z. Yan, M. Gautel, Y.B. Sun, and M. Irving. 2014. Myosin binding protein-C activates thin filaments and inhibits thick filaments in heart muscle cells. *Proceedings of the National Academy of Sciences of the United States of America*. 111:18763-18768.

Katrukha, I.A. 2013. Human cardiac troponin complex. Structure and functions. *Biochemistry. Biokhimiia*. 78:1447-1465.

Kehat, I., and J.D. Molkentin. 2010. Molecular pathways underlying cardiac remodeling during pathophysiological stimulation. *Circulation*. 122:2727-2735.

Kentish, J.C., H.E. ter Keurs, L. Ricciardi, J.J. Bucx, and M.I. Noble. 1986. Comparison between the sarcomere length-force relations of intact and skinned trabeculae from rat right ventricle. Influence of calcium concentrations on these relations. *Circulation research*. 58:755-768.

Knollmann, B.C., S.A. Blatt, K. Horton, F. de Freitas, T. Miller, M. Bell, P.R. Housmans, N.J. Weissman, M. Morad, and J.D. Potter. 2001. Inotropic stimulation induces cardiac dysfunction in transgenic mice expressing a troponin T (I79N) mutation

linked to familial hypertrophic cardiomyopathy. *The Journal of biological chemistry*. 276:10039-10048.

Knollmann, B.C., P. Kirchhof, S.G. Sirenko, H. Degen, A.E. Greene, T. Schober, J.C. Mackow, L. Fabritz, J.D. Potter, and M. Morad. 2003. Familial hypertrophic cardiomyopathy-linked mutant troponin T causes stress-induced ventricular tachycardia and Ca^{2+}-dependent action potential remodeling. *Circ Res*. 92:428-436.

Knollmann, B.C., and J.D. Potter. 2001. Altered regulation of cardiac muscle contraction by troponin T mutations that cause familial hypertrophic cardiomyopathy. *Trends in cardiovascular medicine*. 11:206-212.

Kobayashi, T., L. Jin, and P.P. de Tombe. 2008. Cardiac thin filament regulation. *Pflugers Archiv : European journal of physiology*. 457:37-46.

Kobayashi, T., and R.J. Solaro. 2005. Calcium, thin filaments, and the integrative biology of cardiac contractility. *Annu Rev Physiol*. 67:39-67.

Konhilas, J.P., T.C. Irving, and P.P. de Tombe. 2002a. Frank-Starling law of the heart and the cellular mechanisms of length-dependent activation. *Pflugers Archiv : European journal of physiology*. 445:305-310.

Konhilas, J.P., T.C. Irving, and P.P. de Tombe. 2002b. Length-dependent activation in three striated muscle types of the rat. *J Physiol*. 544:225-236.

Konhilas, J.P., T.C. Irving, B.M. Wolska, E.E. Jweied, A.F. Martin, R.J. Solaro, and P.P. de Tombe. 2003. Troponin I in the murine myocardium: influence on length-dependent activation and interfilament spacing. *The Journal of physiology*. 547:951-961.

Kooij, V., M. Saes, K. Jaquet, R. Zaremba, D.B. Foster, A.M. Murphy, C. Dos Remedios, J. van der Velden, and G.J. Stienen. 2010. Effect of troponin I Ser23/24 phosphorylation on Ca2+-sensitivity in human myocardium depends on the phosphorylation background. *Journal of molecular and cellular cardiology*. 48:954-963.

Kranias, E.G., and R.J. Solaro. 1982. Phosphorylation of troponin I and phospholamban during catecholamine stimulation of rabbit heart. *Nature*. 298:182-184.

Krenz, M., and J. Robbins. 2004. Impact of beta-myosin heavy chain expression on cardiac function during stress. *Journal of the American College of Cardiology*. 44:2390-2397.

Kruger, M., G. Pfitzer, and R. Stehle. 2003. Expression and purification of human cardiac troponin subunits and their functional incorporation into isolated cardiac mouse myofibrils. *J Chromatogr B Analyt Technol Biomed Life Sci*. 786:287-296.

Kudryashov, D.S., and E. Reisler. 2013. ATP and ADP actin states. *Biopolymers*. 99:245-256.

Landstrom, A.P., D. Dobrev, and X.H.T. Wehrens. 2017. Calcium Signaling and Cardiac Arrhythmias. *Circulation research*. 120:1969-1993.

Lankford, E.B., N.D. Epstein, L. Fananapazir, and H.L. Sweeney. 1995. Abnormal contractile properties of muscle fibers expressing beta-myosin heavy chain gene mutations in patients with hypertrophic cardiomyopathy. *The Journal of clinical investigation*. 95:1409-1414.

Lata, K.R., P. Penczek, and J. Frank. 1995. Automatic particle picking from electron micrographs. *Ultramicroscopy*. 58:381-391.

Lee, T.M., D.T. Hsu, P. Kantor, J.A. Towbin, S.M. Ware, S.D. Colan, W.K. Chung, J.L. Jefferies, J.W. Rossano, C.D. Castleberry, L.J. Addonizio, A.K. Lal, J.M. Lamour, E.M. Miller, P.T. Thrush, J.D. Czachor, H. Razoky, A. Hill, and S.E. Lipshultz. 2017. Pediatric Cardiomyopathies. *Circulation research*. 121:855-873.

Leger, J., P. Bouveret, K. Schwartz, and B. Swynghedauw. 1976. A comparative study of skeletal and cardiac tropomyosins: subunits, thiol group content and biological activities. *Pflugers Archiv : European journal of physiology*. 362:271-277.

Lehman, W., R. Craig, and P. Vibert. 1994. Ca(2+)-induced tropomyosin movement in Limulus thin filaments revealed by three-dimensional reconstruction. *Nature*. 368:65-67.

LeWinter, M.M., and H. Granzier. 2010. Cardiac titin: a multifunctional giant. *Circulation*. 121:2137-2145.

Li, A.Y., C.M. Stevens, B. Liang, K. Rayani, S. Little, J. Davis, and G.F. Tibbits. 2013a. Familial hypertrophic cardiomyopathy related cardiac troponin C L29Q mutation alters length-dependent activation and functional effects of phosphomimetic troponin I*. *PloS one*. 8:e79363.

Li, K.L., M. Methawasin, B.C.W. Tanner, H.L. Granzier, R.J. Solaro, and W.J. Dong. 2019. Sarcomere length-dependent effects on Ca(2+)-troponin regulation in myocardium expressing compliant titin. *The Journal of general physiology*. 151:30-41.

Li, M.X., and P.M. Hwang. 2015. Structure and function of cardiac troponin C (TNNC1): Implications for heart failure, cardiomyopathies, and troponin modulating drugs. *Gene*. 571:153-166.

Li, X., P. Mooney, S. Zheng, C.R. Booth, M.B. Braunfeld, S. Gubbens, D.A. Agard, and Y. Cheng. 2013b. Electron counting and beam-induced motion correction enable near-atomic-resolution single-particle cryo-EM. *Nature methods*. 10:584-590.

Li, X.E., L.S. Tobacman, J.Y. Mun, R. Craig, S. Fischer, and W. Lehman. 2011. Tropomyosin position on F-actin revealed by EM reconstruction and computational chemistry. *Biophys J*. 100:1005-1013.

Lin, D., A. Bobkova, E. Homsher, and L.S. Tobacman. 1996. Altered cardiac troponin T in vitro function in the presence of a mutation implicated in familial hypertrophic cardiomyopathy. *The Journal of clinical investigation*. 97:2842-2848.

Lin, T., S. Ichihara, Y. Yamada, T. Nagasaka, H. Ishihara, N. Nakashima, and M. Yokota. 2000. Phenotypic variation of familial hypertrophic cardiomyopathy caused by the Phe(110)-->Ile mutation in cardiac troponin T. *Cardiology*. 93:155-162.

Liu, B., R.S. Lee, B.J. Biesiadecki, S.B. Tikunova, and J.P. Davis. 2012a. Engineered troponin C constructs correct disease-related cardiac myofilament calcium sensitivity. *The Journal of biological chemistry*. 287:20027-20036.

Liu, B., J.J. Lopez, B.J. Biesiadecki, and J.P. Davis. 2014. Protein kinase C phosphomimetics alter thin filament Ca2+ binding properties. *PloS one*. 9:e86279.

Liu, B., S.B. Tikunova, K.P. Kline, J.K. Siddiqui, and J.P. Davis. 2012b. Disease-related cardiac troponins alter thin filament Ca2+ association and dissociation rates. *PloS one*. 7:e38259.

Lodish H, B.A., Zipursky SL, et al. 2000. The Dynamics of Actin Assembly. *In* Molecular Cell Biology, New York: W. H. Freeman.

Lovelock, J.D., M.M. Monasky, E.M. Jeong, H.A. Lardin, H. Liu, B.G. Patel, D.M. Taglieri, L. Gu, P. Kumar, N. Pokhrel, D. Zeng, L. Belardinelli, D. Sorescu, R.J. Solaro, and S.C. Dudley, Jr. 2012. Ranolazine improves cardiac diastolic dysfunction through modulation of myofilament calcium sensitivity. *Circulation research*. 110:841-850.

Lowey, S. 2002. Functional consequences of mutations in the myosin heavy chain at sites implicated in familial hypertrophic cardiomyopathy. *Trends in cardiovascular medicine*. 12:348-354.

Lu, Q.W., X.Y. Wu, and S. Morimoto. 2013. Inherited cardiomyopathies caused by troponin mutations. *Journal of geriatric cardiology : JGC*. 10:91-101.

Mamidi, R., K.S. Gresham, S. Verma, and J.E. Stelzer. 2016. Cardiac Myosin Binding Protein-C Phosphorylation Modulates Myofilament Length-Dependent Activation. *Frontiers in physiology*. 7:38.

Manning, E.P., J.C. Tardiff, and S.D. Schwartz. 2011. A model of calcium activation of the cardiac thin filament. *Biochemistry*. 50:7405-7413.

Maron, B.J., J.M. Gardin, J.M. Flack, S.S. Gidding, T.T. Kurosaki, and D.E. Bild. 1995. Prevalence of hypertrophic cardiomyopathy in a general population of young adults. Echocardiographic analysis of 4111 subjects in the CARDIA Study. Coronary Artery Risk Development in (Young) Adults. *Circulation*. 92:785-789.

Maron, B.J., and M.S. Maron. 2013. Hypertrophic cardiomyopathy. *Lancet*. 381:242-255.

Maron, B.J., M.S. Maron, and C. Semsarian. 2012. Genetics of hypertrophic cardiomyopathy after 20 years: clinical perspectives. *Journal of the American College of Cardiology*. 60:705-715.

Maron, B.J., J. Shirani, L.C. Poliac, R. Mathenge, W.C. Roberts, and F.O. Mueller. 1996. Sudden death in young competitive athletes. Clinical, demographic, and pathological profiles. *Jama*. 276:199-204.

Marston, S.B., and C.S. Redwood. 2003. Modulation of thin filament activation by breakdown or isoform switching of thin filament proteins: physiological and pathological implications. *Circulation research*. 93:1170-1178.

McMullan, G., S. Chen, R. Henderson, and A.R. Faruqi. 2009. Detective quantum efficiency of electron area detectors in electron microscopy. *Ultramicroscopy*. 109:1126-1143.

Memo, M., M.C. Leung, D.G. Ward, C. dos Remedios, S. Morimoto, L. Zhang, G. Ravenscroft, E. McNamara, K.J. Nowak, S.B. Marston, and A.E. Messer. 2013. Familial dilated cardiomyopathy mutations uncouple troponin I phosphorylation from changes in myofibrillar Ca(2)(+) sensitivity. *Cardiovascular research*. 99:65-73.

Menon, S.C., V.V. Michels, P.A. Pellikka, J.D. Ballew, M.L. Karst, K.J. Herron, S.M. Nelson, R.J. Rodeheffer, and T.M. Olson. 2008. Cardiac troponin T mutation in

familial cardiomyopathy with variable remodeling and restrictive physiology. *Clinical genetics*. 74:445-454.

Messer, A.E., C.R. Bayliss, M. El-Mezgueldi, C.S. Redwood, D.G. Ward, M.C. Leung, M. Papadaki, C. Dos Remedios, and S.B. Marston. 2016. Mutations in troponin T associated with Hypertrophic Cardiomyopathy increase Ca(2+)-sensitivity and suppress the modulation of Ca(2+)-sensitivity by troponin I phosphorylation. *Archives of biochemistry and biophysics*. 601:113-120.

Methawasin, M., K.R. Hutchinson, E.J. Lee, J.E. Smith, 3rd, C. Saripalli, C.G. Hidalgo, C.A. Ottenheijm, and H. Granzier. 2014. Experimentally increasing titin compliance in a novel mouse model attenuates the Frank-Starling mechanism but has a beneficial effect on diastole. *Circulation*. 129:1924-1936.

Metzger, J.M., D.E. Michele, E.M. Rust, A.R. Borton, and M.V. Westfall. 2003. Sarcomere thin filament regulatory isoforms. Evidence of a dominant effect of slow skeletal troponin I on cardiac contraction. *The Journal of biological chemistry*. 278:13118-13123.

Metzger, J.M., and M.V. Westfall. 2004. Covalent and noncovalent modification of thin filament action: the essential role of troponin in cardiac muscle regulation. *Circ Res*. 94:146-158.

Meznaric, M., and E. Cvetko. 2016. Size and Proportions of Slow-Twitch and Fast-Twitch Muscle Fibers in Human Costal Diaphragm. *BioMed research international*. 2016:5946520.

Miller, T., D. Szczesna, P.R. Housmans, J. Zhao, F. de Freitas, A.V. Gomes, L. Culbreath, J. McCue, Y. Wang, Y. Xu, W.G. Kerrick, and J.D. Potter. 2001. Abnormal contractile function in transgenic mice expressing a familial hypertrophic cardiomyopathy-linked troponin T (I79N) mutation. *The Journal of biological chemistry*. 276:3743-3755.

Monteiro, P.B., R.C. Lataro, J.A. Ferro, and C. Reinach Fde. 1994. Functional alpha-tropomyosin produced in Escherichia coli. A dipeptide extension can substitute the amino-terminal acetyl group. *The Journal of biological chemistry*. 269:10461-10466.

Morimoto, S., F. Yanaga, R. Minakami, and I. Ohtsuki. 1998. Ca2+-sensitizing effects of the mutations at Ile-79 and Arg-92 of troponin T in hypertrophic cardiomyopathy. *The American journal of physiology*. 275:C200-207.

Moss, R.L., M. Razumova, and D.P. Fitzsimons. 2004. Myosin crossbridge activation of cardiac thin filaments: implications for myocardial function in health and disease. *Circ Res*. 94:1290-1300.

Muthuchamy, M., L. Pajak, P. Howles, T. Doetschman, and D.F. Wieczorek. 1993. Developmental analysis of tropomyosin gene expression in embryonic stem cells and mouse embryos. *Molecular and cellular biology*. 13:3311-3323.

Nagueh, S.F., G. Shah, Y. Wu, G. Torre-Amione, N.M. King, S. Lahmers, C.C. Witt, K. Becker, S. Labeit, and H.L. Granzier. 2004. Altered titin expression, myocardial stiffness, and left ventricular function in patients with dilated cardiomyopathy. *Circulation*. 110:155-162.

Nakanishi, T., and J.M. Jarmakani. 1984. Developmental changes in myocardial mechanical function and subcellular organelles. *The American journal of physiology*. 246:H615-625.

Nogales, E. 2016. The development of cryo-EM into a mainstream structural biology technique. *Nature methods*. 13:24-27.

O'Mahony, C., P. Elliott, and W. McKenna. 2013. Sudden cardiac death in hypertrophic cardiomyopathy. *Circulation. Arrhythmia and electrophysiology*. 6:443-451.

Ohi, M., Y. Li, Y. Cheng, and T. Walz. 2004. Negative Staining and Image Classification - Powerful Tools in Modern Electron Microscopy. *Biol Proced Online*. 6:23-34.

Ohtsuki, I. 1979. Molecular arrangement of troponin-T in the thin filament. *Journal of biochemistry*. 86:491-497.

Olivotto, I., F. Girolami, M.J. Ackerman, S. Nistri, J.M. Bos, E. Zachara, S.R. Ommen, J.L. Theis, R.A. Vaubel, F. Re, C. Armentano, C. Poggesi, F. Torricelli, and F. Cecchi. 2008. Myofilament protein gene mutation screening and outcome of patients with hypertrophic cardiomyopathy. *Mayo Clinic proceedings*. 83:630-638.

Opic, P., E.M. Utens, P. Moons, D.A. Theuns, A.P. van Dijk, E.S. Hoendermis, H.W. Vliegen, N.M. de Groot, M. Witsenburg, M. Schalij, and J.W. Roos-Hesselink. 2012. Psychosocial impact of implantable cardioverter defibrillators (ICD) in young adults with Tetralogy of Fallot. *Clinical research in cardiology : official journal of the German Cardiac Society*. 101:509-519.

Otterbein, L.R., P. Graceffa, and R. Dominguez. 2001. The crystal structure of uncomplexed actin in the ADP state. *Science*. 293:708-711.

Palm, T., S. Graboski, S.E. Hitchcock-DeGregori, and N.J. Greenfield. 2001. Disease-causing mutations in cardiac troponin T: identification of a critical tropomyosin-binding region. *Biophys J*. 81:2827-2837.

Parmley, W.W., and L. Chuck. 1973. Length-dependent changes in myocardial contractile state. *The American journal of physiology*. 224:1195-1199.

Pasquale, F., P. Syrris, J.P. Kaski, J. Mogensen, W.J. McKenna, and P. Elliott. 2012. Long-term outcomes in hypertrophic cardiomyopathy caused by mutations in the cardiac troponin T gene. *Circulation. Cardiovascular genetics*. 5:10-17.

Patel, M.D., J. Mohan, C. Schneider, G. Bajpai, E. Purevjav, C.E. Canter, J. Towbin, A. Bredemeyer, and K.J. Lavine. 2017. Pediatric and adult dilated cardiomyopathy represent distinct pathological entities. *JCI insight*. 2.

Paul, D.M., E.P. Morris, R.W. Kensler, and J.M. Squire. 2009. Structure and orientation of troponin in the thin filament. *The Journal of biological chemistry*. 284:15007-15015.

Pi, Y., K.R. Kemnitz, D. Zhang, E.G. Kranias, and J.W. Walker. 2002. Phosphorylation of troponin I controls cardiac twitch dynamics: evidence from phosphorylation site mutants expressed on a troponin I-null background in mice. *Circ Res*. 90:649-656.

Pinnell J., T.S., Howell S. 2007. Cardiac muscle physiology *Continuing Education in Anaesthesia Critical Care & Pain* 7:85-55.

Pinto, J.R., S.W. Yang, M.P. Hitz, M.S. Parvatiyar, M.A. Jones, J. Liang, V. Kokta, M. Talajic, N. Tremblay, M. Jaeggi, G. Andelfinger, and J.D. Potter. 2011. Fetal

cardiac troponin isoforms rescue the increased Ca^{2+} sensitivity produced by a novel double deletion in cardiac troponin T linked to restrictive cardiomyopathy: a clinical, genetic, and functional approach. *The Journal of biological chemistry*. 286:20901-20912.

Pirani, A., M.V. Vinogradova, P.M. Curmi, W.A. King, R.J. Fletterick, R. Craig, L.S. Tobacman, C. Xu, V. Hatch, and W. Lehman. 2006. An atomic model of the thin filament in the relaxed and Ca2+-activated states. *J Mol Biol*. 357:707-717.

Pirani, A., C. Xu, V. Hatch, R. Craig, L.S. Tobacman, and W. Lehman. 2005. Single particle analysis of relaxed and activated muscle thin filaments. *Journal of molecular biology*. 346:761-772.

Pospich, S., E.P. Kumpula, J. von der Ecken, J. Vahokoski, I. Kursula, and S. Raunser. 2017. Near-atomic structure of jasplakinolide-stabilized malaria parasite F-actin reveals the structural basis of filament instability. *Proceedings of the National Academy of Sciences of the United States of America*. 114:10636-10641.

Prinz, C., M. Farr, D. Hering, D. Horstkotte, and L. Faber. 2011. The diagnosis and treatment of hypertrophic cardiomyopathy. *Dtsch Arztebl Int*. 108:209-215.

Purcell, I.F., W. Bing, and S.B. Marston. 1999. Functional analysis of human cardiac troponin by the in vitro motility assay: comparison of adult, foetal and failing hearts. *Cardiovascular research*. 43:884-891.

Putkey, J.A., D.G. Dotson, and P. Mouawad. 1993. Formation of inter- and intramolecular disulfide bonds can activate cardiac troponin C. *The Journal of biological chemistry*. 268:6827-6830.

Racca, A.W., J.M. Klaiman, J.M. Pioner, Y. Cheng, A.E. Beck, F. Moussavi-Harami, M.J. Bamshad, and M. Regnier. 2016. Contractile properties of developing human fetal cardiac muscle. *The Journal of physiology*. 594:437-452.

Rao, V., Y. Cheng, S. Lindert, D. Wang, L. Oxenford, A.D. McCulloch, J.A. McCammon, and M. Regnier. 2014. PKA phosphorylation of cardiac troponin I modulates activation and relaxation kinetics of ventricular myofibrils. *Biophysical journal*. 107:1196-1204.

Razumova, M.V., A.E. Bukatina, and K.B. Campbell. 2000. Different myofilament nearest-neighbor interactions have distinctive effects on contractile behavior. *Biophysical journal*. 78:3120-3137.

Redwood, C., and P. Robinson. 2013. Alpha-tropomyosin mutations in inherited cardiomyopathies. *Journal of muscle research and cell motility*. 34:285-294.

Ren, X., N. Hensley, M.B. Brady, and W.D. Gao. 2018. The Genetic and Molecular Bases for Hypertrophic Cardiomyopathy: The Role for Calcium Sensitization. *Journal of cardiothoracic and vascular anesthesia*. 32:478-487.

Ripoll-Vera, T., J.M. Gamez, N. Govea, Y. Gomez, J. Nunez, L. Socias, A. Escandell, and J. Rosell. 2016. Clinical and Prognostic Profiles of Cardiomyopathies Caused by Mutations in the Troponin T Gene. *Revista espanola de cardiologia*. 69:149-158.

Robertson, S.P., J.D. Johnson, M.J. Holroyde, E.G. Kranias, J.D. Potter, and R.J. Solaro. 1982. The effect of troponin I phosphorylation on the Ca2+-binding properties of the Ca2+-regulatory site of bovine cardiac troponin. *The Journal of biological chemistry*. 257:260-263.

Robinson, P., S. Lipscomb, L.C. Preston, E. Altin, H. Watkins, C.C. Ashley, and C.S. Redwood. 2007. Mutations in fast skeletal troponin I, troponin T, and beta-tropomyosin that cause distal arthrogryposis all increase contractile function. *FASEB journal : official publication of the Federation of American Societies for Experimental Biology*. 21:896-905.

Rohou, A., and N. Grigorieff. 2015. CTFFIND4: Fast and accurate defocus estimation from electron micrographs. *Journal of structural biology*. 192:216-221.

Rosano, G.L., and E.A. Ceccarelli. 2014. Recombinant protein expression in Escherichia coli: advances and challenges. *Frontiers in microbiology*. 5:172.

Rust, E.M., F.P. Albayya, and J.M. Metzger. 1999. Identification of a contractile deficit in adult cardiac myocytes expressing hypertrophic cardiomyopathy-associated mutant troponin T proteins. *The Journal of clinical investigation*. 103:1459-1467.

Saggin, L., L. Gorza, S. Ausoni, and S. Schiaffino. 1989. Troponin I switching in the developing heart. *The Journal of biological chemistry*. 264:16299-16302.

Sasse, S., N.J. Brand, P. Kyprianou, G.K. Dhoot, R. Wade, M. Arai, M. Periasamy, M.H. Yacoub, and P.J. Barton. 1993. Troponin I gene expression during human cardiac development and in end-stage heart failure. *Circulation research*. 72:932-938.

Sata, M., and M. Ikebe. 1996. Functional analysis of the mutations in the human cardiac beta-myosin that are responsible for familial hypertrophic cardiomyopathy. Implication for the clinical outcome. *The Journal of clinical investigation*. 98:2866-2873.

Scheres, S.H. 2012. RELION: implementation of a Bayesian approach to cryo-EM structure determination. *Journal of structural biology*. 180:519-530.

Schevzov, G., S.P. Whittaker, T. Fath, J.J. Lin, and P.W. Gunning. 2011. Tropomyosin isoforms and reagents. *Bioarchitecture*. 1:135-164.

Schiaffino, S., L. Gorza, and S. Ausoni. 1993. Troponin isoform switching in the developing heart and its functional consequences. *Trends in cardiovascular medicine*. 3:12-17.

Schober, T., S. Huke, R. Venkataraman, O. Gryshchenko, D. Kryshtal, H.S. Hwang, F.J. Baudenbacher, and B.C. Knollmann. 2012. Myofilament Ca sensitization increases cytosolic Ca binding affinity, alters intracellular Ca homeostasis, and causes pause-dependent Ca-triggered arrhythmia. *Circ Res*. 111:170-179.

Schober, T., and B.C. Knollmann. 2007. Exercise after myocardial infarction improves contractility and decreases myofilament Ca2+ sensitivity. *Circulation research*. 100:937-939.

Scott, W., J. Stevens, and S.A. Binder-Macleod. 2001. Human skeletal muscle fiber type classifications. *Physical therapy*. 81:1810-1816.

Seok, J., H.S. Warren, A.G. Cuenca, M.N. Mindrinos, H.V. Baker, W. Xu, D.R. Richards, G.P. McDonald-Smith, H. Gao, L. Hennessy, C.C. Finnerty, C.M. Lopez, S. Honari, E.E. Moore, J.P. Minei, J. Cuschieri, P.E. Bankey, J.L. Johnson, J. Sperry, A.B. Nathens, T.R. Billiar, M.A. West, M.G. Jeschke, M.B. Klein, R.L. Gamelli, N.S. Gibran, B.H. Brownstein, C. Miller-Graziano, S.E. Calvano, P.H. Mason, J.P. Cobb, L.G. Rahme, S.F. Lowry, R.V. Maier, L.L. Moldawer, D.N. Herndon, R.W. Davis, W. Xiao, R.G. Tompkins, Inflammation, and L.S.C.R.P.

Host Response to Injury. 2013. Genomic responses in mouse models poorly mimic human inflammatory diseases. *Proceedings of the National Academy of Sciences of the United States of America*. 110:3507-3512.

Sequeira, V., P.J. Wijnker, L.L. Nijenkamp, D.W. Kuster, A. Najafi, E.R. Witjas-Paalberends, J.A. Regan, N. Boontje, F.J. Ten Cate, T. Germans, L. Carrier, S. Sadayappan, M.A. van Slegtenhorst, R. Zaremba, D.B. Foster, A.M. Murphy, C. Poggesi, C. Dos Remedios, G.J. Stienen, C.Y. Ho, M. Michels, and J. van der Velden. 2013. Perturbed length-dependent activation in human hypertrophic cardiomyopathy with missense sarcomeric gene mutations. *Circ Res*. 112:1491-1505.

Seymour, J., and E.J. O'Brien. 1980. The position of tropomyosin in muscle thin filaments. *Nature*. 283:680-682.

Sgro, G.G., and T.R.D. Costa. 2018. Cryo-EM Grid Preparation of Membrane Protein Samples for Single Particle Analysis. *Frontiers in molecular biosciences*. 5:74.

Shafaattalab, S., A.Y. Li, E. Lin, C.M. Stevens, L.J. Dewar, F.C. Lynn, S. Sanatani, Z. Laksman, R.D. Morin, F. van Petegem, L. Hove-Madsen, D.P. Tieleman, J.P. Davis, and G.F. Tibbits. 2019. In vitro analyses of suspected arrhythmogenic thin filament variants as a cause of sudden cardiac death in infants. *Proceedings of the National Academy of Sciences of the United States of America*. 116:6969-6974.

Sheng, J.J., and J.P. Jin. 2016. TNNI1, TNNI2 and TNNI3: Evolution, regulation, and protein structure-function relationships. *Gene*. 576:385-394.

Siddiqui, J.K., S.B. Tikunova, S.D. Walton, B. Liu, M. Meyer, P.P. de Tombe, N. Neilson, P.M. Kekenes-Huskey, H.E. Salhi, P.M. Janssen, B.J. Biesiadecki, and J.P. Davis. 2016. Myofilament Calcium Sensitivity: Consequences of the Effective Concentration of Troponin I. *Frontiers in physiology*. 7:632.

Sievers, F., A. Wilm, D. Dineen, T.J. Gibson, K. Karplus, W. Li, R. Lopez, H. McWilliam, M. Remmert, J. Soding, J.D. Thompson, and D.G. Higgins. 2011. Fast, scalable generation of high-quality protein multiple sequence alignments using Clustal Omega. *Molecular systems biology*. 7:539.

Sirenko, S.G., J.D. Potter, and B.C. Knollmann. 2006. Differential effect of troponin T mutations on the inotropic responsiveness of mouse hearts--role of myofilament Ca2+ sensitivity increase. *J Physiol*. 575:201-213.

Smillie, L.B. 1979. Structure and functions of tropomyosins from muscle and non-muscle sources *Trends in Biochemical Sciences*. 4:7.

Smillie, L.B., M.D. Pato, J.R. Pearlstone, and A.S. Mak. 1980. Periodicity of alpha-helical potential in tropomyosin sequence correlates with alternating actin binding sites. *Journal of molecular biology*. 136:199-202.

Solaro, R.J., and T. Kobayashi. 2011. Protein phosphorylation and signal transduction in cardiac thin filaments. *The Journal of biological chemistry*. 286:9935-9940.

Solaro, R.J., A.J. Moir, and S.V. Perry. 1976. Phosphorylation of troponin I and the inotropic effect of adrenaline in the perfused rabbit heart. *Nature*. 262:615-617.

Solaro, R.J., P. Rosevear, and T. Kobayashi. 2008. The unique functions of cardiac troponin I in the control of cardiac muscle contraction and relaxation. *Biochem Biophys Res Commun*. 369:82-87.

Solaro, R.J., and J. van der Velden. 2010. Why does troponin I have so many phosphorylation sites? Fact and fancy. *Journal of molecular and cellular cardiology*. 48:810-816.

Spudich, J.A., H.E. Huxley, and J.T. Finch. 1972. Regulation of skeletal muscle contraction. II. Structural studies of the interaction of the tropomyosin-troponin complex with actin. *Journal of molecular biology*. 72:619-632.

Szczesna, D., R. Zhang, J. Zhao, M. Jones, G. Guzman, and J.D. Potter. 2000. Altered regulation of cardiac muscle contraction by troponin T mutations that cause familial hypertrophic cardiomyopathy. *The Journal of biological chemistry*. 275:624-630.

Takeda, S., Fujiwara, S. 2016. Core domain of human cardiac troponin. *The ministry of Education, Culture, Sports, Science and Techinology Japan*

Takeda, S., A. Yamashita, K. Maeda, and Y. Maeda. 2003. Structure of the core domain of human cardiac troponin in the Ca(2+)-saturated form. *Nature*. 424:35-41.

Tang, G., L. Peng, P.R. Baldwin, D.S. Mann, W. Jiang, I. Rees, and S.J. Ludtke. 2007. EMAN2: an extensible image processing suite for electron microscopy. *Journal of structural biology*. 157:38-46.

Tardiff, J.C. 2011. Thin filament mutations: developing an integrative approach to a complex disorder. *Circ Res*. 108:765-782.

Tardiff, J.C., L. Carrier, D.M. Bers, C. Poggesi, C. Ferrantini, R. Coppini, L.S. Maier, H. Ashrafian, S. Huke, and J. van der Velden. 2015. Targets for therapy in sarcomeric cardiomyopathies. *Cardiovascular research*. 105:457-470.

Tatman, P.D., K.C. Woulfe, A. Karimpour-Fard, D.A. Jeffrey, J. Jaggers, J.C. Cleveland, K. Nunley, M.R. Taylor, S.D. Miyamoto, B.L. Stauffer, and C.C. Sucharov. 2017. Pediatric dilated cardiomyopathy hearts display a unique gene expression profile. *JCI insight*. 2.

Theopistou, A., A. Anastasakis, A. Miliou, A. Rigopoulos, P. Toutouzas, and C. Stefanadis. 2004. Clinical features of hypertrophic cardiomyopathy caused by an Arg278Cys missense mutation in the cardiac troponin T gene. *The American journal of cardiology*. 94:246-249.

Thierfelder, L., H. Watkins, C. MacRae, R. Lamas, W. McKenna, H.P. Vosberg, J.G. Seidman, and C.E. Seidman. 1994. Alpha-tropomyosin and cardiac troponin T mutations cause familial hypertrophic cardiomyopathy: a disease of the sarcomere. *Cell*. 77:701-712.

Tikunova, S.B., and J.P. Davis. 2004. Designing calcium-sensitizing mutations in the regulatory domain of cardiac troponin C. *The Journal of biological chemistry*. 279:35341-35352.

Tikunova, S.B., B. Liu, N. Swindle, S.C. Little, A.V. Gomes, D.R. Swartz, and J.P. Davis. 2010. Effect of calcium-sensitizing mutations on calcium binding and exchange with troponin C in increasingly complex biochemical systems. *Biochemistry*. 49:1975-1984.

Tobacman, L.S. 1996. Thin filament-mediated regulation of cardiac contraction. *Annual review of physiology*. 58:447-481.

Tobacman, L.S. 2008. Cooperative binding of tropomyosin to actin. *Advances in experimental medicine and biology*. 644:85-94.

Torricelli, F., F. Girolami, I. Olivotto, I. Passerini, S. Frusconi, D. Vargiu, P. Richard, and F. Cecchi. 2003. Prevalence and clinical profile of troponin T mutations among patients with hypertrophic cardiomyopathy in tuscany. *The American journal of cardiology*. 92:1358-1362.

Trivedi, A., and B.P. Knight. 2016. ICD Therapy for Primary Prevention in Hypertrophic Cardiomyopathy. *Arrhythmia & electrophysiology review*. 5:188-196.

Tse, G. 2016. Mechanisms of cardiac arrhythmias. *Journal of arrhythmia*. 32:75-81.

UniProt Consortium, T. 2018. UniProt: the universal protein knowledgebase. *Nucleic acids research*. 46:2699.

van der Velden, J., C.Y. Ho, J.C. Tardiff, I. Olivotto, B.C. Knollmann, and L. Carrier. 2015. Research priorities in sarcomeric cardiomyopathies. *Cardiovascular research*. 105:449-456.

Vandekerckhove, J., G. Bugaisky, and M. Buckingham. 1986. Simultaneous expression of skeletal muscle and heart actin proteins in various striated muscle tissues and cells. A quantitative determination of the two actin isoforms. *The Journal of biological chemistry*. 261:1838-1843.

Veltri, T., M. Landim-Vieira, M.S. Parvatiyar, D. Gonzalez-Martinez, K.M. Dieseldorff Jones, C.A. Michell, D. Dweck, A.P. Landstrom, P.B. Chase, and J.R. Pinto. 2017. Hypertrophic Cardiomyopathy Cardiac Troponin C Mutations Differentially Affect Slow Skeletal and Cardiac Muscle Regulation. *Frontiers in physiology*. 8:221.

von der Ecken, J., S.M. Heissler, S. Pathan-Chhatbar, D.J. Manstein, and S. Raunser. 2016. Cryo-EM structure of a human cytoplasmic actomyosin complex at near-atomic resolution. *Nature*. 534:724-728.

von der Ecken, J., M. Muller, W. Lehman, D.J. Manstein, P.A. Penczek, and S. Raunser. 2015. Structure of the F-actin-tropomyosin complex. *Nature*. 519:114-117.

Wang, D., I.M. Robertson, M.X. Li, M.E. McCully, M.L. Crane, Z. Luo, A.Y. Tu, V. Daggett, B.D. Sykes, and M. Regnier. 2012. Structural and functional consequences of the cardiac troponin C L48Q Ca(2+)-sensitizing mutation. *Biochemistry*. 51:4473-4487.

Wang, L., K. Kim, S. Parikh, A.G. Cadar, K.R. Bersell, H. He, J.R. Pinto, D.O. Kryshtal, and B.C. Knollmann. 2018. Hypertrophic cardiomyopathy-linked mutation in troponin T causes myofibrillar disarray and pro-arrhythmic action potential changes in human iPSC cardiomyocytes. *Journal of molecular and cellular cardiology*. 114:320-327.

Watkins, H., W.J. McKenna, L. Thierfelder, H.J. Suk, R. Anan, A. O'Donoghue, P. Spirito, A. Matsumori, C.S. Moravec, J.G. Seidman, and et al. 1995. Mutations in the genes for cardiac troponin T and alpha-tropomyosin in hypertrophic cardiomyopathy. *N Engl J Med*. 332:1058-1064.

Web. 2017. Difference Between Myofibirl and Msucle Fiber. . Vol. 2018.

Wehland, J., M. Osborn, and K. Weber. 1977. Phalloidin-induced actin polymerization in the cytoplasm of cultured cells interferes with cell locomotion and growth.

Proceedings of the National Academy of Sciences of the United States of America. 74:5613-5617.

Wessels, A., and D. Sedmera. 2003. Developmental anatomy of the heart: a tale of mice and man. *Physiological genomics*. 15:165-176.

Westfall, M.V., A.R. Borton, F.P. Albayya, and J.M. Metzger. 2002. Myofilament calcium sensitivity and cardiac disease: insights from troponin I isoforms and mutants. *Circ Res*. 91:525-531.

Westfall, M.V., E.M. Rust, and J.M. Metzger. 1997. Slow skeletal troponin I gene transfer, expression, and myofilament incorporation enhances adult cardiac myocyte contractile function. *Proceedings of the National Academy of Sciences of the United States of America*. 94:5444-5449.

Whitby, F.G., and G.N. Phillips, Jr. 2000. Crystal structure of tropomyosin at 7 Angstroms resolution. *Proteins*. 38:49-59.

Wijnker, P.J.M., V. Sequeira, D.W.D. Kuster, and J.V. Velden. 2018. Hypertrophic Cardiomyopathy: A Vicious Cycle Triggered by Sarcomere Mutations and Secondary Disease Hits. *Antioxidants & redox signaling*.

Wilkins, M.R., E. Gasteiger, A. Bairoch, J.C. Sanchez, K.L. Williams, R.D. Appel, and D.F. Hochstrasser. 1999. Protein identification and analysis tools in the ExPASy server. *Methods in molecular biology*. 112:531-552.

Willott, R.H., A.V. Gomes, A.N. Chang, M.S. Parvatiyar, J.R. Pinto, and J.D. Potter. 2010. Mutations in Troponin that cause HCM, DCM AND RCM: what can we learn about thin filament function? *Journal of molecular and cellular cardiology*. 48:882-892.

Wolska, B.M., K. Vijayan, G.M. Arteaga, J.P. Konhilas, R.M. Phillips, R. Kim, T. Naya, J.M. Leiden, A.F. Martin, P.P. de Tombe, and R.J. Solaro. 2001. Expression of slow skeletal troponin I in adult transgenic mouse heart muscle reduces the force decline observed during acidic conditions. *The Journal of physiology*. 536:863-870.

Xu, C., R. Craig, L. Tobacman, R. Horowitz, and W. Lehman. 1999. Tropomyosin positions in regulated thin filaments revealed by cryoelectron microscopy. *Biophysical journal*. 77:985-992.

Yang, S., L. Barbu-Tudoran, M. Orzechowski, R. Craig, J. Trinick, H. White, and W. Lehman. 2014. Three-dimensional organization of troponin on cardiac muscle thin filaments in the relaxed state. *Biophysical journal*. 106:855-864.

Zheng, S.Q., E. Palovcak, J.P. Armache, K.A. Verba, Y. Cheng, and D.A. Agard. 2017. MotionCor2: anisotropic correction of beam-induced motion for improved cryo-electron microscopy. *Nature methods*. 14:331-332.

Zhou, P., and W.T. Pu. 2016. Recounting Cardiac Cellular Composition. *Circulation research*. 118:368-370.

Ziegelstein, R.C. 2007. Acute emotional stress and cardiac arrhythmias. *Jama*. 298:324-329.

Appendix

Supporting Materials

Supporting Materials for Chapter 2:

The followings are the representative FPLC chromatogram and the corresponding SDS-PAGE gel for each protein component of the Tn complex and RTF. Purification of WT and mutant protein subunits required similar protocols so only the WT chromatogram and gels are shown here.

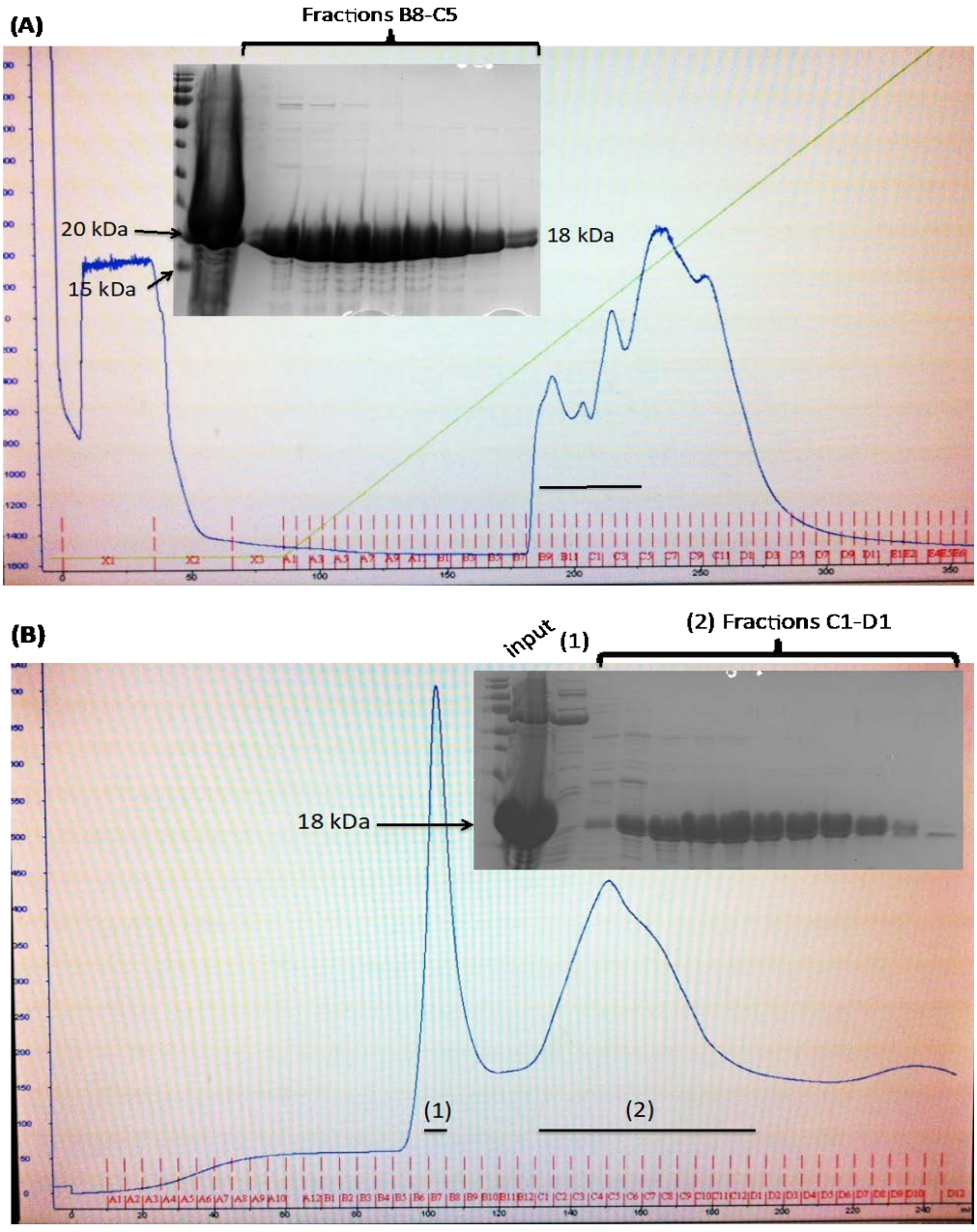

Figure A1. Purification of WT human cTnC by (A) DEAE fast flow anionic exchange column and (B) size exclusion HiPrep Sephacryl S100 column.

(A) The DEAE chromatogram of human cTnC is shown here with a 12% SDS-PAGE demonstrating that cTnC collected from fractions B5 to C5 migrated as an 18 kDa protein species. The proteins were eluted at 30-40% of a 500 mM salt gradient. (B) The size-exclusion chromatogram of human cTnC in which purified cTnC was separated from the higher-molecular weight containment proteins that eluted from the void volume. The purified human cTnC fractions were combined, concentrated and labeled with IAANS.

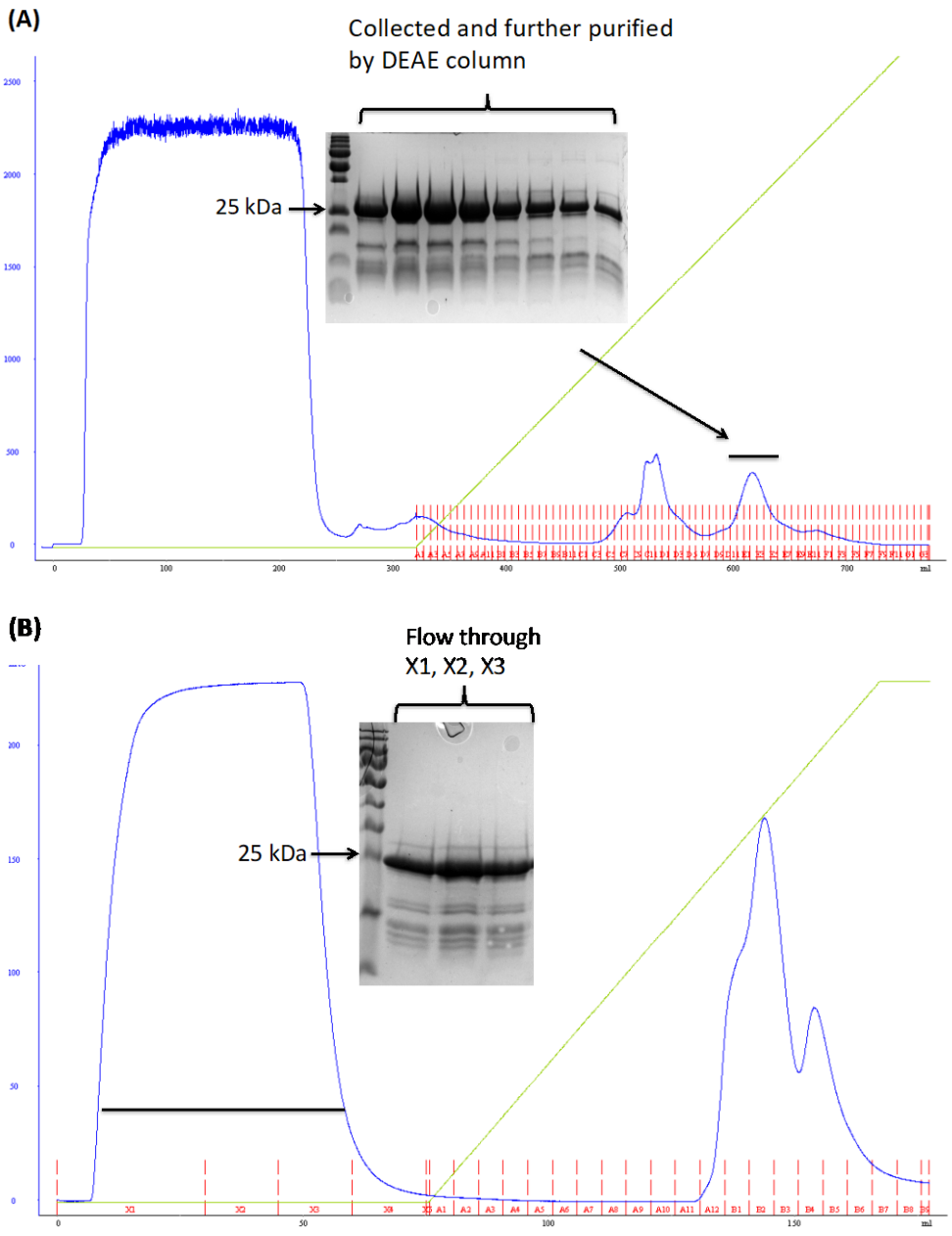

Figure A2. Purification of WT human adult cTnI by (A) CM Sepharose column and (B) DEAE FF column.

(A) The human cTnI eluted at 65-75% of a 500 mM NaCl salt gradient on the chromatogram and migrated as a ~24 kDa protein species on a 12% SDS-PAGE gel. All fractions containing cTnI were combined and further purified by DEAE column. (B) The human cTnI eluted from the flow through in the DEAE FF column while other containment proteins were separated in the salt gradient. All purified WT cTnI proteins were combined, dialyzed against 25 mM ammonium sodium bicarbonate, lyophilized and kept at -20 °C until future use. The containment proteins with lower molecular weights were later removed by dialysis.

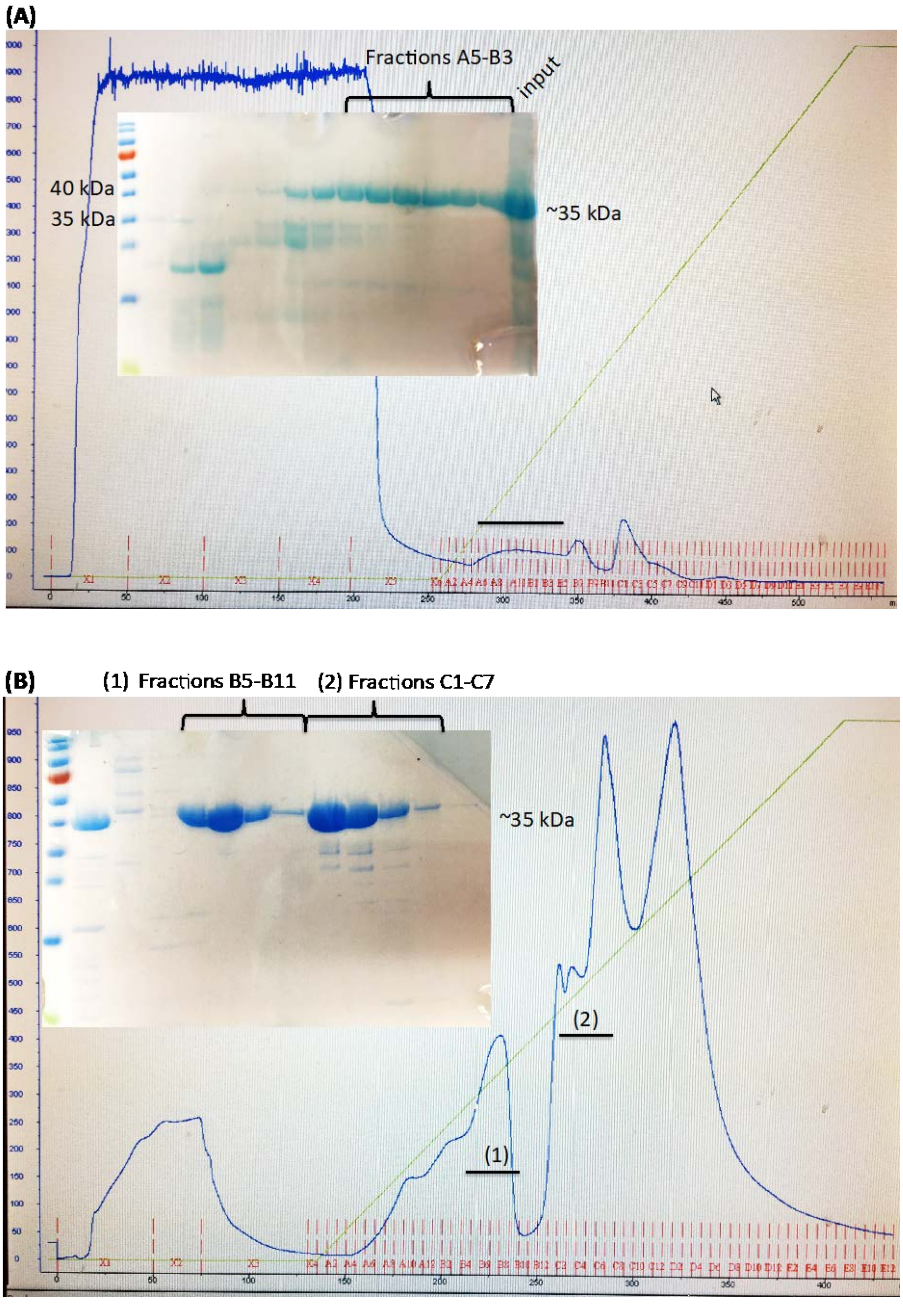

Figure A3. Purification of WT human adult cTnT.

(A) A CM-Sepharose chromatogram and the corresponding SDS-PAGE gel are shown. The fractions of A5 to B3 containing partially purified adult cTnT were eluted at 15-25% of a 500 mM NaCl salt gradient. (B) A DEAE-Sepharose chromatogram and the corresponding SDS-PAGE gel showing the purified cTnT eluted at 25-35% and 45-55% of a 500 mM NaCl salt gradient. All fractions containing purified cTnT were combined,dialyzed against 5 mM ammonium hydrogen bicarbonate, lyophilized and stored at -20 °C until future use.

(A)

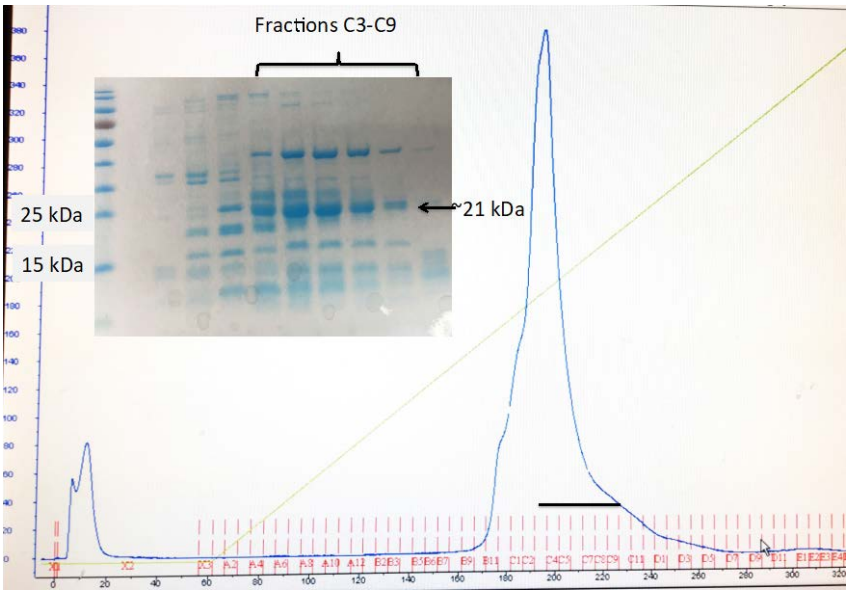

(B)

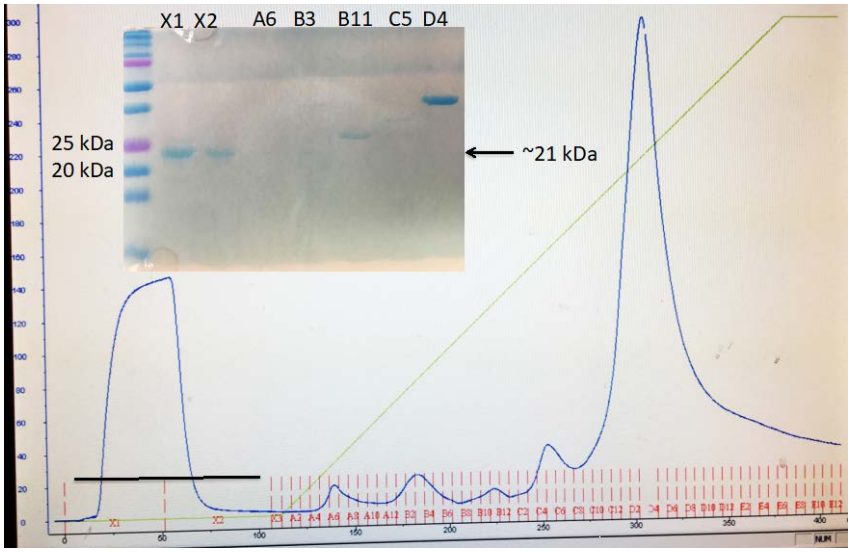

Figure A4. Purification of WT ssTnI.

(A) A CM-Sepharose chromatogram and the corresponding SDS-PAGE gel of partially purified WT ssTnI are shown. WT ssTnI were eluted from 55-65% salt gradient of 500 mM NaCl. Fractions containing WT ssTnI were combined and further purified on a DEAE FF column. (B) A DEAE chromatogram and the corresponding SDS-PAGE gel of purified WT ssTnI are shown. The purified WT ssTnI was eluted in the flow through while other containment proteins were bound to the column and separated from one another during the course of the salt gradient.

(A)

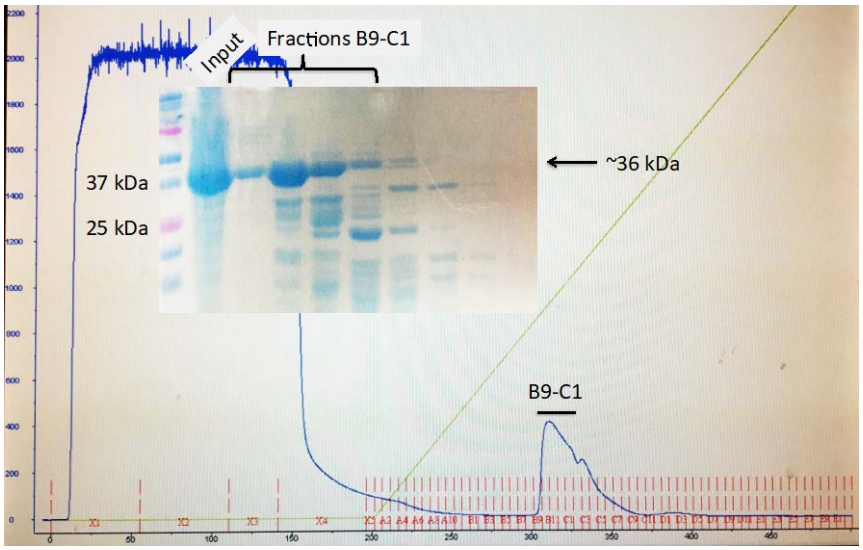

(B)

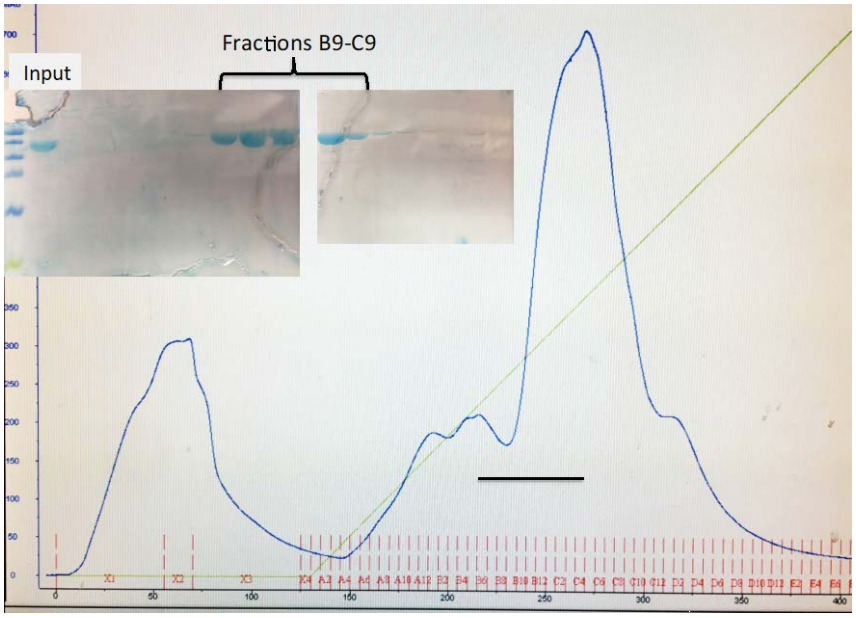

Figure A5. Purification of fetal WT cTnT by (A) CM Sepharose FF column and (B) DEAE FF column.

(A) The CM chromatogram of fetal WT cTnT and the corresponding SDS-PAGE gel are shown. Partially purified fetal WT cTnT was eluted at 30-40% of a 500 mM NaCl salt gradient and migrated as a ~36 kDa species. Fractions from B9-C1 were combined and further purified on a DEAE FF column. (B) The DEAE chromatogram and the corresponding SDS-PAGE gels are shown. Purified fetal WT cTnT were eluted at 30-40% of a 500 mM NaCl salt gradient. Fractions from B9 to C9 were combined, dialyzed against 1% formic acid, lyophilized and stored at -20 °C until future use.

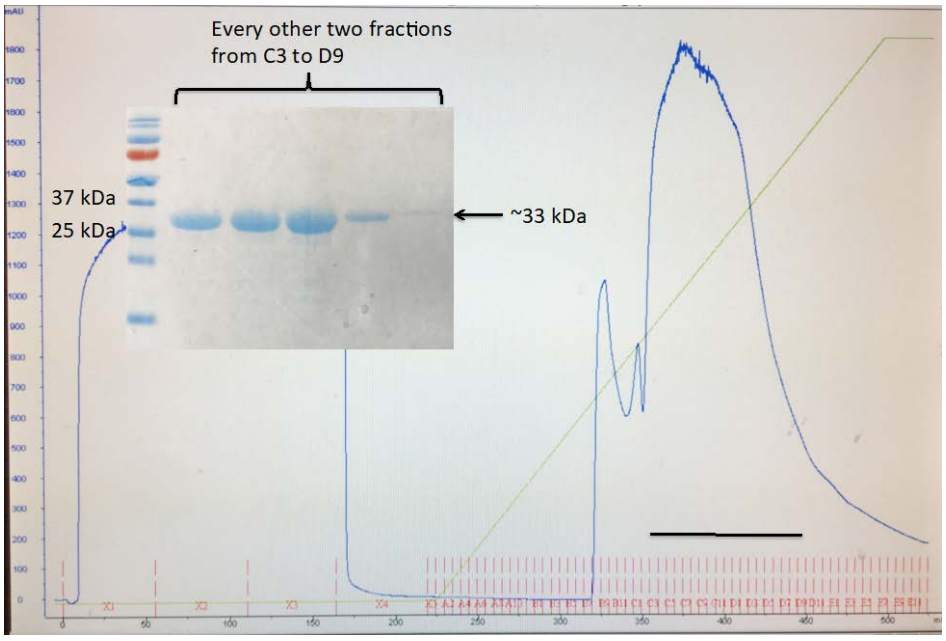

Figure A6. Purification of human MAS-α-Tm.

A Q-Sepharose chromatogram and the corresponding SDS-PAGE of the purified MAS-α-Tm are shown. Tm proteins were eluted at 40-60% of a 900 mM NaCl salt gradient and migrated as a 33 kDa species on a 12% SDS-PAGE gel. Fractions containing purified Tm were combined, lyophilized and stored at -20°C until future use.

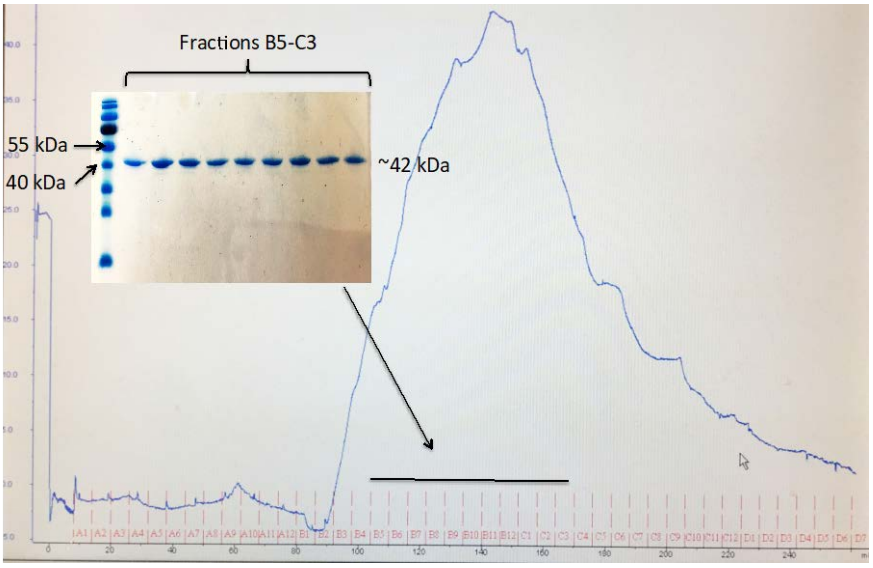

Figure A7. Purification of rabbit skeletal actin by size exclusion HiPrep Sephacryl S100 column.

Fractions containing purified rabbit skeletal monomeric actin (G-actin) proteins shown on the 12% SDS-PAGE gel were combined together. They were converted to filamentous actin (F-actin) before RTF generation.

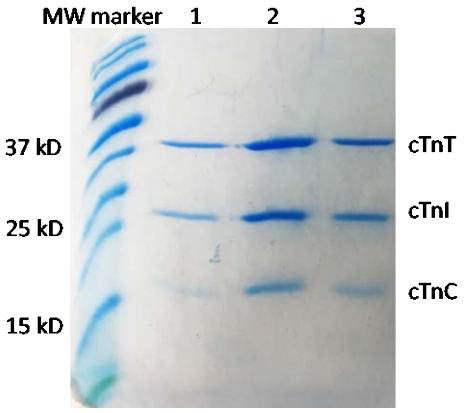

Figure A8. A representative 12% SDS page gel showing the WT Tn complexes.

The gel showing that cTnT migrated as a ~34 kDa species, cTnI migrated as a ~24 kDa species and cTnC as a ~18 kDa species.

Supporting Materials for Chapter 4:

The followings are the original averaged traces (N ≥ 10) obtained from the stopped-flow spectroscopy. The k_{off} (s^{-1}) values derived from the fluorescence traces using first-order reaction are presented as bar graphs throughout the chapters for clarity. The k_{off} (s^{-1}) values are included in the brackets in the following traces. Panel (A), (C), (E), (G), (I), and (K) shows the EGTA-induced time course of Ca^{2+} dissociation from various Tn complexes, reported by an increase in IAANS fluorescence. Panel (B), (D), (F), (H), (J), and (L) shows the EGTA-induced time course of Ca^{2+} dissociation from various RTF, reported by a decrease in IAANS fluorescence.

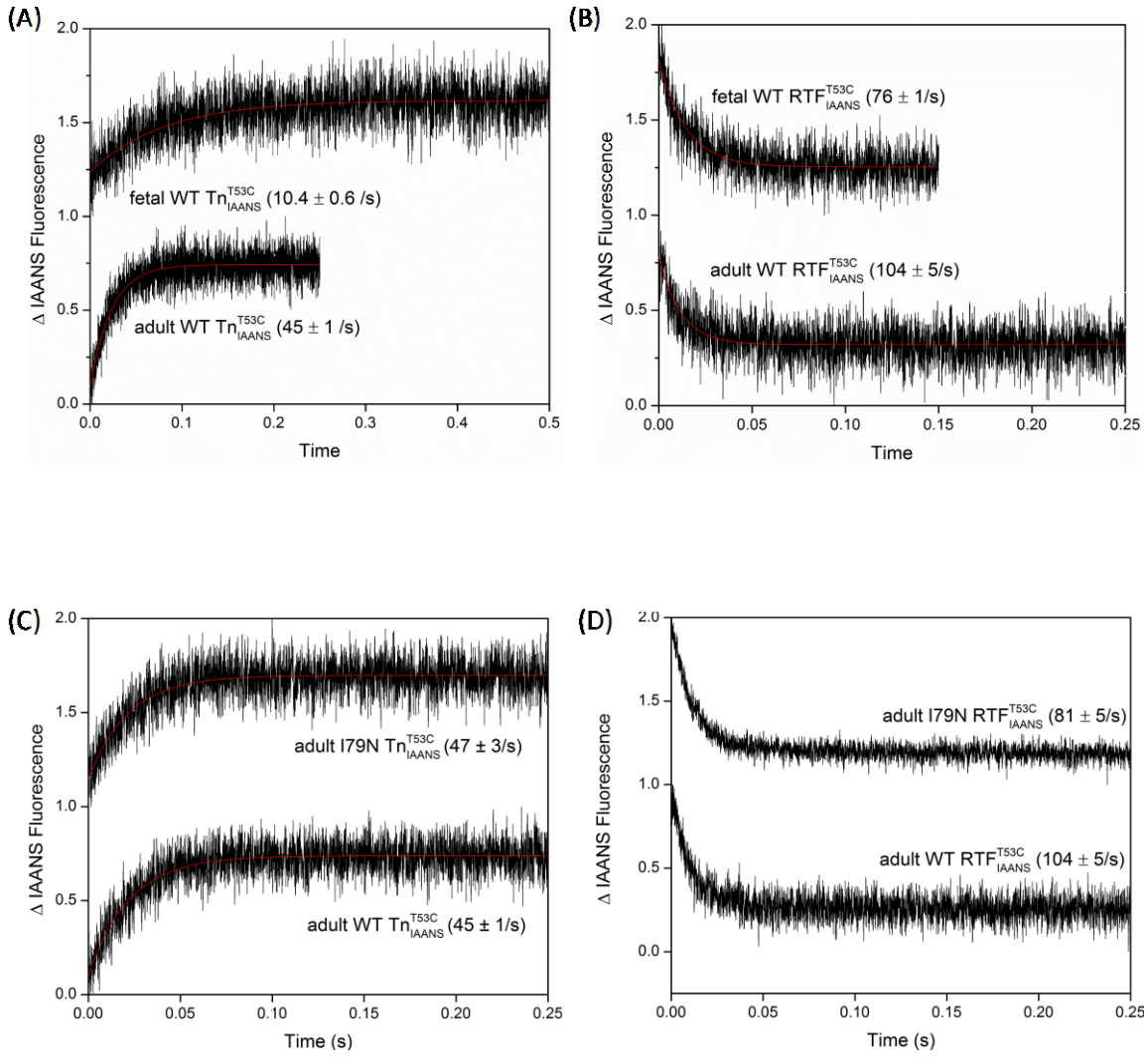

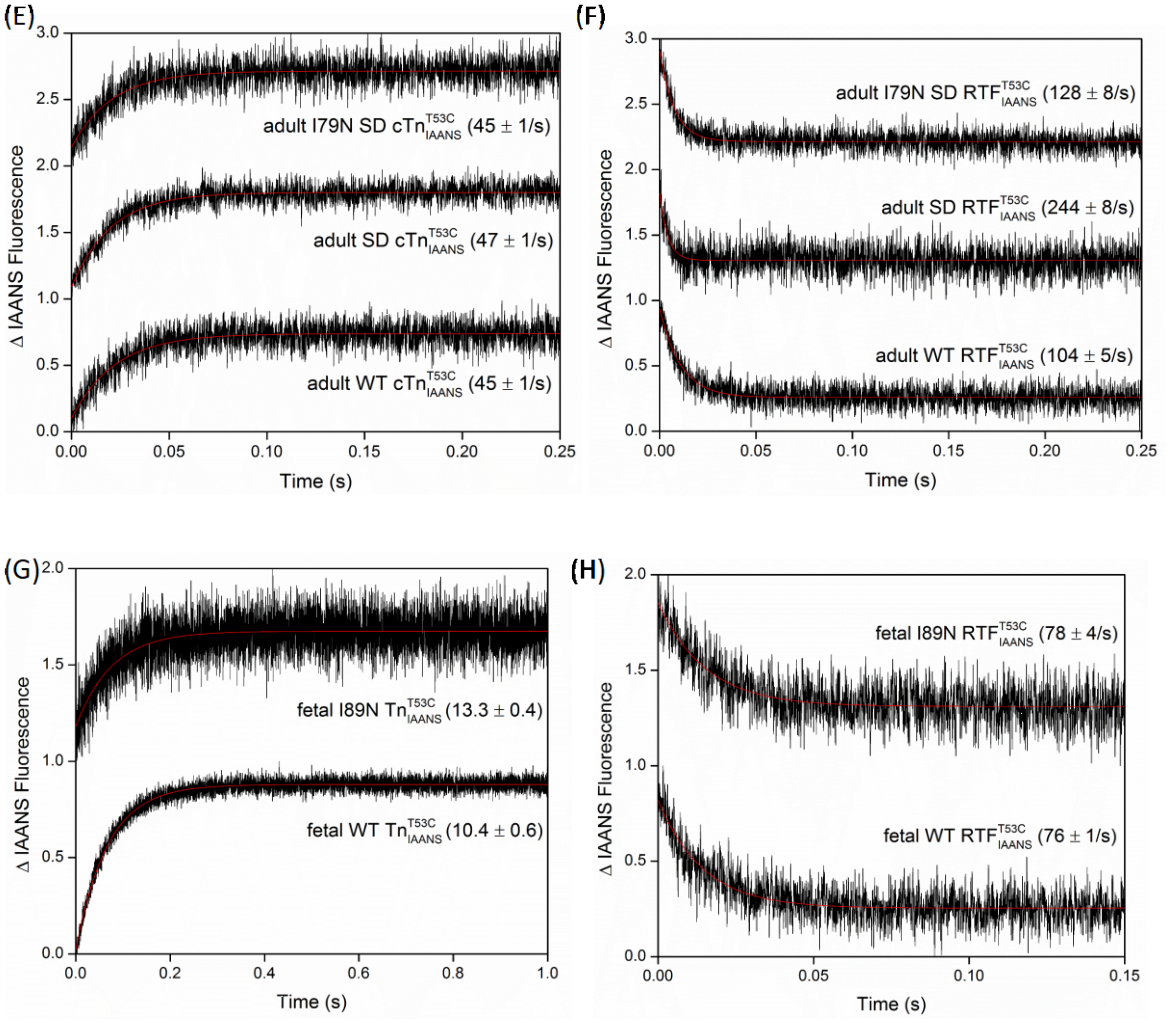
(E)
adult I79N SD cTn$_{IAANS}^{T53C}$ (45 ± 1/s)
adult SD cTn$_{IAANS}^{T53C}$ (47 ± 1/s)
adult WT cTn$_{IAANS}^{T53C}$ (45 ± 1/s)
Δ IAANS Fluorescence
Time (s)
(F)
adult I79N SD RTF$_{IAANS}^{T53C}$ (128 ± 8/s)
adult SD RTF$_{IAANS}^{T53C}$ (244 ± 8/s)
adult WT RTF$_{IAANS}^{T53C}$ (104 ± 5/s)
Δ IAANS Fluorescence
Time (s)
(G)
fetal I89N Tn$_{IAANS}^{T53C}$ (13.3 ± 0.4)
fetal WT Tn$_{IAANS}^{T53C}$ (10.4 ± 0.6)
Δ IAANS Fluorescence
Time (s)
(H)
fetal I89N RTF$_{IAANS}^{T53C}$ (78 ± 4/s)
fetal WT RTF$_{IAANS}^{T53C}$ (76 ± 1/s)
Δ IAANS Fluorescence
Time (s)

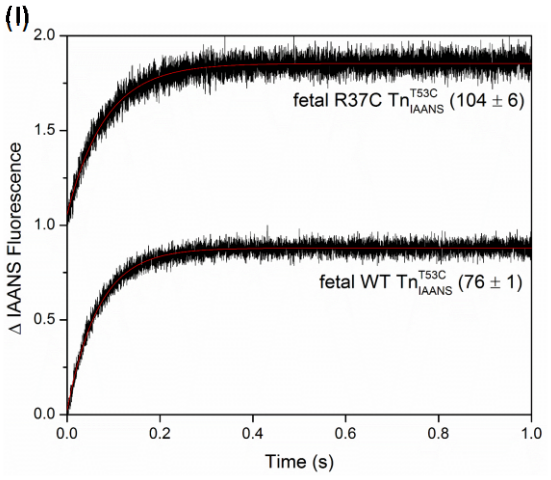
(I)
fetal R37C Tn^{T53C}_{IAANS} (104 ± 6)
fetal WT Tn^{T53C}_{IAANS} (76 ± 1)
Δ IAANS Fluorescence
Time (s)

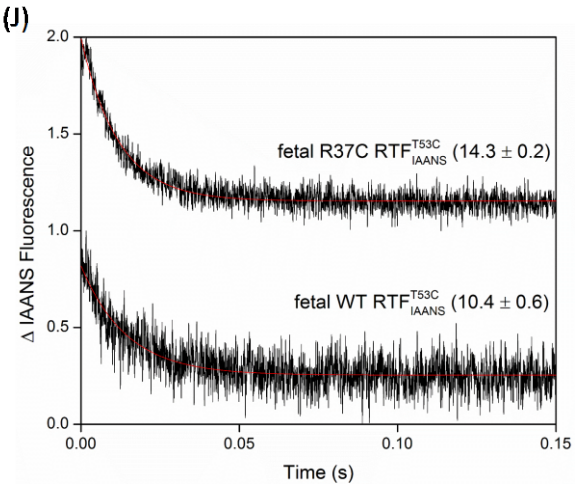
(J)
fetal R37C RTF^{T53C}_{IAANS} (14.3 ± 0.2)
fetal WT RTF^{T53C}_{IAANS} (10.4 ± 0.6)
Δ IAANS Fluorescence
Time (s)

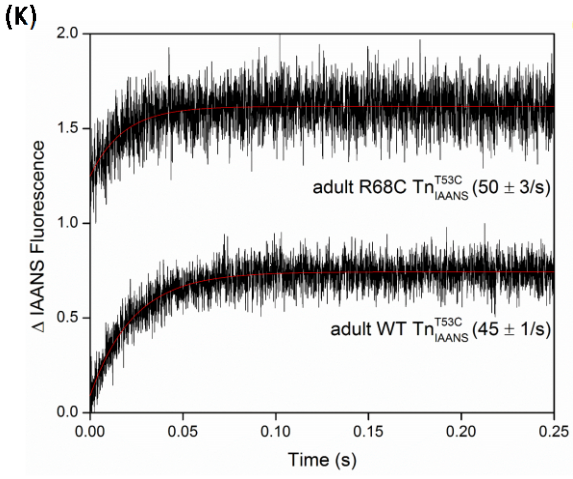
(K)
adult R68C Tn^{T53C}_{IAANS} (50 ± 3/s)
adult WT Tn^{T53C}_{IAANS} (45 ± 1/s)
Δ IAANS Fluorescence
Time (s)

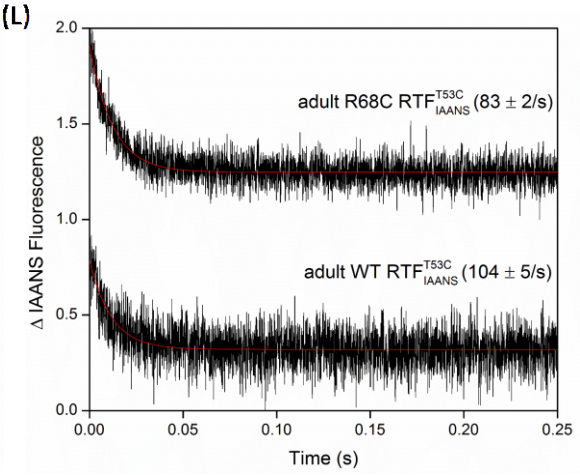
(L)
adult R68C RTF^{T53C}_{IAANS} (83 ± 2/s)
adult WT RTF^{T53C}_{IAANS} (104 ± 5/s)
Δ IAANS Fluorescence
Time (s)